

Frequency Regulation in Conventional, Deregulated and Wind Integrated Power Systems

*A thesis submitted
in partial fulfillment for the degree of*

Doctor of Philosophy

by

DEEPAK M



**DEPARTMENT OF AVIONICS
INDIAN INSTITUTE OF SPACE SCIENCE AND TECHNOLOGY
THIRUVANANTHAPURAM - 695 547, INDIA**

June 2018

Frequency Regulation in Conventional, Deregulated and Wind Integrated Power Systems

*A thesis submitted
in partial fulfillment for the degree of*

Doctor of Philosophy

by

DEEPAK M



**DEPARTMENT OF AVIONICS
INDIAN INSTITUTE OF SPACE SCIENCE AND TECHNOLOGY
THIRUVANANTHAPURAM - 695 547, INDIA**

June 2018

Dedicated to my parents, God Almighty, my guru Dr. K. N. Shubhanaga, my dear brother Mohammed Basim and my dear friend Ananthakrishnan.

Certificate

This is to certify that the thesis titled **Frequency Regulation in Conventional, Deregulated and Wind Integrated Power Systems**, submitted by **Deepak M**, to the Indian Institute of Space Science and Technology, Thiruvananthapuram, for the award of the degree of **Doctor of Philosophy**, is a bonafide record of the research work done by him under my supervision. The contents of this thesis, in full or in parts, have not been submitted to any other Institute or University for the award of any degree or diploma.

Dr. Rajesh Joseph Abraham

(Research Supervisor)

Associate Professor

Department of Avionics

IIST

Dr. B. S. Manoj

Professor & Head

Department of Avionics

IIST

Place: Thiruvananthapuram

Date: June 2018

Declaration

I declare that this thesis titled **Frequency Regulation in Conventional, Deregulated and Wind Integrated Power Systems** submitted in partial fulfillment for the award of the **Degree of Doctor of Philosophy** is a record of original work carried out by me under the supervision of **Dr. Rajesh Joseph Abraham**, and has not formed the basis for the award of any degree, diploma, associateship, fellowship or other titles in this or any other Institution or University of higher learning. In keeping with the ethical practice in reporting scientific information, due acknowledgments have been made wherever the findings of others have been cited.

Place: Thiruvananthapuram

June 2018

Deepak M

Research Student

Department of Avionics

Roll No.: SC13D009

Acknowledgments

Firstly, it is my privilege to express my sincere gratitude to my research supervisor Dr. Rajesh Joseph Abraham for giving me an opportunity to work under his supervision. I am highly indebted to my Doctoral Committee members: Prof. Anil Kulkarni, IIT Bombay, Prof. P. R. Bijwe, IIT Delhi, Prof. B. S. Manoj, Head, Dept. of Avionics, Dr. Selvaganesan, former Head, Dept. of Avionics, Prof. S.S. Moosath, Head, Dept. of Mathematics and Dr. Rajeevan P. P, Dept. of Avionics for their timely reviews and suggestions at various stages of my work. I would like to thank Indian Institute of Space Science & Technology for providing an opportunity to do my research through the IIST Research Fellowship.

I would like to thank my friends and colleagues Mr. Abhilash S, Mr. Sarath Babu, Dr. Rajesh R and Mr. Kiran Stephan for their valuable suggestions and discussions during various stages of my work.

The Guru must teach me and lead me into light, make me a link in that chain of which he himself is a link. The man in the street cannot claim to be a Guru. The Guru must be a man who has known, has actually realised the Divine truth, has perceived himself as the spirit. A mere talker cannot be the Guru. A talkative fool like me can talk much, but cannot be the Guru. A true Guru will tell the disciple, "Go and sin no more"; and no more can he sin, no more has the person the power to sin - Swami Vivekananda. I would like to thank all my teachers who motivated me and laid foundations of basic understanding of science, which inspired me to explore further knowledge.

Last but not least, I would like express my humble gratitude to my parents, their support and strength during my difficulties are invaluable. Their inspiration gave me enough strength to face challenges during my life.

Deepak M

Thiruvananthapuram, India

Abstract

Electric power systems must be maintained at the desired operating level characterized by nominal frequency, voltage profile, and load flow configuration. For power balance, at every instant, the power generated should match with the total load demanded and associated system losses. However, the load-demands fluctuate randomly causing a mismatch in the power balance and, thereby, deviations in the area frequencies and tie-line powers from their respective scheduled values. In this context, Automatic Generation Control (AGC) aims to bring the back frequency error and tie-line power flow error to zero.

In this thesis, we focus on frequency regulation of interconnected power system in conventional and deregulated scenarios. A Thyristor Controlled Series Compensator (TCSC) model suitable for frequency regulation studies has been developed and is tested in conventional as well as deregulated scenarios. It is evident from the analysis that TCSC improves damping performances of the system in terms of better settling time, peak overshoot in area frequencies and tie-line power flow. In traditional power systems, the system inertia is responsible for maintaining the power balance immediately after the load disturbances. With increasing penetration of wind energy system, conventional power plants, which are the prime sources of system inertia, are getting replaced by wind energy systems. Hence, large frequency deviations can be viewed in high wind integrated systems. This thesis also focuses on extracting kinetic energy of the wind generator to make them behave as conventional generating systems in frequency regulation. The proposed hidden inertia emulation and coordinated operation of conventional power generation systems with wind energy can effectively alleviate the frequency excursions during sudden load disturbances. Conventional energy storage device such as Flywheel Energy Storage (FES) system can be used in conjunction with wind integrated power systems to overcome the intermittent nature of power generation. TCSC is found to be effective in damping low frequency oscillations in weak tie-lines and supplement the frequency regulation. The proposed scheme of wind energy system has also been analyzed in deregulated scenario.

New case of contract violation is considered when wind power plant deviates from their contract demand due to variation in the power generation from forecasted value.

Table of Contents

List of Tables	xv
List of Figures	xvii
Abbreviations	xxv
Notations	xxvii
1 Introduction	1
1.1 Motivation, Objectives and Scope	2
1.2 Automatic Generation Control	3
1.2.1 Literature Review	6
1.2.2 Problem Formulation	12
1.2.3 Objectives	13
1.3 Outline of the Thesis	13
2 Improving the AGC Performance in a Power System with Thyristor Controlled Series Compensator	15
2.1 Introduction	15
2.2 Linearized Model of TCSC	16
2.3 Case Studies	18
2.3.1 Case-1: Thermal-Thermal System	19
2.3.2 Case-2: Hydro-Thermal System	29
2.4 Summary	38

3	Load Following in a Deregulated Power System with Thyristor Controlled Series Compensator	39
3.1	Introduction	39
3.2	Deregulated Environment	40
3.3	TCSC in Deregulated Power System	42
3.4	Case Studies	43
3.4.1	Case-1: Thermal-Thermal System	43
3.4.2	Case-2: Hydro-Thermal System	61
3.5	Summary	74
4	Frequency Support in a Wind Integrated Power System	75
4.1	Introduction	75
4.2	Models for Frequency Regulation	77
4.2.1	Power System Model	77
4.2.2	Variable Speed Wind Turbine Systems	78
4.2.3	Wind Turbine Aerodynamic model	79
4.3	Schemes for Frequency Regulation using Wind Turbines	80
4.3.1	Linearized Model of TCSC	82
4.3.2	Flywheel Energy Storage	83
4.4	Case Studies	84
4.4.1	Case-1: Thermal-Thermal System	85
4.4.2	Case-2: Hydro-Thermal System	103
4.5	Summary	115
5	Load Following by Wind Power Plants	117
5.1	Introduction	117
5.2	Frequency Support from Wind Energy System	119

5.3	Deregulated Power System	120
5.3.1	Power Market with Wind Energy System	122
5.4	Case Studies	124
5.4.1	Case-1: Thermal-Thermal Systems	124
5.4.2	Case-2: Hydro-Thermal System	147
5.5	Summary	164
6	Conclusions and Future Scope of Work	165
6.1	Conclusions	165
6.2	Future Scope	167
	Appendix	169
	Bibliography	171
	Publications Based on the Thesis	189

List of Tables

2.1	Optimum values of integral gain settings without and with TCSC for 1% step load disturbance in either of the areas for different combinations of apfs	22
2.2	Optimum values of of integral gain settings for 1% step load perturbation in either of the areas	30
2.3	Optimum values of of integral gain settings under parameter variation for 1% step load perturbation in either of the areas	37
3.1	GA parameters	47
3.2	Optimized Gain Settings of Control Areas	47
3.3	Optimized Gain Settings of Control Areas	63
4.1	PSO parameters	88
4.2	Optimum values of controller gains for 1% step load perturbation in Area-1 for various cases	90
4.3	Optimum values of controller gains for 1% step load perturbation in Area-1 for various cases	105
5.1	Optimization parameters used for tuning	127
5.2	Optimum values of controller gains for various cases with 30% wind penetration level	128
5.3	Optimum values of controller gains for various cases	150

List of Figures

1.1	A typical frequency response plot (Courtesy: NREL) [1]	5
2.1	Schematic diagram of an interconnected power system with TCSC in series with tie-line near to area-1	16
2.2	Linearized model of an interconnected thermal-thermal system	20
2.3	Variations in area frequencies (Δf_1 and Δf_2) and tie-line power (ΔP_{tie12}) with 1% step load disturbance in Area-1	23
2.4	Deviations in power generations of units (ΔP_{G1} and ΔP_{G2}) in Area-1 for 1% step load disturbance in Area-1	24
2.5	Deviations in generation generations of units (ΔP_{G3} and ΔP_{G4}) in Area-2 for 1% step load disturbance in Area-1	25
2.6	Variations in area frequencies (Δf_1 and Δf_2) and tie-line power (ΔP_{tie12}) with 1% step load disturbance in Area-2	26
2.7	Deviations in generation (ΔP_{G1} and ΔP_{G2}) in Area-1 and (ΔP_{G3} and ΔP_{G4}) in Area-2 for 1% step load disturbance in Area-2	27
2.8	Variation in the incremental change of the percentage compensation (Δk_c) of TCSC with 0.01 pu step load disturbance in Area-1 and Area-2, respectively	28
2.9	Transfer function block diagram of the interconnected hydro-thermal power system with TCSC in series with tie-line	29
2.10	Variation of the performance index with integral gain value for the hydro area (K_{I2}) with disturbance in the hydro area	31
2.11	Variations in area frequencies (Δf_1 and Δf_2) and tie-line power (ΔP_{tie12}) when load change in Area-1	32

2.12	Variations in power output of thermal (ΔP_{G1}) and hydro (ΔP_{G2}) units when load change in Area-1	33
2.13	Variations in area frequencies (Δf_1 and Δf_2) and tie-line power (ΔP_{tie12}) when load change in Area-2	34
2.14	Variations in power output of thermal (ΔP_{G1}) and hydro (ΔP_{G2}) units when load change in Area-2	35
2.15	Variation in the incremental change of the percentage compensation (Δk_c) of TCSC with 0.01 pu step load disturbance in Area-1 and Area-2 respectively	36
3.1	Schematic diagram of the interconnected power system with TCSC in series with tie-line near to Area-1 in deregulated scenario	42
3.2	Linearized model of an interconnected thermal-thermal system under deregulation	46
3.3	Generation vs fitness values obtained from GA optimization	48
3.4	Unilateral contract: Variations in area frequencies (Δf_1 and Δf_2) and tie-line power (ΔP_{tie12})	50
3.5	Unilateral contract: Deviation in generation (ΔP_{G1} and ΔP_{G2}) of GENCOs in Area-1	52
3.6	Unilateral contract: Deviation in generation (ΔP_{G3} and ΔP_{G4}) of GENCOs in Area-2	53
3.7	Bilateral contract: Variations in area frequencies (Δf_1 and Δf_2) actual tie-line power (ΔP_{tie12}) and tie-line power error ($\Delta P_{tie12error}$)	54
3.8	Bilateral contract: Deviation in generation (ΔP_{G1} and ΔP_{G2}) of GENCOs in Area-1	55
3.9	Bilateral contract: Deviation in generation (ΔP_{G3} and ΔP_{G4}) of GENCOs in Area-2	56
3.10	Variations in area frequencies (Δf_1 and Δf_2) and actual tie-line power (ΔP_{tie12}) and ($\Delta P_{tie12error}$) for contract violation	58

3.11	Deviation in generation (ΔP_{G1} and ΔP_{G2}) of GENCOs in Area-1 for contract violation	59
3.12	Deviation in generation (ΔP_{G3} and ΔP_{G4}) of GENCOs in Area-2 for contract violation	60
3.13	Variation in the incremental change of the percentage compensation (Δk_c) of TCSC for case-1, Case-2 and Case-3	60
3.14	Linearized model of an interconnected hydro-thermal system under deregulation	62
3.15	Case 1: Variations in area frequencies (Δf_1 and Δf_2) and tie-line power (ΔP_{tie12})	65
3.16	Case 1: Deviation in generation (ΔP_{G1} and ΔP_{G2}) of GENCOs in Area-1	66
3.17	Case 1: Deviation in generation (ΔP_{G3} and ΔP_{G4}) of GENCOs in Area-2	67
3.18	Case 1: Variations in area frequencies (Δf_1 and Δf_2) actual tie-line power (ΔP_{tie12}) and tie-line power error ($\Delta P_{tie12error}$)	68
3.19	Case 2: Deviation in generation (ΔP_{G1} and ΔP_{G2}) of GENCOs in Area-1	69
3.20	Case 2: Deviation in generation (ΔP_{G3} and ΔP_{G4}) of GENCOs in Area-2	70
3.21	Case 3: Variations in area frequencies (Δf_1 and Δf_2) and actual tie-line power (ΔP_{tie12}) and ($\Delta P_{tie12error}$)	71
3.22	Case 3: Deviation in generation (ΔP_{G1} and ΔP_{G2}) of GENCOs in Area-1	72
3.23	Case 3: Deviation in generation (ΔP_{G3} and ΔP_{G4}) of GENCOs in Area-2	73
3.24	Variation in the incremental change of the percentage compensation (Δk_c) of TCSC for Case-1, Case-2 and Case-3	73
4.1	Single area with non conventional generation	78
4.2	Equivalent energy conversion system of DFIG	79
4.3	Control strategy and WECS model	80
4.4	Schematic model of the interconnected two area wind integrated power system with TCSC in series with the tie-line	82

4.5	Small signal model of TCSC used for AGC studies	83
4.6	Flywheel energy storage	84
4.7	Two-area thermal-thermal test system with WECS, FES and TCSC	86
4.8	PSO Flow Chart [2]	89
4.9	Iteration vs fitness values obtained from PSO optimization for 10% wind penetration	91
4.10	Variations in area frequencies (Δf_1 and Δf_2) and tie-line power (ΔP_{tie12}) when load change in Area-1 for 10% wind penetration	94
4.11	Variations in power generations in Area-1 (ΔP_{G1} , ΔP_{G2}) and deviation in the injected wind power (ΔP_{wind}) when load change in Area-1 for 10% wind penetration	95
4.12	Variations in area frequencies (Δf_1 and Δf_2) and tie-line power (ΔP_{tie12}) when load change in Area-1 for 20% wind penetration	97
4.13	Variations in power generations in Area-1 (ΔP_{G1} , ΔP_{G2}) and deviation in the injected wind power (ΔP_{wind}) when load change in Area-1 for 20% wind penetration	98
4.14	Variations in area frequencies (Δf_1 and Δf_2) and tie-line power (ΔP_{tie12}) when load change in Area-1 for 30% wind penetration	100
4.15	Variations in power generations in Area-1 (ΔP_{G1} , ΔP_{G2}) and deviation in the injected wind power (ΔP_{wind}) when load change in Area-1 for 30% wind penetration	101
4.16	Variations in power output of wind power plant (ΔP_{Wind}) and power output of FES (ΔP_{FES}) for different penetration levels	102
4.17	WTG rotor speed variation during grid disturbance for 30% wind penetration	103
4.18	Two-area hydro-thermal test system with WECS, FES and TCSC	104
4.19	Variations in area frequencies (Δf_1 and Δf_2) and tie-line power (ΔP_{tie12}) when load change in Area-1 for 10% wind penetration	107

4.20	Variations in power generations in Area-1 (ΔP_{G1} , ΔP_{G2}) and deviation in the injected wind power (ΔP_{wind}) when load change in Area-1 for 10% wind penetration	108
4.21	Variations in power generations in Area-2 (ΔP_{G3} , ΔP_{G4}) when load change in Area-1 for 10% wind penetration	109
4.22	Variations in area frequencies (Δf_1 and Δf_2) and tie-line power (ΔP_{tie12}) when load change in Area-1 for 20% wind penetration	110
4.23	Variations in power generations in Area-1 (ΔP_{G1} , ΔP_{G2}) and deviation in the injected wind power (ΔP_{wind}) when load change in Area-1 for 20% wind penetration	111
4.24	Variations in power generations in Area-2 (ΔP_{G3} , ΔP_{G4}) when load change in Area-1 for 20% wind penetration	112
4.25	Variations in area frequencies (Δf_1 and Δf_2) and tie-line power (ΔP_{tie12}) when load change in Area-1 for 30% wind penetration	113
4.26	Variations in power generations in Area-1 (ΔP_{G1} , ΔP_{G2}) and deviation in the injected wind power (ΔP_{wind}) when load change in Area-1 for 30% wind penetration	114
4.27	Variations in power generations in Area-2 (ΔP_{G3} , ΔP_{G4}) when load change in Area-1 for 10% wind penetration	115
5.1	Schemes used for the analysis	120
5.2	Schematic model of a two area deregulated power system	122
5.3	Linearized model of an interconnected thermal-thermal system with high wind integration under deregulation	125
5.4	Flow chart of TLBO algorithm [3,4].	127
5.5	Iteration vs fitness values obtained from TLBO for 30% wind penetration	129
5.6	Variations in area frequencies (Δf_1 and Δf_2) and tie-line power (ΔP_{tie12}) in unilateral contract case	131

5.7	Variations in tie-line power ($\Delta P_{tie\ 12\ actual}$) and and power output of wind power plant (ΔP_{wind}) in unilateral contract case	132
5.8	Deviation in generation (ΔP_{G1} and ΔP_{G2}) of GENCOs in Area-1 for unilateral contract case	133
5.9	Deviation in generation (ΔP_{G3} and ΔP_{G4}) of GENCOs in Area-2 for unilateral contract case	134
5.10	Variations in area frequencies (Δf_1 and Δf_2) actual tie-line power (ΔP_{tie12}) and tie-line power error ($\Delta P_{tie12error}$) in bilateral contract case	135
5.11	Deviation in power output of GENCO-wind	136
5.12	Deviation in generation (ΔP_{G1} and ΔP_{G2}) of GENCOs in Area-1 for bilateral contract case	138
5.13	Deviation in generation (ΔP_{G3} and ΔP_{G4}) of GENCOs in Area-2 for bilateral contract case	139
5.14	Variations in area frequencies (Δf_1 and Δf_2) and actual tie-line power (ΔP_{tie12}) and ($\Delta P_{tie12error}$) for contract violation (excess demand)	141
5.15	Deviation in power output of GENCO-wind for contract violation (excess demand)	142
5.16	Deviation in generation (ΔP_{G1} and ΔP_{G2}) of GENCOs in Area-1 for contract violation (excess demand)	142
5.17	Deviation in generation (ΔP_{G3} and ΔP_{G4}) of GENCOs in Area-2 for contract violation (excess demand)	143
5.18	Variations in area frequencies (Δf_1 and Δf_2) and actual tie-line power (ΔP_{tie12}) and ($\Delta P_{tie12error}$) for contract violation (deficit in wind power)	144
5.19	Deviation in generation (ΔP_{G1} and ΔP_{G2}) of GENCOs in Area-1 for contract violation (deficit in wind power)	145
5.20	Deviation in generation (ΔP_{G3} and ΔP_{G4}) of GENCOs in Area-2 for contract violation (deficit in wind power)	146

5.21	Deviation in power output of GENCO-wind for contract violation (deficit in wind power)	147
5.22	Linearized model of an interconnected thermal-thermal system with high wind integration under deregulation	148
5.23	Variations in area frequencies (Δf_1 and Δf_2) and tie-line power (ΔP_{tie12}) in case-1	151
5.24	Variations in tie-line power ($\Delta P_{tie\ 12\ actual}$) and and power output of wind power plant (ΔP_{wind}) in Case-1	152
5.25	Deviation in generation (ΔP_{G1} and ΔP_{G2}) of GENCOs in Area-1 for Case-1	153
5.26	Deviation in generation (ΔP_{G3} and ΔP_{G4}) of GENCOs in Area-2 for Case-1	154
5.27	Variations in area frequencies (Δf_1 and Δf_2) actual tie-line power (ΔP_{tie12}) and tie-line power error ($\Delta P_{tie12error}$)	155
5.28	Deviation in power output of GENCO-wind	156
5.29	Deviation in generation (ΔP_{G1} and ΔP_{G2}) of GENCOs in Area-1 for Case-2	156
5.30	Deviation in generation (ΔP_{G3} and ΔP_{G4}) of GENCOs in Area-2 for Case-2	157
5.31	Deviation in power output of GENCO-wind for Case-3 (excess demand)	158
5.32	Variations in area frequencies (Δf_1 and Δf_2) and actual tie-line power (ΔP_{tie12}) and ($\Delta P_{tie12error}$) for Case-3 (excess demand)	159
5.33	Deviation in generation (ΔP_{G1} and ΔP_{G2}) of GENCOs in Area-1 for Case-3 (excess demand)	160
5.34	Deviation in generation (ΔP_{G3} and ΔP_{G4}) of GENCOs in Area-2 for Case-3 (excess demand)	161
5.35	Variations in area frequencies (Δf_1 and Δf_2) and actual tie-line power (ΔP_{tie12}) and ($\Delta P_{tie12error}$) for Case-3 (deficit in wind power)	162

5.36	Deviation in power output of GENCO-wind for Case-3 (deficit in wind power)	163
5.37	Deviation in generation (ΔP_{G1} and ΔP_{G2}) of GENCOs in Area-1 for Case-3 (deficit in wind power)	163
5.38	Deviation in generation (ΔP_{G3} and ΔP_{G4}) of GENCOs in Area-2 for Case-3 (deficit in wind power)	164

Abbreviations

ACE	Area Control Error
AGC	Automatic Generation Control
DISCO	Distribution Company
FACTS	Flexible AC Transmission System
FES	Flywheel Energy Storage
GA	Genetic Algorithm
GENCO	Generating Company
ISO	Independent System Operator
LFC	Load frequency Control
PSO	Particle swarm Optimization
TCSC	Thyristor Controlled Series Compensator
TLBO	Teaching Learning based Optimization
TRANSCO	Transmission Company
VSWT	Variable Speed Wind Turbine
WECS	Wind Energy Conversion System
WTG	Wind Turbine Generator

Notations

f	Nominal System Frequency in Hz
$P_{tie\ ij}$	Tie line power flow from i^{th} area to j^{th} area
P_{ri}	Rated Power in the i^{th} area in MW
H	Inertia Constant in seconds
ΔP_{Di}	Incremental load change in i^{th} area in pu MW
ΔP_{Gi}	Incremental generation change in i^{th} area in pu MW
T_{12}	Synchronizing coefficient in pu MW/rad
R_i	Governor speed regulation parameters in Hz/pu MW
T_{Gi}	Steam turbine time constant in seconds
T_{Ri}	Reheat unit time constant in seconds
T_{Ti}	Turbine time constant in seconds
B_i	Frequency bias constant in pu MW/Hz
K_{Ri}	Steam turbine reheat constant in seconds
J	Cost Index
T_{TCSC}	TCSC time constant in seconds
K_{TCSC}	TCSC gain constant
T_{FES}	FES time constant in seconds
K_{FES}	FES gain constant
K_{Ii}	Integral gain of the i^{th} area
T_w	Washout filter time constant in seconds
T_R	Frequency transducer time constant in seconds
T_A	Controlled WECS time constant in seconds
T_c	Communication link time constant in seconds
K_P	Proportional gain constant of the speed recovery loop
K_I	Integral gain constant of the speed recovery loop
D	Damping constant in an area

Chapter 1

Introduction

Electric power systems comprise different control areas that are interconnected over a wide range through tie-lines for better reliability and continuous operation. Such systems must be maintained at desired operating level characterized by nominal frequency, voltage profile, and load flow configuration by the close control of the real and reactive powers generated in the controllable sources of the system. For power balance, the power generated should match with the total load demanded and associated system losses. However, the load-demands fluctuate randomly, causing a mismatch in the power balance and thereby deviations in the area frequencies and tie-line powers from their respective scheduled values. In this context, Automatic Generation Control (AGC) helps in bringing back frequency error and tie-line power flow error to zero so as to obtain better power balance following the load perturbations [5–7].

An imbalance between generation and load degrades the power system performance severely following the load perturbation. A mismatch in the real power balance primarily affects the system frequency. Frequency error is the most sensitive indicator that real power balance is not maintained [8].

Frequency control is becoming more significant today due to the increasing size of interconnected power systems, its changing structure and complexity of operation. High economic demand for power system efficiency and reliability led to a requirement for maintaining system frequency and tie-line power flows closer to scheduled values as much as possible. Therefore, in modern power systems, AGC plays a vital role as an ancillary service in supporting power exchanges and providing better operating conditions for power trading.

1.1 Motivation, Objectives and Scope

Today power systems are being operated under increasingly stressed conditions due to increased competition, open transmission access, integration of various Renewable Energy Systems (RES), and environmental constraints. Deregulation in electrical power systems has changed the nature of electricity from a service to commodity, so as to participate in open energy market. This leads to different ownership of generation, transmission and distribution makes power system control more difficult, and results in a lack of coordination among generation and transmission utilities as they target for maximizing their profit. This causes increasing uncertainty of operation and control [9].

In traditional power systems, load balancing is achieved by controlling the power output of dispatchable generating sources. Typically a small portion of hydro and thermal generating units in a control area are responsible for maintaining frequency regulation after sudden load demands. Integration of various renewable energy sources into the grid pose challenges to system operators due to their variability in power generation. In conventional systems, system inertia (linked to kinetic energy stored in the rotating mass) is responsible for maintaining power balance following a sudden load perturbation, which is termed as inertial control. Increasing integration of renewable energy sources into the grid has replaced conventional generating sources. At present, wind energy system occupies the major share in the installed capacity around the globe. Among various available wind energy conversion techniques, variable speed Doubly Fed Induction Generator (DFIG) wind turbines are the most commonly used ones. However, DFIG wind turbine generator (WTG) does not provide inertia support to the system as the power electronics interface decouples the rotor from the grid [10–14]. This in turn decreases the system inertia with increase in the wind penetration level. Thus, maintaining the system frequency after a load change becomes cumbersome. At the same time, competition in the power market also allows the Wind Energy Conversion System (WECS) to participate in power trading. Hence, maintaining load balance as an ancillary service becomes challenging in current power system operation and control.

With such complexities, maintaining generation-consumption equilibrium is an arduous task following the load perturbation. If the power balance is not met immediately

after the disturbance, it leads to variations in system frequency and tie-line power flow, resulting from non-availability of energy following the load demand. This brings up the question, why should we maintain system frequency constant?

1. Steam turbines are designed to operate in a narrow frequency band. Any deviation beyond this band causes gradual or even immediate damage to turbine.
2. For power transformers, under frequency operation increases the flux in the magnetic core. This may result in low efficiency and over-heating of transformer, which is highly undesirable.
3. Change in system frequency primarily affects the speed of AC motors, where speed consistency is expected to be high.
4. Variation in system frequency affects the accuracy of system clocks, which is driven by synchronous motors.

For stable and reliable operation, at steady state, the frequency should be maintained at its nominal value with help of AGC, where frequency and inter area power flow can be regulated.

1.2 Automatic Generation Control

The prime objective of an electric power system is to provide quality and reliable power to consumers in accordance with varying system operating conditions. The power system operator has to maintain the supply-demand balance at every instant of time. As we know, power is expressed as a complex quantity, which changes with variation in generator output and affects the system frequency, whereas change in excitation primarily affects the system voltage. For small load changes, it is fairly straight forward to divide the control of power system into frequency control and voltage control. It is also well known that frequency regulation mechanisms constitute slow responding mechanical systems, whereas in voltage control (excitation control) constitutes fast responding electromechanical systems. Through linear control theory perspective, the small load changes, the frequency

regulation and voltage control can be individually controlled. The control of real power output of generator, in response to the changing system frequency and tie-line power exchange is termed as Automatic Generation Control [5, 6].

Automatic Generation Control constitutes:

- Primary control
- Secondary control

Primary control refers to the governor action in response to load changes and is done by changing the valve settings so as to change the input of hydro or thermal turbines. Conventionally, at steady state, the generation matches with system loads and associated system losses. Any change in generation or load disturbs the power balance in the system, which may perturb the system operating conditions. This can be viewed through fundamental Swing equation of the system.

$$\frac{2H}{\omega_s} \frac{d\delta^2}{dt^2} = P_m - P_e \quad (1.1)$$

where,

- P_m – Input mechanical power
- P_e – Electrical output power
- δ – Internal angle/load angle
- H – Inertia cost
- ω_s – Synchronous speed

It can be seen that any system perturbation primarily affects the system frequency. Hence, frequency is the sensitive indication of system power imbalance. In conventional power systems, where all generators are connected in synchronous, any load change results in frequency change.

When a load change occurs, it may disturb the system power balance. Since all synchronous generators are rotating, to balance the mismatches, the kinetic energy stored in

the generator rotors gets released resulting in rotor speed changes. The rotor speed change ultimately results in system frequency changes. The release of stored kinetic energy from the rotor of generator is normally termed as inertia control, which may last for a few seconds immediately after the load change.

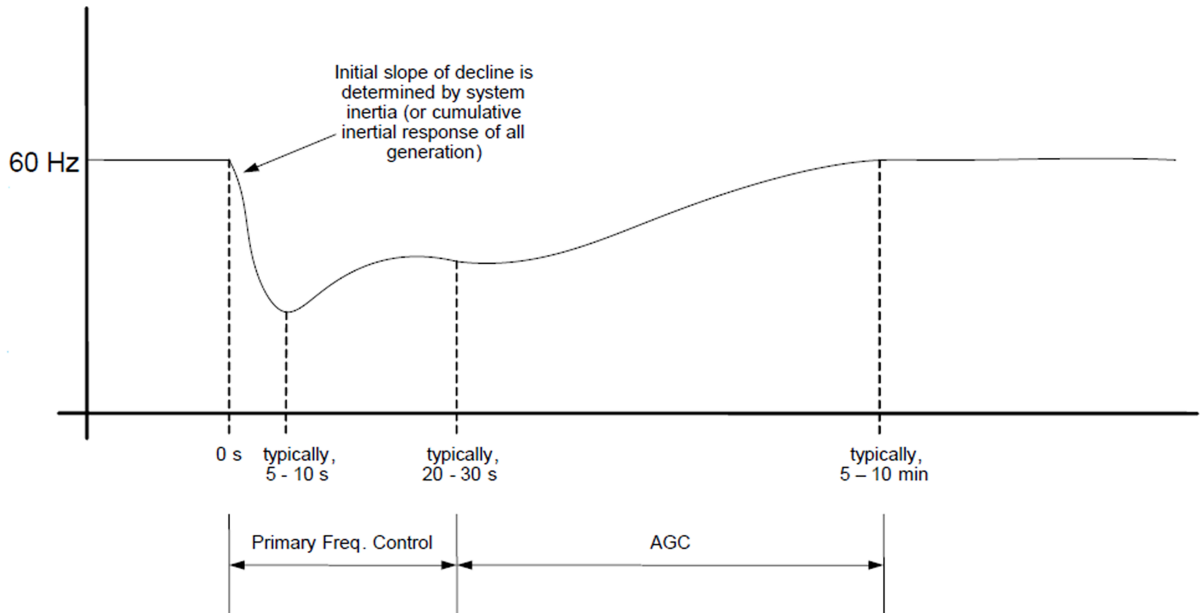


Fig. 1.1: A typical frequency response plot (Courtesy: NREL) [1]

A typical frequency regulation plot is shown in Fig. 1.1. It is clear that initial decline in the system frequency from the nominal grid frequency depends on the system inertia. The initial decline or Rate of Change of Frequency (RoCoF) is governed by the net kinetic energy released from the synchronous generators, which is termed as inertia control. As already mentioned, the change in frequency activates the governors so as to change its gate valve position either to increase or decrease the water/steam output. The action is carried out in line with regulation parameter ' R ' of the governors so as to maintain the proper load sharing between the generators. Basically, R is a proportional control, which results in a steady state error. To bring back the grid frequency to its nominal value a secondary control, typically an integral control is employed. The secondary control restores the frequency by properly adjusting the power reference of individual generating units. Normally, inertia response last for a few seconds immediately after the load perturbation, whereas primary control/governor action for 10 s to 30 s and slow responding secondary

control last for few minutes.

1.2.1 Literature Review

There exist available literature in AGC problem ever since the interconnection of power system began. This can be broadly divided into the following:

- Traditional AGC
- AGC in restructured power systems
- AGC in renewable integrated power systems

Traditional AGC

Literature survey shows that many researchers have tried to address the AGC problem ever since operation of interconnected power systems began. A robust adaptive AGC scheme with system parametric uncertainties combining riccati equation approach and adaptive model reference control has been proposed in [15]. However, the designed adaptive robust controller was suitable for single area system, whereas the practical electric power systems are highly interconnected. Hence, the proposed model lacks a real world issue and extending this design to a multi-area interconnection becomes too complex. A systematic control design approach that utilizes the loop shaping ideas and Quantitative Feedback Theory to improve the load frequency controller which has many intrinsic complexities has been suggested in [16]. The proposed control scheme in [16] needs complex computation in loop shaping design and it is quite difficult to achieve in real world problems. In [17], authors have studied the control performance of Redox flow batteries for frequency control applications. However, the losses occurring, were found to be more. A novel approach for steady-state analysis of generation control using computational intelligence techniques has been proposed in [18]. Training data and test data have been formed over a large range of input and output, however which has no physical significance to practical system. It can be seen that range set for deviation in system system frequency (Δf) lies between -0.5 to 0.5 pu, which indicates a faulty assumption made during analysis. Tuning

the PID controller by the lozi map-based chaotic algorithm to solve the Load Frequency Control (LFC) problem for a two-area power system has been reported in [19]. Simulation results of paper [19] show that with proposed controller the system exhibits a delayed response.

A new AGC structure has been proposed in [20] that overcomes the intermittency control problems in smart power grids. The proposed AGC control structure can accommodate high penetration of intermittent nondispatchable distributed energy sources. A new method of designing a multivariable self tuning regulator through speed governor control and excitation control has been suggested in [21]. The use of recursive least square algorithm for acquiring the system parameters in real time has been reported in [22]. An online estimation method for determining the frequency bias coefficient of a control area using variables commonly available from existing AGC system has been proposed in [23]. The proposed scheme in [24] has been very effective in frequency control of an isolated small hydro power plant in addition to reducing the size of the dump load. However, it is evident from the paper that with proposed scheme the frequency varies upto ± 2 to 3 Hz, which cannot be accepted as far as the LFC problem is concerned. In [25], authors have presented a sliding mode based automatic generation control. However, it requires full state feedback necessitating the estimation of unmeasured system states and disturbance. A sub-optimal AGC regulator design of an interconnected power system using constrained feedback control strategy has been proposed in [26]. An advanced frequency control based on H_∞ approach to integrate energy storage system into frequency control has been suggested in [27]. The proposed strategy take care of balancing frequency deviations introduced by renewable energy source and load variations according to the capabilities of storage and generators. The model based predictive control suggested in [28] for load frequency control employs a linear matrix inequality based approach. A design of decentralized PID load frequency controller based on Quantitative Feedback Theory has been proposed in [29]. The proposed method not only handles the parametric uncertainties in power system, but also covers a wide range of load change. Authors of [30] presented a wide area measurement, centralized, load frequency control using model predictive control for multi-area power systems. A new fuzzy sliding mode controller has been proposed for load frequency control of large hydro power plant in [31]. However,

a non-linear estimator is necessary for estimating and identifying the system state variables. A multi-agent reinforcement learning approach for load frequency control problem has been proposed in [9]. Most of the solutions proposed for AGC, however, have not yet been implemented due to system operational constraints and additional cost and complexities in implementation.

Restructured Power Systems and Renewable Integration

Literature survey shows that several researchers have proposed different methods to tackle the load frequency control problem in deregulated environment [32–43]. In [32], authors have proposed an introductory idea of LFC control in deregulated power system considering bilateral contract and contract violation. A PID tuning technique using internal mode control for decentralized load frequency control in deregulated environment has been investigated in [33]. The authors of [34] has proposed a decentralized robust LFC design technique through mixed H_2/H_∞ for three area power system under bilateral policy scheme. However, the proposed scheme lacks realization of various market scenarios such as bilateral market, pool based schemes. The paper has not addressed a common scenario of bilateral market, i.e., a case of contract violation, where any of DISCOs may violates contract by demanding excess or less power than it contracted early. A new robust controller for load frequency control in a deregulated electricity environment based on H_∞ norm and structured singular values of each control area has been reported in [35]. In practical environment, access to all state variables of a system is limited and measuring them is either difficult or impossible. In [36], authors have suggested some practical viewpoints on load frequency control problem in deregulated power system. A decentralized neural network based controller for load frequency control in a deregulated power system has been explored in [37]. The impact of interline power flow controller and Redox flow batteries on a two area multiple unit thermal reheat power system in restructured environment has been investigated in [38]. The effect of Superconducting Magnetic Energy Storage in load frequency control of a deregulated system with decentralized controller based on mixed H_2/H_∞ technique has been explored in [39]. Load frequency control

for an interconnected system with multi-source power generation under deregulated environment has been presented in [40]. A new robust strategy to adapt classical automatic generation control system to changing environment of power system operation based on bilateral AGC scheme has been proposed in [41]. A robust decentralized approach based on μ -synthesis for load frequency controller design of a restructured multi-area power system under possible contract has been reported in [42]. An intelligent solution for load frequency control in a restructured power system using extended classifier system has been explored in [43]. The proposed method of robust control technique such as H_2/H_∞ , μ -synthesis method, neural network based control techniques are insufficient to explain the effect of FACTS based system in deregulated scenario. Most of the proposed schemes merely address issues pertaining to the bilateral power market. The main drawback of the above tuning techniques are they require high computation efficiency to obtain better system performances.

In a traditional power systems, conventional sources like hydro and thermal are the main sources of inertia that is stored in the form of kinetic energy in the rotor. However, the inertia provided by DFIG type wind turbine is negligibly small because the rotor is decoupled from the grid through power electronic interface. With decreasing levels of inertia, an increased frequency excursion is observed after a sudden load perturbation which is of concern for plant operators as well as turbine manufacturers. Plenty of research works that are concerned with frequency support using variable speed wind turbines are available in the literature based on (a) inertia control [10–13, 44–53] (b) speed recovery [44, 45] and (c) coordinated operation with neighbouring conventional sources [45, 46].

In inertia control, the stored kinetic energy in rotor mass of wind turbine is fed back to the grid when a sudden load demand occurs. This fast acting energy reserve can be delivered only for a short period [12]. Inertia control is normally activated when load change occurs. This is done by adding a control loop for enhancing the inertia support from DFIG wind turbine [54]. A method to emulate inertia to support primary frequency control has been presented in [47], which involves releasing kinetic energy stored in the rotating mass of the turbine. Coordinated inertial control, rotor speed control and pitch angle control

have been presented in [13] for regulating frequency with DFIG wind turbines under various wind conditions. Normally modern wind turbines such as GE 1.5 MW are equipped with inertial control, which emulates the inertia of wind turbines and support during transients [55–57]. A control strategy for variable speed wind turbines to participate in primary frequency control has been proposed in [58]. It deploys the stored kinetic energy in the rotating masses to reduce the need of deloaded operation. A modified control that introduces inertia response to the DFIG wind turbine with high-voltage DC interconnection to alter the frequency behavior has been proposed in [59]. The study in [49] has developed a control strategy to mitigate the impact of reduced inertia in high wind penetrated system. The proposed scheme deals with reintroducing inertia using power electronics converter and pitch angle adjustment, to provide improved inertia response during grid frequency excursion. The use of wind turbines in primary frequency control considering transient and droop characteristics has been discussed in [60] while authors of [61] have presented a load frequency control design using Model Predictive Control (MPC) technique in a multi-area power system with wind turbines. The authors of [62] have suggested two main de-loading techniques: over-speeding and pitch controlled de-loading of wind generators which could enable wind generators to participate in load frequency control. To behave like a conventional synchronous machine, a supplementary control with variable droop has been introduced to deloaded turbines during depressed frequency [63]. As shown in recent works [14, 44, 46, 47, 54], additional schemes can be implemented to give the turbines a virtual/synthetic inertia. Available work [10–14, 44–63] suggest extracting kinetic energy from the rotating rotating mass of the WTG rotor through inertia emulating schemes. Due to the inertia emulation from rotor, rotor starts decelerating from its nominal value. To bring back the rotor speed to its nominal speed a recovery control need to be activated soon after the inertia control. During speed recovery, energy will be absorbed from the grid to bring back rotor speed its rated value as decided by the MPPT algorithm. Thus, sudden loss of temporary active power support from WTG through inertia control and speed recovery results in a second dip in the system frequency, which may be severe due to varying power output from the wind turbine. However, most literature has not addressed above issue to solve this problem so far.

Most of the proposed solutions available for frequency regulation with high wind

integration have considered either inertial emulation, droop control or pitch angle adjustment. Meanwhile, various literature are available in application of FACTS devices to improve load following in deregulated power systems [38, 64–66]. Similarly, various energy storage devices are also used in conjunction with renewable sources to enhance their performance [67]. Among them, Flywheel Energy storage (FES) is found to be the most efficient in storing this intermittent energy whenever available and supplying it to the grid as required [68]. Apart from stabilizing the intermittent energy sources, FES can also be used for controlling frequency and tie-line power flows [69]. Their advantages include operability at normal temperature, low losses during standby and long life time.

Various literature are available in frequency control of deregulated power systems ever since the operation of power system in deregulated scenario began. Most of the available research work on frequency regulation of deregulated power systems deal with the application of various modern control techniques such as optimal control, adaptive control, robust control, and intelligent techniques [70–72]. Application of energy storage devices and FACTS devices to damp out the area frequency oscillations as well as tie-line power flow in deregulated systems to improve the frequency regulation services were discussed in [38, 73, 74]. Many of the researchers have tried to incorporate various soft computing techniques for improving the load following in deregulated systems [75, 76].

Many works exist that deal with market operation of wind energy systems. Most of them have proposed the way to reduce the uncertainty associated with wind power forecasting, which is crucial for bidding in the energy market [77, 78]. Practical aspects associated with optimal operation of energy market with wind energy systems is described in [79]. Authors of [80] have analyzed the effect of wind penetration levels and wind power forecasting techniques in US market conditions. A disaggregate framework for integrating various renewable energy sources in deregulated power systems to improve the various ancillary services has been proposed [81]. Wind curtailment due to excess production or error in forecasting leads to revenue loss of power producers. To tackle this, various energy storage devices such as Battery Energy Storage, Superconducting Magnetic Energy Storage (SMES) System, and electric vehicles have been used to reduce the wind power curtailment by optimally charging these storage devices during excess wind power production [82–84]. Authors of [85] have investigated the importance of energy

storage, its sizing, and location to improve the system reserve in open market scenario. An optimal bidding mechanism for energy storage in open power market has also been proposed.

1.2.2 Problem Formulation

From the available literature, AGC problem can be tackled through design of proper controller and coordinated operation with suitable energy storage devices. During power imbalance, AGC guarantees improvement in transient behaviour with faster settling of frequency and tie-line deviations with less overshoot and small settling time. As complexities in power systems increase day by day, maintaining the system power balance under various operating conditions of interconnected power system is a matter of concern. Frequency regulation in turn means balancing generation and demand through the reduction in their gap. With competitive markets and renewable integration the frequency regulation becomes a concern for plant operators and system engineers.

Conventionally, AGC problem has been solved through two techniques - (i) proper controller design, and (ii) use of energy storage device. Balancing of generation-load problem through AGC is still an attractive arena for researchers due to lack of immediate availability of energy in the wake of sudden load. Even though technologies have been advanced over the years, there is no absolute solution to the AGC problem so far. As system operator demands fast settling of frequency deviation immediately after load perturbation, the use of fast acting energy sources like batteries, ultra capacitors, fly wheel energy storage, compressed air storage technologies still needs improvements in capacity enhancement and fast response. The use of various control strategy for designing controllers may help mitigate problem to a lesser extent. Most of the literature available are dealt with tuning the controllers (basically PI) using various advanced tuning techniques such as H_2/H_∞ , μ -synthesis method, neural network based control techniques. The prime aim of these techniques were better system performance in terms of settling time, peak overshoot etc.,. At the same time, designing of those controllers is a herculean task due to the parameter uncertainties associated with system nature. There is still scope for availing property of FACTS devices to improve better damping while enhancing the

power flow capability of tie-lines. Hence, in this work we have explored the possibility of existing TCSC in system to damp out the low frequency oscillations and achieving better system performance.

This thesis tries to address this problem in conventional, deregulated and wind integrated system through FACTS and energy storage device.

1.2.3 Objectives

The main objectives of this research work are as follows:

1. Study the effect of Thyristor Controlled Series Compensator (TCSC) in improving frequency regulation and analyze its performance in
 - (a) Conventional power system and a
 - (b) Deregulated power system
2. Develop a modified model for wind power plants suitable for load frequency analysis
3. Study the effect of load following by wind power plants in deregulated system
4. Study the effect of Flywheel (FES) system in the wind integrated scenarios.

1.3 Outline of the Thesis

The outline of the thesis is as follows:

Chapter 2 deals with the application of Thyristor Controlled Series Compensator (TCSC) in frequency control of two area interconnected power system. The analysis has been carried out to study the effect of TCSC in thermal-thermal as well as hydro-thermal power systems.

Chapter 3 presents the impact of TCSC in load following in a two area power system. The analysis has been extended for various market scenarios.

Chapter 4 proposes an FES-TCSC combination in improving the primary frequency capability of a wind power plant, where traditional Variable Speed Wind Turbines (VSWT) lack the primary frequency control capabilities. The issues associated with high wind penetration on load frequency control is also analyzed.

Chapter 5 suggests the possibility of using wind power plant potential on load following in open competitive power market. This chapter also conveys the importance of energy storage to enhance the system regulation reserve as well as to avoid wind power curtailment following excess production in imperialistic power market.

Chapter 6 summarizes the contributions of this research followed by scope for future work.

Chapter 2

Improving the AGC Performance in a Power System with Thyristor Controlled Series Compensator

2.1 Introduction

Electric power systems comprise different control areas that are interconnected over a wide range through tie-lines for better reliability and continuous operation. They must be maintained at the desired operating level characterized by nominal frequency, voltage profile, and load flow configuration by the close control of the real and reactive powers generated in the controllable sources of the system. For power balance, the power generated should match with the total load demanded and associated system losses. However, the load-demands fluctuate randomly causing a mismatch in the power balance and, thereby, deviations in the area frequencies and tie-line powers from their respective scheduled values, called Automatic Generation Control (AGC) [5, 6, 8].

In the mean time, several studies have investigated the potential of using Flexible AC Transmission Systems (FACTS) devices for better power system control since it provides more flexibility. Not only the power system dynamics can be enhanced and power transfer capability of transmission lines can be increased [86–92], but also, the dynamic stability can be enhanced using TCSC [93]. However, literature survey shows that, the effect of a TCSC on low frequency oscillations in area frequencies and tie-line power following a load perturbations is yet to be established. Hence in this chapter, our work aims to

1. Develop a linear incremental mathematical model of TCSC suitable for AGC applications
2. Optimize the integral gain settings of control areas using Integral Squared Error (ISE) technique for different combinations of area participation factors (apfs) and

3. Study and compare the effect of TCSC on AGC of (a) Two area Thermal-Thermal Power system (b) Two area Hydro-Thermal Power system considering non linearities.

2.2 Linearized Model of TCSC

Thyristor Controlled Series Compensator (TCSC) is a series compensating device to govern the power flow by compensating for the reactance of transmission line. TCSC consists of a series capacitor shunted by a Thyristor controlled inductive reactor whose reactance is varied according to the firing angle [94]. TCSC is considered as a variable reactance, the value of which is adjusted automatically to constrain the power flow across the branch to a specified value. The variable reactance X_{TCSC} represents the net equivalent reactance of the TCSC, when operating in either the inductive or the capacitive mode.

Fig. 2.1 shows the schematic diagram of a sample two area interconnected thermal-thermal power system with TCSC in series with the tie-line. For analysis, it is assumed that TCSC is connected near to the Area-1. Resistance of the tie-line is neglected, since the effect on the dynamic performance is negligible. Further, the reactance to resistance ratio in a practically interconnected power system is quite high. The incremental tie-line power flow without TCSC is given in [7] as

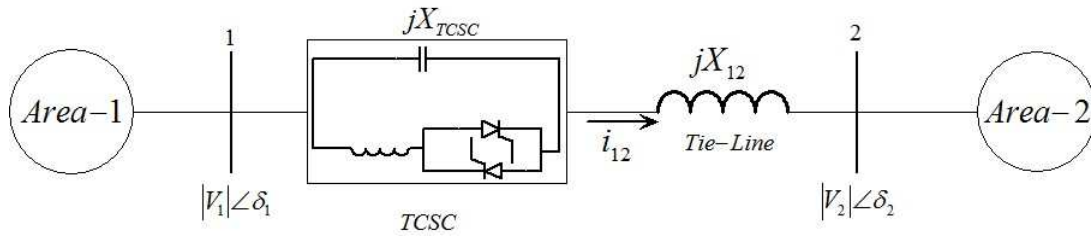


Fig. 2.1: Schematic diagram of an interconnected power system with TCSC in series with tie-line near to area-1

$$\Delta P_{tie12}(s) = \frac{2\pi T_{12}^0}{s} [\Delta f_1(s) - \Delta f_2(s)], \quad (2.1)$$

where, T_{12}^0 is the synchronizing coefficient without TCSC and Δf_1 and Δf_2 are the fre-

quency deviations in Areas 1 and 2 respectively. When TCSC is connected in series with the tie-line, the current flow from Area-1 to Area-2 can be written as

$$i_{12} = \frac{|V_1|\angle(\delta_1) - |V_2|\angle(\delta_2)}{j(X_{12} - X_{TCSC})}, \quad (2.2)$$

where X_{12} and X_{TCSC} are the tie-line reactance and TCSC reactance respectively.

From Fig. 2.1,

$$P_{tie12} - jQ_{tie12} = V_1^* I_{12} = |V_1|\angle(-\delta_1) \left[\frac{|V_1|\angle(\delta_1) - |V_2|\angle(\delta_2)}{j(X_{12} - X_{TCSC})} \right] \quad (2.3)$$

Therefore,

$$P_{tie12} - jQ_{tie12} = \frac{|V_1||V_2|}{(X_{12} - X_C)} \sin(\delta_1 - \delta_2) - j \left[\frac{|V_1|^2 - |V_1||V_2| \cos(\delta_1 - \delta_2)}{(X_{12} - X_C)} \right] \quad (2.4)$$

Separating the real part of Eqn. 2.3,

$$P_{tie12} = \frac{|V_1||V_2|}{(X_{12} - X_{TCSC})} \sin(\delta_1 - \delta_2) \quad (2.5)$$

Let k_c be the percentage of compensation offered by the TCSC, $k_c = \frac{X_{TCSC}}{X_{12}}$. The tie-line flow can be represented in terms of k_c as

$$P_{tie12} = \frac{|V_1||V_2|}{X_{12}(1 - k_c)} \sin(\delta_1 - \delta_2) \quad (2.6)$$

To obtain the linear incremental model, δ_1 , δ_2 and k_c are perturbed by $\Delta\delta_1$, $\Delta\delta_2$, Δk_c from their respective nominal values δ_1^0 , δ_2^0 and k_c^0 , so that, from Eqn. 2.6

$$\Delta P_{tie12} = \frac{|V_1||V_2|}{X_{12}(1 - k_c^0)^2} \sin(\delta_1^0 - \delta_2^0) \Delta k_c + \frac{|V_1||V_2|}{X_{12}(1 - k_c^0)} \cos(\delta_1^0 - \delta_2^0) (\Delta\delta_1 - \Delta\delta_2) \quad (2.7)$$

If $J_{12}^0 = \frac{|V_1||V_2|}{X_{12}} \sin(\delta_1^0 - \delta_2^0)$, and $T_{12}^0 = \frac{|V_1||V_2|}{X_{12}} \cos(\delta_1^0 - \delta_2^0)$, then Eqn. 2.7 becomes

$$\Delta P_{tie12} = \frac{J_{12}^0}{(1 - k_c^0)^2} \Delta k_c + \frac{T_{12}^0}{(1 - k_c^0)} (\Delta \delta_1 - \Delta \delta_2) \quad (2.8)$$

Since $\Delta \delta_1 = 2\pi \int \Delta f_1 dt$ and $\Delta \delta_2 = 2\pi \int \Delta f_2 dt$ and taking Laplace transform, Eqn. 2.8 yields

$$\Delta P_{tie12}(s) = \frac{J_{12}^0}{(1 - k_c^0)^2} \Delta k_c(s) + \frac{2\pi T_{12}^0}{s(1 - k_c^0)} [\Delta f_1(s) - \Delta f_2(s)] \quad (2.9)$$

Eqn. 2.9 reveals that the tie-line power flow can be regulated by controlling $\Delta k_c(s)$, the percentage compensation of TCSC. If the control input signal to TCSC damping controller is assumed to be $\Delta Error(s)$ and the transfer function of the signal conditioning circuit is $\frac{K_{TCSC}}{1 + sT_{TCSC}}$, then

$$\Delta k_c(s) = \frac{K_{TCSC}}{1 + sT_{TCSC}} \Delta Error(s), \quad (2.10)$$

where K_{TCSC} is the gain of the TCSC controller and T_{TCSC} is the time constant of the TCSC. Since TCSC is kept near to Area-1, frequency deviation Δf_1 may be suitably used as the control signal $\Delta Error(s)$, to the TCSC unit to control the percentage incremental change in the system compensation level. Hence,

$$\Delta k_c(s) = \frac{K_{TCSC}}{1 + sT_{TCSC}} \Delta f_1(s) \quad (2.11)$$

Thus, the deviation in the tie-line power flow after the perturbation becomes,

$$\Delta P_{tie12} = \frac{2\pi T_{12}^0}{s(1 - k_c^0)} [\Delta f_1(s) - \Delta f_2(s)] + \left[\frac{J_{12}^0}{(1 - k_c^0)^2} \right] \frac{K_{TCSC}}{1 + sT_{TCSC}} \Delta f_1(s) \quad (2.12)$$

2.3 Case Studies

The effect of Thyristor Controlled Series Compensator in improving frequency regulation on a conventional two area interconnected power system is studied for the following cases.

■ Case-1: Thermal-Thermal System

■ Case-1: Hydro-Thermal System

2.3.1 Case-1: Thermal-Thermal System

2.3.1.1 System Investigated

The sample AGC system on which investigations have been carried out comprises a two area interconnected thermal system with Generation Rate Constraints and Governor Dead Band non linearities. Area 1 consists of two reheat thermal power generation units and Area 2 comprises two non reheat thermal units. In a reheat thermal unit, the steam upon leaving the high pressure section of the turbine returns to the boiler where it is passed to a reheater before returning to the intermediate pressure section [8]. Typical values of Generation Rate Constraints (GRC) considered for non-reheat and reheat thermal units are 10%/min and 3%/min, respectively [95, 96]. A typical value of 0.06 % is considered for governor dead-band non-linearity as well [97]. Governor dead-band is defined as the total magnitude of a sustained speed change without change in valve position. The governor dead band affects the dynamic performance of load frequency control by introducing a zero in the governor transfer function through describing function approach [98] which leads to the inherent time-lag associated with it. In real system simulations, it is represented as backlash hysteresis. The governor deadband non-linearity has a destabilizing effect on the load-frequency control of a power system [98, 99]. A linearized model of governor dead band is developed in [100] has been used for the analysis. The paper [100] elaborately modelled the governor dead band as hysteresis backlash through describing function approach. In this thesis work we have adopted this modelling strategy in the entire analysis.

K_{I1} and K_{I2} are the integral gain settings in Area-1 and Area-2, respectively. apf_{11} and apf_{12} are the area participation factors in Area-1 while apf_{21} and apf_{22} are the area participation factors in Area-2. It may be noted that $apf_{11} + apf_{12} = 1$ and $apf_{21} + apf_{22} = 1$. ΔP_{D1} is the load perturbation in Area-1 and the load disturbance in Area-2 is ΔP_{D2} . Fig. 2.2 shows the linearized transfer function model of the interconnected power system with two area thermal system with TCSC in series with tie-line. The system parameters

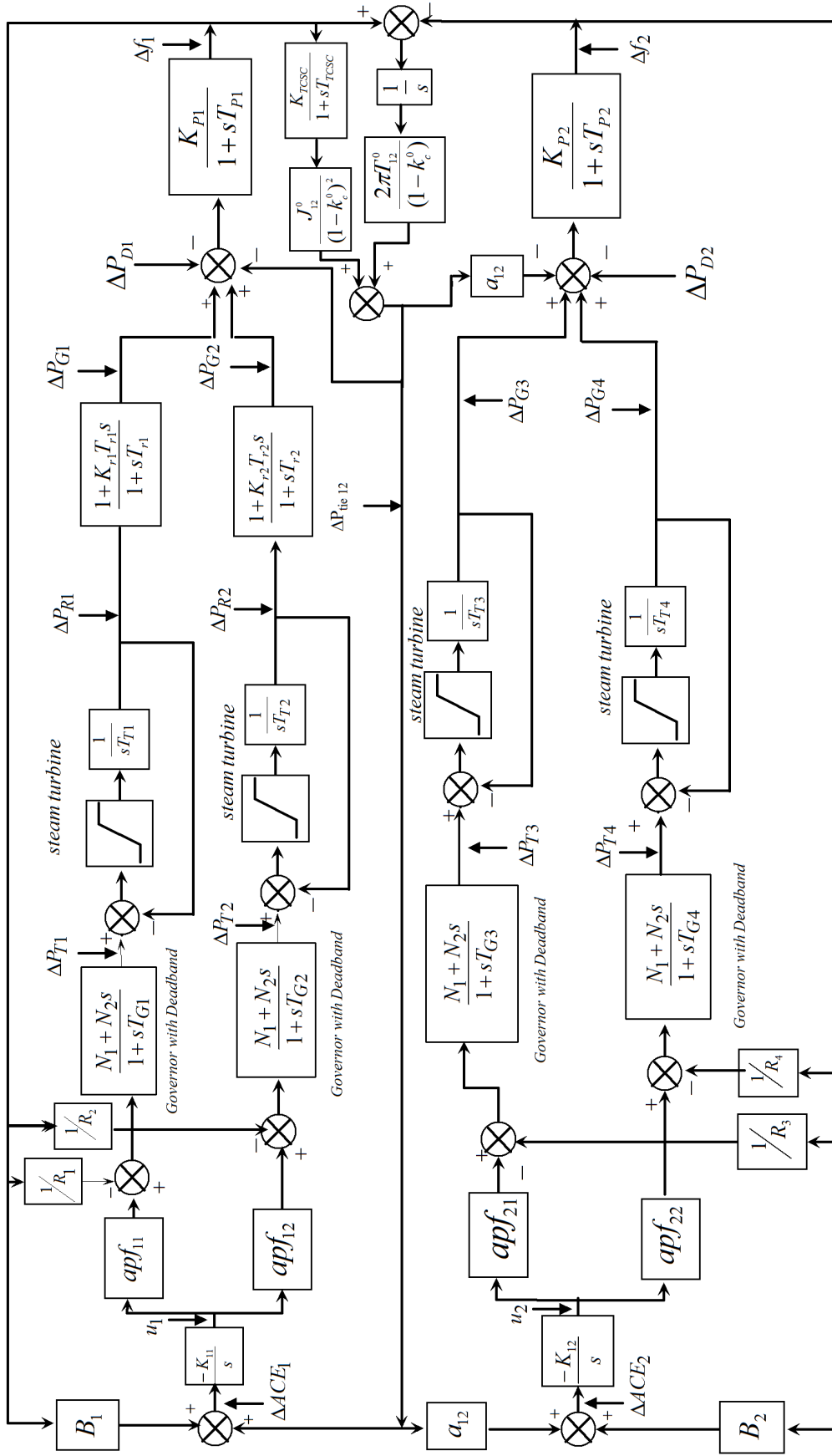


Fig. 2.2: Linearized model of an interconnected thermal-thermal system

are given in Appendix. The standard state space form of the system can be expressed as

$$\dot{X} = AX + BU + \Gamma p, \quad (2.13)$$

where X, U and p are the state, control and load disturbance input vectors, respectively whereas A, B and Γ are the respective matrices of appropriate dimensions. The vectors X, U and p are given by

$$X = \begin{bmatrix} \Delta f_1 \\ \Delta P_{G1} \\ \Delta P_{G2} \\ \Delta P_{R1} \\ \Delta P_{R2} \\ \Delta P_{T1} \\ \Delta P_{T2} \\ \Delta f_2 \\ \Delta P_{G3} \\ \Delta P_{G4} \\ \Delta P_{T3} \\ \Delta P_{T4} \\ \Delta P_{tie12} \end{bmatrix}, \quad U = \begin{bmatrix} u_1 \\ u_2 \end{bmatrix}, \quad p = \begin{bmatrix} \Delta P_{D1} \\ \Delta P_{D2} \end{bmatrix},$$

where the states are chosen as deviations in frequencies ($\Delta f_1, \Delta f_2$) in Area-1 and Area-2 respectively, the deviations in the power outputs in Area-1 ($\Delta P_{G1}, \Delta P_{G2}$) and ($\Delta P_{G3}, \Delta P_{G4}$) in Area-2, the deviations in reheat outputs in Area-1 ($\Delta P_{R1}, \Delta P_{R2}$), the deviations in turbine outputs in Area-1 ($\Delta P_{T1}, \Delta P_{T2}$) and ($\Delta P_{T3}, \Delta P_{T4}$) in Area-2 and the deviations in tie-line power flow (ΔP_{tie12}). The states chosen are also shown in Fig. 2.2.

2.3.1.2 Tuning the Controller Gain Settings

The ultimate objective of AGC is to maintain the frequency and inter-area tie-line powers within their respective scheduled values with minimum settling time following a sudden load perturbation. Hence, the integral gains of the control areas (K_{I1}, K_{I2}) are to be opti-

mally tuned for different combinations of *apfs*. Integral Squared Error (ISE) technique is used to formulate the objective function, since the ISE criterion weighs large errors heavily and small errors lightly. Furthermore, the criterion can be easily handled analytically to establish the frequency regulation capacity via a feedback controller. The objective is to maintain frequency within in the acceptable limit, i.e., very nearer to nominal value as soon as possible after the sudden load disturbance. At steady state, the tie-line power flow has to be maintained at its scheduled values between the control areas. To do so, the integral gains of the feedback controller of AGC (K_{I1} , K_{I2}) are to be tuned optimally to obtain the area frequencies and power exchange with minimum overshoot and lower settling time. A quadratic performance index defined by,

$$J = \int_0^t (\Delta f_1^2 + \Delta f_2^2 + \Delta P_{tie12}^2) dt \quad (2.14)$$

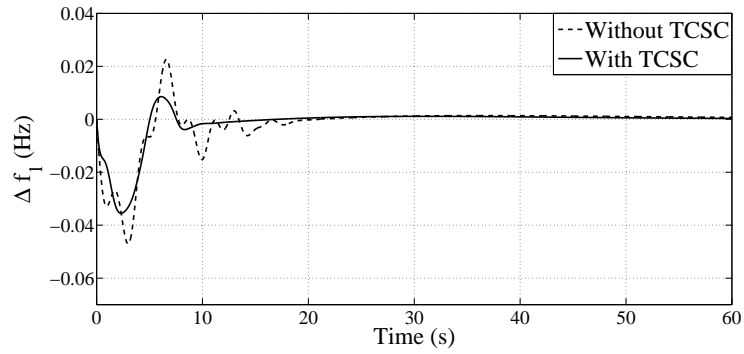
Table 2.1

Optimum values of integral gain settings without and with TCSC for 1% step load disturbance in either of the areas for different combinations of *apfs*

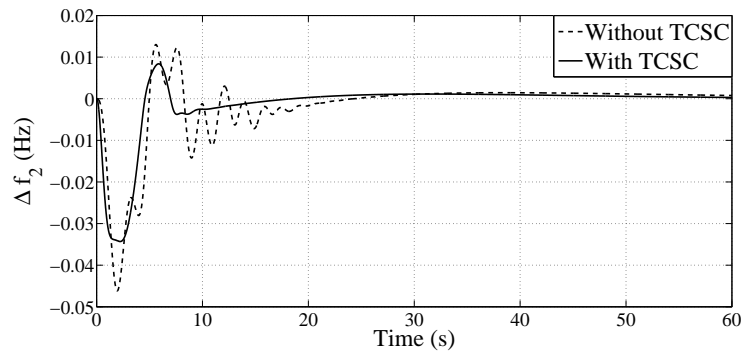
Step Load Perturbation 0.01 pu		Optimum integral gain settings for Area-1		Optimum integral gain settings for Area-2	
apf_{11}	apf_{12}	Without TCSC	With TCSC	Without TCSC	With TCSC
0.5	0.5	$K_{I1}=0.053$	$K_{I1}=0.071$	$K_{I2}=0.042$	$K_{I2}=0.069$
0.1	0.9	$K_{I1}=0.0483$	$K_{I1}=0.0827$	$K_{I2}=0.0392$	$K_{I2}=0.0764$
0.25	0.75	$K_{I1}=0.0514$	$K_{I1}=0.0756$	$K_{I2}=0.0411$	$K_{I2}=0.0729$
0.75	0.25	$K_{I1}=0.0582$	$K_{I1}=0.0651$	$K_{I2}=0.0475$	$K_{I2}=0.0612$

is minimized for 1% step load disturbance in either of the areas considering GRCs to obtain the optimum values of K_{I1} and K_{I2} . The controller gain settings of either areas are optimized by keeping the other area uncontrolled as in [96,98]. The optimal integral gains

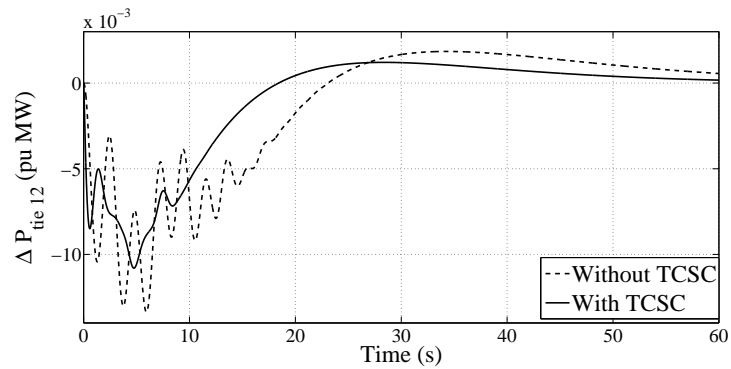
with and without TCSC and the corresponding performance index values so obtained are tabulated as in Table 2.1. It may be noted that, the optimal integral values with TCSC are higher than those without TCSC.



(a) Deviation in frequency of Area-1



(b) Deviation in frequency of Area-2

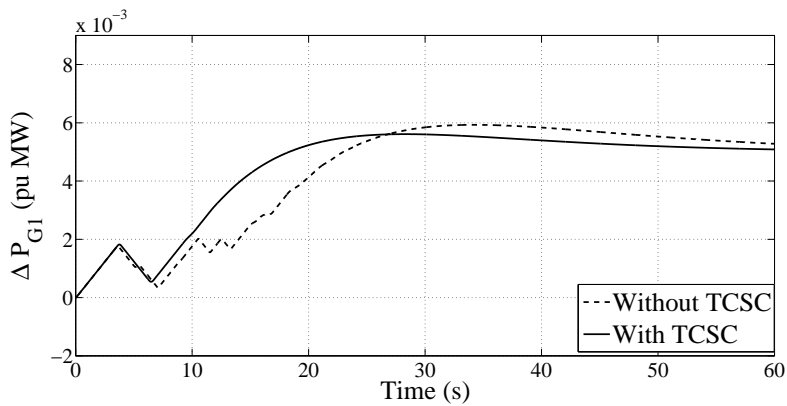


(c) Deviation in tie-line power flow

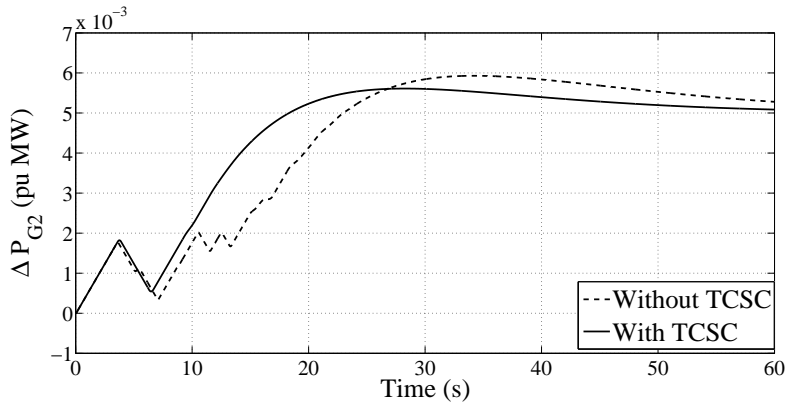
Fig. 2.3: Variations in area frequencies (Δf_1 and Δf_2) and tie-line power (ΔP_{tie12}) with 1% step load disturbance in Area-1

2.3.1.3 Simulation Results and Discussion

Time domain simulations using MATLAB have been carried out for the AGC system with a step load perturbation of 1% in either of the control areas with $apf_{11} = apf_{12} = apf_{21} = apf_{22} = 0.5$. The output of the TCSC is within 25 % to 75 %, a compensation range which can be easily achieved by TCSC manufacturers [89]. Hence, a compensation level of 50% was chosen for simulation studies. TCSC is placed near Area-1 considering 50% compensation. Fourth-order Runge-Kutta method with an integration step size of 0.01s is used for simulations.



(a) Deviation in power output of reheat Unit-1

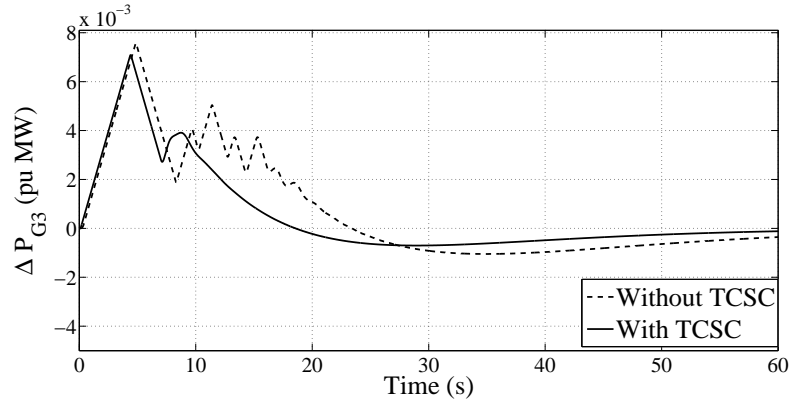


(b) Deviation in power output of reheat Unit-2

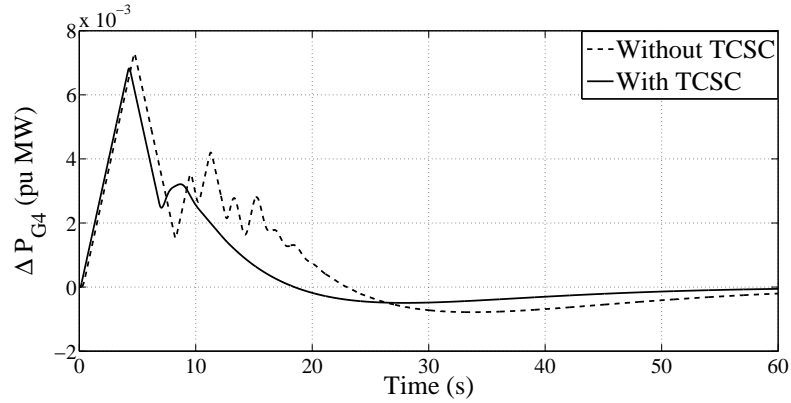
Fig. 2.4: Deviations in power generations of units (ΔP_{G1} and ΔP_{G2}) in Area-1 for 1% step load disturbance in Area-1

With optimal gain settings and a step load disturbance of 0.01 pu in Area-1, the different dynamic responses with and without TCSC are plotted in Figs. 2.3-2.7. The frequency

deviations ($\Delta f_1, \Delta f_2$) and tie-line power deviations (ΔP_{tie12}) as depicted in Fig. 2.3, show appreciable improvement in damping of oscillations with TCSC when compared with those without TCSC. Similarly with TCSC, the responses settle down quickly with 60 s whereas without TCSC the settling time is found to be 100 s. Furthermore, with TCSC, the settling time has been improved to a considerable extent.



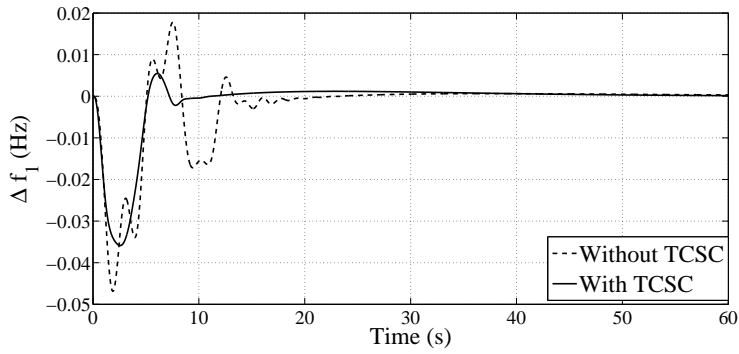
(a) Deviation in power output of non-reheat Unit-1



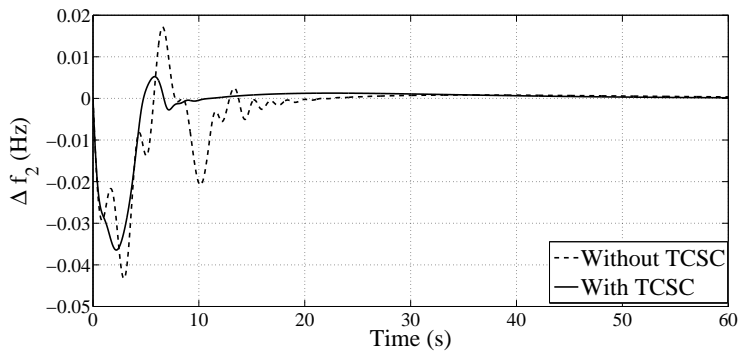
(b) Deviation in power output of non-reheat Unit-2

Fig. 2.5: Deviations in generation generations of units (ΔP_{G3} and ΔP_{G4}) in Area-2 for 1% step load disturbance in Area-1

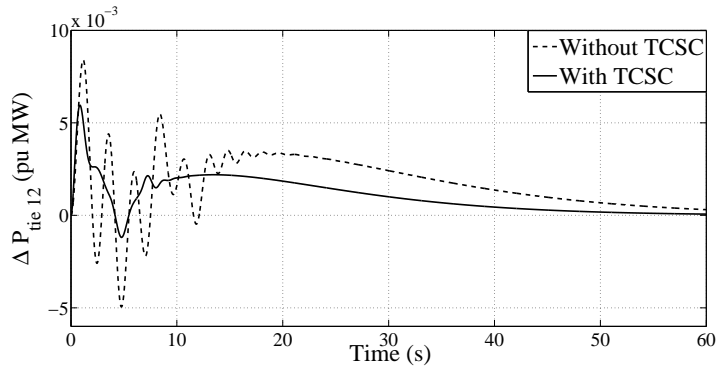
Figs. 2.4(a)-2.4(b) show the dynamic responses for the deviations in reheat thermal unit generations ($\Delta P_{G1}, \Delta P_{G2}$) in Area-1. Since load perturbation is in Area-1, the reheat units have to raise their generation to satisfy the local load requirement as per the followed practices in interconnected power system operation. Because we considered $apf_{11} = apf_{12} = 0.5$, at steady state, each reheat thermal unit has to generate 0.005 pu MW so that together, they satisfy 0.01 pu MW load demand in Area-1.



(a) Deviation in frequency of Area-1



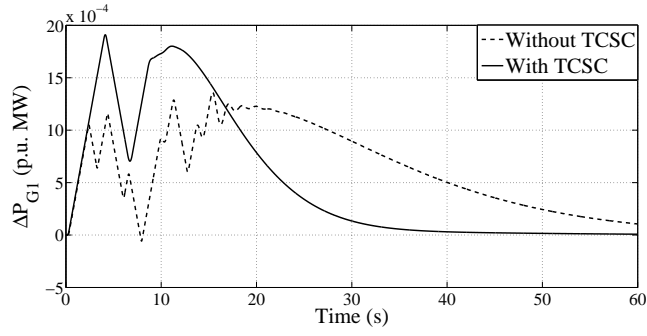
(b) Deviation in frequency of Area-2



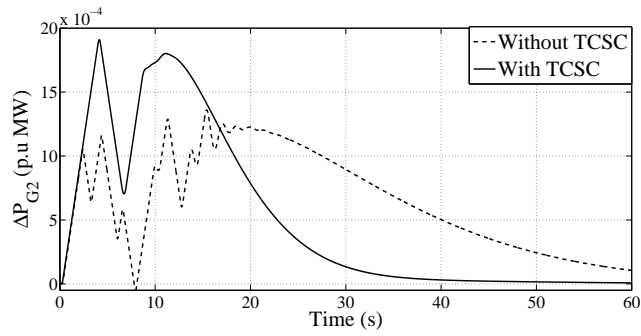
(c) Deviation in tie-line power flow

Fig. 2.6: Variations in area frequencies (Δf_1 and Δf_2) and tie-line power (ΔP_{tie12}) with 1% step load disturbance in Area-2

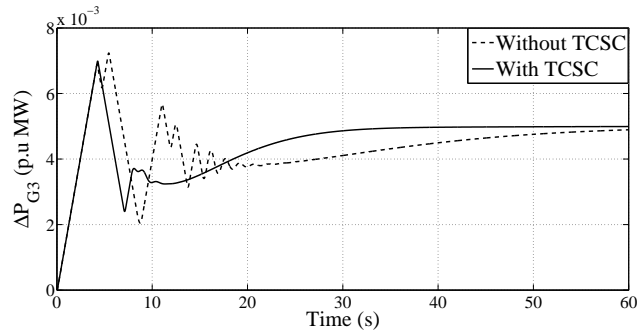
Further, from Figs. 2.4(a)-2.4(b), it can be observed that with TCSC there is a remarkable improvement in the settling time of the generation responses. The chasing of the load demand is smooth and almost free of ripples.



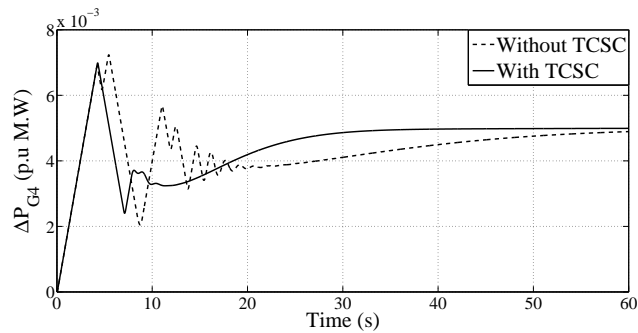
(a) Deviation in power output of reheat Unit-1



(b) Deviation in power output of reheat Unit-2



(c) Deviation in power output of non-reheat Unit-1



(d) Deviation in power output of non-reheat Unit-2

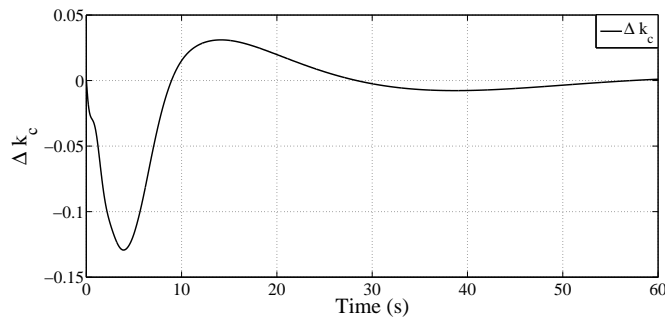
Fig. 2.7: Deviations in generation (ΔP_{G1} and ΔP_{G2}) in Area-1 and (ΔP_{G3} and ΔP_{G4}) in Area-2 for 1% step load disturbance in Area-2

Depicted in Fig. 2.5(a)-2.5(b) are deviations in generations of non reheat units (ΔP_{G3} and ΔP_{G4}) in Area-2. The non reheat unit generation deviations settle down to zero because the load disturbance occurred in Area-1. It can be seen that with TCSC, settling time has been considerably reduced and responses are almost ripple free.

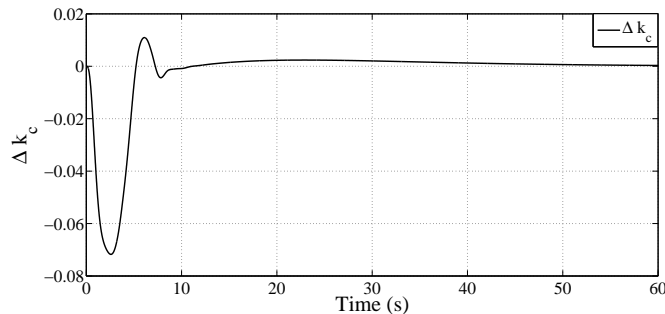
Similar conclusions can be drawn from the dynamic responses when a 1% step load perturbation occurs Area-2 (see Figs. 2.6-2.7).

Fig. 2.8 shows the variations in incremental change in percentage compensation of TCSC with 0.01 pu load perturbation in Area-1 and Area-2. Δk_c settles down to zero as frequency and tie-line power deviations from their respective scheduled values become zero.

Therefore, the low frequency oscillations in area frequencies and tie-power deviations pertaining to sudden load perturbations can be damped out effectively by a TCSC.



(a) Δk_c when loading in Area-1



(b) Δk_c when loading in Area-2

Fig. 2.8: Variation in the incremental change of the percentage compensation (Δk_c) of TCSC with 0.01 pu step load disturbance in Area-1 and Area-2, respectively

2.3.2 Case-2: Hydro-Thermal System

2.3.2.1 State Space Modeling

The effect of TCSC on AGC is also studied on a sample two area hydro-thermal system shown in Fig. 2.9. The two area system consist of a reheat unit in Area-1 and a hydro system in Area-2. Various non-linearities in the system such as GRC and governor dead-band are considered in the sample model. The linearized transfer function block diagram model of the power system under study is shown in Fig. 2.9 and can be expressed in the standard state space form as

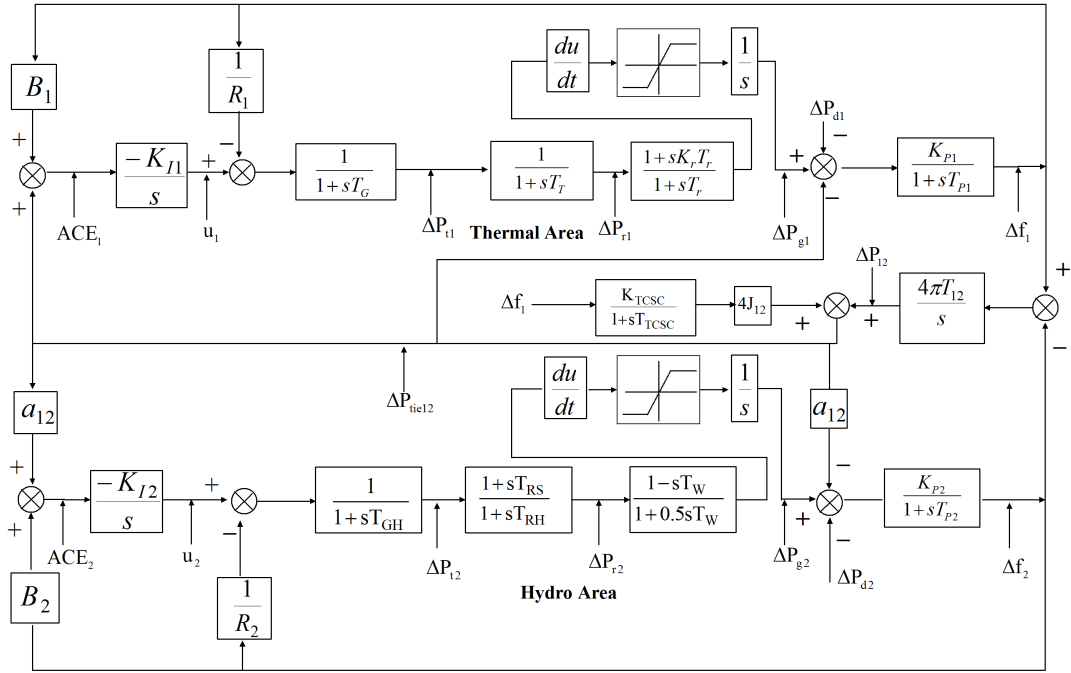


Fig. 2.9: Transfer function block diagram of the interconnected hydro-thermal power system with TCSC in series with tie-line

$$\dot{X} = AX + BU + \Gamma p, \quad (2.15)$$

where X , U and p are the states, control input, and load disturbance input vectors and A , B and Γ are the respective matrices of appropriate dimensions associated with them. The

vectors X , U and p are given by

$$X = \begin{bmatrix} \Delta f_1 \\ \Delta f_2 \\ \Delta P_{12} \\ \Delta P_{G1} \\ \Delta P_{R1} \\ \Delta P_{T1} \\ \Delta P_{G2} \\ \Delta P_{R2} \\ \Delta P_{T2} \\ \Delta k_c \end{bmatrix}, U = \begin{bmatrix} u_1 \\ u_2 \end{bmatrix}, p = \begin{bmatrix} \Delta P_{D1} & \Delta P_{D2} \end{bmatrix}$$

The state variables chosen are as shown in the power system model given in Fig. 2.9. The dynamic state space equations pertaining to the above AGC system are presented in Appendix.

2.3.2.2 Optimization of Integral Gain Settings

The optimal integral gain setting of each area (K_{I1} and K_{I2}) is obtained by the Integral Squared Error (ISE) method.

Table 2.2

Optimum values of of integral gain settings for 1% step load perturbation in either of the areas

Condition	K_{11}	K_{12}
Without TCSC	0.1124	0.0743
With TCSC	0.0590	0.2925

A quadratic performance index is formulated as in Eqn. 2.14 using the error terms in area frequencies and tie-line power and is minimized, for 1% step load disturbance in either of the areas in the presence of GRCs to obtain the optimal values of K_{I1} and K_{I2} . The controller settings of either thermal or hydro areas are optimized by considering the other area as uncontrolled [96].

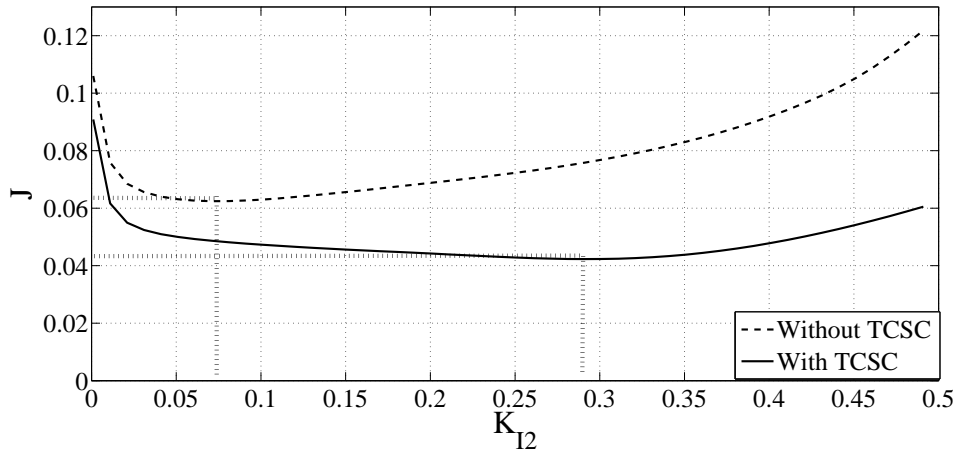
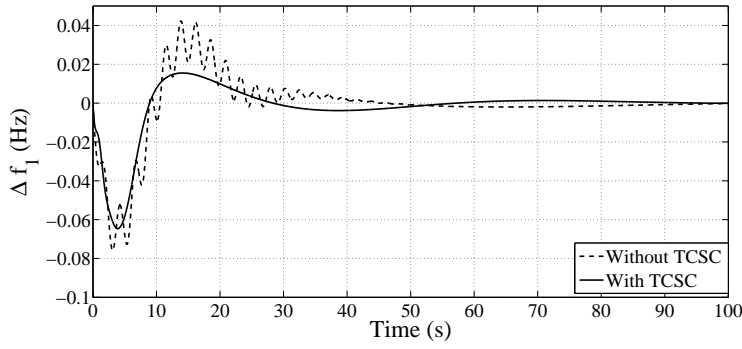


Fig. 2.10: Variation of the performance index with integral gain value for the hydro area (K_{I2}) with disturbance in the hydro area

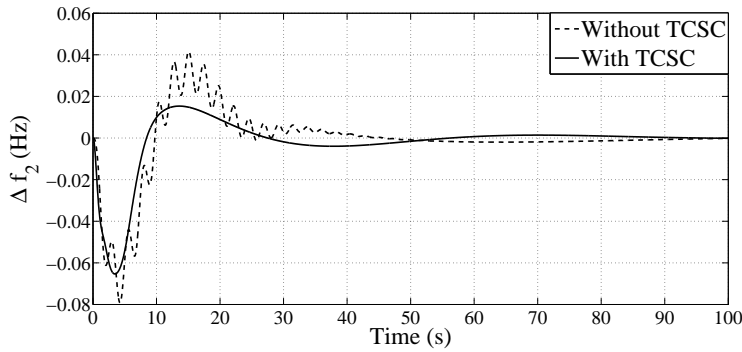
Fig. 2.10 shows the plot of the performance index against the integral gain setting (K_{I2}) of the hydro area in the presence and absence of TCSC for 1% step load disturbance in hydro area and keeping the thermal area uncontrolled. The optimal gain values of K_{I2} obtained for with and without TCSC are 0.2925 and 0.0743, respectively. Similar plots are also obtained for the thermal area by keeping the hydro area uncontrolled and with a step load of 0.01 pu in the thermal area. All the optimum values of Area-1 and Area-2 with and without TCSC are tabulated as in Table 2.2.

2.3.2.3 Results and Discussion

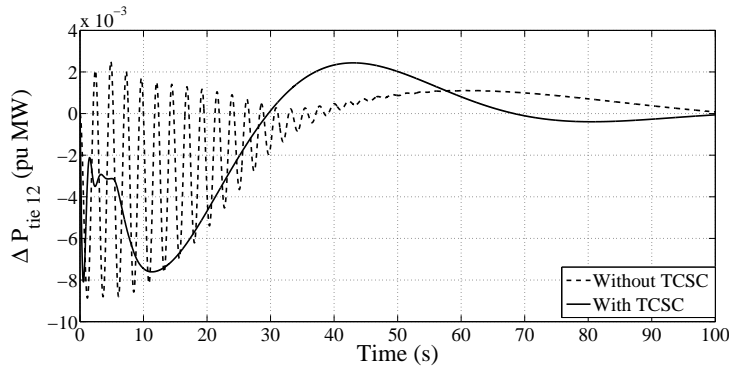
MATLAB simulation studies are performed to investigate the performance of the AGC system under consideration without and with TCSC in series with the tie-line. A step load perturbation of 1% nominal load is considered in either of the areas.



(a) Deviation in frequency of Area-1



(b) Deviation in frequency of Area-2

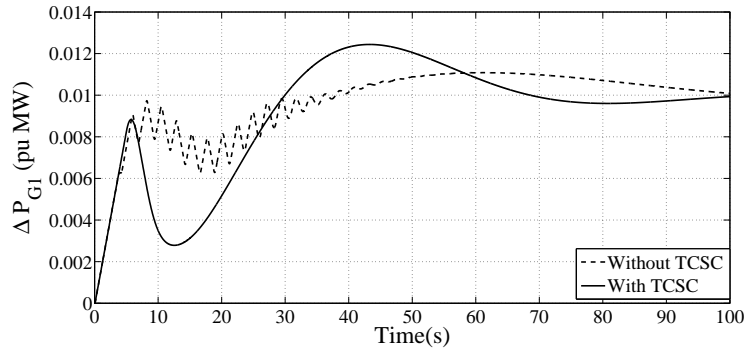


(c) Deviation in tie-line power flow

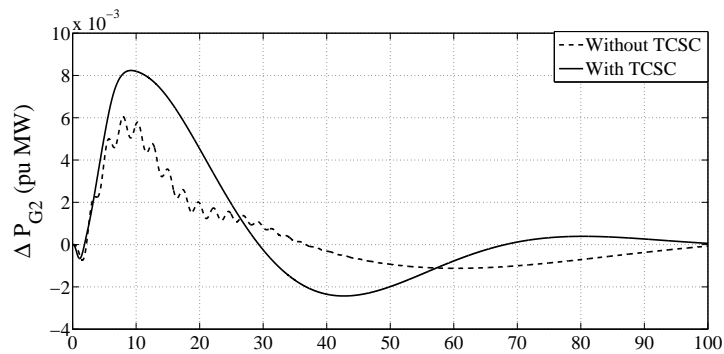
Fig. 2.11: Variations in area frequencies (Δf_1 and Δf_2) and tie-line power (ΔP_{tie12}) when load change in Area-1

With and without TCSC for a step load disturbance of 0.01 pu in the thermal area keeping the hydro area uncontrolled, Fig. 2.11 shows the dynamic responses for frequency deviations (Δf_1 and Δf_2) and tie-line power (ΔP_{tie12}) perturbations. It can be seen that, with TCSC, the deviations in area frequencies have been damped out to a great extent.

Further, the responses settle down at about 60 s, much faster than that without TCSC. Also, with TCSC, the dynamic response of ΔP_{tie12} , has improved remarkably in terms of oscillations and settling time.



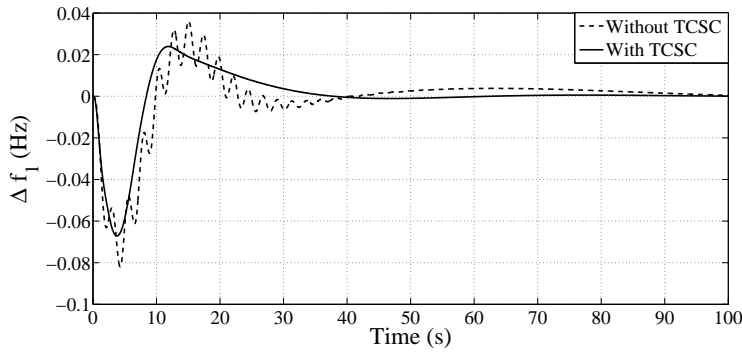
(a) Deviation in power output of thermal plant in Area-1



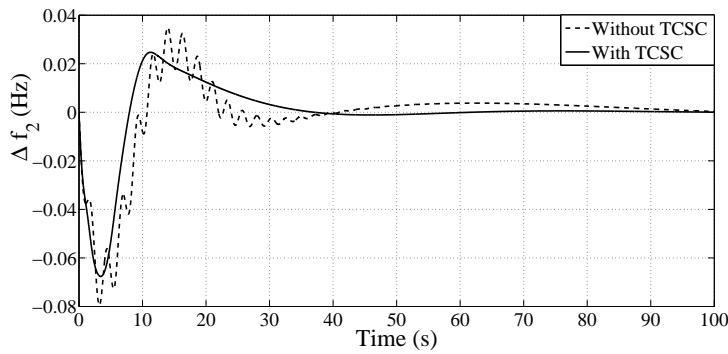
(b) Deviation in power output of hydro plant in Area-1

Fig. 2.12: Variations in power output of thermal (ΔP_{G1}) and hydro (ΔP_{G2}) units when load change in Area-1

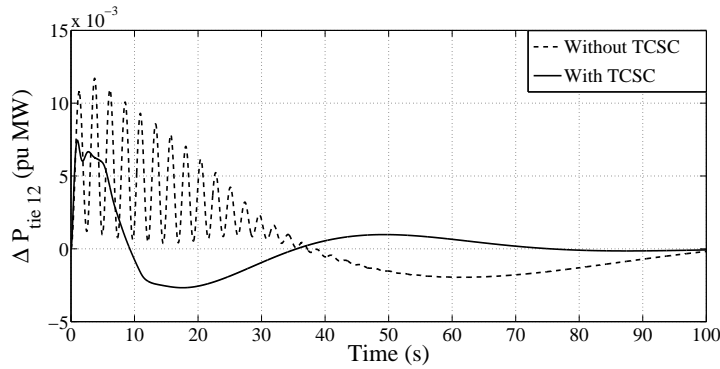
When subjected to a step load perturbation of 0.01 pu in the thermal area, the generation responses are presented in Fig. 2.12. Since the step load disturbance has occurred in the thermal area, the thermal unit should adjust its output as quickly as possible so that the local load perturbation in its area can be taken up as per its obligation which is reflected in Fig. 2.12.



(a) Deviation in frequency of Area-1



(b) Deviation in frequency of Area-2

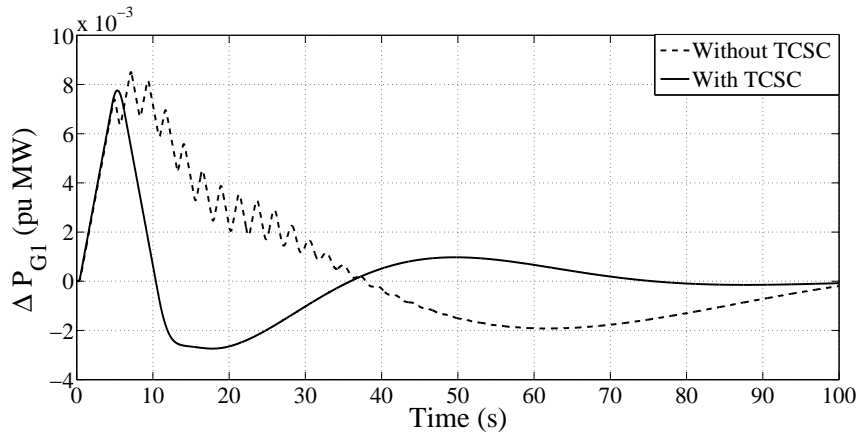


(c) Deviation in tie-line power flow

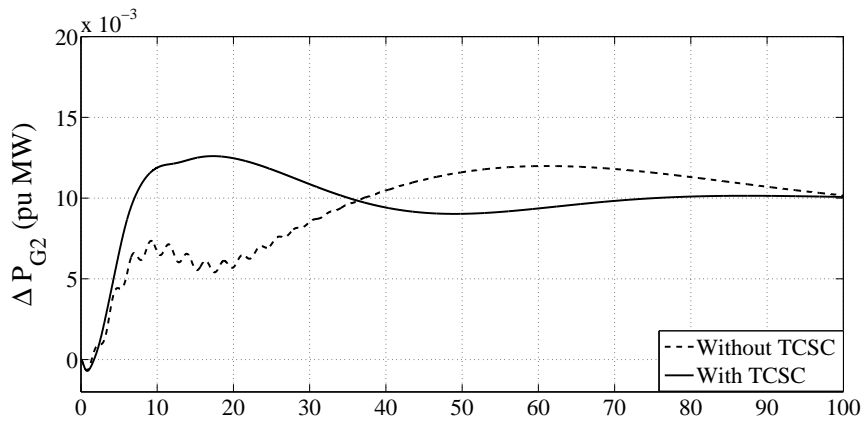
Fig. 2.13: Variations in area frequencies (Δf_1 and Δf_2) and tie-line power (ΔP_{tie12}) when load change in Area-2

The hydro area need not contribute to the local load fluctuation in the thermal area as per the approved practices of interconnected power system operations and hence should settle down to zero steady state value as early as possible which is also evident from Fig. 2.12. It may be noted that, the water hammer effect causes the initial negative deflec-

tion of the transient response of the hydro unit output.



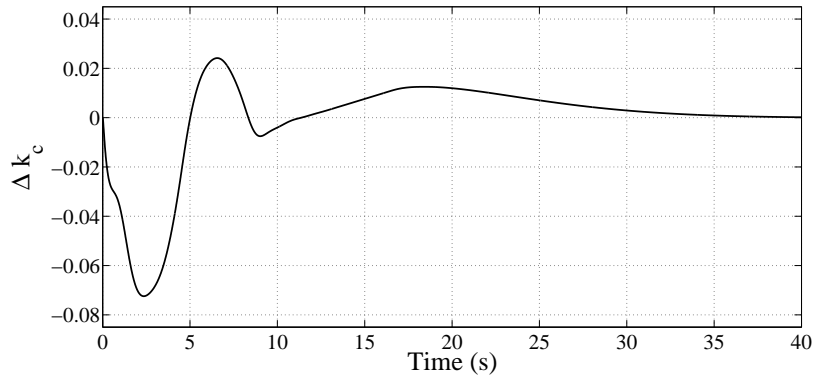
(a) Deviation in power output of thermal plant in Area-1



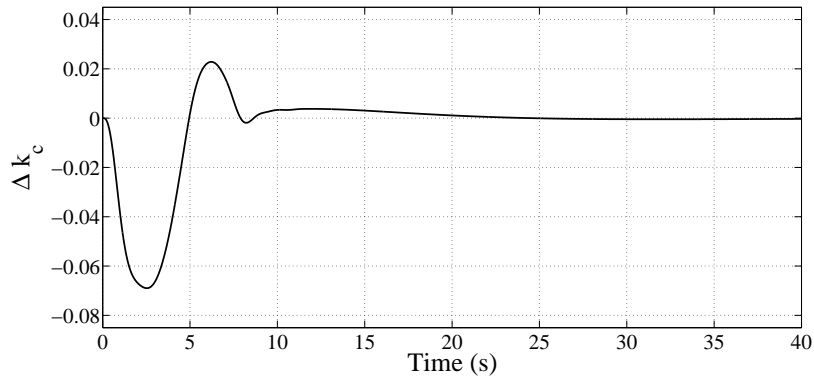
(b) Deviation in power output of hydro plant in Area-1

Fig. 2.14: Variations in power output of thermal (ΔP_{G1}) and hydro (ΔP_{G2}) units when load change in Area-2

With step load disturbance of 1% in hydro area, the variations in area frequencies and tie power deviations are depicted in Fig. 2.13. Similar findings as in the case of Fig. 2.11 can be observed in Fig. 2.13 too. The generation responses for the thermal and hydro units with 1% step load disturbance in the hydro area have been plotted in Fig. 2.14.



(a) Δk_c when loading in Area-1



(b) Δk_c when loading in Area-2

Fig. 2.15: Variation in the incremental change of the percentage compensation (Δk_c) of TCSC with 0.01 pu step load disturbance in Area-1 and Area-2 respectively

Fig. 2.15 shows the variation of the incremental change in TCSC percentage compensation (Δk_c). With Δf_1 feedback, the maximum negative variation is -0.126 approximately and on the positive side the maximum variation in percentage compensation is 0.042 approximately.

The TCSC computes its percentage compensation from the frequency deviation of Area-1 and it becomes zero as the area frequency oscillations die out as can be seen from Fig. 2.15.

Hence, it can be concluded that the oscillations in frequencies and tie-line power deviations due to load perturbation can be damped out by controlling the percentage compensation of TCSC which in turn controls the tie-line power flow of interconnected power system.

2.3.2.4 Sensitivity Analysis

Table 2.3

Optimum values of of integral gain settings under parameter variation for 1% step load perturbation in either of the areas

Parameter	% Change	With TCSC		Without TCSC	
		K_{11}	K_{12}	K_{11}	K_{12}
Nominal loading	0	0.059	0.2925	0.1124	0.0624
T_G	+10	0.058	0.291	0.11	0.072
	-10	0.059	0.294	0.115	0.077
T_{RH}	+10	0.058	0.286	0.114	0.079
	-10	0.059	0.299	0.108	0.069
K_r	+10	0.064	0.303	0.135	0.076
	-10	0.054	0.279	0.086	0.076
T_W	+10	0.057	0.269	0.106	0.067
	-10	0.054	0.3085	0.119	0.084

The motivation of doing a sensitivity analysis is to deal with the small parametric uncertainties and to check the robustness of the designed controller for large parametric uncertainties so that stability of the overall system and good performance can both be achieved for all admissible uncertainties.

A sensitivity analysis has been carried out to study the system robustness to changes in system parameters in the range of $\pm 10\%$. Table 2.3 shows that controller values more

or less remains the same and do not change appreciably with the variations in the system parameters.

2.4 Summary

In this chapter, a maiden attempt to study the effect of a Thyristor Controlled Series Compensator (TCSC) on frequency regulation of interconnected power system has been analysed on a two area Thermal-Thermal power system and Hydro-Thermal power system with considering appropriate Generation Rate Constraints and Dead band non linearity. A linear incremental mathematical model for a TCSC has also been used which is suitable for AGC applications. When TCSC connected in series with tie-line near to a control area, computes its percentage compensation from frequency deviation of that particular control area which in turn damps out the low frequency oscillations. In this work, we have done the analysis with TCSC placed near to Area-1. The deviation in frequency of Area-1 (Δf_1) is given as the error signal to the model. Since TCSC is placed near to Area-1 and Δf_1 as the control signal the effect of TCSC on frequency regulation is more with load perturbation in Area-1. The optimal integral gain settings of the control areas are obtained using ISE technique by minimizing a quadratic performance index. Simulation studies reveal that a Thyristor Controlled Series Compensator can effectively suppress the low frequency oscillations in area frequencies and tie-line power following a sudden load perturbation in either of the areas. It may therefore be concluded that a TCSC may be utilised for controlling the inter-area tie-line power flow which also stabilises the oscillations in area frequencies.

In comparison with existing schemes proposed by various literature, the proposed method in this chapter has given an insight into the advantage of existing TCSC in the system, which can enhance the frequency regulation performance through damping out the low frequency oscillations in the system. We have explored the add-on advantage on existing TCSC rather not to implement any special schemes to improve the performance of AGC.

Chapter 3

Load Following in a Deregulated Power System with Thyristor Controlled Series Compensator

3.1 Introduction

Conventionally, the electricity supply industry has been a natural monopoly, wherein electricity was considered as merely an energy supply sector. In this monopolistic market, the same agency is responsible for power generation, transmission, distribution and control. For a few decades, electric power industry has undergone rapid changes from the conventional, monopolistic Vertically Integrated Utility (VIU) configuration to Horizontally Integrated Utility configuration with distinct entities namely GENCOs, TRANSCOs and DISCOs [32, 101–104]. This has introduced an open power market and competition among different market players where customers/DISCOs can buy power from different suppliers/GENCOs at competitive prices. Since power generation, transmission, distribution, and control tasks are segregated, they have to be separately paid for, by the transacting parties [102]. In the new competitive electricity market, maintaining the physical flow of electricity, satisfying consumer's demand at proper voltage and frequency level, maintaining security, economy and reliability of the system, ensuring proper protection, control and all measures for the proper functioning of the system are treated as separate ancillary services [104].

Load following is one among such ancillary services. In a power system, changes in power supply or demand affect the operating conditions. Hence, a power system must be kept tightly controlled in two ways. First, power coming into the system must be exactly balanced against power flowing out, at every moment. Second, the system frequency must be held constant as far as possible [103]. It too, can wander as power flow changes, and as a result, the system can become unstable. Instant adjustment of the generation to track the fluctuations between the power supply and demand so that the system is in perfect

balance is called speed regulation or load following.

In the mean time, several studies have investigated the potential of using Flexible AC Transmission Systems (FACTS) devices for better power system control since it provides more flexibility. Not only the power transfer capability of transmission lines can be increased [86–92, 105], but also, the dynamic stability can be enhanced using TCSC [93]. In this chapter our aim is to

1. Study the effect of TCSC in load following in competitive power market.
2. Optimize the integral gain settings of control areas using Genetic Algorithm and
3. Compare the effect on AGC in deregulated environment of following cases without and with TCSC
 - (a) Thermal - Thermal System
 - (b) Hydro - Thermal System

3.2 Deregulated Environment

In a restructured power market, there are distinct and separate entities namely GENCOs, TRANSCOs and DISCOs exclusively for generation, transmission and distribution of electric power. In such a scenario, any DISCO can have individual and independent power contracts with any GENCO either in the same area (Unilateral Contract) or in other areas (Bilateral Contract) but under the supervision of Independent System Operator (ISO) [32]. Since the DISCOs are free to choose any GENCOs for power contract based on prices, various combinations of GENCO-DISCO contracts are possible in practice which can be visualized through DISCO Participation Matrix (DPM). Number of rows of the DPM is equal to number of GENCOs, whereas number of DISCOs determine the number of columns of DPM. Each entry in this matrix called contract participation factor (cpf), corresponds to the fraction of the total load contracted by a DISCO (column) towards a GENCO (row). Thus the i_j^{th} entry of the DPM corresponds to the fraction of the total power contracted by $DISCO_j$ from $GENCO_i$. Thus for a two area system with two GENCOs ($GENCO_1, GENCO_2$) and two DISCOs ($DISCO_1, DISCO_2$) in Area-1

and two GENCOs($GENCO_3, GENCO_4$) and two DISCOs ($DISCO_3, DISCO_4$) in Area-2, DPM is given by

$$DPM = \begin{bmatrix} cpf_{11} & cpf_{12} & cpf_{13} & cpf_{14} \\ cpf_{21} & cpf_{22} & cpf_{23} & cpf_{24} \\ cpf_{31} & cpf_{32} & cpf_{33} & cpf_{34} \\ cpf_{41} & cpf_{42} & cpf_{43} & cpf_{44} \end{bmatrix} \quad (3.1)$$

The sum of all the entries in a column of this matrix is unity. i.e.,

$$\sum_{i=1}^{NGENCO} cpf_{ij} = 1; \text{ for } j = 1, 2, \dots, NDISCO, \quad (3.2)$$

where NGENCO is the total number of GENCOs and NDISCO is the total number of DISCOs. The expression for contracted power of i^{th} GENCO with DISCOs is given as

$$\Delta P_{gci} = \sum_{j=1}^{NDISCO} cpf_{ij} \Delta P_{Lj}; \text{ for } i = 1, 2, \dots, NGENCO, \quad (3.3)$$

where ΔP_{gci} is the contracted power of i^{th} GENCO and ΔP_{Lj} is the total load demand of j^{th} DISCO. The scheduled steady state power flow on the tie-line is given as:

$\Delta P_{tie12scheduled} = (\text{Demand of DISCOs in Area-2 from GENCOs in Area-1}) - (\text{Demand of DISCOs in Area-1 from GENCOs in Area-2})$

The scheduled steady state power flow through the tie-line is given as:

$$\Delta P_{tie12scheduled} = \sum_{i=1}^2 \sum_{j=3}^4 cpf_{ij} \Delta P_{Lj} - \sum_{i=3}^4 \sum_{j=1}^2 cpf_{ij} \Delta P_{Lj} \quad (3.4)$$

$$= (cpf_{13} \Delta P_{L3} + cpf_{14} \Delta P_{L4} + cpf_{23} \Delta P_{L3} + cpf_{24} \Delta P_{L4}) \quad (3.5)$$

$$- (cpf_{31} \Delta P_{L1} + cpf_{32} \Delta P_{L2} + cpf_{41} \Delta P_{L1} + cpf_{42} \Delta P_{L2})$$

The tie-line power error is defined as:

$$\Delta P_{tie12,error} = \Delta P_{tie12,actual} - \Delta P_{tie12,scheduled} \quad (3.6)$$

At steady state, the tie-line power error, $\Delta P_{tie12,error}$, vanishes as the actual tie-line power flow reaches the scheduled power flow. This error signal is used to generate the respective Area Control Error (ACE) signal as similar to that of traditional scenario. i.e.,

$$ACE_1 = B_1 \Delta f_1 + \Delta P_{tie12,error} \quad (3.7)$$

$$ACE_2 = B_2 \Delta f_2 + a_{12} \Delta P_{tie12,error}, \quad (3.8)$$

where $a_{12} = -\frac{P_{r1}}{P_{r2}}$ with P_{r1} and P_{r2} being the rated area capacities of Area-1 and Area-2 respectively.

In a deregulated power system, DPM varies with a fixed time interval, which may be decided by system operator. Normally, time interval is fixed for 15-minutes. However, frequency regulation studies (AGC) operates typically for a few seconds to minutes. Hence, the analysis can be done with a constant DPM. Thus, a constant DPM is considered for our analysis.

3.3 TCSC in Deregulated Power System

Fig. 3.1 shows the schematic diagram of a two area interconnected power system with TCSC connected in series with the tie-line under deregulated environment. For analysis, it is assumed that TCSC is connected near to the Area-1. The TCSC model developed in Chapter-2 is used for the analysis. The deviation in the tie-line power flow in deregulated

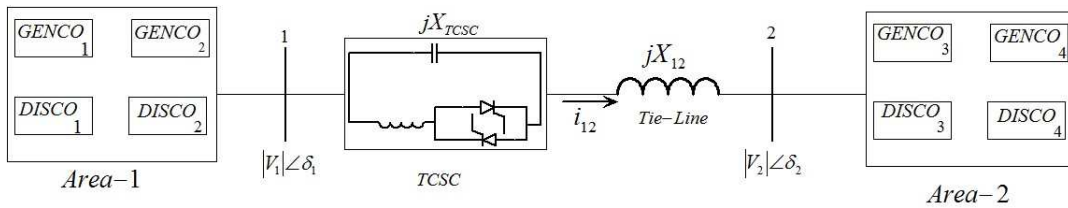


Fig. 3.1: Schematic diagram of the interconnected power system with TCSC in series with tie-line near to Area-1 in deregulated scenario

power system after the perturbation becomes,

$$\Delta P_{tie12} = \frac{2\pi T_{12}^0}{s(1 - k_c^0)} \left[\Delta f_1(s) - \Delta f_2(s) \right] + \left[\frac{J_{12}^0}{(1 - k_c^0)^2} \right] \frac{K_{TCSC}}{1 + sT_{TCSC}} \Delta f_1(s) \quad (3.9)$$

3.4 Case Studies

The effect of TCSC on load following of a deregulated power system is studied for the following scenarios.

■ Case 1 - Thermal-Thermal System

■ Case 2 - Hydro-Thermal system

3.4.1 Case-1: Thermal-Thermal System

Space Model of the Two-area Deregulated System with TCSC

The block schematic shown in Fig. 3.2 represents the detailed block diagram model of a two area multi-unit thermal system in deregulated environment. The AGC in a deregulated power market should be designed to accommodate all possible transactions, such as unilateral based transactions, bilateral transactions, and a combination of these two transactions. The system on which investigations have been carried out comprises a two area interconnected thermal system as shown in Fig. 3.2. Area-1 consists of two GENCOs ($GENCO_1$ and $GENCO_2$) of reheat thermal power generation units and Area-2 comprises two GENCOs ($GENCO_3$ and $GENCO_4$) of non reheat thermal units. K_{I1} and K_{I2} are the integral gain settings in Area-1 and Area-2 respectively. The state space model of the two area system is characterized by the state space form as

$$\dot{X} = AX + BU + \Gamma p, \quad (3.10)$$

where X, U and p are the state, control and load disturbance input vectors respectively whereas A, B and Γ are the respective matrices of appropriate dimensions. The vectors

X, U and p are given by

$$X = \begin{bmatrix} \Delta f_1 \\ \Delta P_{G1} \\ \Delta P_{G2} \\ \Delta P_{R1} \\ \Delta P_{R2} \\ \Delta P_{T1} \\ \Delta P_{T2} \\ \Delta f_2 \\ \Delta P_{G3} \\ \Delta P_{G4} \\ \Delta P_{T3} \\ \Delta P_{T4} \\ \Delta P'_{tie} \\ \Delta k_c \end{bmatrix}, \quad U = \begin{bmatrix} u_1 \\ u_2 \end{bmatrix}, \quad p = \begin{bmatrix} \Delta P_{D1} \\ \Delta P_{D2} \end{bmatrix}$$

Total load demand of i^{th} Area, $\Delta P_{Di} = \sum_{i=1}^N \Delta P_{Li} +$ Uncontracted load demands of DISCOs in i^{th} area, where ΔP_{Li} denotes the contract demand i^{th} DISCO, N is the number of DISCOs in i^{th} area. The states are chosen as deviations in frequencies ($\Delta f_1, \Delta f_2$) in Area-1 and Area-2 respectively, the deviations in the power outputs of DISCOs in Area-1 ($\Delta P_{G1}, \Delta P_{G2}$) and ($\Delta P_{G3}, \Delta P_{G4}$) in Area-2, the deviations in reheat outputs in Area-1 ($\Delta P_{R1}, \Delta P_{R2}$), the deviations in turbine outputs in Area-1 ($\Delta P_{T1}, \Delta P_{T2}$) and ($\Delta P_{T3}, \Delta P_{T4}$) in Area-2 and the deviations in tie-line power flow (ΔP_{tie12}) and are also shown in Fig. 3.2.

3.4.1.1 Objective function formulation for AGC

In conventional controller tuning scheme, a quadratic performance index is formulated using the error terms in area frequencies and tie-line power and is minimized, for 1% step load disturbance in either of the areas to obtain the optimal values of K_{I1} and K_{I2} . The controller settings of either thermal or hydro areas are optimized by considering the

other area as uncontrolled. This assumption is not valid in the cases of bilateral contract and contract violation. As the load demand is met from the inter area power contract, the conventional controller tune technique where other area is kept as uncontrolled can not be employed for tuning the gain settings of the control areas. Hence, nature inspired algorithm will be a suitable option for finding the optimal gain values in a deregulated power system.

The ultimate objective of AGC is to maintain area frequencies and inter-area tie-line power flow within their respective scheduled values following a sudden load perturbation at the earliest. To do so, the integral gains of the control areas (K_{I1}, K_{I2}) are tuned optimally to obtain the area frequencies and power exchange with minimum overshoot and lower settling time. A quadratic performance index defined by,

$$J = \int_0^t (\Delta f_1^2 + \Delta f_2^2 + \Delta P_{tie12error}^2) dt \quad (3.11)$$

is minimized for 10% load demand on each DISCO to obtain the optimum values of K_{I1} and K_{I2} using Genetic Algorithm.

3.4.1.2 Genetic Algorithm

Genetic Algorithm (GA) is a directed random search technique that uses *the survival of the fittest* concept in search of better solutions. Normally the parameters to be optimized are represented as individual strings in a GA population which are reproduced as in nature [106]. To start the optimization, GA uses randomly produced initial population and then, each individual string in the population is evaluated by their fitness, normally represented by the value of objective function. Individuals with higher fitness values are selected and are then modified through selection, crossover and mutation to obtain the next generation of individuals strings. The new generation on average, will be *better* than the current population [107]. In this way, the above process is repeated to create the subsequent new generations until some termination condition is reached.

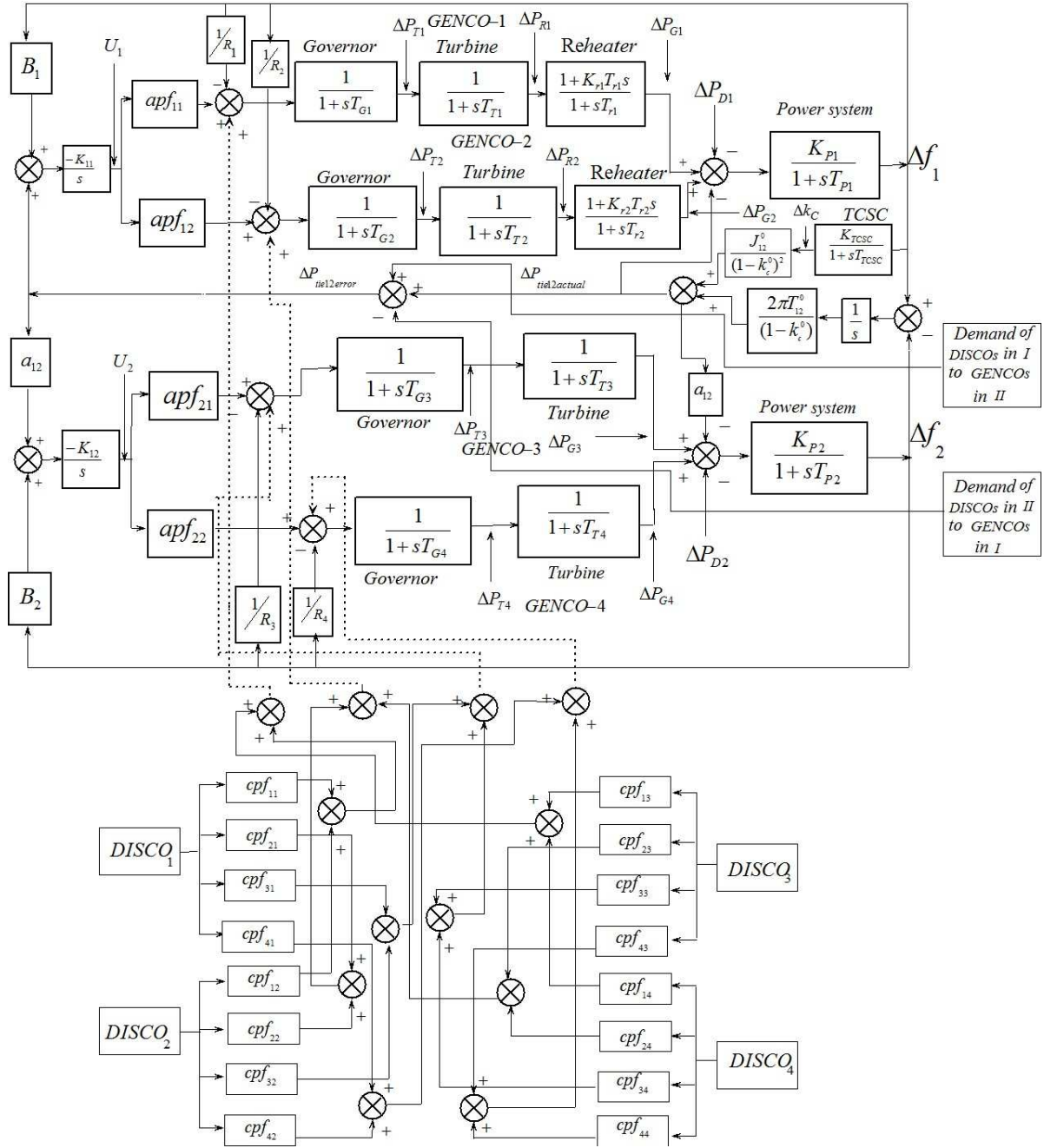


Fig. 3.2: Linearized model of an interconnected thermal-thermal system under deregulation

In this work, GA is used to tune the integral gain settings (K_{I1} , K_{I2}) of Area-1 and Area-2 respectively with and without TCSC. An initial generation of 100 individual strings representing K_{I1} and K_{I2} is chosen randomly. The performance index (J) given by Eqn. 3.11 is evaluated for each individual string in the population and individuals strings with higher fitness values are selected for cross over and mutation to obtain

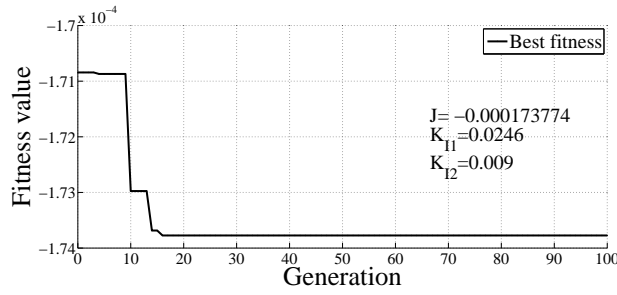
the next generation. The GA parameters used are given in Table 3.1. The algorithm is repeated for 100 number of generations and computation is terminated until for a particular generation, average fitness is within 1% of best fitness value in the generations. This indicates convergence in the population. The gain settings based on the best fittest value from the current generation is chosen as optimal gain settings.

Table 3.1
GA parameters

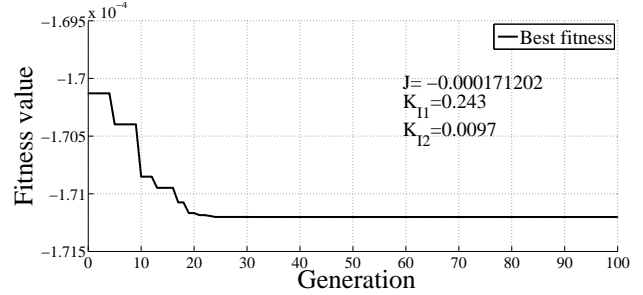
Population Size	100
Cross Over	0.8
Elite Count	2
Mutation	0.2
No. of Generations	100
Initial penalty	10
Penalty factor	100

Table 3.2
Optimized Gain Settings of Control Areas

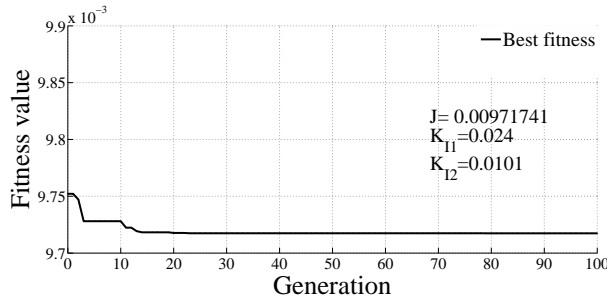
	Unilateral Contract		Bilateral Contract		Contract Violation	
	K_{I1}	K_{I2}	K_{I1}	K_{I2}	K_{I1}	K_{I2}
Without TCSC	0.0246	0.0090	0.0240	0.0101	0.0710	0.0220
With TCSC	0.2430	0.0097	0.0248	0.0100	0.0712	0.0222



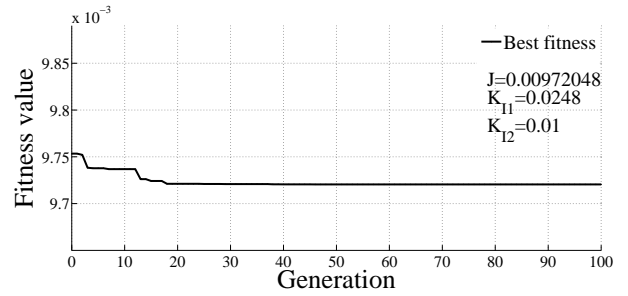
(a) Case-1: Unilateral contract without TCSC



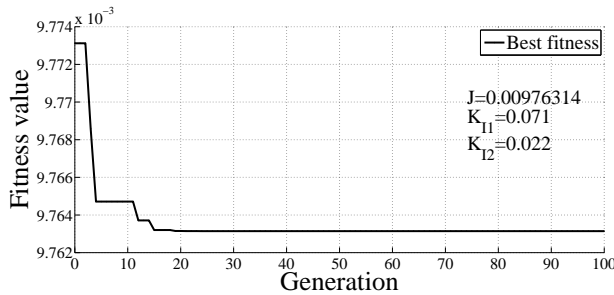
(b) Case-1: Unilateral contract with TCSC



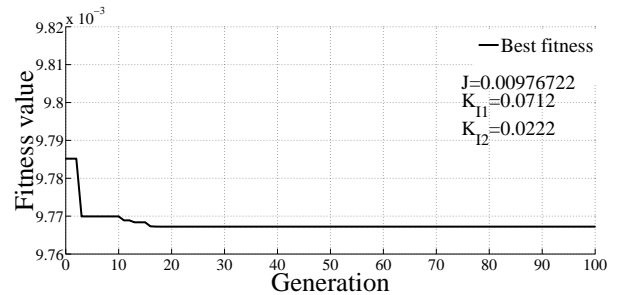
(c) Case-2: Bilateral contract without TCSC



(d) Case-2: Bilateral contract with TCSC



(e) Case-3: Contract violation without TCSC



(f) Case-3: Contract Violation With TCSC

Fig. 3.3: Generation vs fitness values obtained from GA optimization

The optimized gain settings for (1) Unilateral Contract (2) Bilateral Contract and (3) Contract violation for Areas 1 and 2 are given in Table 3.2. Presented in Fig. 3.3 are plots showing the generation versus fitness function for different cases.

From Table 3.2, it is clear that with TCSC for unilateral contract case, there is considerable change in the controller parameter whereas in other two cases the change were feeble. In bilateral and contract violation cases load change occurred in both areas, which

has more influence on controller parameter rather than the inclusion TCSC. However, in unilateral contract case load change occurred in Area-1 only.

3.4.1.3 Simulation Results and Discussion

Time domain simulations using MATLAB have been carried out for the AGC system with 10% load demand on each DISCO, ie $\Delta P_{L1} = \Delta P_{L2} = \Delta P_{L3} = \Delta P_{L4} = 0.1$ pu. TCSC is placed near Area-1 considering 50% compensation. Fourth-order Runge-Kutta method with an integration step size of 0.01 s is adopted for simulations. Studies are carried out on AGC in deregulated environment, for three different possibilities as given below

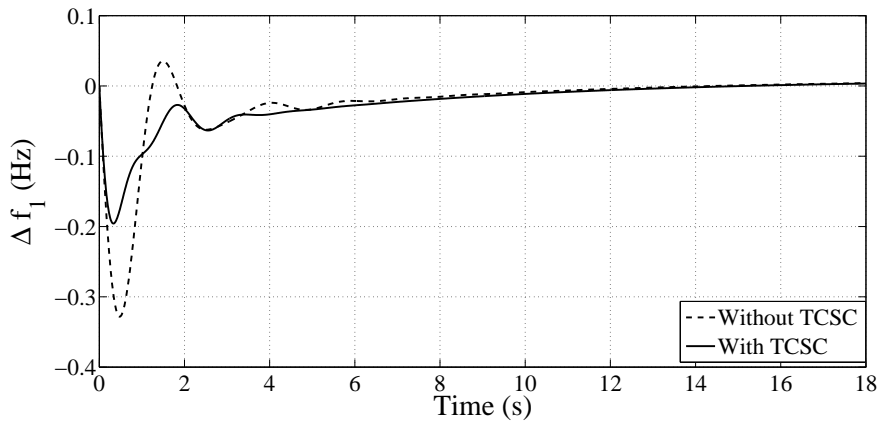
- Case 1: Unilateral contract
- Case 2: Bilateral contract
- Case 3: With contract violation

Case 1-Unilateral Contract/ Poolco based transaction

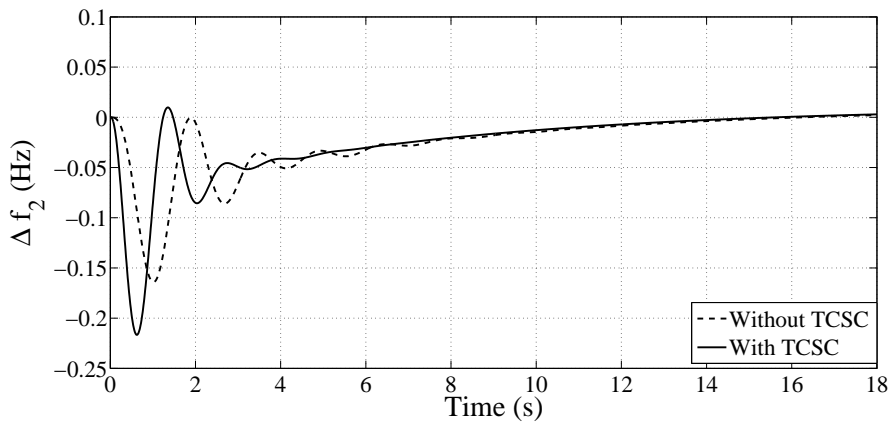
In unilateral contract, DISCOs in an area can have power contract with GENCOs in the same area only. Assume that each DISCO has a total load demand of 0.1 pu MW. Let $DISCO_1$ & $DISCO_2$ in Area-1 have power contract with $GENCO_1$ and $GENCO_2$ in Area-1 as per the following DPM,

$$DPM = \begin{bmatrix} 0.6 & 0.7 & 0 & 0 \\ 0.4 & 0.3 & 0 & 0 \\ 0 & 0 & 0 & 0 \\ 0 & 0 & 0 & 0 \end{bmatrix} \quad (3.12)$$

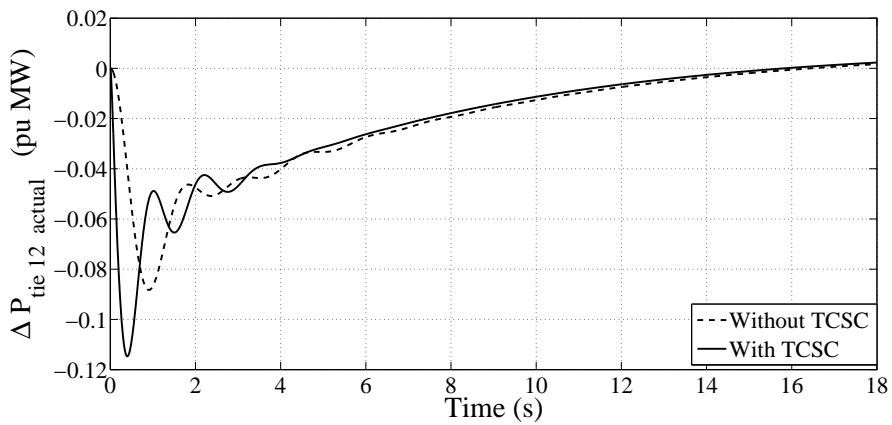
The dynamic responses with and without TCSC are plotted in Fig. 3.4. It can be observed that, with TCSC, the transient response has been improved in terms of ripples as well as settling time. In unilateral contract, GENCOs in Area-1 are having power contracts with DISCOs in Area-1 only. Hence as per the DPM given by Eqn. 3.12, $\Delta P_{tie12 \text{ scheduled}}$ given in Eqn. 3.5 becomes zero and is depicted in Fig. 3.4(c).



(a) Deviation in frequency of Area-1



(b) Deviation in frequency of Area-2



(c) Deviation in tie-line power flow

Fig. 3.4: Unilateral contract: Variations in area frequencies (Δf_1 and Δf_2) and tie-line power (ΔP_{tie12})

It may be noted that as per Eqn. 3.12, at steady state,

$$\begin{aligned}
 \text{Power output of GENCO-1 } (\Delta P_{G1}) &= (cpf_{11} \times \Delta P_{L1}) + (cpf_{12} \times \Delta P_{L2}) + \\
 &\quad (cpf_{13} \times \Delta P_{L3}) + (cpf_{14} \times \Delta P_{L4}) \\
 &= (0.6 \times 0.1) + (0.7 \times 0.1) + \\
 &\quad (0 \times 0.1) + (0 \times 0.1) \\
 &= 0.13 \text{ pu MW}
 \end{aligned}$$

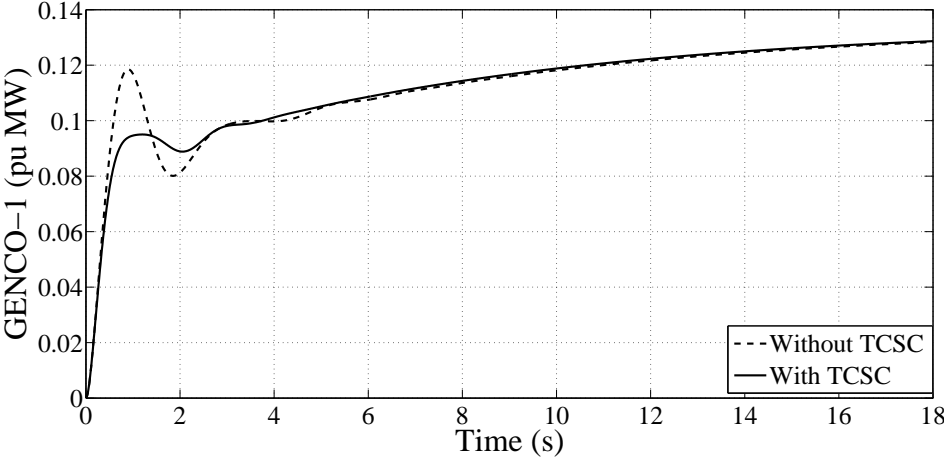
$$\begin{aligned}
 \text{Power output of GENCO-2 } (\Delta P_{G2}) &= (cpf_{21} \times \Delta P_{L1}) + (cpf_{22} \times \Delta P_{L2}) + \\
 &\quad (cpf_{23} \times \Delta P_{L3}) + (cpf_{24} \times \Delta P_{L4}) \\
 &= (0.4 \times 0.1) + (0.3 \times 0.1) + \\
 &\quad (0 \times 0.1) + (0 \times 0.1) \\
 &= 0.07 \text{ pu MW}
 \end{aligned}$$

$$\begin{aligned}
 \text{Power output of GENCO-3 } (\Delta P_{G3}) &= (cpf_{31} \times \Delta P_{L1}) + (cpf_{32} \times \Delta P_{L2}) + \\
 &\quad (cpf_{33} \times \Delta P_{L3}) + (cpf_{34} \times \Delta P_{L4}) \\
 &= (0 \times 0.1) + (0 \times 0.1) + \\
 &\quad (0 \times 0.1) + (0 \times 0.1) \\
 &= 0 \text{ pu MW}
 \end{aligned}$$

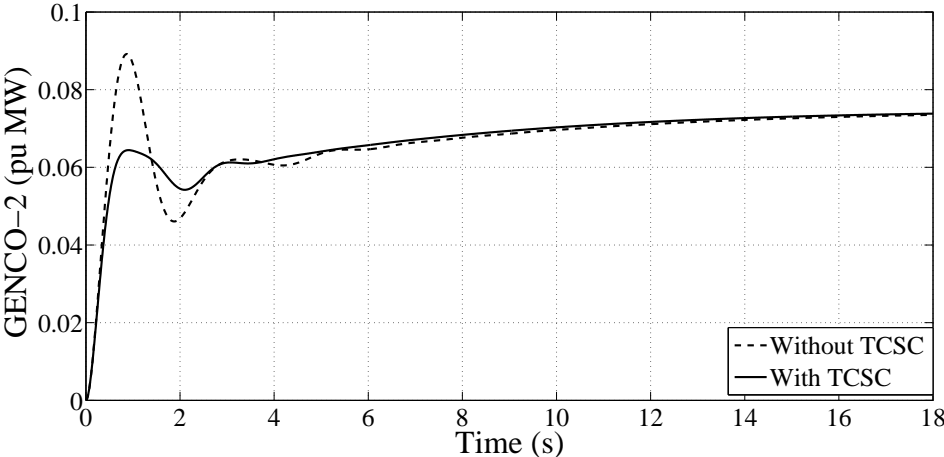
$$\begin{aligned}
 \text{Power output of GENCO-4 } (\Delta P_{G4}) &= (cpf_{41} \times \Delta P_{L1}) + (cpf_{42} \times \Delta P_{L2}) + \\
 &\quad (cpf_{43} \times \Delta P_{L3}) + (cpf_{44} \times \Delta P_{L4}) \\
 &= 0 \text{ pu MW}
 \end{aligned}$$

In Poolco based power exchange, there is only single buyer for all energy generated by the GENCOs. Poolco provides all ancillary services and the auctions are single sided

auctions. This kind of operation is similar to unilateral contract, which discussed in the thesis.



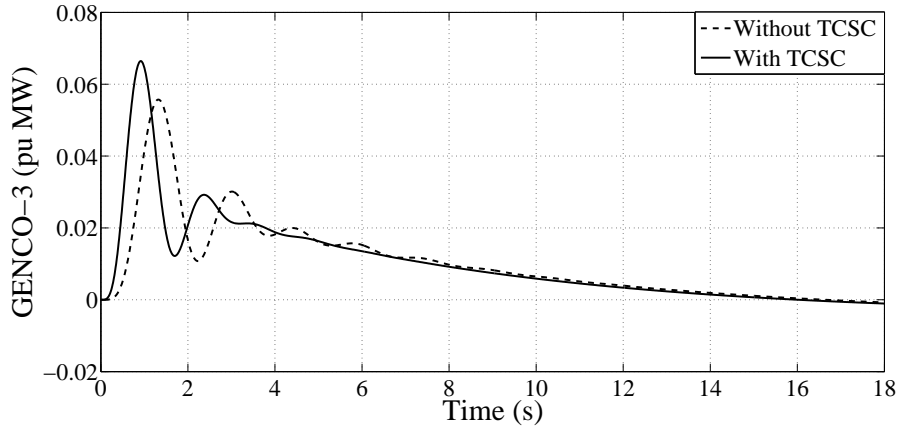
(a) Deviation in power output of GENCO-1



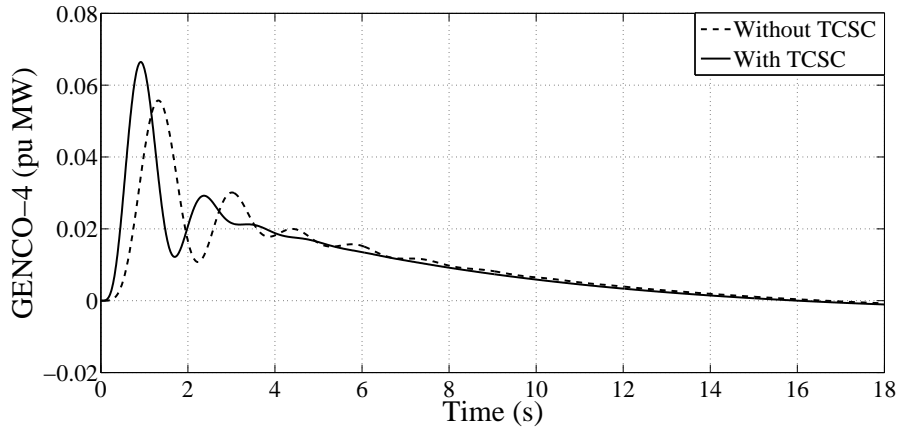
(b) Deviation in power output of GENCO-2

Fig. 3.5: Unilateral contract: Deviation in generation (ΔP_{G1} and ΔP_{G2}) of GENCOs in Area-1

The power outputs of various GENCOs with and without TCSC cases are plotted in Figs. 3.5-3.6 and simulation results matches with calculated values. It can be seen from Figs. 3.5-3.6 that TCSC improves the power outputs in terms of overshoots and the responses are more smooth.



(a) Deviation in power output of GENCO-3



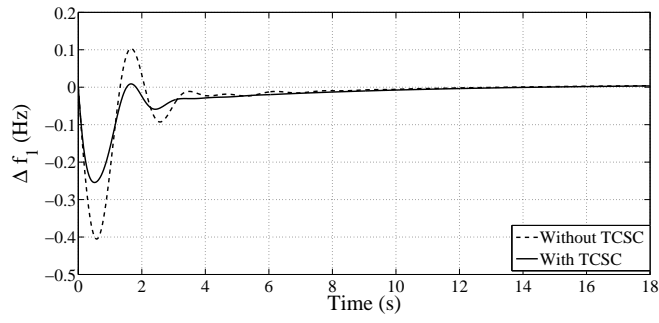
(b) Deviation in power output of GENCO-4

Fig. 3.6: Unilateral contract: Deviation in generation (ΔP_{G3} and ΔP_{G4}) of GENCOs in Area-2

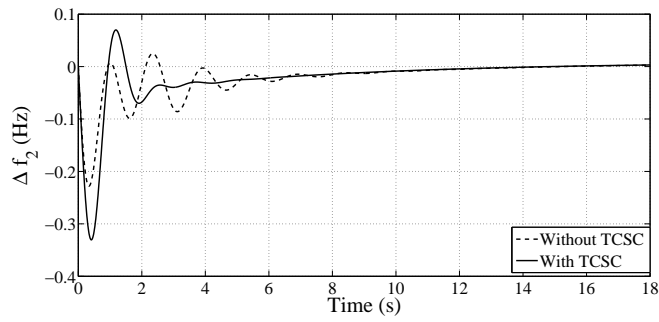
Case 2-Bilateral Transactions

In this scenario, a DISCO in an area has freedom to have power contract with any GENCOs in other control areas. The bilateral contracts between DISCOs and various GENCOs are simulated based on the following DPM, given by

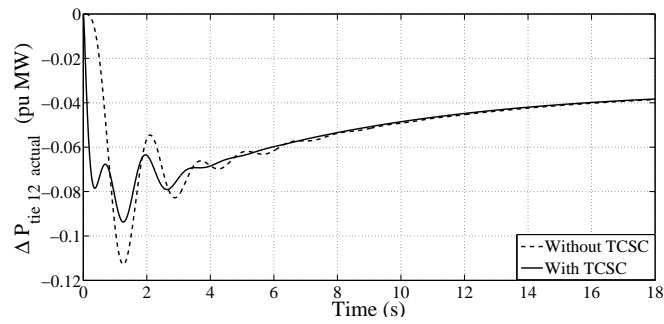
$$DPM = \begin{bmatrix} 0.1 & 0.24 & 0.33 & 0.18 \\ 0.2 & 0.16 & 0.17 & 0.22 \\ 0.27 & 0.4 & 0.5 & 0 \\ 0.43 & 0.2 & 0 & 0.6 \end{bmatrix} \quad (3.13)$$



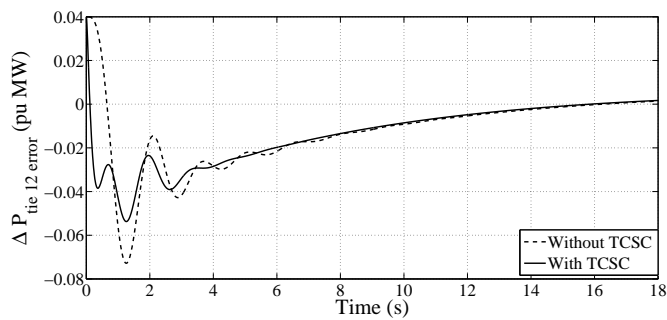
(a) Deviation in frequency of Area-1



(b) Deviation in frequency of Area-2

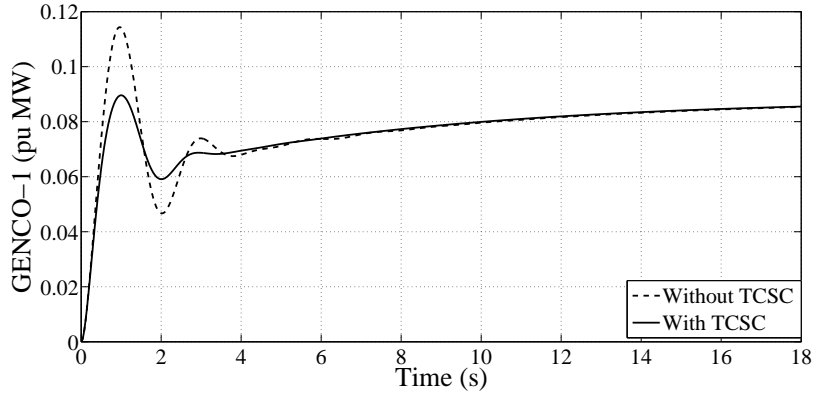


(c) Deviation in tie-line power flow

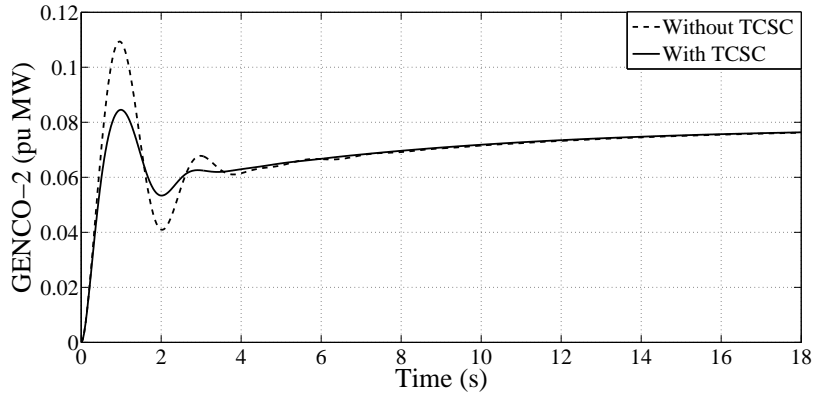


(d) Deviation in tie-line power flow error

Fig. 3.7: Bilateral contract: Variations in area frequencies (Δf_1 and Δf_2) actual tie-line power (ΔP_{tie12}) and tie-line power error ($\Delta P_{tie12error}$)



(a) Deviation in power output of GENCO-1



(b) Deviation in power output of GENCO-2

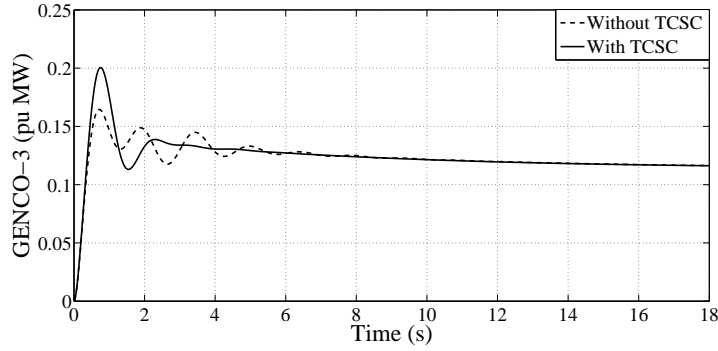
Fig. 3.8: Bilateral contract: Deviation in generation (ΔP_{G1} and ΔP_{G2}) of GENCOs in Area-1

Figs. 3.7-3.9 depict the corresponding simulation results with and without TCSC. It may be noted that with TCSC, the transient oscillations and settling times have been reduced. It is clear from Fig. 3.7(d) that with TCSC, $\Delta P_{tie12error}$ vanishes faster.

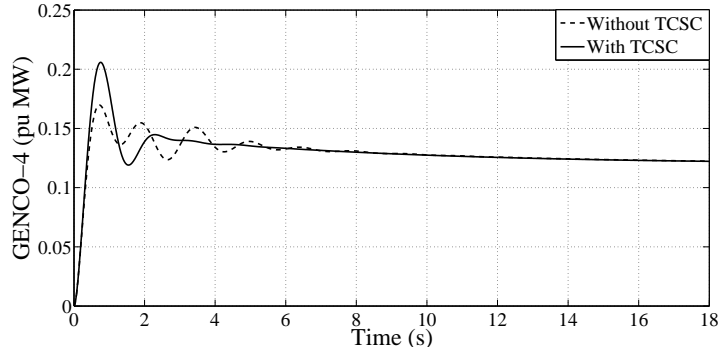
In this case, calculated value of $\Delta P_{tie12scheduled} = -0.04$ pu MW, as given by Eqn. 3.5 matches with simulation result. At steady state,

$$\begin{aligned}
 \text{Power output of GENCO-1 } (\Delta P_{G1}) &= (0.1 \times 0.1) + (0.24 \times 0.1) + \\
 &\quad (0.33 \times 0.1) + (0.18 \times 0.1) \\
 &= 0.085 \text{ pu MW}
 \end{aligned}$$

$$\begin{aligned}
\text{Power output of GENCO-2 } (\Delta P_{G2}) &= (0.2 \times 0.1) + (0.16 \times 0.1) + \\
&\quad (0.17 \times 0.1) + (0.22 \times 0.1) \\
&= 0.075 \text{ pu MW}
\end{aligned}$$



(a) Deviation in power output of GENCO-3



(b) Deviation in power output of GENCO-4

Fig. 3.9: Bilateral contract: Deviation in generation (ΔP_{G3} and ΔP_{G4}) of GENCOs in Area-2

$$\begin{aligned}
\text{Power output of GENCO-3 } (\Delta P_{G3}) &= (0.27 \times 0.1) + (0.4 \times 0.1) + \\
&\quad (0.5 \times 0.1) + (0 \times 0.1) \\
&= 0.117 \text{ pu MW}
\end{aligned}$$

$$\begin{aligned}
\text{Power output of GENCO-4 } (\Delta P_{G4}) &= (0.43 \times 0.1) + (0.2 \times 0.1) + \\
&\quad (0 \times 0.1) + (0.6 \times 0.1) \\
&= 0.123 \text{ pu MW}
\end{aligned}$$

The corresponding plots are presented in Figs. 3.8-3.9. TCSC has improved the transient behaviour of the response.

Case 3-Contract Violation

In this scenario, DISCOs in an area may have an excess uncontracted power demand. As per industrial practice, this uncontracted load must be supplied by the GENCOs in the same area according to their respective ACE participation factor. Consider a case where DISCO-1 demands 0.1 pu MW uncontracted excess power

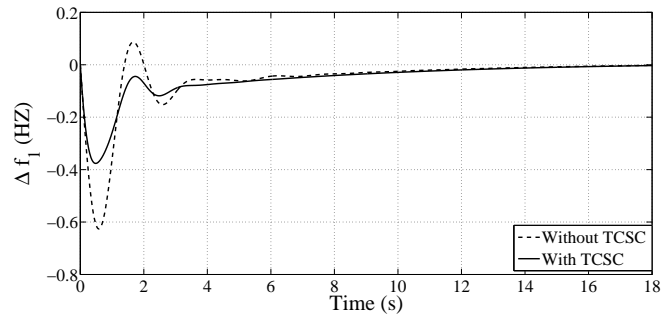
The total load in Area-1 (ΔP_{D1}) = Contracted Load of $DISCO_1$ + Contracted Load of $DISCO_2$ + Uncontracted power = $(0.1+0.1) + 0.1 = 0.3$ pu MW

Similarly for Area-2 (ΔP_{D2}) = Contracted Load of $DISCO_3$ + Contracted Load of $DISCO_4$ = $(0.1+0.1) = 0.2$ pu MW

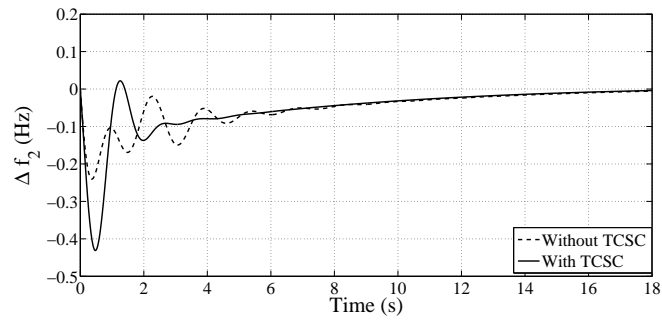
With the DPM given by Eqn. 3.13, at steady state,

$$\begin{aligned}
\text{GENCO-1 generates, } \Delta P_{G1} &= (cpf_{11} \times \Delta P_{L1}) + (cpf_{12} \times \Delta P_{L2}) + \\
&\quad (cpf_{13} \times \Delta P_{L3}) + (cpf_{14} \times \Delta P_{L4}) + \\
&\quad (apf_{11} \times \text{uncontractedpower}) \\
&= (0.1 \times 0.1) + (0.24 \times 0.1) + \\
&\quad (0.33 \times 0.1) + (0.18 \times 0.1) + \\
&\quad (0.5 \times 0.1) \\
&= 0.135 \text{ pu MW.}
\end{aligned}$$

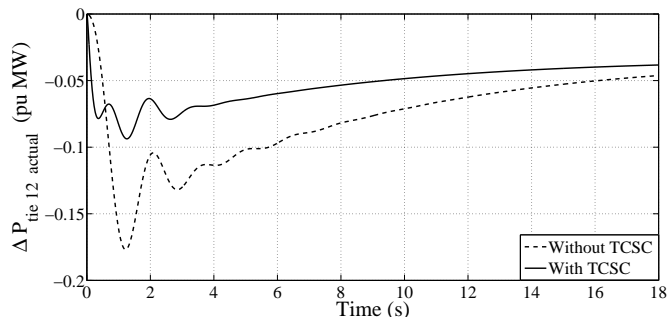
The dynamic responses pertain to contract violation case is depicted in Fig. 3.10.



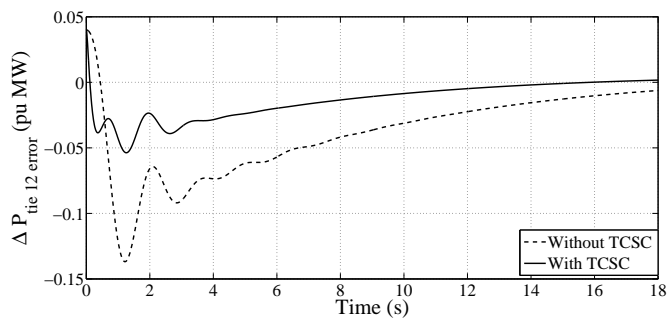
(a) Deviation in frequency of Area-1



(b) Deviation in frequency of Area-2

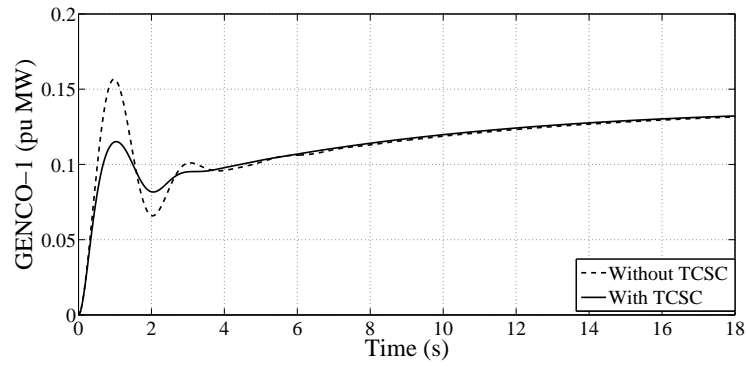


(c) Deviation in tie-line power flow

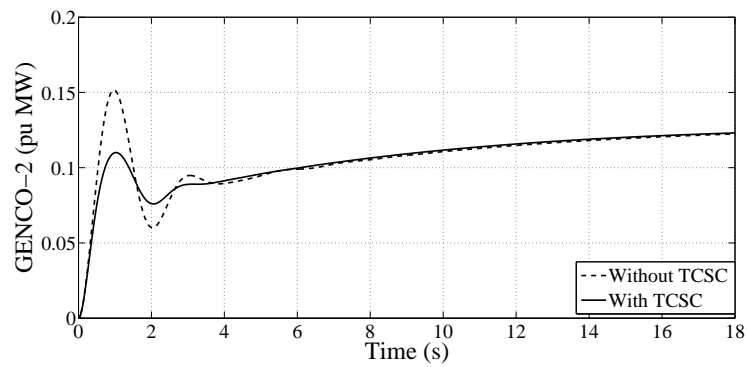


(d) Deviation in tie-line power flow error

Fig. 3.10: Variations in area frequencies (Δf_1 and Δf_2) and actual tie-line power (ΔP_{tie12}) and ($\Delta P_{tie12error}$) for contract violation



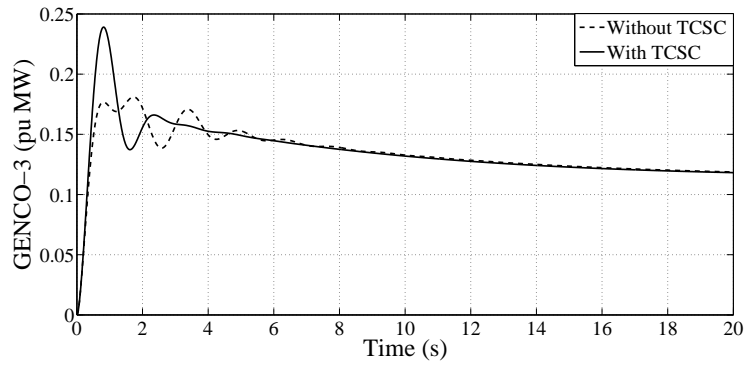
(a) Deviation in power output of GENCO-1



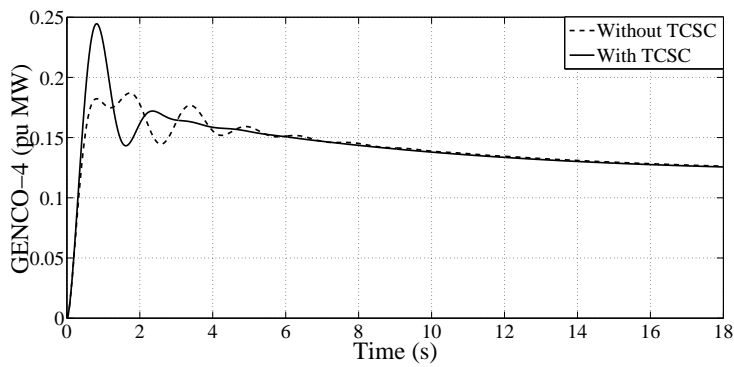
(b) Deviation in power output of GENCO-2

Fig. 3.11: Deviation in generation (ΔP_{G1} and ΔP_{G2}) of GENCOs in Area-1 for contract violation

Similarly at steady state, $\Delta P_{G2} = 0.125$ pu MW. Further, $\Delta P_{G3} = 0.117$ pu MW and $\Delta P_{G4} = 0.123$ pu MW which are same as in previous case. The uncontracted load of DISCO-1 is reflected in generations of GENCO-1 and GENCO-2 in its area. The responses obtained for this case are shown in Figs. 3.11-3.12 and clearly reveal the superiority of TCSC over those without TCSC. The uncontracted load of DISCO-1 is reflected in ΔP_{G1} and ΔP_{G2} at steady state as shown in Fig. 3.11 and matches with calculated (desired) value. As shown in Fig. 3.12, the generation of GENCOs-3 and 4 is not affected by the excess uncontracted load of DISCO-1.



(a) Deviation in power output of GENCO Unit-1



(b) Deviation in power output of GENCO Unit-2

Fig. 3.12: Deviation in generation (ΔP_{G3} and ΔP_{G4}) of GENCOs in Area-2 for contract violation

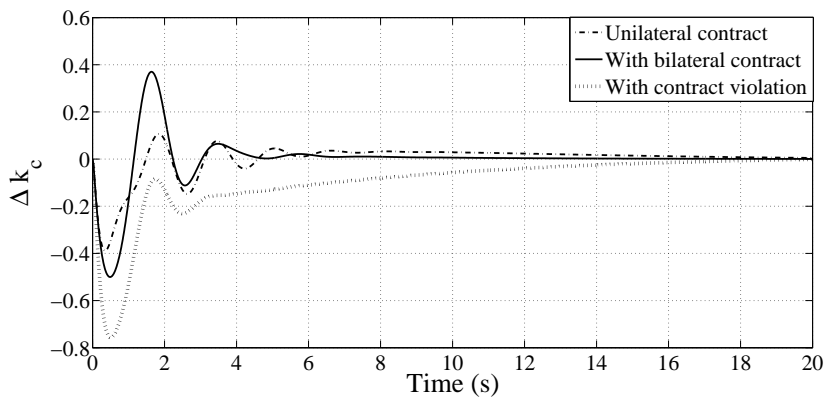


Fig. 3.13: Variation in the incremental change of the percentage compensation (Δk_c) of TCSC for case-1, Case-2 and Case-3

In deregulated environment the contract affects not only the load demand of an area

but also the exchanged tie-line power flow. Inclusion of TCSC in the existing system enables better performance in terms of settling time and faster response.

Fig. 3.13 shows the variation in incremental change of the percentage compensation (Δk_c) of TCSC for the deregulated power system with unilateral, bilateral and contract violation cases. It may be noted that, the TCSC reactance varies in accordance with tie-line power flow deviations.

In bilateral power market, ISO is responsible for providing various ancillary services such as frequency regulation, reactive power management etc. In frequency regulation scheme, the generation-load balancing is done by ISO through power balance market. A balance service is used for secondary regulation of frequency, which is done by taking regulating bids from generators willing to quickly increase or decrease generation or even consumers willing to quickly increase or decrease consumption. The same scenario is explained in terms as contract violation case, where an excess load demand arrives from any of the DISCOs in bilateral market, certain GENCOs in that area itself supplies this excess load demand.

3.4.2 Case-2: Hydro-Thermal System

3.4.2.1 State Space Model of the Two-area Deregulated System with TCSC

Fig. 3.14 shows the schematic representation of a two area hydro-thermal power system in deregulated environment. The investigations are carried out on a two area hydro-thermal power system with two thermal generation based GENCOs in Area-1 ($GENCO_1$ and $GENCO_2$) and two hydro based GENCOs in Area-2 ($GENCO_3$ and $GENCO_4$). The integral gains of the control areas are given as K_{I1} and K_{I2} for Area-1 and Area-2 respectively. The controllers gains are obtained by tuning the quadratic performance index as shown in Eqn. 3.11 using GA.

The state space model of the two area system is characterized by the state space form as

$$\dot{X} = AX + BU + \Gamma p, \quad (3.14)$$

where X, U and p are the state, control and load disturbance input vectors, respectively, whereas A, B and Γ are the respective matrices of appropriate dimensions.

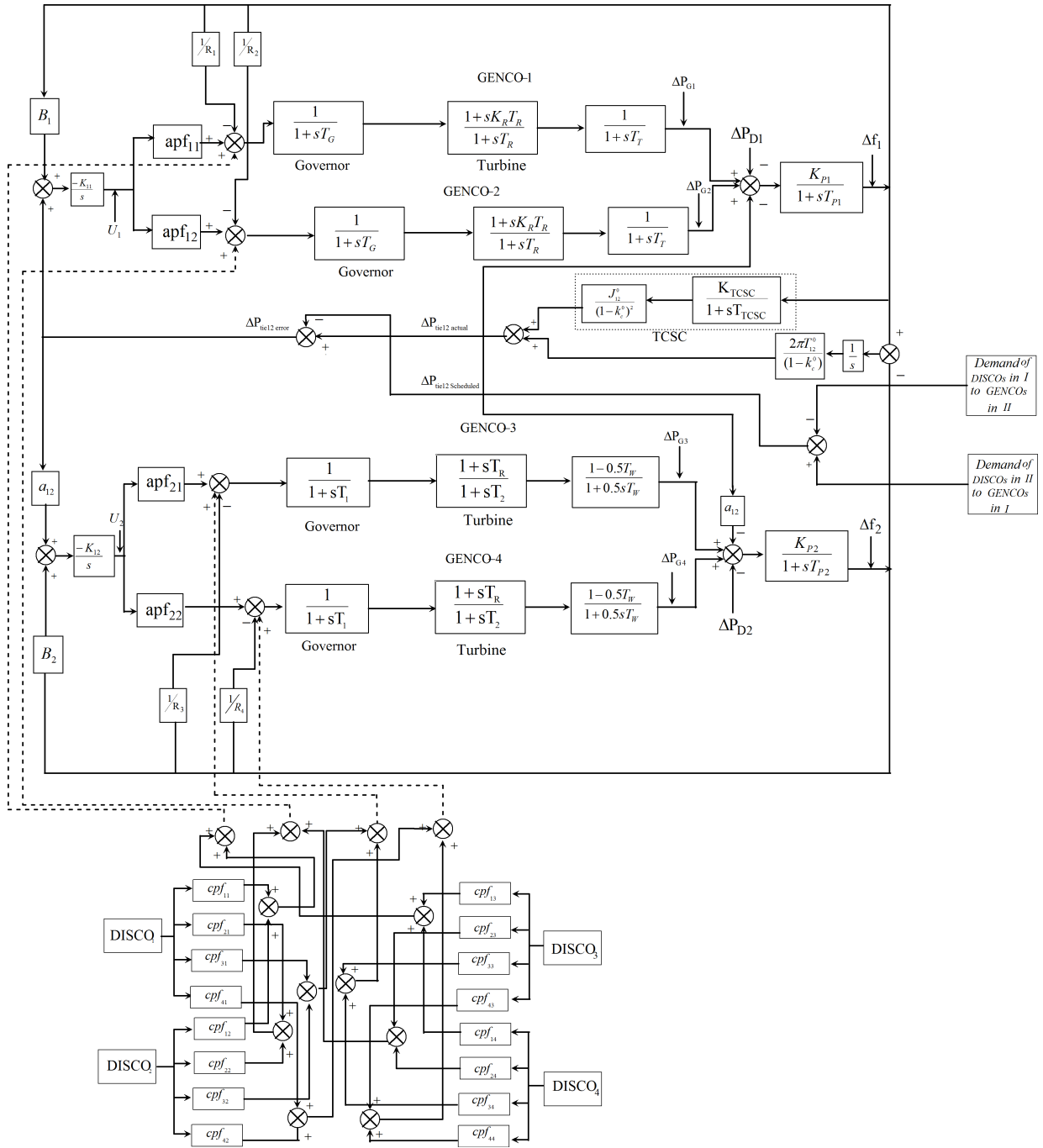


Fig. 3.14: Linearized model of an interconnected hydro-thermal system under deregulation

Table 3.3
Optimized Gain Settings of Control Areas

	Unilateral Contract		Bilateral Contract		Contract Violation	
	K_{I1}	K_{I2}	K_{I1}	K_{I2}	K_{I1}	K_{I2}
Without TCSC	0.0216	0.039	0.434	0.0840	0.4590	0.0820
With TCSC	0.0331	0.0425	0.3970	0.0839	0.0495	0.0831

3.4.2.2 Simulation Results and Discussion

Time domain simulations are carried out using MATLAB on a two area hydro-thermal deregulated power system shown in Fig. 3.14. Similar to thermal-thermal system as already explained in Section 3.4.1, each DISCO demands 0.1 pu MW, i.e., $\Delta P_{L1} = \Delta P_{L2} = \Delta P_{L3} = \Delta P_{L4} = 0.1$ pu. For analysis, TCSC is connected in series with tie-line near to Area-1. Table 3.3 shows the optimal gain settings of the control areas (K_{I1} and K_{I2}) for different market conditions using GA for the sample hydro-thermal system. Simulations are carried out on given sample system with three possible market scenarios as following.

1. Unilateral contract
2. Bilateral contract
3. With contract violation

Case 1-Unilateral Contract/ Poolco based transaction

As explained in the earlier section, in unilateral contract, DISCOs in an area can have power contract with GENCOs in the same area only. It is assumed that each DISCO has a total load demand of 0.1 pu MW. Let $DISCO_1$ & $DISCO_2$ in Area-1 have power contract with $GENCO_1$ and $GENCO_2$ in Area-1 as per the following DPM,

$$DPM = \begin{bmatrix} 0.45 & 0.55 & 0 & 0 \\ 0.55 & 0.45 & 0 & 0 \\ 0 & 0 & 0 & 0 \\ 0 & 0 & 0 & 0 \end{bmatrix} \quad (3.15)$$

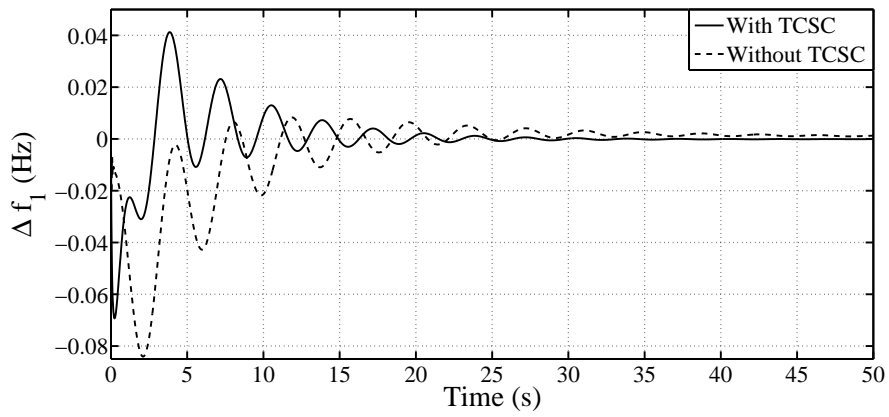
Fig. 3.15 shows the variations of area frequencies and tie-line power flow with and without TCSC for unilateral contract. It is observed that, in unilateral contract, GENCOs in Area-1 meet the load contracts from DISCOs in Area-1. It is seen that at steady state, deviation in tie-line power flow settles down to zero as there is no additional inter area power contract between GENCOs and DISCOs, which can viewed in Fig. 3.15(c). It is also seen that the power generations at various GENCOs settles down to their respective calculated as per the DPM. At steady state,

$$\begin{aligned}
 \text{Power output of GENCO-1 } (\Delta P_{G1}) &= (cpf_{11} \times \Delta P_{L1}) + (cpf_{12} \times \Delta P_{L2}) + \\
 &\quad (cpf_{13} \times \Delta P_{L3}) + (cpf_{14} \times \Delta P_{L4}) \\
 &= (0.45 \times 0.1) + (0.55 \times 0.1) + \\
 &\quad (0 \times 0.1) + (0 \times 0.1) \\
 &= 0.1 \text{ pu MW}
 \end{aligned}$$

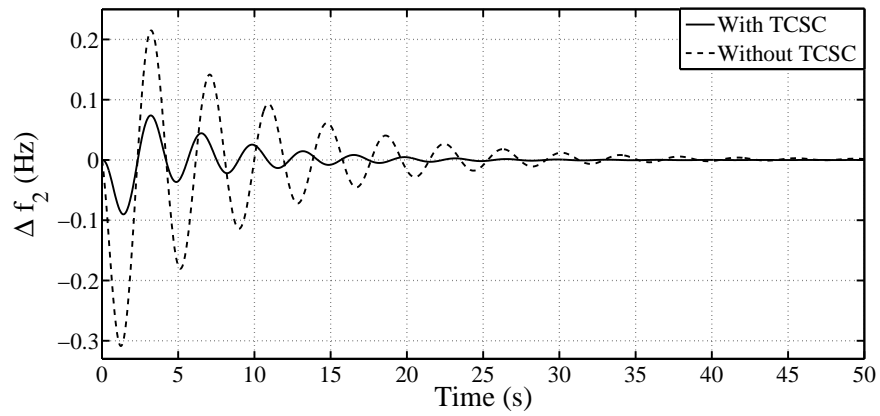
$$\begin{aligned}
 \text{Power output of GENCO-2 } (\Delta P_{G2}) &= (cpf_{21} \times \Delta P_{L1}) + (cpf_{22} \times \Delta P_{L2}) + \\
 &\quad (cpf_{23} \times \Delta P_{L3}) + (cpf_{24} \times \Delta P_{L4}) \\
 &= (0.55 \times 0.1) + (0.45 \times 0.1) + \\
 &\quad (0 \times 0.1) + (0 \times 0.1) \\
 &= 0.1 \text{ pu MW.}
 \end{aligned}$$

Similarly at steady state,

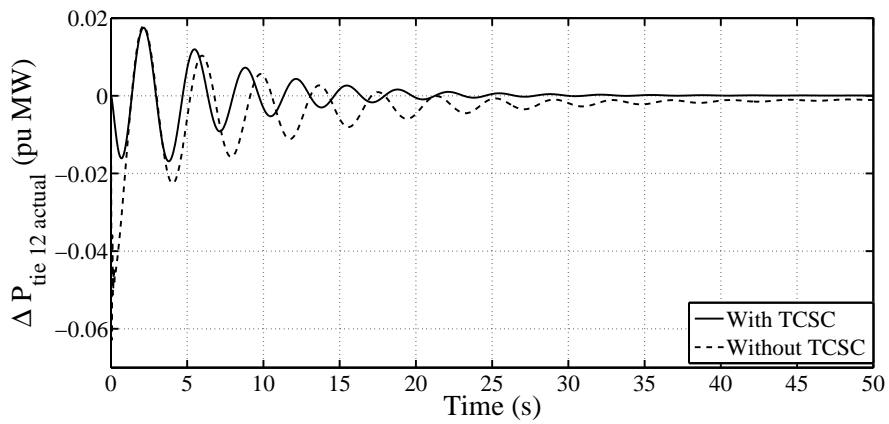
$$\begin{aligned}
 \text{Power output of GENCO-3 } (\Delta P_{G3}) &= (cpf_{31} \times \Delta P_{L1}) + (cpf_{32} \times \Delta P_{L2}) + \\
 &\quad (cpf_{33} \times \Delta P_{L3}) + (cpf_{34} \times \Delta P_{L4}) \\
 &= (0 \times 0.1) + (0 \times 0.1) + \\
 &\quad (0 \times 0.1) + (0 \times 0.1) \\
 &= 0 \text{ pu MW}
 \end{aligned}$$



(a) Deviation in frequency of Area-1



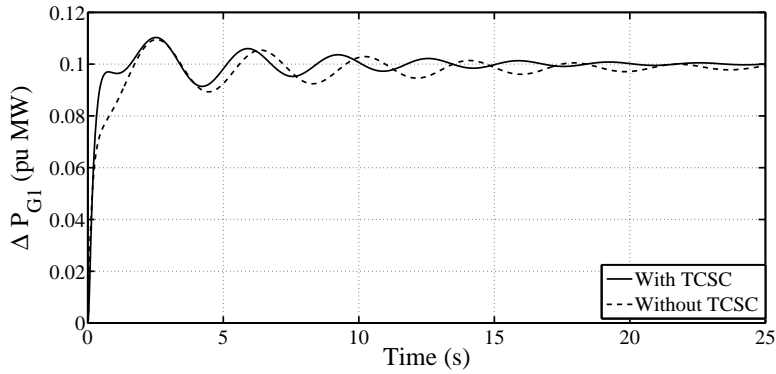
(b) Deviation in frequency of Area-2



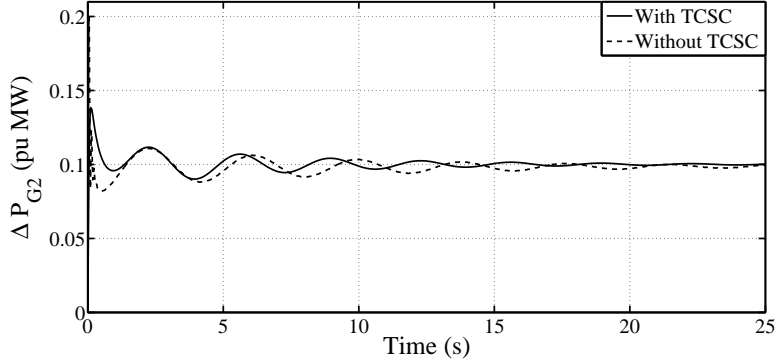
(c) Deviation in tie-line power flow

Fig. 3.15: Case 1: Variations in area frequencies (Δf_1 and Δf_2) and tie-line power (ΔP_{tie12})

$$\begin{aligned}
\text{Power output of GENCO-4 } (\Delta P_{G4}) &= (cpf_{41} \times \Delta P_{L1}) + (cpf_{42} \times \Delta P_{L2}) + \\
&\quad (cpf_{43} \times \Delta P_{L3}) + (cpf_{44} \times \Delta P_{L4}) \\
&= 0 \text{ pu MW.}
\end{aligned}$$



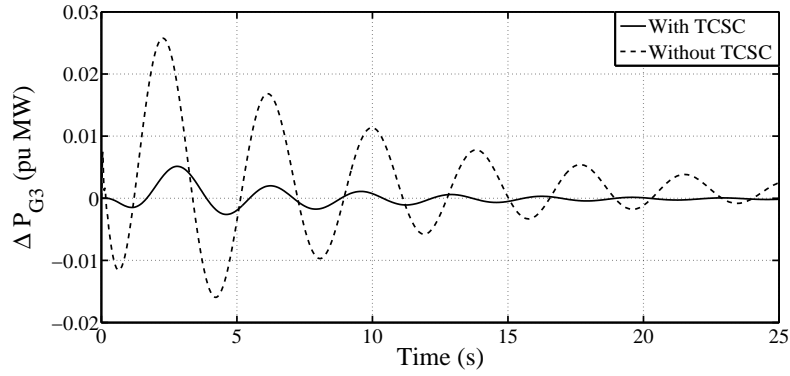
(a) Deviation in power output of GENCO-1



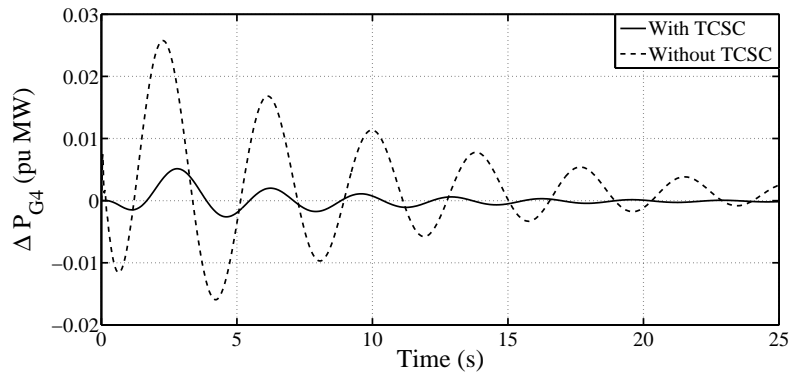
(b) Deviation in power output of GENCO-2

Fig. 3.16: Case 1: Deviation in generation (ΔP_{G1} and ΔP_{G2}) of GENCOs in Area-1

The power outputs of various GENCOs are plotted with and without TCSC in Figs. 3.16-3.17 and simulation results match with calculated values. Fig. 3.17 shows the generation output of $GENCO_3$ and $GENCO_4$ in Area-2, which do not take part in load contract during unilateral contract, which is clear from DPM shown in Eqn. 3.15 as their corresponding contract participation factors are zero.



(a) Deviation in power output of GENCO-3



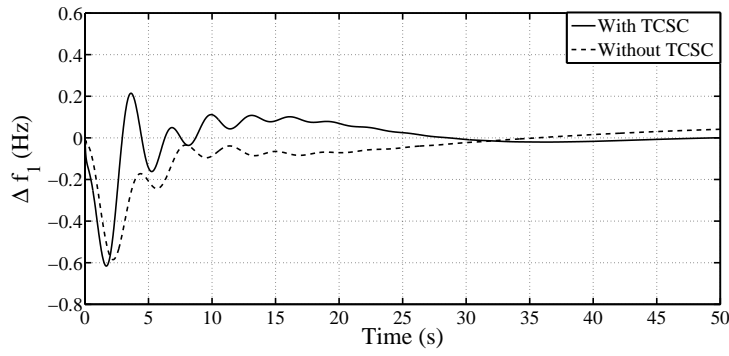
(b) Deviation in power output of GENCO-4

Fig. 3.17: Case 1: Deviation in generation (ΔP_{G3} and ΔP_{G4}) of GENCOs in Area-2

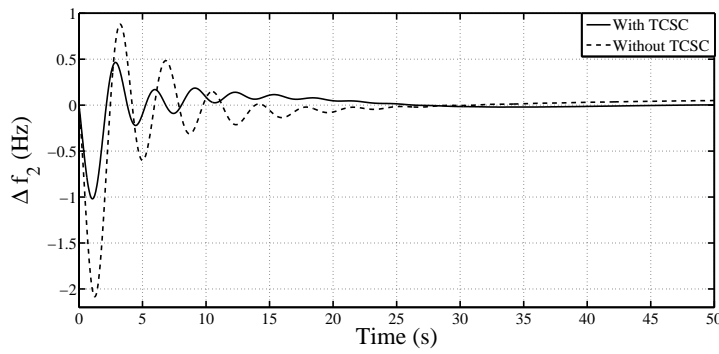
Case 2-Bilateral Transactions

As previously explained, in bilateral transactions, a DISCO in an area have independent power contract with GENCOs in any area. The load contract made by various DISCOs-GENCOs combination can be realized through DPM given by,

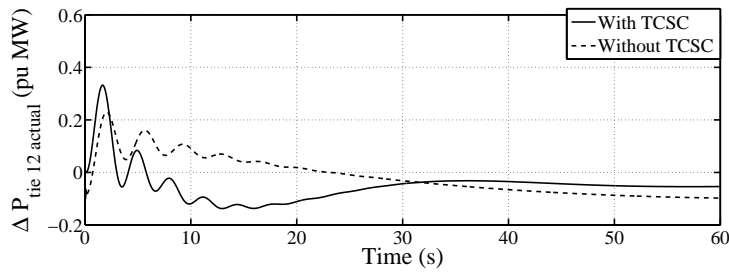
$$DPM = \begin{bmatrix} 0.1 & 0.24 & 0.33 & 0.18 \\ 0.2 & 0.16 & 0.17 & 0.22 \\ 0.27 & 0.4 & 0.5 & 0 \\ 0.43 & 0.2 & 0 & 0.6 \end{bmatrix} \quad (3.16)$$



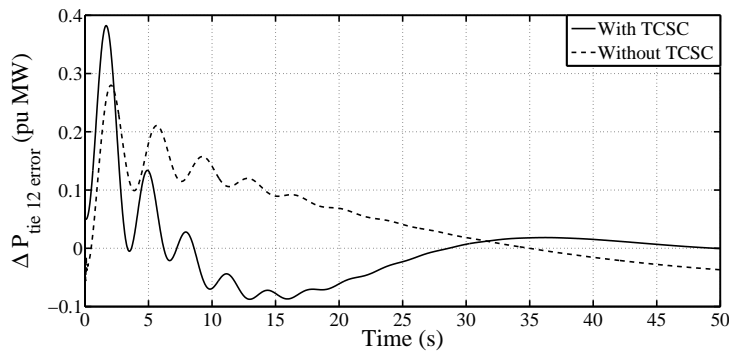
(a) Deviation in frequency of Area-1



(b) Deviation in frequency of Area-2

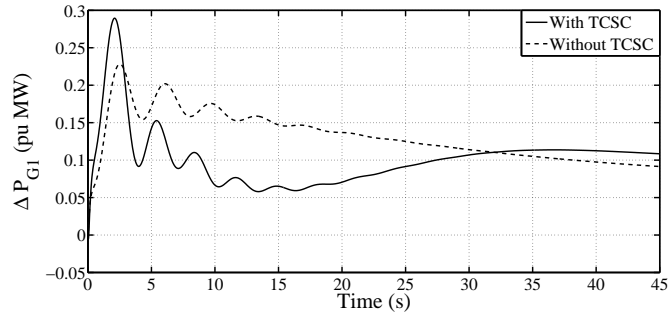


(c) Deviation in tie-line power flow

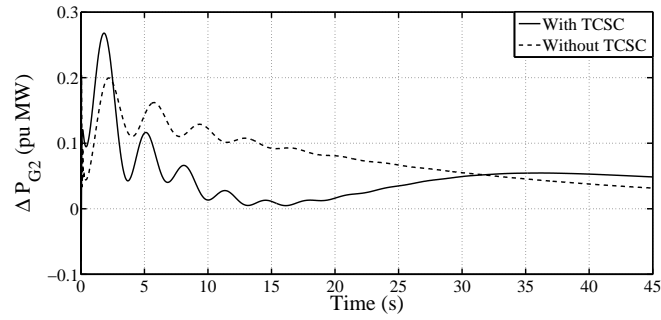


(d) Deviation in tie-line power flow error

Fig. 3.18: Case 1: Variations in area frequencies (Δf_1 and Δf_2) actual tie-line power (ΔP_{tie12}) and tie-line power error ($\Delta P_{tie12error}$)



(a) Deviation in power output of GENCO-1



(b) Deviation in power output of GENCO-2

Fig. 3.19: Case 2: Deviation in generation (ΔP_{G1} and ΔP_{G2}) of GENCOs in Area-1

The dynamic responses pertaining to load following in a hydro-thermal system with and without TCSC case are shown in Figs. 3.18-3.20. It is clear that with TCSC, transient specifications such as peak time, overshoot, and rise time has improved. It is evident from Fig. 3.18(c) that at steady state, the tie-line power flow settles to its scheduled value $\Delta P_{tie12scheduled} = -0.04$ pu MW, as calculated from DPM. The generations from various GENCOs are presented in Figs. 3.19-3.20. It is found that, the generations at various GENCOs settle down to their respective values as calculated from DPM. At steady state,

$$\begin{aligned}
 \text{Power output of GENCO-1 } (\Delta P_{G1}) &= (0.1 \times 0.1) + (0.24 \times 0.1) + \\
 &\quad (0.33 \times 0.1) + (0.18 \times 0.1) \\
 &= 0.085 \text{ pu MW.}
 \end{aligned}$$

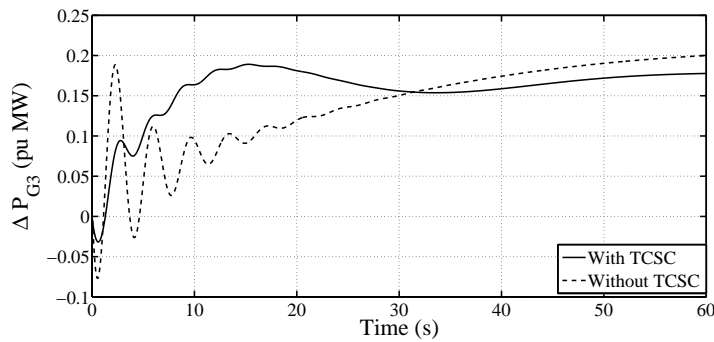
Similarly, at steady state,

$$\begin{aligned}
 \Delta P_{G2} &= (0.2 \times 0.1) + (0.16 \times 0.1) + (0.17 \times 0.1) + (0.22 \times 0.1) \\
 &= 0.075 \text{ pu MW.}
 \end{aligned}$$

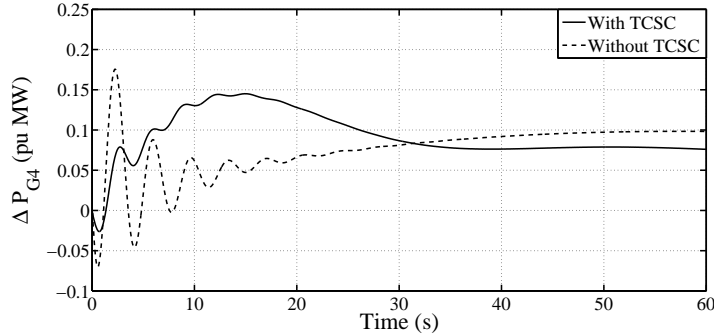
Further, at steady state,

$$\begin{aligned}\Delta P_{G3} &= (0.27 \times 0.1) + (0.4 \times 0.1) + (0.5 \times 0.1) + (0 \times 0.1) \\ &= 0.117 \text{ pu MW},\end{aligned}$$

$$\begin{aligned}\Delta P_{G4} &= (0.43 \times 0.1) + (0.2 \times 0.1) + (0 \times 0.1) + (0.6 \times 0.1) \\ &= 0.123 \text{ pu MW}.\end{aligned}$$



(a) Deviation in power output of GENCO-3

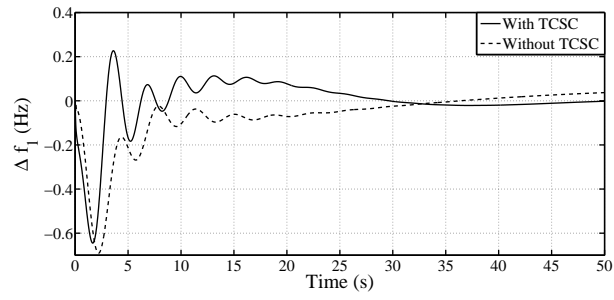


(b) Deviation in power output of GENCO-4

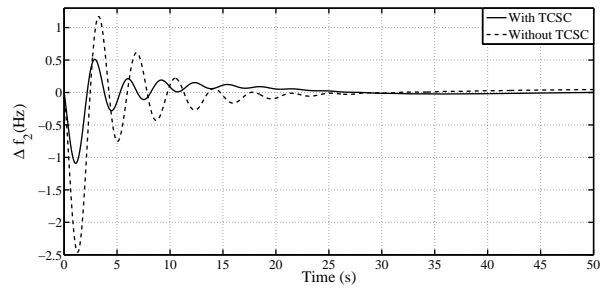
Fig. 3.20: Case 2: Deviation in generation (ΔP_{G3} and ΔP_{G4}) of GENCOs in Area-2

Case 3-Contract Violation

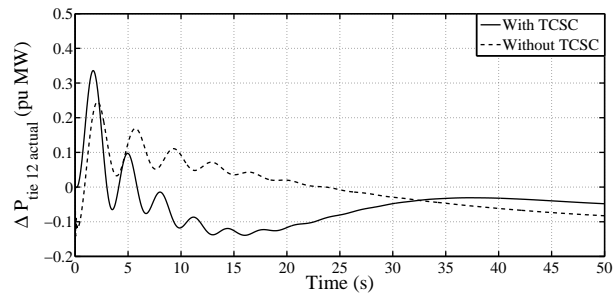
This is an extension of Case-2 where DISCO in area may demands more power than it contracted earlier. To maintain the power balance, this extra demand must be supplied by the GENCOs in the same area. In this analysis, we have considered a case where DISCO-1 demands 0.1 pu MW power extra than it contracted.



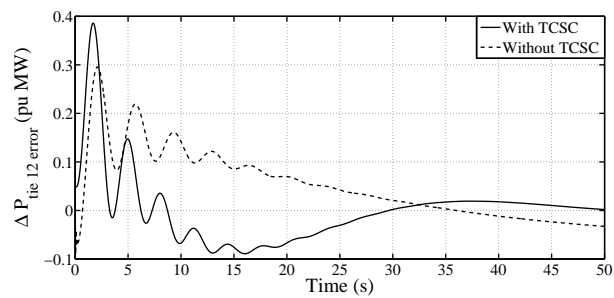
(a) Deviation in frequency of Area-1



(b) Deviation in frequency of Area-2

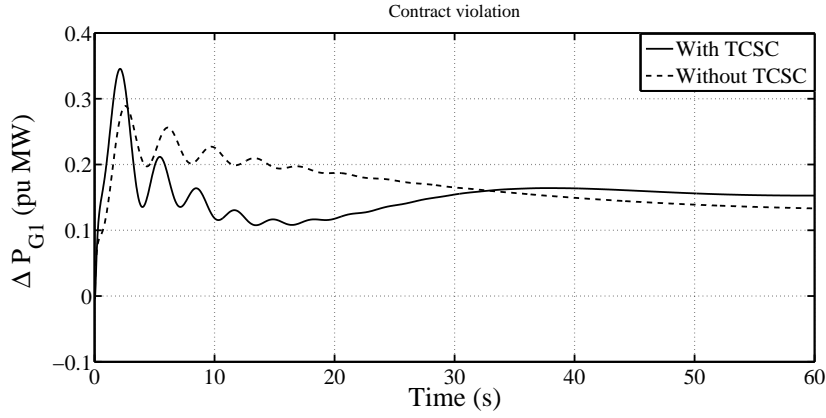


(c) Deviation in tie-line power flow

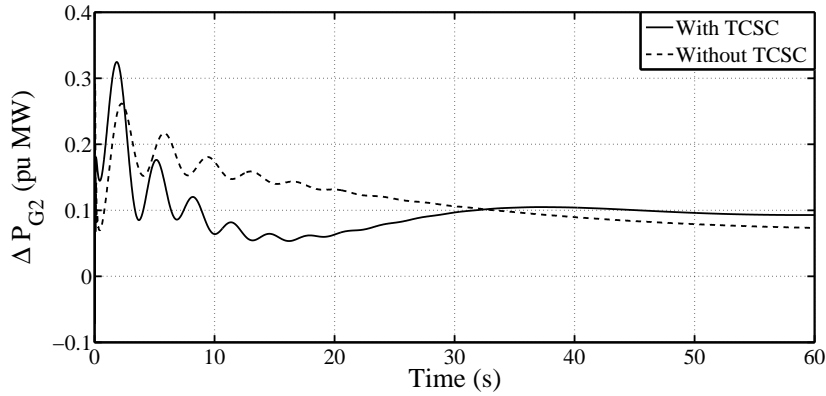


(d) Deviation in tie-line power flow error

Fig. 3.21: Case 3: Variations in area frequencies (Δf_1 and Δf_2) and actual tie-line power (ΔP_{tie12}) and ($\Delta P_{tie12error}$)



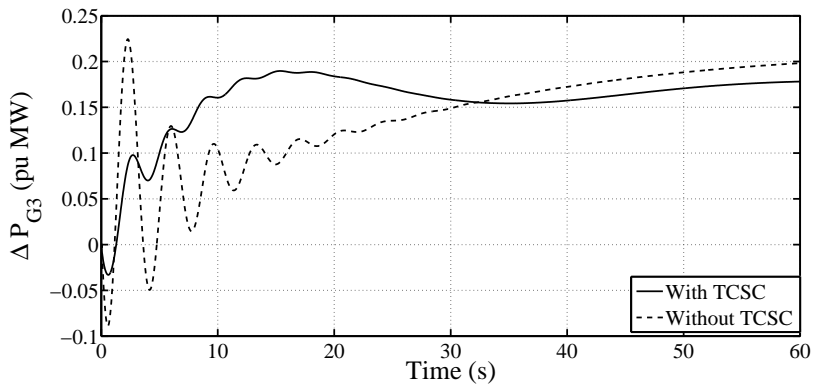
(a) Deviation in power output of GENCO-1



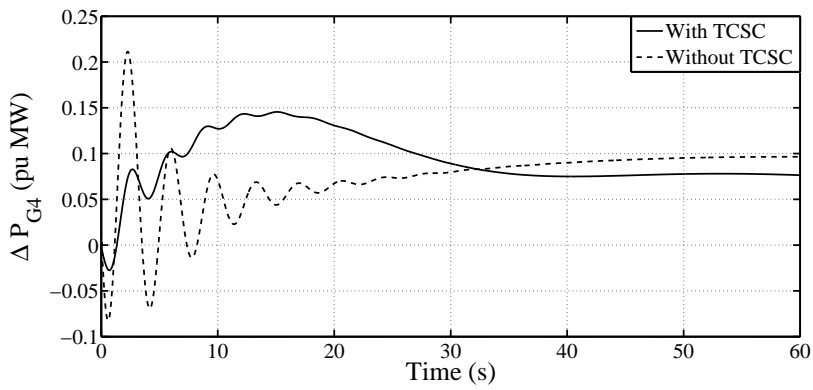
(b) Deviation in power output of GENCO-2

Fig. 3.22: Case 3: Deviation in generation (ΔP_{G1} and ΔP_{G2}) of GENCOs in Area-1

As explained in the thermal-thermal system, this extra load will be shared among GENCOs in Area-1 according to area participation factor. It is seen that, at steady state, power output of GENCO-1 becomes, $\Delta P_{G1} = \text{contracted power} + (apf_{11} \times \text{uncontracted load-demand of GENCO-1}) = 0.135 \text{ pu MW}$, which can be viewed in Fig. 3.22(a). In order to maintain the tie-line power flow unaltered, this extra load is met by the GENCOs in Area-1. It is also clear from Fig. 3.21(c) and Fig. 3.23 that tie-line power flow and generations of GENCOs in Area-2 remain same as that of bilateral contract.



(a) Deviation in power output of GENCO-3



(b) Deviation in power output of GENCO-4

Fig. 3.23: Case 3: Deviation in generation (ΔP_{G3} and ΔP_{G4}) of GENCOs in Area-2

From the above simulations, it is clear that with TCSC improves the system performance in terms of fast settling and less overshoot.

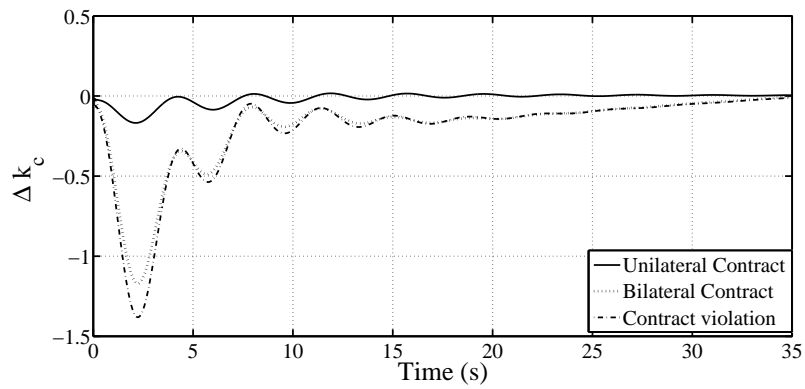


Fig. 3.24: Variation in the incremental change of the percentage compensation (Δk_c) of TCSC for Case-1, Case-2 and Case-3

Fig. 3.24 shows the variation in incremental change of the percentage compensation (Δk_c) of TCSC for the deregulated power system with unilateral, bilateral and contract violation cases. It may be noted that, the TCSC reactance varies in accordance with tie-line power flow deviations.

3.5 Summary

An attempt has been made to damp out the area frequency oscillations and tie-line power flow after a sudden load demand using TCSC in a deregulated power system, thereby, improving the load following. A linearized model of the TCSC is used to study its effect in load following. Extensive analysis is done for AGC scheme considering unilateral transactions, bilateral transactions and contract violation. Genetic algorithm has been used to tune the integral gain settings of both the areas with and without TCSC considering a quadratic performance index for the above three scenarios. It is found that in all the cases, the area frequency error becomes zero at the steady state. Performance of AGC has been improved in terms of settling time, peak overshoot and damping with the use of TCSC in all the three cases. It is found that actual values of generations and tie-line power exchanges of GENCOs obtained from simulations are matching with the corresponding calculated (desired) values. Hence, a Thyristor Controlled Series Compensator (TCSC) can be used effectively for load following in a deregulated power system.

Chapter 4

Frequency Support in a Wind Integrated Power System

4.1 Introduction

Power generation using renewable energy sources such as solar, wind, biomass and geothermal has gained momentum among electric power utilities owing to increase in electric energy demands, fast depleting sources of fossil fuels and considerations for environmental concerns such as emission of carbon dioxide and other green house gases. Currently, wind energy penetration has gone up significantly with variable speed type wind turbines. Thus conventional sources are getting replaced by Doubly Fed Induction Generator (DFIG) type wind turbine as the penetration level increases [10, 11, 108]. In a traditional power system, conventional sources such as hydro and thermal are the main sources of inertia that is stored in the form of kinetic energy in the rotor. However, the inertia provided by the DFIG type wind turbine is negligibly small because the rotor is decoupled from the grid through power electronic interface. With decreasing levels of inertia, an increased frequency excursion is observed after a sudden load perturbation which is of concern for plant operators as well as turbine manufacturers. Plenty of research works that are concerned with frequency support using variable speed wind turbines are available in the literature based on (a) inertia control [10–13, 44–53] (b) speed recovery [44, 45] and (c) coordinated operation with neighbouring conventional sources [45, 46].

Primary frequency control with wind turbines in comparison with conventional system is more cumbersome. Existing methods of inertia emulation [12, 13, 44–55] suggest the extraction of stored kinetic energy from the wind turbine rotor in the wake of sudden load disturbances which leads to a reduction in its rotor speed. To work at a specified speed limit, a recovery system should bring back Wind Turbine Generator (WTG) rotor speed to its nominal value by absorbing energy from the grid. This results in a second frequency dip in the system that may be worse than the first one. If the WTG rotor speed

is not recovered, wind turbine will not inject additional energy into the grid [109]. This will result in reduction in overall system efficiency [110]. Hence, this work emphasizes on reducing the stress in the WTG rotor by allowing it to less release energy for a short duration.

This work aims at enhancing the primary frequency support from DFIG by incorporating inertia response, in tandem with conventional sources and coordinated operation with TCSC-FES. When a load perturbation occurs, the kinetic energy associated with the system inertia that is stored in the rotor of conventional generators will be released to the grid. Hence, the rotor speed changes. However, with the inclusion of WTG, the effective system inertia gets reduced which needs to be compensated for. With inertia response, the kinetic energy stored in the rotating mass of WTG rotor will be released to the grid. This results in the variation of the rotor speed which will be reset to the rated value later. Since the stored kinetic energy linked to machine inertia constant is limited and available for short duration of time, the conventional generating units should take up the extra load demand. Communication must be established between conventional sources and wind turbines so as to mitigate load imbalance as fast as possible. Meanwhile, Flywheel Energy Storage (FES) can effectively serve as an energy source and sink, i.e., storing energy during low load condition and dispatching the stored energy to meet the load requirement when needed. On the other hand, a TCSC can dynamically control the transmission line reactance, thereby, controlling the power flow transfer and hence the tie-line power flow perturbations. The TCSC-FES combination further enhances the frequency regulation by not letting the DFIG to release the entire stored energy but forcing the FES to release the already available stored energy instantaneously. Hence, combined together, FES-TCSC combination has the capability to control the dynamic characteristics of frequency regulation effectively by not letting the DFIG to release the entire stored energy but making FES to release the already available stored energy. Hence, the main contributions of this chapter are as follows:

- A modelling approach enabling the simulation of dynamic frequency events in a multi-area power system with wind penetration.
- Proposal of a FES system to improve primary frequency regulation in a power sys-

tem with high wind penetration.

- A combined frequency control scheme using FES, TCSC, and conventional generation.

Simulation of various wind penetration scenarios with the above have been carried out using MATLAB®R2013b. Further, the proposed scheme has been compared with one of the already existing methods [54]. Since load frequency control analysis is done for short duration of time, a constant wind speed is assumed.

4.2 Models for Frequency Regulation

The power system model to accommodate non conventional generation for simulation studies is presented below.

4.2.1 Power System Model

Fig. 4.1 shows a classical single area power system model for frequency regulation studies [45]. Block G denotes a conventional generation unit and simulates the dynamics of an equivalent machine representing a system with different kinds of generation technologies (hydro turbine, gas turbine, steam turbine and alternative engine), along with its governor. Power reference U is the input to block G and the change in generated power ΔP_G is the output.

The change in system active power demand (ΔP_D) and the change in power interchanged with neighbour systems as (ΔP_{tie}) are subtracted from the change in generated power (ΔP_G). To consider the change in power injection from wind power generation unit, a new term ΔP_{wind} is added.

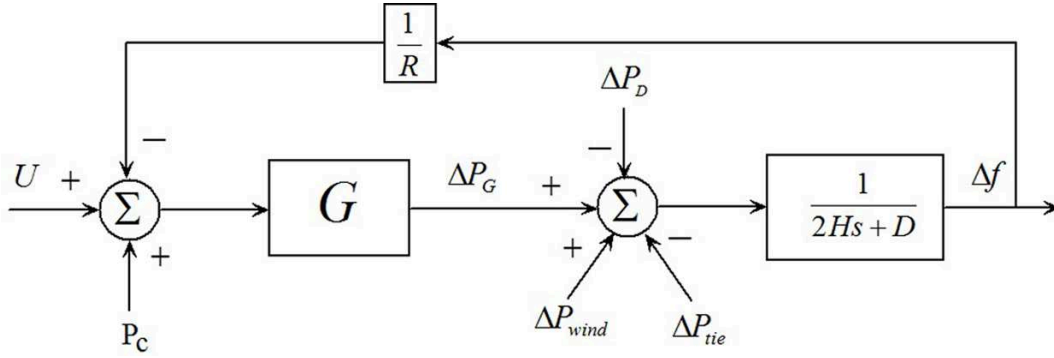


Fig. 4.1: Single area with non conventional generation

At steady state, the total power balance is given as,

$$\Delta P_G - \Delta P_{tie} + \Delta P_{wind} - \Delta P_D = 0 \quad (4.1)$$

The term U stands for the secondary control or Automatic Generation Control power reference while P_c is a coordination signal coming from the Wind Energy Conversion System (WECS), which will make conventional generators aware of frequency support from the WECS.

4.2.2 Variable Speed Wind Turbine Systems

Fig. 4.2 depicts the most commonly used variable-speed machine for WECS [typical Doubly Fed Induction Generation) unit]. Variable speed operation is commonly used in wind energy system due to their wide range of operating speeds, robust structure, less investment in power conditioning system [111], reduced inverter cost, reduced cost of the inverter filters and EMI filters, improved system efficiency and ease of power-factor control at lower cost [112]. DFIG can be considered as a conversion system that links a mechanical force (wind) through an asynchronous electrical link to the rest of the power system, as shown in Fig. 4.2. It can effectively control both active and reactive powers injected into the grid through the power electronics interface so that the desired operating conditions can be achieved. Optimum power extraction from the available wind is carried out using Maximum Power Point Tracking (MPPT) implemented in power electronic controllers. Various primary frequency strategies like inertia emulation, speed recovery control etc.

are associated with these controllers to make DFIGs behave like a conventional generator. In this work, DFIG is assumed to work in the optimal power extraction curve thereby extracting the maximum available energy from wind.

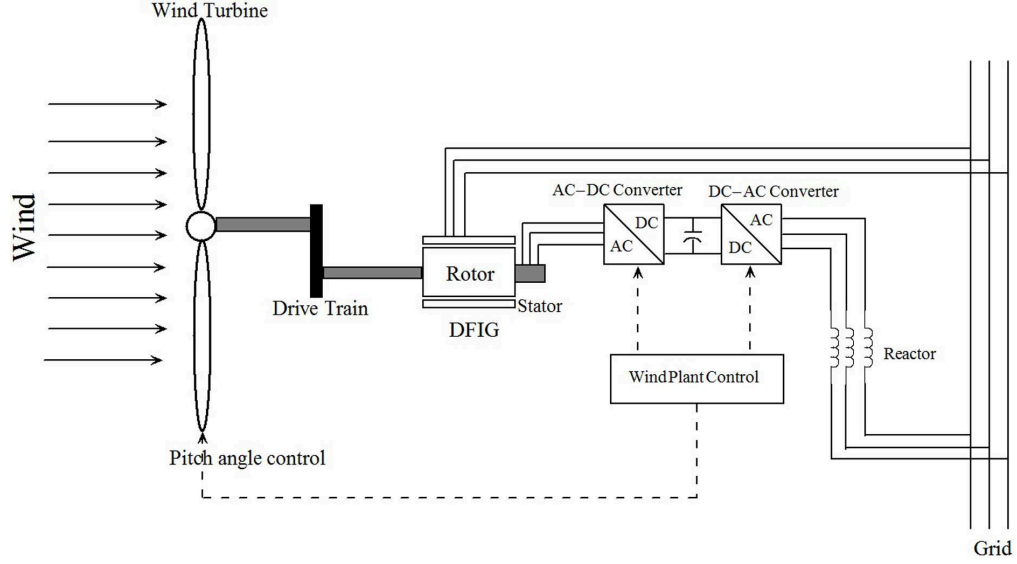


Fig. 4.2: Equivalent energy conversion system of DFIG

4.2.3 Wind Turbine Aerodynamic model

This work addresses the frequency regulation with variable speed wind turbines utilizing inertia control and coordinated operation of Wind Turbine (WT) and conventional generators. The maximum mechanical power that can be extracted from the wind by WT is given by [113]

$$P_{opt} = \frac{1}{2} \rho C_{popt}(\lambda_{opt}, \beta) A U_m^3, \quad (4.2)$$

where C_{popt} is the optimal power coefficient of the wind turbine expressed as a function of tip speed ratio (λ) and pitch angle (β), A is the effective swept area in m^2 , U_m is the wind speed in m/s and ρ is the air density in kg/m^3 . The optimal power coefficient C_{popt} is given by the following function [113]

$$C_{popt}(\lambda_{opt}, \beta) = 0.22 \left(\frac{116}{\lambda_i} - 0.4\beta - 5 \right) e^{-\frac{12.5}{\lambda_i}} \quad (4.3)$$

$$\frac{1}{\lambda_i} = \frac{1}{\lambda_{opt} + 0.08\beta} - \frac{0.035}{\beta^3 + 1}, \quad (4.4)$$

where the optimal tip speed ratio is given as

$$\lambda_{opt} = \frac{\omega_{t_{opt}} R}{U_w} \quad (4.5)$$

Here, R being the blade radius in m and $\omega_{t_{opt}}$ being the optimal WT rotor speed for a given wind speed in rad/s .

4.3 Schemes for Frequency Regulation using Wind Turbines

The scheme is a combination of primary droop control with speed recovery and coordinated operation with conventional sources. Fig. 4.3 gives a schematic overview of the model.

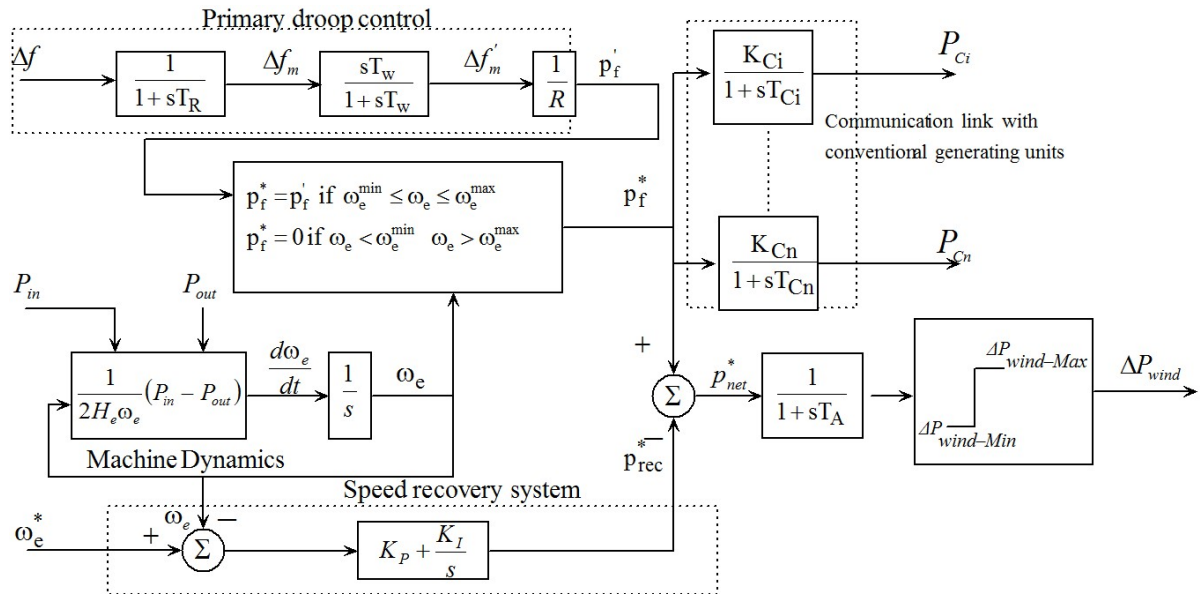


Fig. 4.3: Control strategy and WECS model

Primary Droop Control

A wind generator possesses significant amount of stored kinetic energy in the rotating mass similar to that of its conventional counterpart. Due to the power electronic interface, the rotor of the variable speed wind turbines are decoupled from the grid causing negligi-

ble contribution of inertia from WECS. This leads to reduction in overall system inertia with high wind penetration, which is the prime cause of larger frequency nadir during load disturbances. To overcome this and to emulate *hidden inertia*, a droop based control strategy has been used in this work to support primary frequency control for a short period of time (in the order of seconds) after the load perturbation.

Active power injected from WTG is proportional to the deviation in system frequency, ($\Delta f_{sys} = f_{sys_measured} - f_{sys_nominal}$) and the primary droop control is activated only when grid frequency exceeds certain limit, similar to the droop control in conventional generating units. Fig. 4.3 shows the primary frequency control characterized by R , with frequency deviation as the control signal. A filter is used in this loop to remove the steady state frequency error. The power injected is given follows:

$$\Delta P'_f = \frac{-1}{R} \Delta f'_m, \quad (4.6)$$

where $\Delta P'_f$ is the signal given to power electronics controllers, which effectively releases the stored kinetic energy and $\Delta f'_m$ is the filter frequency deviation.

Speed Recovery

Due to sudden release of the stored kinetic energy from the WTG rotor, the primary droop control gets activated resulting in reduction of the rotor speed. To bring the WTG rotor speed back to its optimal rated value, a Proportional Integral (PI) controller is activated soon after the occurrence of load disturbance. This speed recovery loop absorbs energy from the grid when the frequency deviation settles down to zero and is relatively slow in comparison with primary droop control. This avoids a negative impact on WECS performance.

Coordination with Conventional Sources

A sudden load perturbation results in frequency changes which activates the primary droop control. This ensures the contribution of extra kinetic energy to the grid to avoid the large frequency nadir. Due to this, conventional generators does not take up the excess load, resulting in reduction of WTG rotor speed, which may force the WTG to move out

from the grid. To avoid this, communication signals are given to conventional generators to take up this extra load demand. It should be noted that

$$\sum_{i=1}^n K_{ci} = 1, \quad (4.7)$$

where K_{Ci} is the gain of i^{th} communication link. Thus coordination between conventional and WECS helps in reducing the negative impact of primary droop control. The power output of the WTG is limited to a range of 0 to 1.2 pu. Modern power systems are designed to supply power on demand with high reliability. For the satisfactory operation of power, system frequency and voltage should be kept fairly constant.

4.3.1 Linearized Model of TCSC

Fig. 4.4 shows a linearized model used in Chapter-2 is analyzed with wind integrated power system. Normally FACTS devices are used to improve the power flow through weak tie-lines as well as to evacuate the renewable energy from the far away locations to load centers.

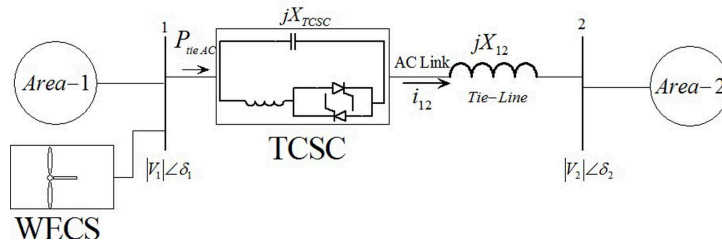


Fig. 4.4: Schematic model of the interconnected two area wind integrated power system with TCSC in series with the tie-line

Considering TCSC in series with the tie-line and near to Area-1, Fig. 4.4 shows the schematic diagram of a sample two area interconnected thermal dominated power system with wind penetration. Generally the reactance to resistance ratio of the tie-line is quite high ($X/R \gg 10$) so that, while modeling the power system, the effects of tie-line resistance can be neglected.

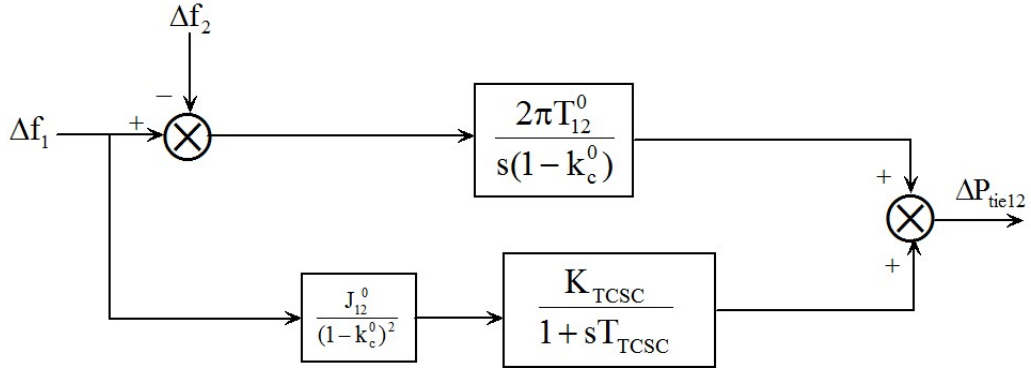


Fig. 4.5: Small signal model of TCSC used for AGC studies

The deviation in the tie-line power flow with TCSC after the perturbation becomes,

$$\begin{aligned} \Delta P_{tie12} = & \frac{2\pi T_{12}^0}{s(1 - k_c^0)} [\Delta f_1(s) - \Delta f_2(s)] \\ & + \left[\frac{J_{12}^0}{(1 - k_c^0)^2} \right] \frac{K_{TCSC}}{1 + sT_{TCSC}} \Delta f_1(s) \end{aligned} \quad (4.8)$$

The equivalent representation of TCSC corresponding to Eqn. 4.8 is shown in Fig. 4.5. It is evident that a TCSC in series with tie line can effectively vary the tie-line reactance, thereby changing the net power flow through the line. Hence, by suitably adjusting the TCSC compensation, tie line power flow perturbations can be controlled which in turn controls the frequency perturbations. Thus, TCSC can damp out the low frequency oscillations in tie-line power flow and area frequencies which in turn helps to achieve better frequency regulation in system.

4.3.2 Flywheel Energy Storage

A Flywheel Energy Storage (FES) system mainly comprises a Flywheel (rotor), motor/-generator, power conversion system and magnetic bearings [67]. Flywheel is a mechanical battery that stores energy in the form kinetic energy. FES takes electrical energy as the input to accelerate the rotor and stores it in the form of mechanical energy. When required, this stored energy is converted to electrical energy by using the same motor/generator [114]. Permanent magnetic motors dispense higher energy density due to higher magnetic flux as compared to an induction motor. Reduction of mechanical and aerodynamic fric-

tion can be achieved by using magnetic bearings and by operating the flywheel in vacuum [67].

The amount of stored energy is high in the case of a flywheel having lower mass density and higher tensile strength. Stored energy in FES is given by $E = \frac{1}{2}I\omega^2$, where I is the moment of inertia and ω is the angular velocity. For a fixed shape flywheel, moment of inertia is constant and hence, angular velocity is the only measure of stored energy.

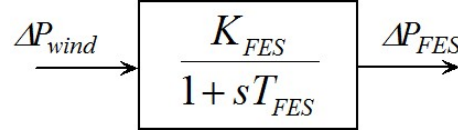


Fig. 4.6: Flywheel energy storage

The small signal model of FES can be represented as a first order model by considering the change of stored energy Q in an energy storage device equal to the difference between the grid power P_G and load demand P_D multiplied by efficiency. A simple model of the flywheel system given in [114] (see Fig. 4.6)

$$\frac{dQ_{fw}}{dt} = (P_G - P_D)f - \frac{1}{T_{fw}}Q_{fw}, \quad (4.9)$$

where $T_{fw} = \frac{I_{fw}}{2B_{loss}}$. The above equation gives a first-order approximation of flywheel system with load demand P_D and grid power P_G . The energy stored in the flywheel acts as a buffer between the grid and the load [114]. The economic benefits of using FES in conjunction with wind power plants in frequency control, and load leveling have been reported in literature [69, 115, 116].

4.4 Case Studies

The wind integrated AGC model is analyzed for the following cases.

- Case 1 - Thermal-Thermal System
- Case 2 - Hydro-Thermal system

4.4.1 Case-1: Thermal-Thermal System

4.4.1.1 System Configuration

Fig. 4.7 shows a sample AGC system on which investigations have been carried out. The system comprises a two area thermal dominated interconnected system with wind integration considering Generation Rate Constraints and Governor Dead Band non linearities. Area-1 consists of two reheat thermal power generation units with wind integrated system and Area-2 comprises two non reheat thermal units. Typical values of Generation Rate Constraints (GRC) considered for non-reheat and reheat thermal units are 10%/min and 3%/min respectively [99, 117]. Regulatory agencies such as NERC [118], has specified governor deadband settings to be within ± 36 mHz [$0.06\% \times$ nominal frequency]. Hence, a typical value of 0.06 % is considered for governor dead-band non-linearity as well [119]. The governor deadband non-linearity has a destabilizing effect on the load-frequency control of a power system [119]. K_{I1} and K_{I2} are the integral gain settings in Area-1 and Area-2 respectively. The nominal parameters of the system are given in Appendix.

In recent years, a control area has been a mixture of conventional units such as hydro and thermal power generating units along with DFIG based wind turbines generators. On increase in the wind penetration level in the control area affects the droop settings and system inertia: equivalent droop increases whereas system inertia constant decreases. This result in the deterioration of system frequency regulation capability of the system in the absence of any frequency support from DFIG [46]. The change in system droop is given by [66]

$$R_{new} = \frac{R}{(1 - L_P)} \quad (4.10)$$

and change in system inertia given by [66]

$$H_{new} = H \times (1 - L_P) \quad (4.11)$$

where L_P is the wind penetration level, i.e., the percentage reduction in the existing gen-

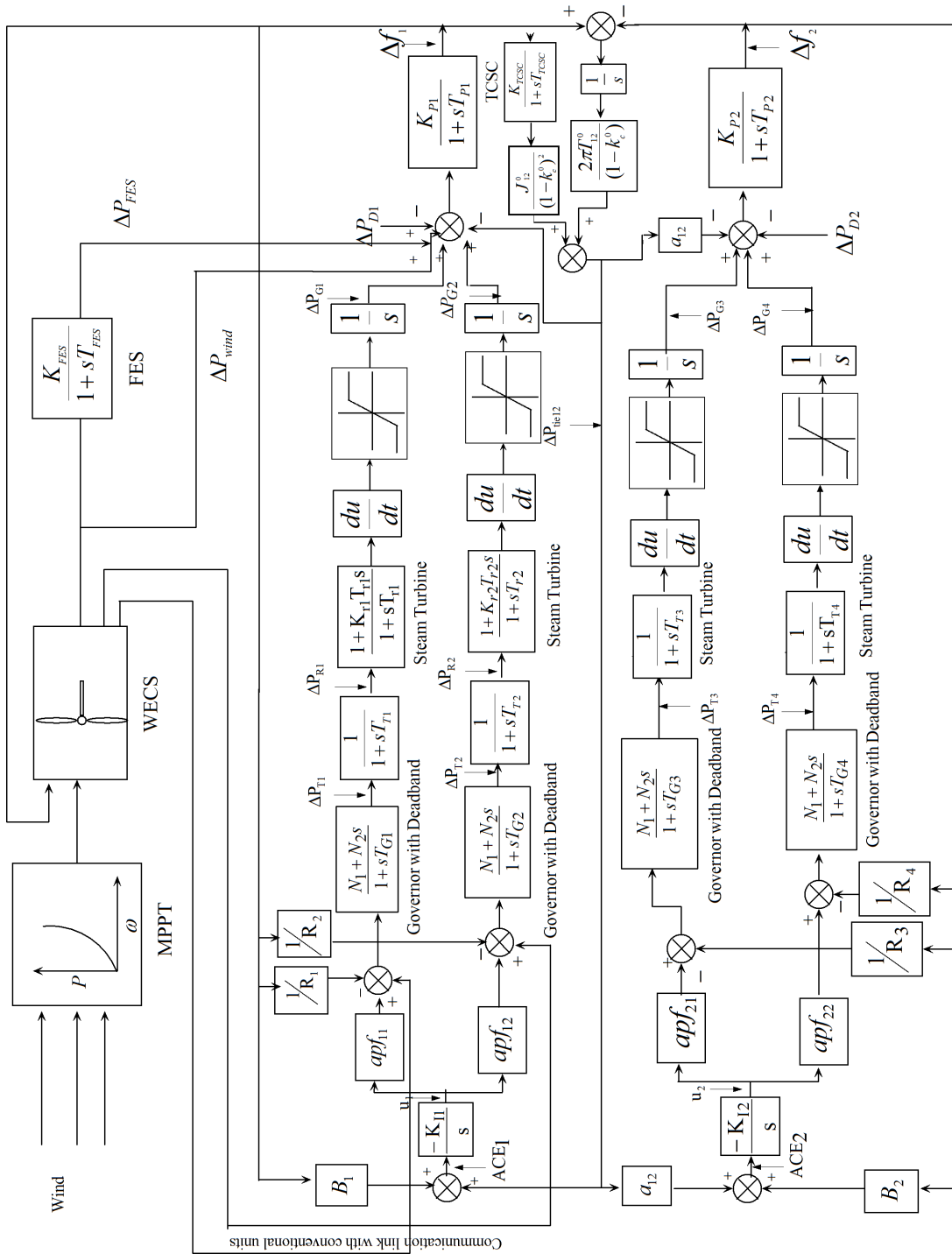


Fig. 4.7: Two-area thermal-thermal test system with WECS, FES and TCSC

erating units.

4.4.1.2 Particle Swarm Optimization

Particle Swarm Optimization (PSO) is a population based stochastic technique introduced by Kennedy and Eberhart [120]. It is modeled through simplified social model simulation inspired by bird flocking, fishing schooling and swarm theory. This optimization techniques finds application in wide variety of areas including combinatorial optimization, different types of controls including adaptive inverse, predictive or PID controls, design applications, optimization of reflect array antennas and fault tolerant power systems [121]. PSO is a computational intelligence based technique that is not largely affected by the size and nonlinearity of the problem, and can converge to the optimal solution where most analytical methods fails to converge [122]. Further, easier implementation, adjustment of fewer parameters, requirement of relatively lesser memory are the added advantages.

PSO operates by simultaneously keeping candidate solutions in a search space. Candidate solutions are evaluated by objective functions which are being optimized to find out fitness of that solution during each iteration [122]. Candidate solutions can be initialized randomly. Particle position is the candidate solution and velocity is updated during each iteration as

$$v_i(t + 1) = wv(t) + C_1R_1(g_{best} - cur) + C_2R_2(p_{best} - cur) \quad (4.12)$$

The first term in the above equation is momentum term, which signifies that its velocity cannot be changed abruptly. Second term shows cognitive thinking, i.e., contribution from its own experience while the third term highlights social behavior, collaboration among particles to choose the optimal value [2]. In a nutshell, the three main steps of PSO that occur in each iteration are

1. Evaluation of fitness of each particle
2. Updating individual and global fitness and positions

3. Updating velocity and position of each particle

A flow chart of PSO technique is given in Fig. 4.8. The parameters used for this analysis is tabulated in Table-1 for which there are no strict methods. Experience of the designer and the application for which PSO is being used play a crucial role in the PSO parameter selection. The computation accuracy and efficiency also depends on how the problem is being formulated.

Optimization of Integral Gains Using PSO

In this work, PSO is used to optimize the integral gains. Simulations are done (a) without wind support, (b) with wind support alone and (3) with wind support and FES-TCSC combination.

Automatic Generation Control maintains frequencies and tie-line power flows at scheduled values at the same time keeping settling time and overshoot as low as possible. An objective function that takes into account, the wind power generation change (ΔP_{wind}) in addition to frequency perturbations (Δf_1 and Δf_2) and tie-line power deviation (ΔP_{tie12}) is formulated to tune the controller gains as given below.

$$J = \int_0^t [\Delta f_1^2 + \Delta f_2^2 + \Delta P_{tie12}^2 + \Delta P_{wind}^2] dt \quad (4.13)$$

J is minimized for 1% step load perturbation in Area-1 to obtain the optimum values of K_{I1} , K_{I2} , K_P and K_I . The PSO parameters used for tuning are given in Table 4.1.

Table 4.1
PSO parameters

No of Birds	100
Bird Step	100
PSO parameter C_1	1.8
PSO parameter C_2	2.1
PSO momentum or inertia w	1.4

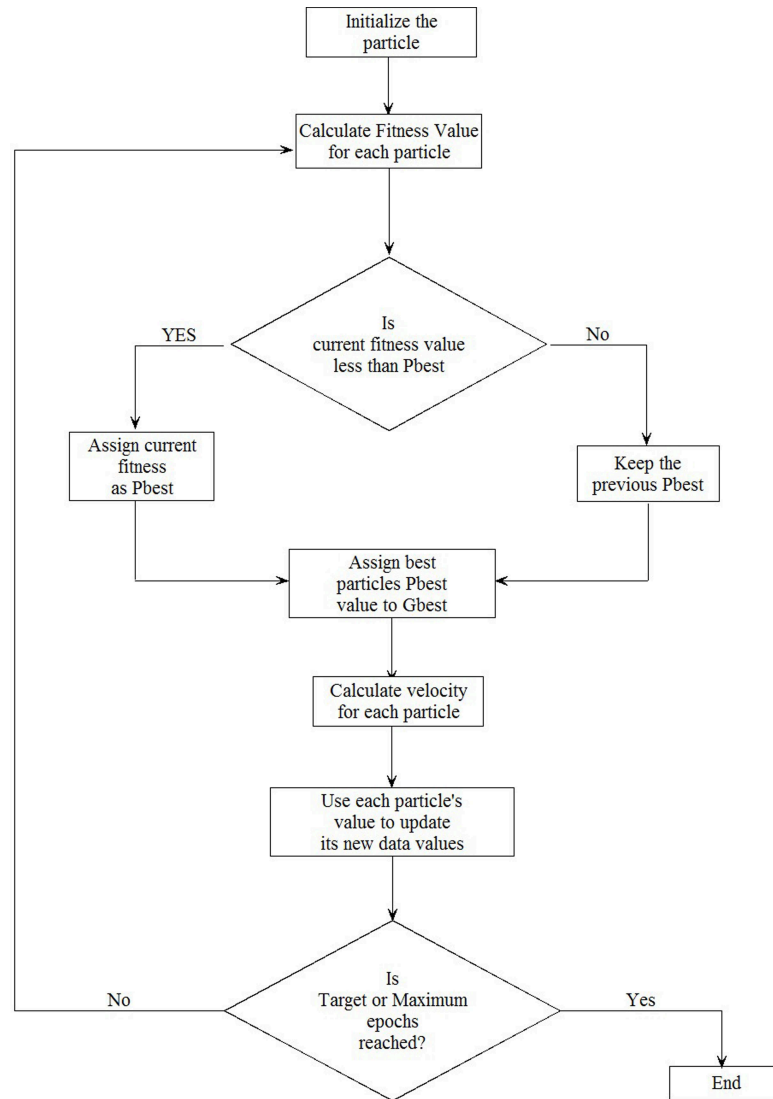
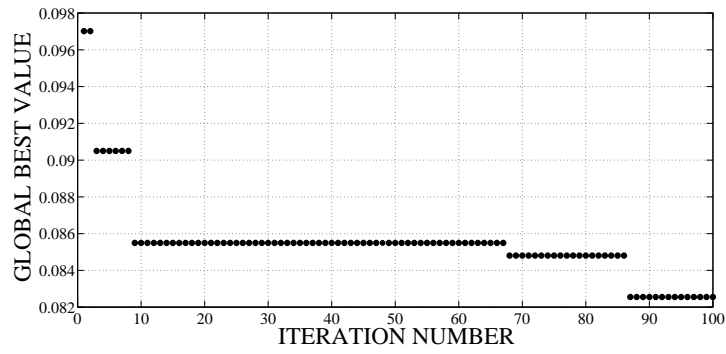


Fig. 4.8: PSO Flow Chart [2]

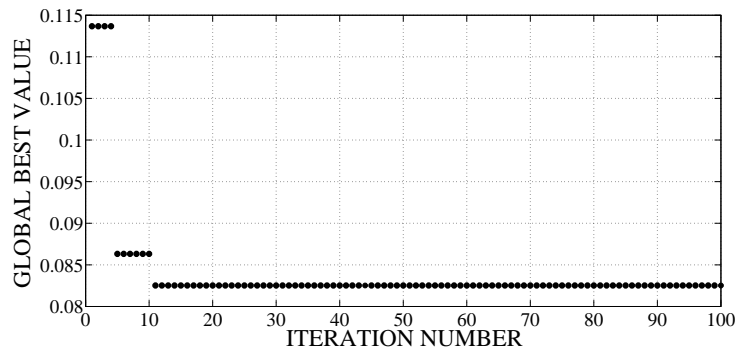
The optimal values of controller gains in the speed recovery loop of WECS obtained are used in the simulation studies. It is seen that the K_P values decreases with wind penetration level while K_I values increases. Also, the integral values of the control areas increase with wind penetration level. The optimized gain settings for (1) 10% wind penetration, (2) 20% wind penetration and (3) 30% wind penetration for Areas-1 and 2 are given in Table 4.2. Presented in Fig. 4.9 are plots showing the global best value versus iteration no. for different cases.

Table 4.2
Optimum values of controller gains for 1% step load perturbation in Area-1 for various cases

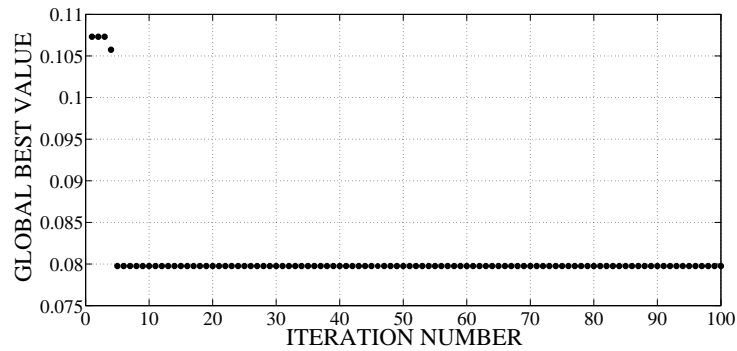
Parameters	Without wind support			With wind support			With wind support and TCSC-FES combination		
	10%	20%	30%	10%	20%	30%	10%	20%	30%
K_{I1}	0.1236	0.1197	1.103	0.2547	0.2768	0.0969	0.1180	0.1287	0.1404
K_{I2}	0.0200	0.0226	0.0025	0.0762	0.0852	0.0095	0.5144	0.5517	0.5886
K_P	-	-	-	0.3698	0.4434	0.4270	2.3235	1.4901	1.1356
K_I	-	-	-	0.0064	0.8260	0.0394	1.6511	1.8538	1.9807



(a) Without wind support



(b) With wind support



(c) With wind support and TCSC-FES

Fig. 4.9: Iteration vs fitness values obtained from PSO optimization for 10% wind penetration

4.4.1.3 Results and Discussions

The power system model shown in Fig. 4.7 is simulated using MATLAB[®]R2013b for the system data given in Appendix. A TCSC is placed near area-1 considering 50%

compensation and FES system placed near to Area-1. Studies are carried out on AGC with wind penetration, for three different possibilities as given below

- Case 1: 10% Wind Penetration
- Case 2: 20% Wind Penetration
- Case 3: 30% Wind Penetration

A comparison has also been done with the existing model available in [54].

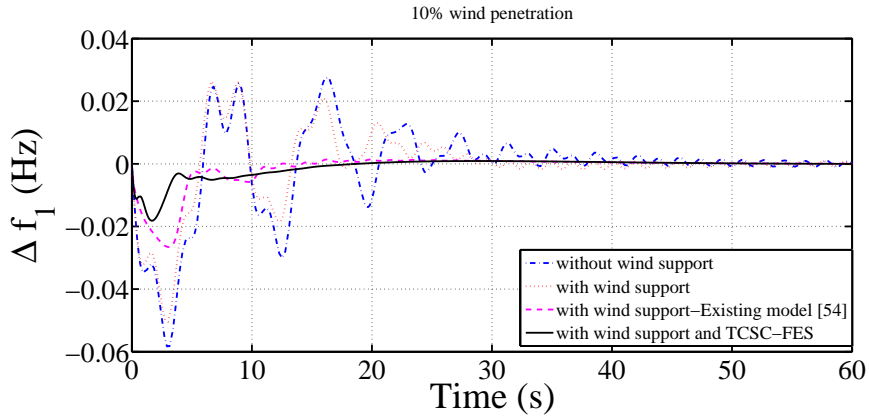
Case 1: 10% Wind Penetration

The dynamic responses for the three combinations: (a) without wind support, (b) with wind support and (c) with wind support TCSC-FES are plotted in Figs. 4.10-4.11. With TCSC-FES combination, the transient response is improved in terms of ripples as well as settling time. Fig. 4.10 shows improvement in the deviations in area frequencies (Δf_1 & Δf_2) and tie-line power flow (ΔP_{tie12}) with TCSC-FES combination in comparison with that of with wind support alone and without wind support cases. It is clear from Fig. 4.11 that loading in Area-1 results in corresponding increase in the power generation in the thermal units of Area-1. With wind integration alone, the inertia contribution from the conventional system reduces considerably, resulting in large frequency nadir. This can be reduced by providing an extra inertia support from wind turbines through inertia control. The TCSC-FES combination, in addition to wind support, helps to reduce this low inertia problem to a greater extent.

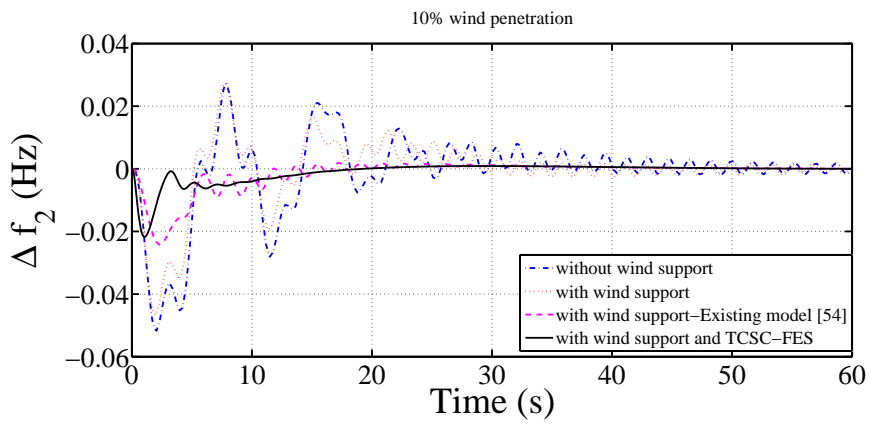
It is evident from Fig. 4.10 that during power imbalance, the system frequency deviates widely when wind turbines are not supporting primary frequency control. It establishes the well known fact that without any auxiliary control like inertia control or active power control, DFIG based WTG does not take part in frequency control. It can also be observed that, with primary active power control, WTG releases the stored kinetic energy from rotor to the grid, thereby, improving the frequency regulation using synthetic inertia. It is also well clear from the plots that, with TCSC-FES combination the frequency nadir point gets improved and satisfies the prevailing grid codes [118] with fast settling in a short duration of time.

At steady state, the excess load is shared between the conventional sources based on their area participation factor(see Fig. 4.11(a) and Fig. 4.11(b)) [$\Delta P_D = \Delta P_{G1} + \Delta P_{G2} = apf_{11} \times 0.1 + apf_{12} \times 0.1 = 0.06 + 0.04 = 0.1$]. Fig. 4.11(c) shows the additional power injection from wind turbines during the load disturbance in Area-1. The power injection from the wind turbine reduces considerably with TCSC-FES combination due to the extra power support from FES in the event of load perturbation. Hence, it can be concluded that, excess power available from the wind energy system is stored as kinetic energy in flywheels during off peak periods. At the same time in the event of load perturbation during peak hours, this stored energy in the FES is dispatched back to grid for energy balancing. This in turn enables the wind turbines to run their rotor at near optimal speed even when load disturbances occur.

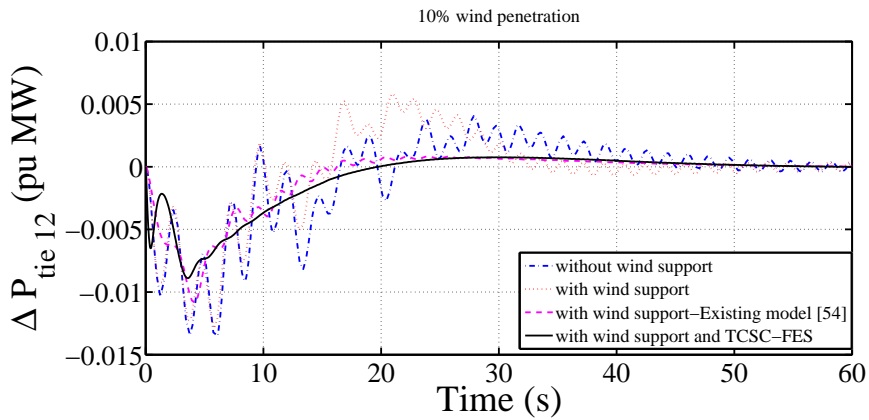
The responses of thermal power plants are slower than that of wind turbines. Thermal units have longer time constants [44]. However, the power electronic converters associated with WTG are fast switching with shorter time constant. Hence, the response of thermal power plant in Fig. 4.11(a) and Fig. 4.11(b) are naturally slower than wind turbine response in Fig. 4.11(c).



(a) Deviation in frequency of Area-1

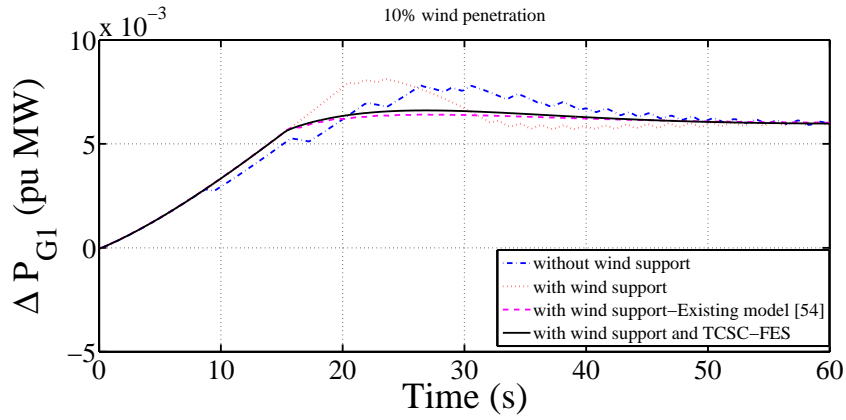


(b) Deviation in frequency of Area-2

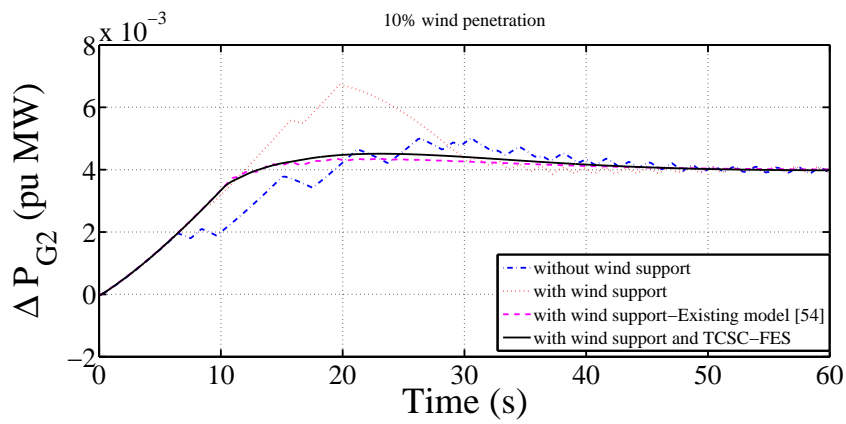


(c) Deviation in tie-line power flow

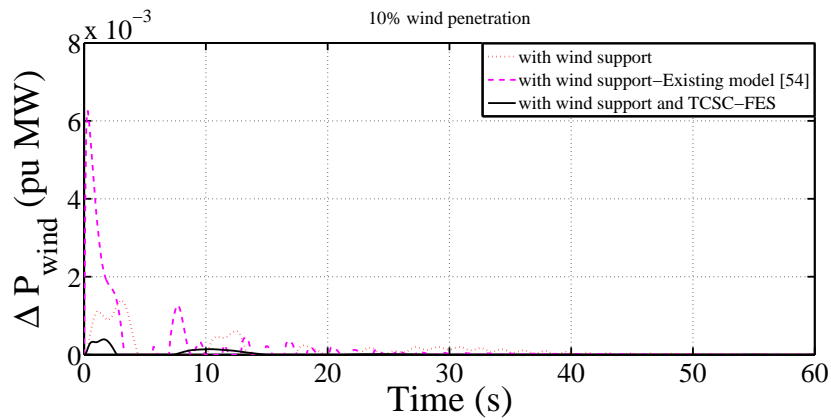
Fig. 4.10: Variations in area frequencies (Δf_1 and Δf_2) and tie-line power (ΔP_{tie12}) when load change in Area-1 for 10% wind penetration



(a) Deviation in power output of reheat thermal plant-1 in Area-1



(b) Deviation in power output of reheat thermal plant-2 in Area-1



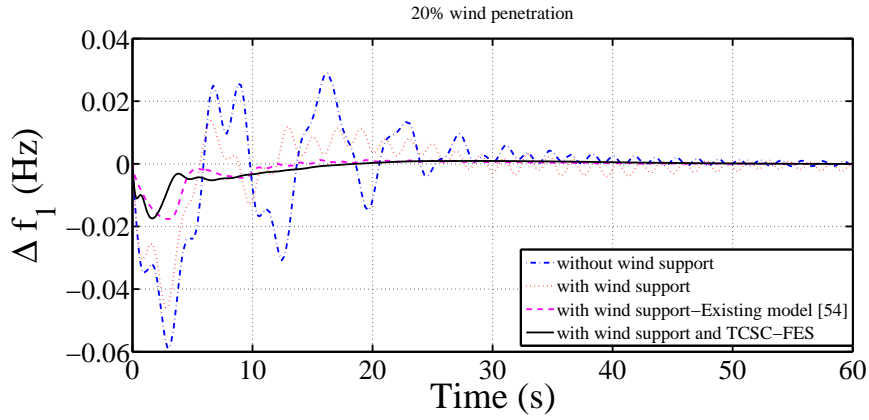
(c) Deviation in power injected from WECS

Fig. 4.11: Variations in power generations in Area-1 (ΔP_{G1} , ΔP_{G2}) and deviation in the injected wind power (ΔP_{wind}) when load change in Area-1 for 10% wind penetration

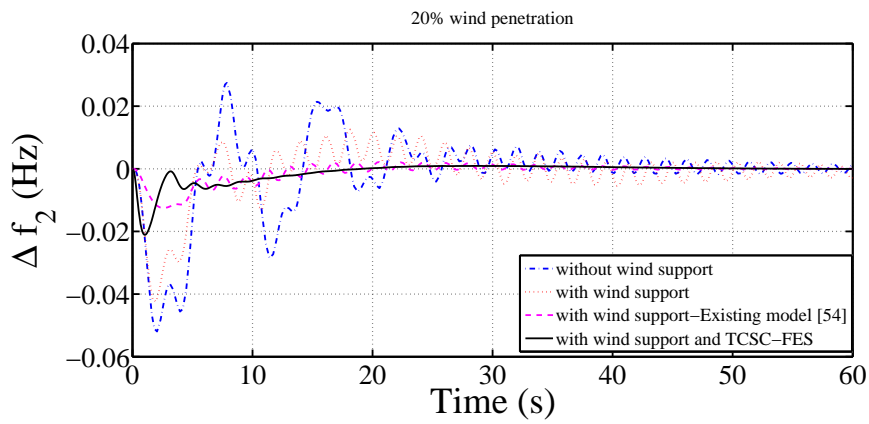
Case 2: 20% Wind Penetration

Figs. 4.12-4.13 depict the corresponding simulation results for the following three scenarios: (a) without wind support, (b) with wind support and (c) with wind support and TCSC-FES combination. It may be noted that with TCSC-FES, the transient oscillations and settling times have been reduced and the deviations in area frequencies (Δf_1 and Δf_2) and tie-line power flow (ΔP_{tie12}) vanish to zero relatively faster. It is also evident that as the wind penetration level increases, the system shows more oscillatory behaviour in their responses. Hence, TCSC could be considered as a suitable choice to damp out these oscillations in high wind penetrated system.

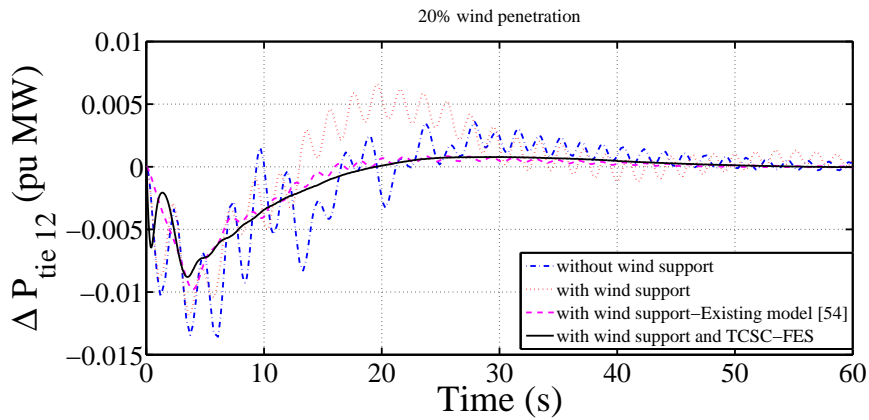
Fig. 4.13(c) shows the extra power injected from the wind power plants during frequency excursion. With TCSC-FES combination, the change in power output of wind turbine has been reduced considerably. This is due to power support from the FES, which acts as an auxiliary source. Thus, it allows the rotor speed of WTG to vary over a narrow band and hence reduces the stress on WTG rotor during grid imbalances. Faster response of FES enables the grid to balance faster, thereby, letting WTG release less energy as previously supplied to the grid.



(a) Deviation in frequency of Area-1

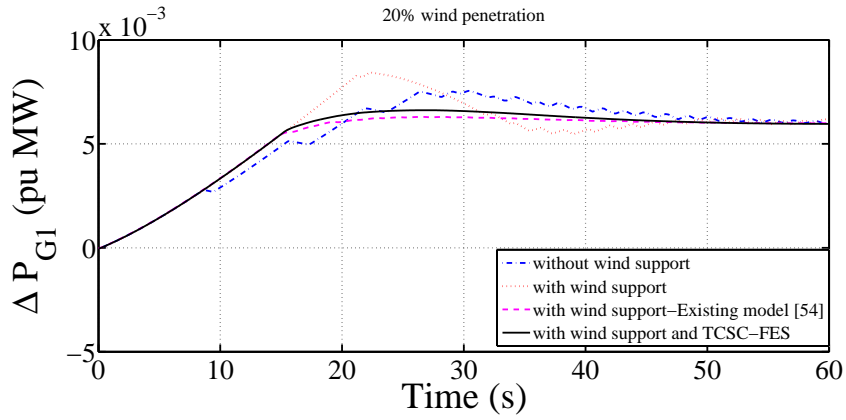


(b) Deviation in frequency of Area-2

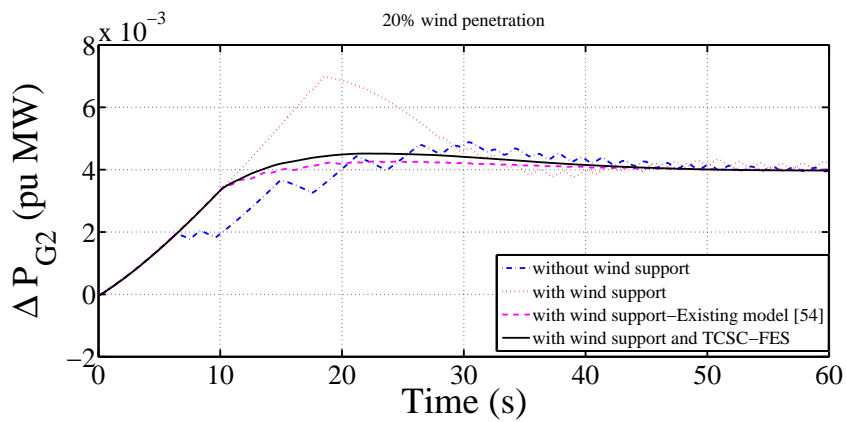


(c) Deviation in tie-line power flow

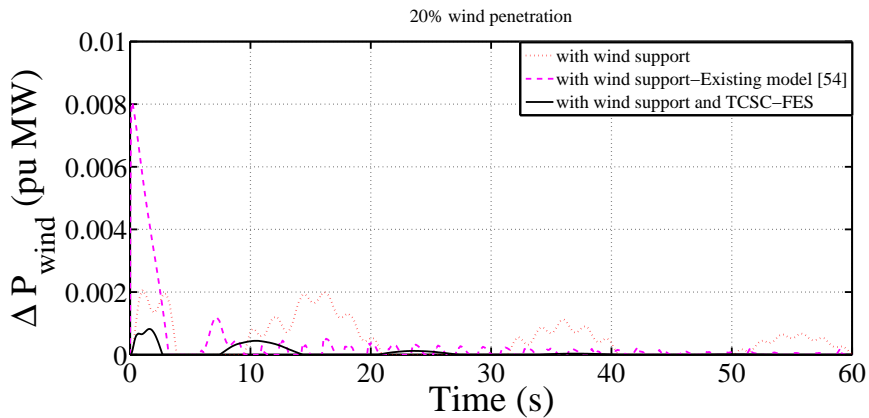
Fig. 4.12: Variations in area frequencies (Δf_1 and Δf_2) and tie-line power (ΔP_{tie12}) when load change in Area-1 for 20% wind penetration



(a) Deviation in power output of reheat thermal plant-1 in Area-1



(b) Deviation in power output of reheat thermal plant-2 in Area-1



(c) Deviation in power injected from WECS

Fig. 4.13: Variations in power generations in Area-1 (ΔP_{G1} , ΔP_{G2}) and deviation in the injected wind power (ΔP_{wind}) when load change in Area-1 for 20% wind penetration

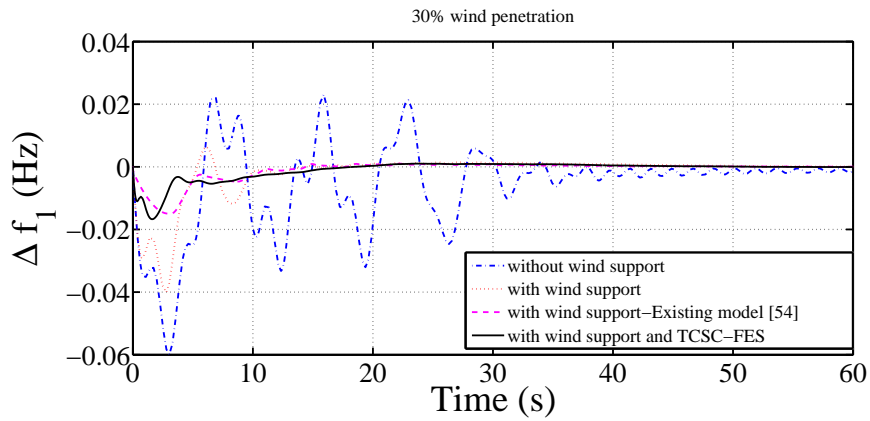
Case 3: 30% Wind Penetration

In this scenario, 30% wind penetration level is considered. Figs. 4.14-4.15 depict the corresponding simulation results for (a) without wind support, (b) with wind support and (c) with wind support and TCSC-FES combination. It is evident from Fig. 4.14 that without any support from wind turbines at 30% wind penetration level, area frequencies as well as tie-line power flow, takes more time to settle down to their respective scheduled values. Further, with wind support, both frequencies and tie power settle down faster as expected. It is clear from the simulation studies that, the TCSC-FES combination along with wind support, helps to achieve better performance in terms of overshoot, settling time and damping. As expected, TCSC in series with tie-line provides extra damping to system to damp out low frequency oscillations in both area frequencies and tie-power. FES in conjunction wind energy system provides the *frequency shaving effect* with fast responses to load demands.

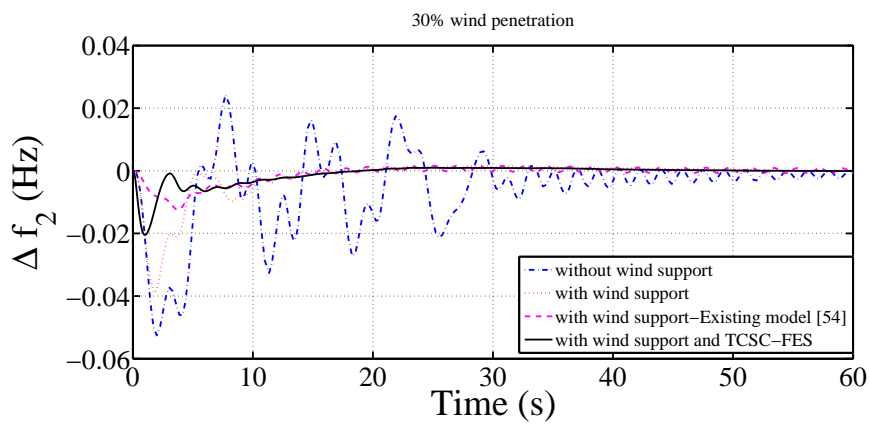
Figs. 4.15(a)-4.15(b) show the deviations in power output from the generating units in Area-1. As anticipated, the excess load demand is met by the thermal generating units in Area-1. With the TCSC-FES combination, it is evident that, the power output from the generating units settles down to their respective values with lesser overshoot and fast settling time. Fig. 4.15(c) reveals that with TCSC-FES combination the extra power injected from the WTG reduces considerably in comparison with case of wind support alone.

From above results, it is clear that as penetration level increases the effect of WECS is more significant whereas at low penetration levels role of TCSC-FES combination is more predominant.

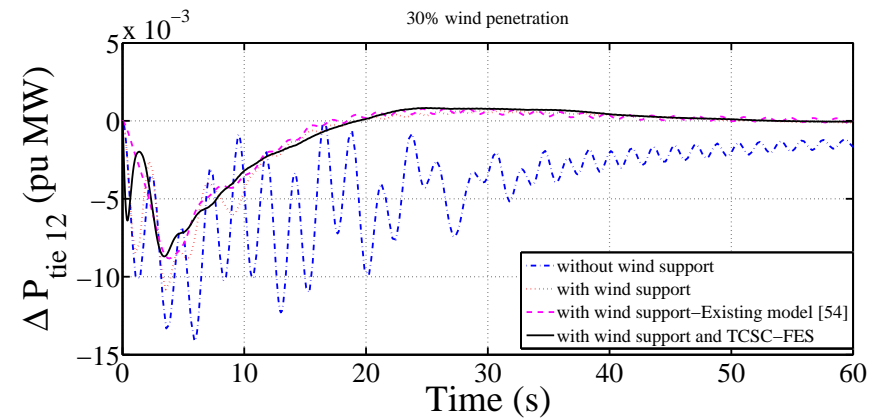
Since increasing wind power penetration results in lowering the overall synchronous inertia response of the system, synthetic inertia must be provided for better system reliability. Different methods to compensate for this inertia response includes various inertia emulation methods and fast acting energy storage such as FES to compile with the existing grid codes.



(a) Deviation in frequency of Area-1

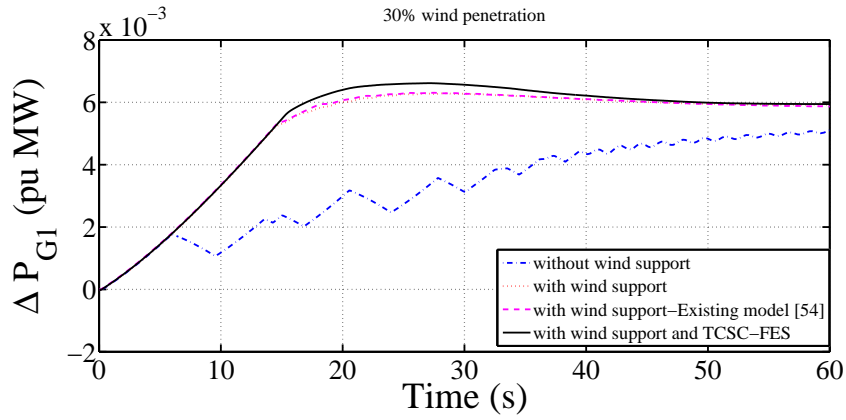


(b) Deviation in frequency of Area-2

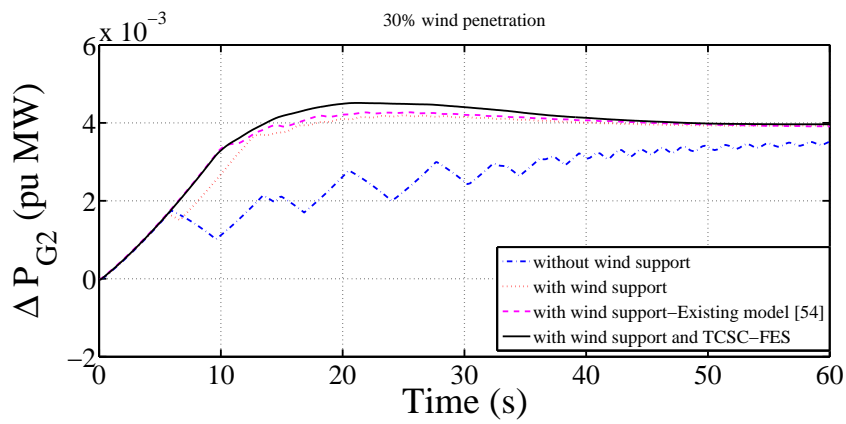


(c) Deviation in tie-line power flow

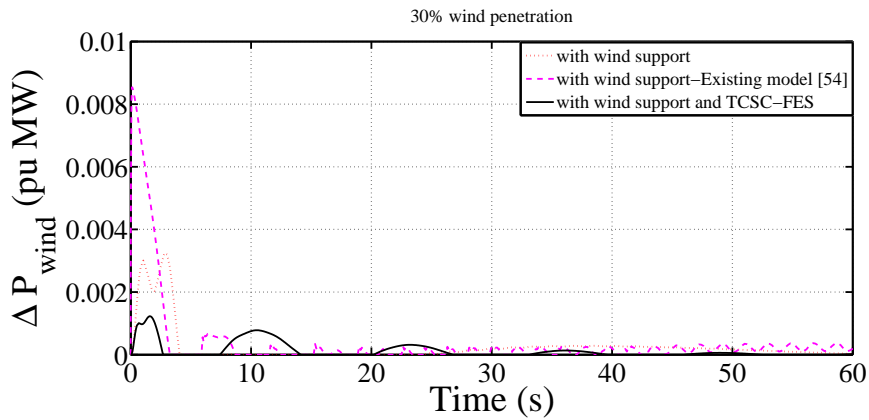
Fig. 4.14: Variations in area frequencies (Δf_1 and Δf_2) and tie-line power (ΔP_{tie12}) when load change in Area-1 for 30% wind penetration



(a) Deviation in power output of reheat thermal plant-1 in Area-1

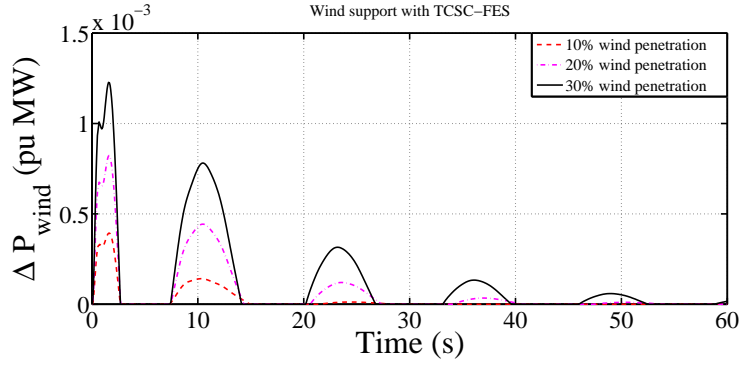


(b) Deviation in power output of reheat thermal plant-2 in Area-1

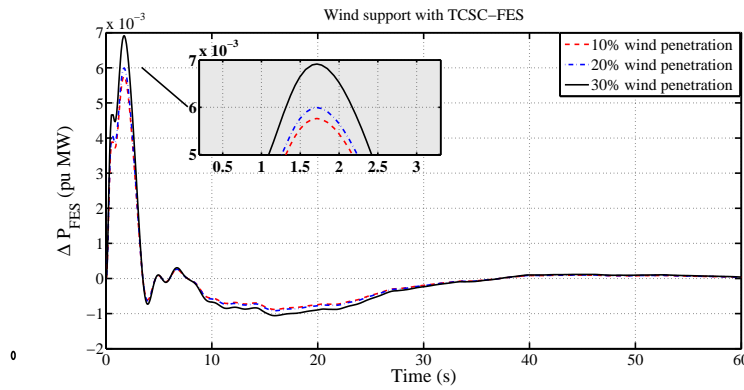


(c) Deviation in power injected from WECS

Fig. 4.15: Variations in power generations in Area-1 (ΔP_{G1} , ΔP_{G2}) and deviation in the injected wind power (ΔP_{wind}) when load change in Area-1 for 30% wind penetration



(a) Deviation in power output of wind power plant for different level of wind penetration level



(b) Deviation in power output of FES for different level of wind penetration level

Fig. 4.16: Variations in power output of wind power plant (ΔP_{Wind}) and power output of FES (ΔP_{FES}) for different penetration levels

Fig. 4.16(a) shows deviations in power generation from wind power plant for TCSC-FES combination during grid disturbances. It is clear that, with increase in wind penetration level (30%) the power output from WECS on primary frequency control is more in comparison with low wind penetration levels (10%). This is due the considerable improvement in the inertia response from WECS. The power output from the FES system for TCSC-FES combination which is shown Fig. 4.16(b) remains more or less same at different penetration levels. As the wind penetration level increases, inertia response from WECS (equipped with inertia emulation techniques) also increases, which results in the same power output from the FES system.

A plot of variation in rotor speed versus time after 1% load perturbation with 30%

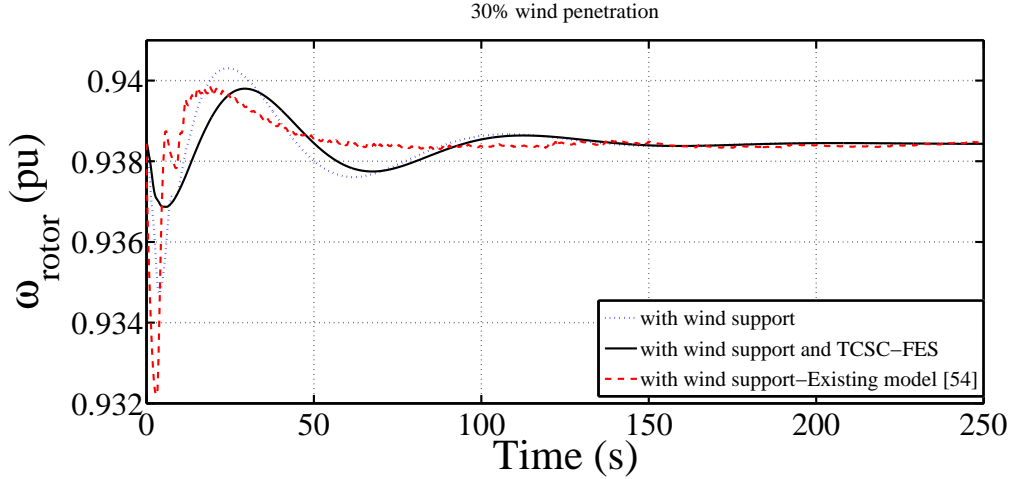


Fig. 4.17: WTG rotor speed variation during grid disturbance for 30% wind penetration

wind penetration level is presented in Fig. 4.17. In the presence of the TCSC-FES combination, the WTG rotor speed varies over a small range even for 30% wind level penetration. It can be observed that with our proposed scheme, the rotor speed varies over a narrow band (i.e., $\pm 10\%$ of the nominal rating, which is highly desirable), which helps WTG to continuously deliver its optimal power to grid without stepping out. This establishes that, during grid imbalances FES releases stored kinetic energy to supply extra demand for short duration. Thus, it allows the WTG to release less kinetic energy than it would otherwise allowing the WTGs to run close to their rated operating point. Hence, FES avoids WTG stalling out from service by releasing its stored energy during large grid disturbances.

4.4.2 Case-2: Hydro-Thermal System

4.4.2.1 System Investigated

The effect of high wind penetration on frequency control has also been examined on a hydro-thermal system as shown in Fig. 4.18. The two area hydro-thermal system consist of two reheat thermal generating units in Area-1 and two hydro generating units in Area - 2. The integral gains (K_{I1} and K_{I2}) of the control areas are optimally tuned to obtain better transient responses similar to thermal-thermal case. PSO is used to optimally tune the controller gains.

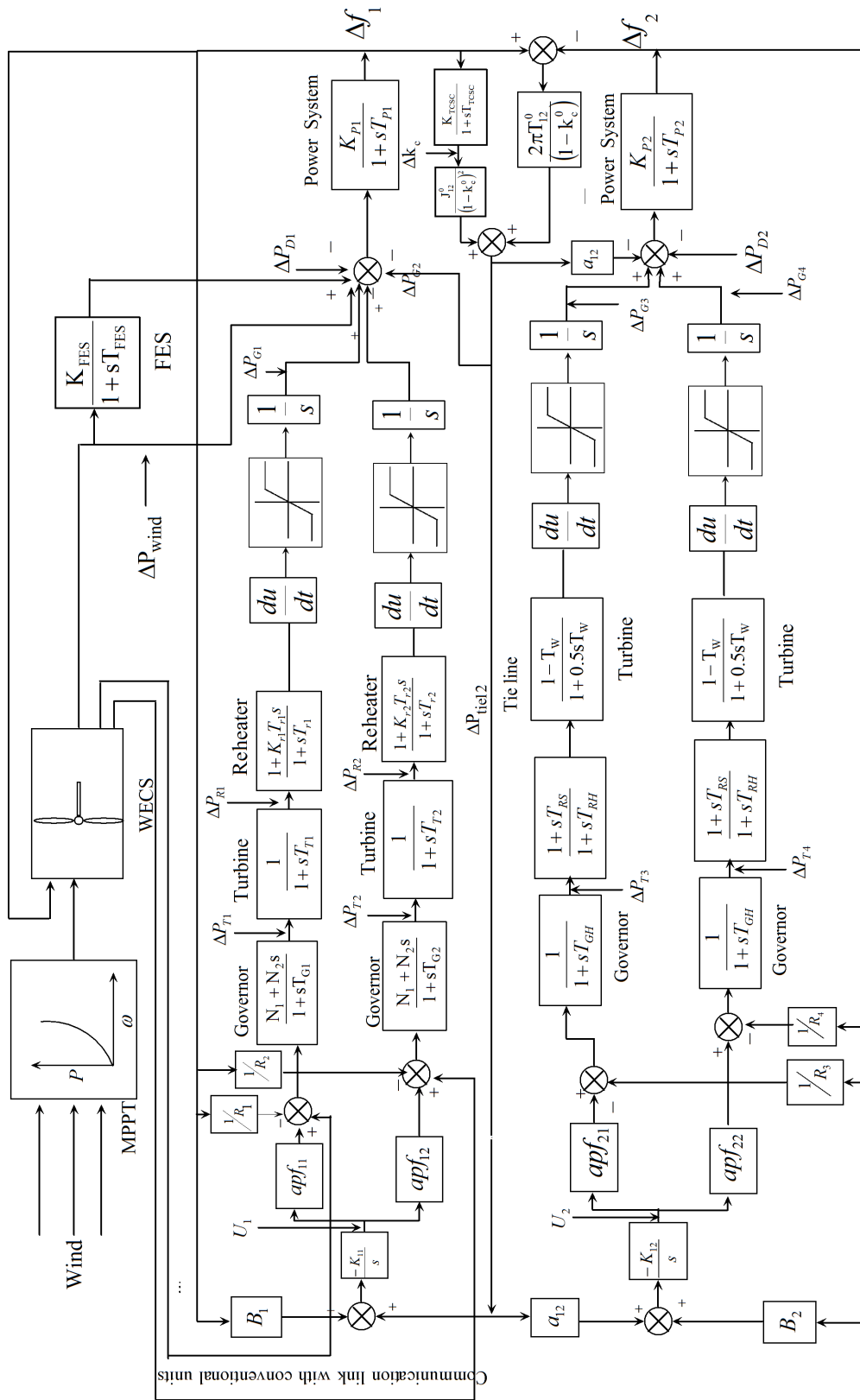


Fig. 4.18: Two-area hydro-thermal test system with WECS, FES and TCSC

Table 4.3
Optimum values of controller gains for 1% step load perturbation in Area-1 for various cases

Parameters	Without wind support			With wind support			With wind support and TCSC-FES combination		
	10%	20%	30%	10%	20%	30%	10%	20%	30%
K_{I1}	0.193	0.203	0.2218	0.2691	0.2704	0.2794	0.2768	0.3268	0.3568
K_{I2}	0.0942	0.1107	0.1296	0.0442	0.0484	0.0513	0.0852	0.0912	0.0942
K_P	-	-	-	2.0937	2.1504	2.256	1.9469	2.1469	2.674
K_I	-	-	-	2.415	2.573	2.962	8.089	7.289	6.315

Contoller Tuning

Controller gains are obtained by optimizing the objective function formulated as

$$J = \int_0^t [\Delta f_1^2 + \Delta f_2^2 + \Delta P_{tie12}^2 + \Delta P_{wind}^2] dt \quad (4.14)$$

J is minimized for 1% step load perturbation in area-1 to obtain the optimum values of K_{I1} , K_{I2} , K_P and K_I . Table 4.3 gives the optimal values of controller gains for different possible combinations.

4.4.2.2 Results and Discussions

Fig. 4.18 shows the two area hydro-thermal system with wind integration in Area-1. For analysis, TCSC is placed near to Area-1 in series with tie-line. FES is also placed near to Area-1. Three possible wind penetration levels are considered for AGC studies.

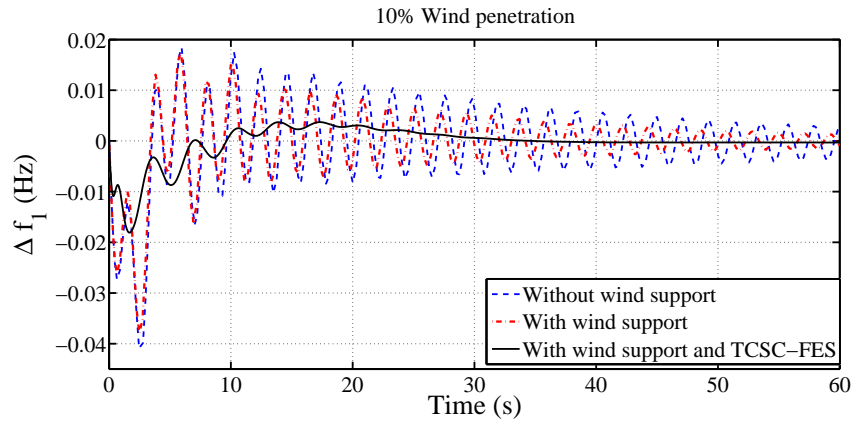
- Case 1: 10% Wind Penetration

- Case 2: 20% Wind Penetration

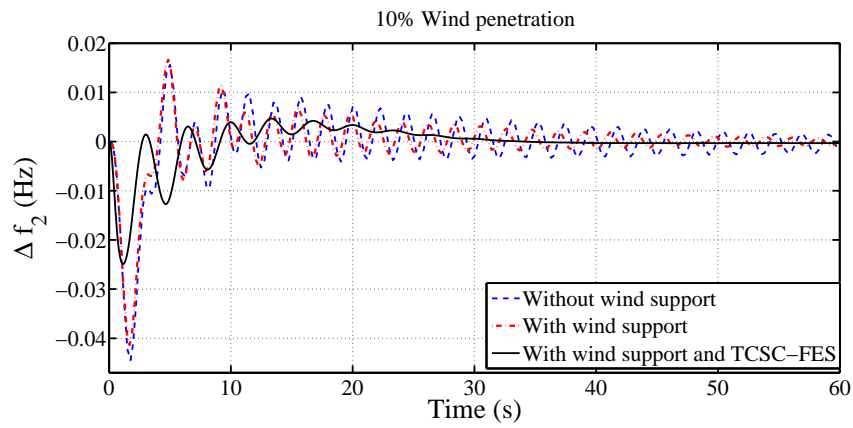
- Case 3: 30% Wind Penetration

Case 1: 10% wind penetration

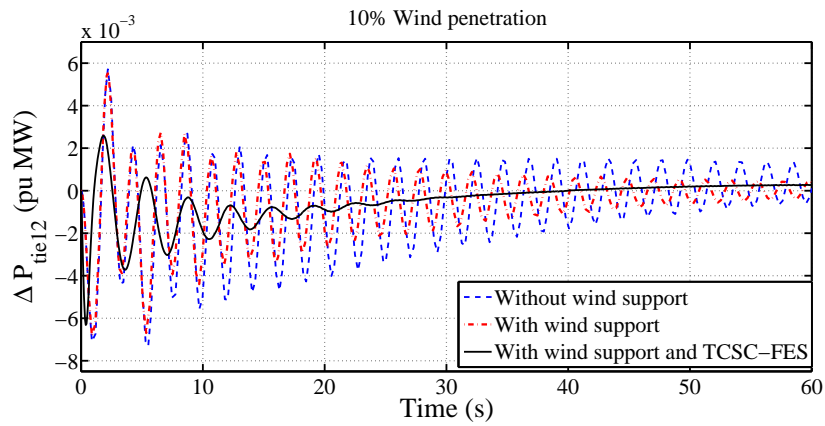
Figs. 4.19-4.21 show the dynamic responses of hydro-thermal system for three possible combination: (a) without wind support, (b) with wind support and (c) with wind support TCSC-FES. It is evident that with TCSC-FES combination, the system transient performance has improved in terms of ripples and settling time. As the load change has occurred in Area-1, it clear from Fig. 4.20(c) that load-demand is met by the conventional thermal generating units in Area-1. It is also observed that with TCSC-FES combination, the deviations in area frequencies and tie-line power flow has improved.



(a) Deviation in frequency of Area-1

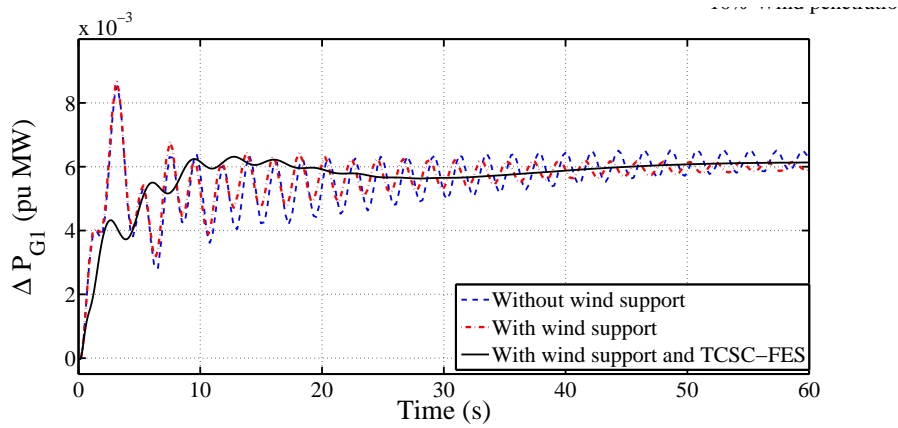


(b) Deviation in frequency of Area-2

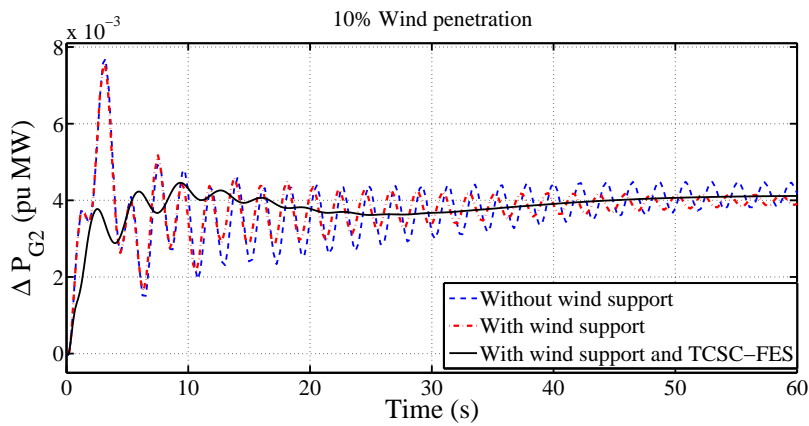


(c) Deviation in tie-line power flow

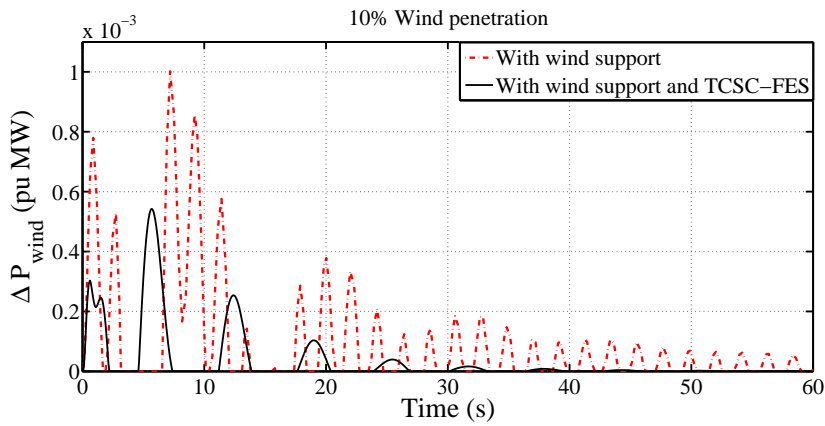
Fig. 4.19: Variations in area frequencies (Δf_1 and Δf_2) and tie-line power (ΔP_{tie12}) when load change in Area-1 for 10% wind penetration



(a) Deviation in power output of reheat thermal plant-1 in Area-1

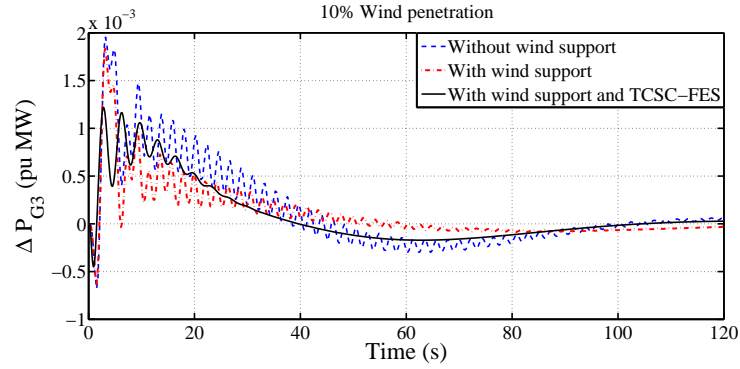


(b) Deviation in power output of reheat thermal plant-2 in Area-1

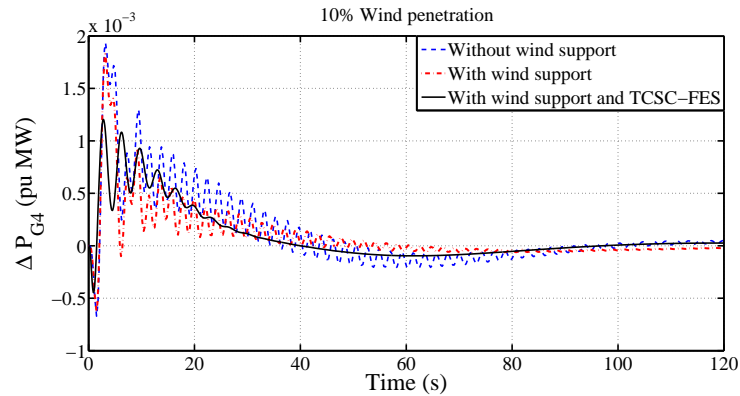


(c) Deviation in power injected from WECS

Fig. 4.20: Variations in power generations in Area-1 (ΔP_{G1} , ΔP_{G2}) and deviation in the injected wind power (ΔP_{wind}) when load change in Area-1 for 10% wind penetration



(a) Deviation in power output of hydro plant-1 in Area-2

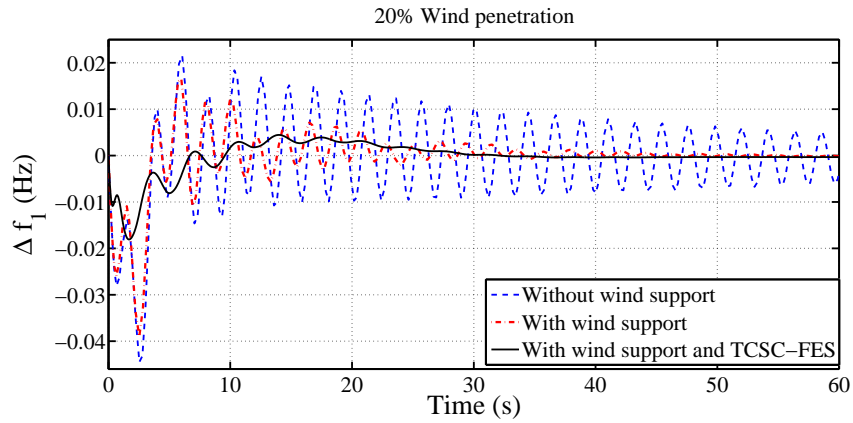


(b) Deviation in power output of hydro plant-2 in Area-2

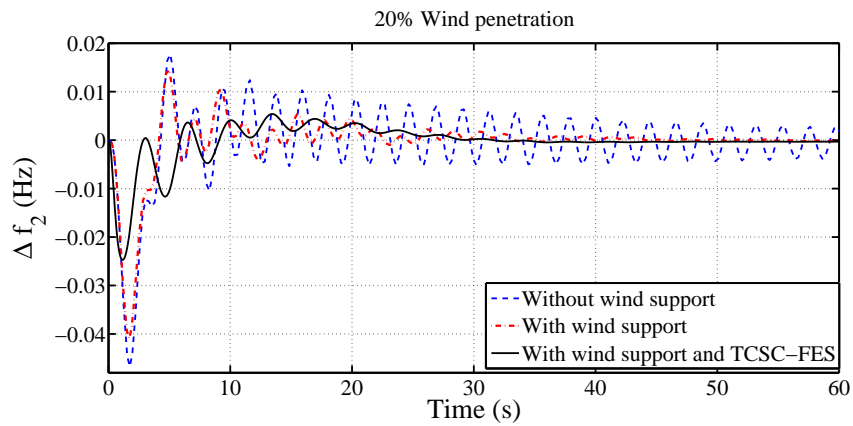
Fig. 4.21: Variations in power generations in Area-2 (ΔP_{G3} , ΔP_{G4}) when load change in Area-1 for 10% wind penetration

Case 2: 20% Wind Penetration

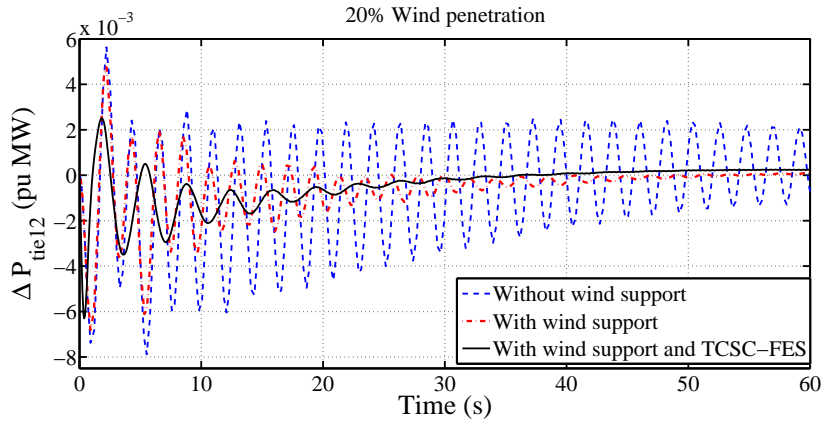
Figs. 4.22-4.24 shows the system dynamic responses for 20% wind penetration for following three scenarios: (a) without wind support, (b) with wind support and (c) with wind support and TCSC-FES combination. It is clear that with TCSC-FES combination, the transient performances such as settling time, overshoot of area frequencies and tie-line power flow has improved. FES acts as an auxiliary energy source during grid imbalances, thereby supplying a part of load immediately after perturbation. This results in considerably less kinetic energy from WTG rotor, thus rotor of WTG varies over the narrow range, that reduces the stress on WTG rotor. As already explained, TCSC-FES combination ensures a better inertial support from wind turbines.



(a) Deviation in frequency of Area-1

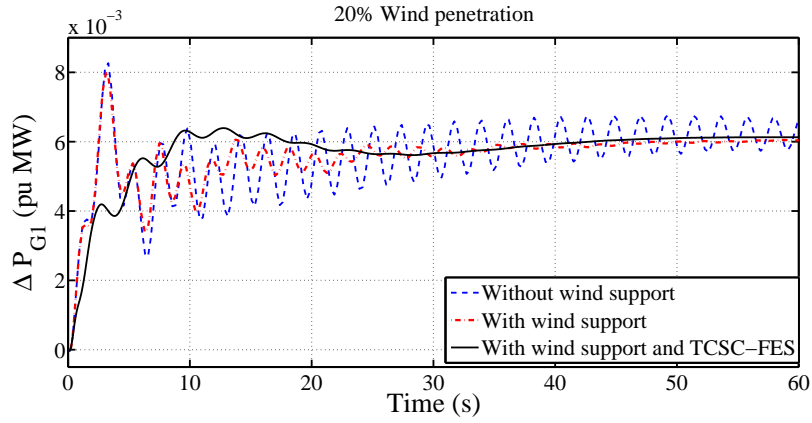


(b) Deviation in frequency of Area-2

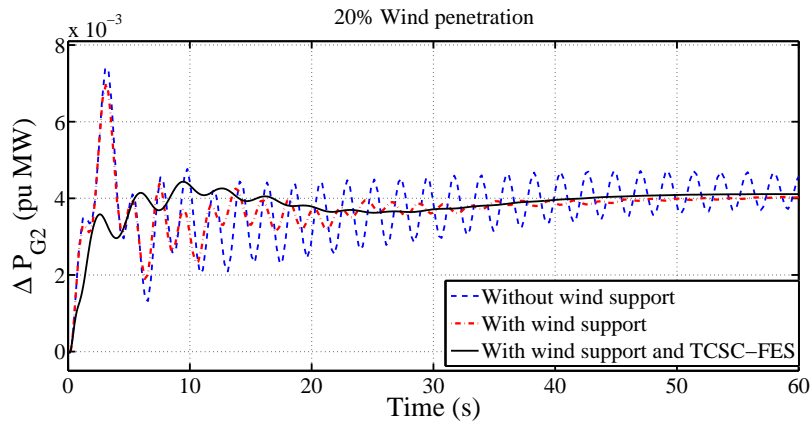


(c) Deviation in tie-line power flow

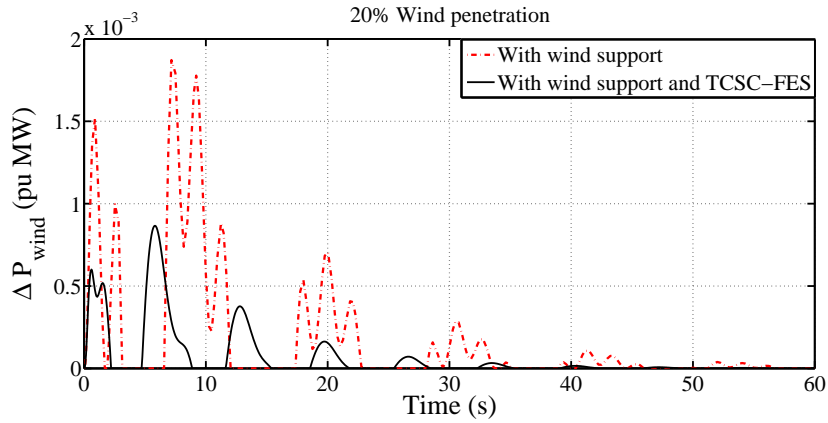
Fig. 4.22: Variations in area frequencies (Δf_1 and Δf_2) and tie-line power (ΔP_{tie12}) when load change in Area-1 for 20% wind penetration



(a) Deviation in power output of reheat thermal plant-1 in Area-1

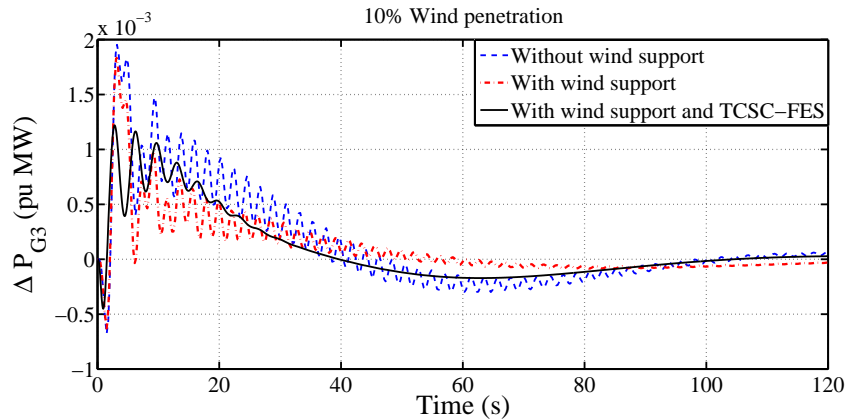


(b) Deviation in power output of reheat thermal plant-2 in Area-1

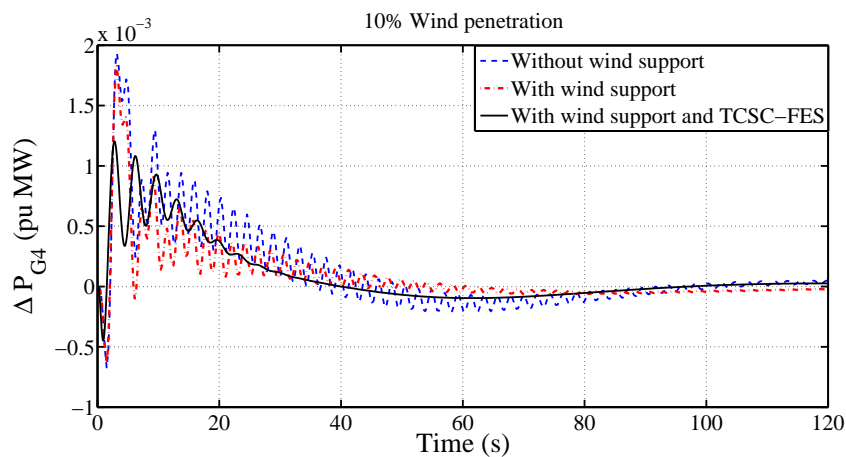


(c) Deviation in power injected from WECS

Fig. 4.23: Variations in power generations in Area-1 (ΔP_{G1} , ΔP_{G2}) and deviation in the injected wind power (ΔP_{wind}) when load change in Area-1 for 20% wind penetration



(a) Deviation in power output of hydro plant-1 in Area-2

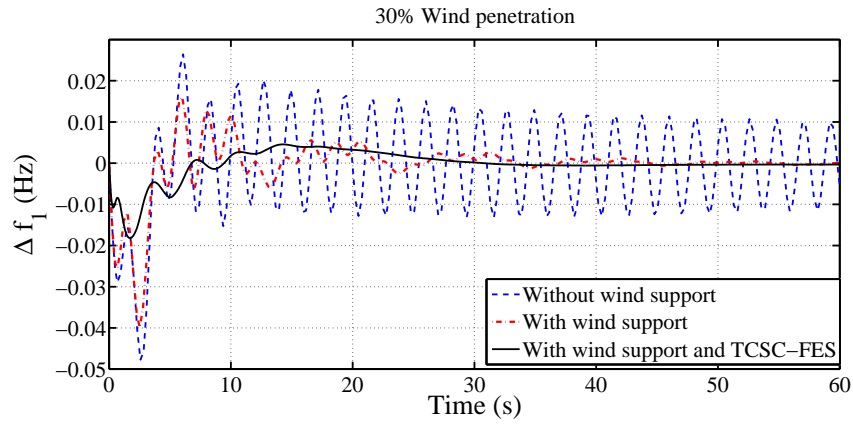


(b) Deviation in power output of hydro plant-2 in Area-2

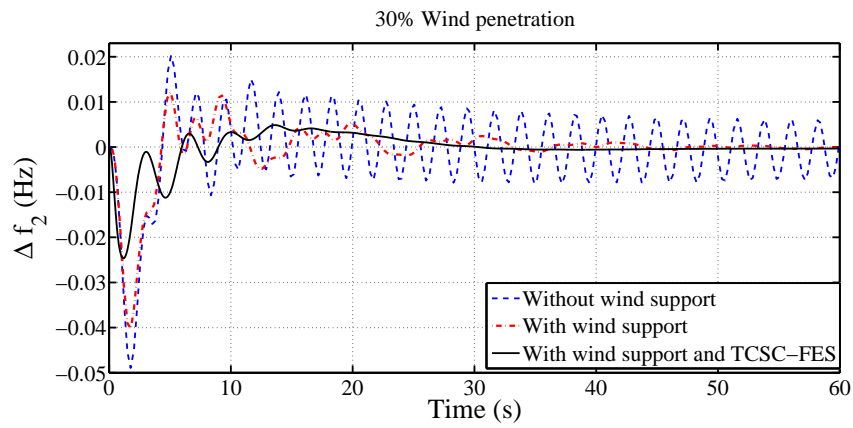
Fig. 4.24: Variations in power generations in Area-2 (ΔP_{G3} , ΔP_{G4}) when load change in Area-1 for 20% wind penetration

Case 3: 30% Wind Penetration

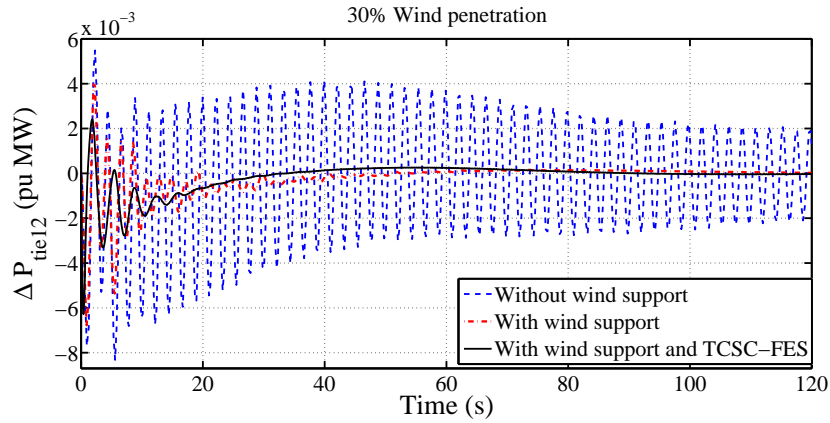
Figs. 4.25-4.27 show the system dynamic responses for hydro-thermal restructured power system with 30% wind penetration level. The results were obtained for (a) without wind support, (b) with wind support and (c) with wind support and TCSC-FES combination. It is evident from from Fig. 4.25 that without wind support case the system frequency dips much lower than other two cases. The increase in penetration level results in decrease in system inertia.



(a) Deviation in frequency of Area-1

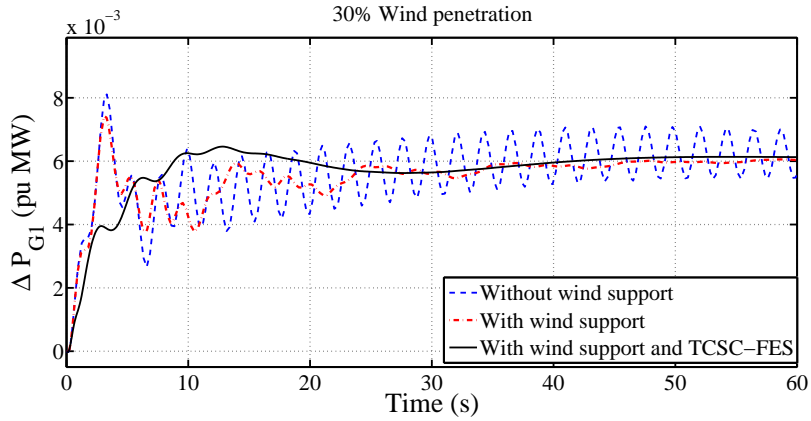


(b) Deviation in frequency of Area-2

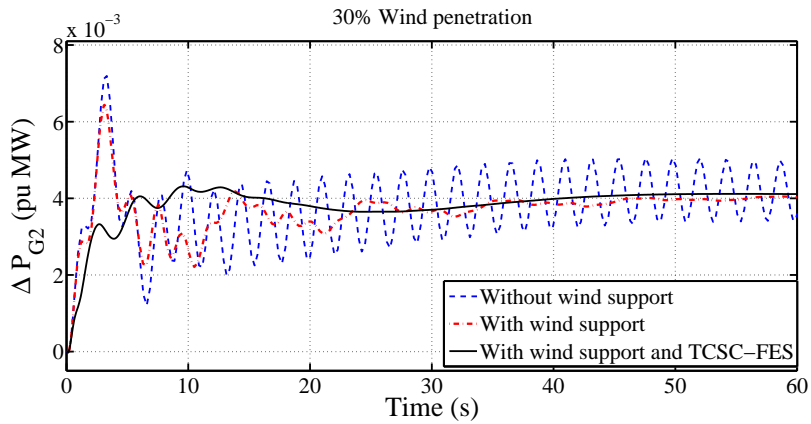


(c) Deviation in tie-line power flow

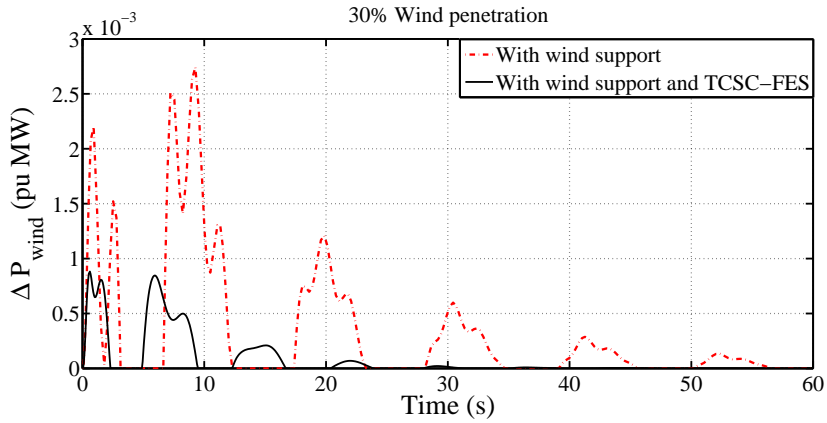
Fig. 4.25: Variations in area frequencies (Δf_1 and Δf_2) and tie-line power (ΔP_{tie12}) when load change in Area-1 for 30% wind penetration



(a) Deviation in power output of reheat thermal plant-1 in Area-1

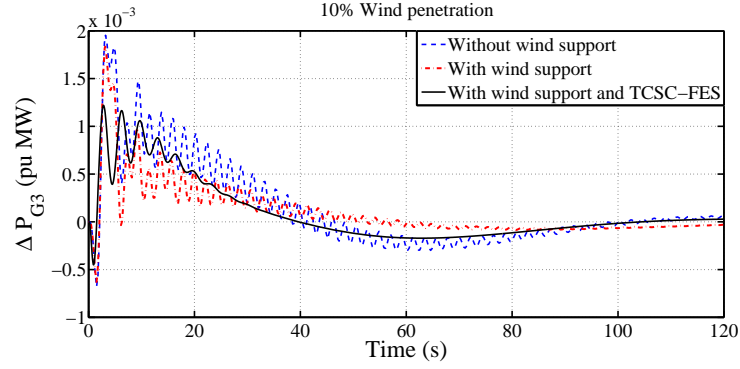


(b) Deviation in power output of reheat thermal plant-2 in Area-1

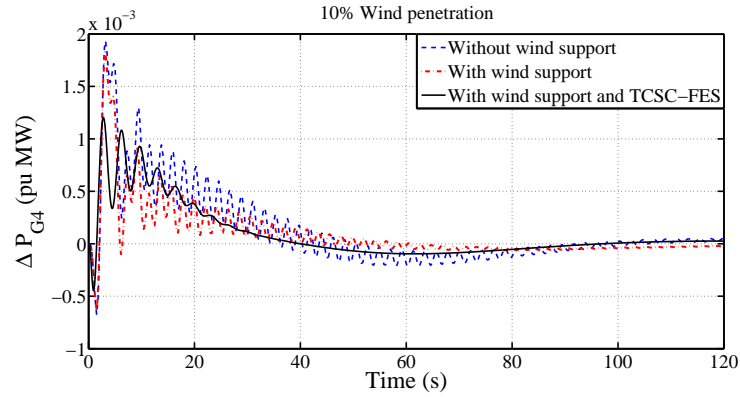


(c) Deviation in power injected from WECS

Fig. 4.26: Variations in power generations in Area-1 (ΔP_{G1} , ΔP_{G2}) and deviation in the injected wind power (ΔP_{wind}) when load change in Area-1 for 30% wind penetration



(a) Deviation in power output of hydro plant-1 in area-2



(b) Deviation in power output of hydro plant-2 in area-2

Fig. 4.27: Variations in power generations in Area-2 (ΔP_{G3} , ΔP_{G4}) when load change in Area-1 for 10% wind penetration

4.5 Summary

An attempt has been made to damp out the area frequency oscillations and tie-line power flow after a sudden load demand using TCSC-FES in an interconnected power system with wind integration. Both thermal-thermal and hydro-thermal cases have been analyzed. The proposed TCSC-FES combination with wind support has been used to study its effect in primary frequency support with 10%, 20% and 30% wind penetration levels. Particle Swarm Optimization has been used to tune the integral gain settings of both the areas as well as controller gains of speed recovery loop considering a quadratic performance index for the above three scenarios. It is found that in all the cases, the area frequency error becomes zero at the steady state. A comparison with existing method shows that with the

proposed method, dynamic responses have been improved in terms of settling time, peak overshoot and damping with the use of TCSC-FES in all the three cases. Further, it is clear that as the wind penetration level increases, the effect of WECS on primary frequency control is more pronounced while the effect of FES-TCSC is more predominant with low wind penetration levels.

Chapter 5

Load Following by Wind Power Plants

5.1 Introduction

The urge for reduction in carbon emission from fossil fuel powered energy sources and the availability of advanced technologies at reasonable cost have paved the way for integrating different clean and affordable renewable energy sources into the electric grid. Among the most widely used, Wind Energy Conversion Systems occupy significant share in the global installed capacity [81, 123, 124]. Variable speed Doubly Fed Induction Generator type wind turbine has become a favourite option due to their technical and economical benefits [125].

DFIG type Wind Turbine Generator (WTG) has power electronic interface/coupling between the rotor and grid, which prevents the release of stored kinetic energy from WTG rotor to grid during grid imbalances (normally termed as inertia control in conventional sources). Increase in wind penetration level reduces system inertia and thereby, urges the need for participation of WECS in primary frequency regulation. Available literature [46, 47, 63, 126–128] has suggested the synthetic inertia support from WECS, where kinetic energy stored in the rotating mass of WTG is released to the grid following a load perturbation. A supplementary control is initiated after the load change to release the stored kinetic energy from rotor of WECS, which is equipped with inertial control schemes. Inertia control leads to the slowing down of WTG rotor. Input to the WECS is the wind upon which no control can be exercised and for optimal operation, rotor must be brought back to its nominal speed. A speed recovery loop will be activated soon after the inertia control by absorbing energy from the grid. As per the existing literature, primary frequency support from WECS can be broadly classified into (a) primary control [46, 47, 126, 127] (b) droop control [63, 128] (c) de-loading technique [63, 128], and (d) speed recovery control [45, 50].

In many countries, electricity industries have undergone drastic changes from conventional monopolistic Vertically Integrated Utility (VIU) to competitive open market based deregulated power systems. Since electricity is considered as a commodity rather than a service in the new paradigm, it has to participate in open energy market or power exchanges. A trend in power market moving from old monopolistic market (owned by a single owner) to oligopolistic (a state of limited competition) then to open competitive market has introduced stress in power system operation. This transition creates challenges to system operators in maintaining power balance following the load perturbation. Since, separate entities namely GENCOs, TRANSCOs and DISCOs exclusively for generation, transmission and distribution are owned by different independent owners, there exists an uncertainty in maintaining generation - consumption equilibrium. In order to operate these entities in coherence, an independent entity namely Independent System Operator (ISO), capable of maintaining system power balance, takes the controls of other entities through proper ancillary service management. In this open competitive energy market, it is not mandatory for all GENCOs to contribute in frequency regulation. Any DISCO can make free and independent power contract with GENCOs in any control area.

With the emergence of power market, an increase in wind penetration level paved the participation of WECS to actively contribute in ancillary service management. Among various ancillary services, frequency control is important for maintaining the power balance in the open accessed interconnected power system. The availability of different forecasting algorithms to accurately predict the power output of wind power plants, enables the WECS to get involved in load following. This in turn enhances further capital investment in renewable integration. Our work focuses on analyzing the effect of wind energy system on load following in a deregulated power system with Flywheel Energy Storage (FES) system. In this thesis, WECS is considered as an independent GENCO so that it can actively participate in energy market under the supervision of Independent System Operator (ISO). WECS system under a particular power producer can have independent contract with DISCOs in same or different control areas through competitive bidding. Normally the energy biddings are done in day-ahead market, based on available prediction from forecasting algorithms. In this thesis, we have considered three cases.

- Operation under unilateral contract.
- With bilateral contract
- Contract violation

We have also extended a case of contract violation, where WECS violates the load contract that is already made in the energy market. Contract violation may be either a deficit or surplus power production from WECS due to the error in forecasting. The effect of FES system in enhancing the system regulation margin is also analyzed in this work.

Simulations have been carried with 30% wind penetration level using MATLAB[®]R2013b. A constant wind speed is assumed for the analysis.

5.2 Frequency Support from Wind Energy System

In traditional DFIG type WECS does not have any role in primary frequency regulation. Currently, various schemes have been proposed to operate them as conventional generating units in primary frequency control. Most of the proposed techniques utilize the instantaneous power reserve from WTG rotor. In this work, we have also considered a technique to emulate the stored kinetic energy from rotating mass of WTG. The schemes used in this work is shown in Fig. 5.1, which consist of

- Primary control
- Speed recovery
- Communication between WECS and the conventional units

Primary control is one of the inertia control technique which provides short term energy support during power imbalances. In this scheme, kinetic energy stored in the rotating mass of the wind turbine is exploited. The active power injected is being proportional to the difference in measured and nominal system frequencies. Normally, this loop will be activated only after the grid frequency exceeds certain limit.

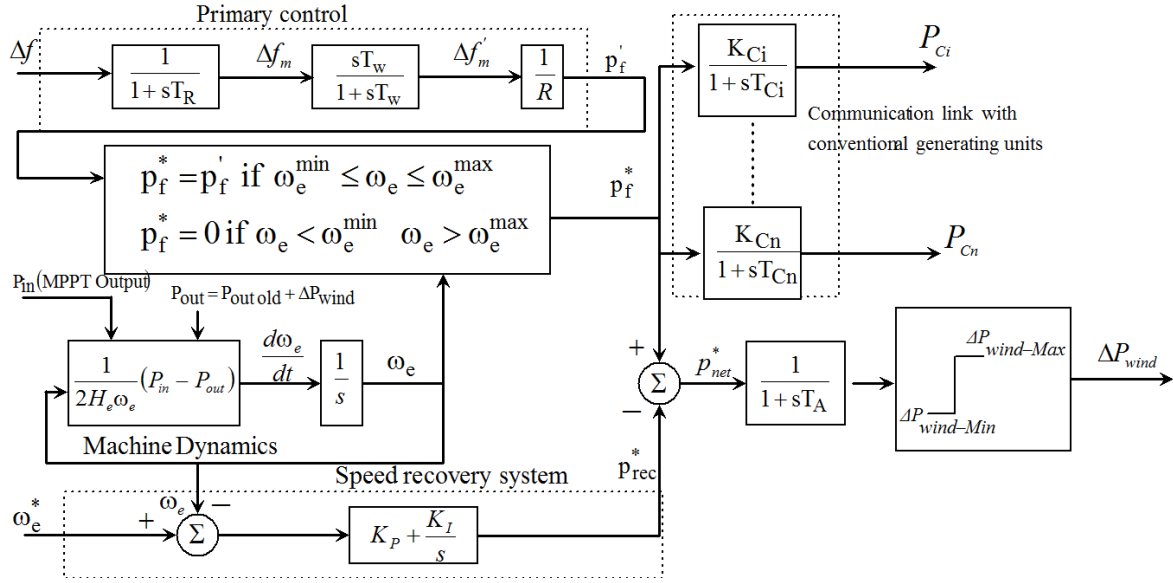


Fig. 5.1: Schemes used for the analysis

Since there is no control over the input of WECS, primary control results in release of kinetic energy from WTG rotor which in turn reduces the rotor speed. In order to operate them at their nominal values, a PI controller is activated which absorbs the energy from the grid. Thus rotor speed will be brought back by speed recovery loop.

Due to the inertia contribution from WECS, conventional generating units respond to load variations slowly. The extra load should be met by the conventional generating units and to have a faster performance, a communication link must be established between WECS and conventional sources. This is helpful in deregulated system too, when there is a deficit in wind power output. This communication channel enables the conventional generating units to supply extra power for maintaining system power balance as well as the contracted load for consumers.

5.3 Deregulated Power System

At present, electric industry has undergone drastic structural as well as regulatory changes from Vertically Integrated Utilities (VIU) to separate and independent entities such as GENCOs, TRANSCO and DISCOs for generation, transmission and distribution system, respectively, to provide reliable power to consumers at competitive tariff under the control

of a separate entity namely Independent System Operator (ISO) in an unbiased manner. In this scenario, GENCOs may or may not participate in frequency regulation [129] and DISCOs have the freedom to make contract with any GENCOs in their own as well as other control areas [130]. In deregulated framework, the power transactions owing to load contract can be classified into three [131].

1. Unilateral contract
2. Bilateral contract
3. Contract violation

Various combinations of DISCO-GENCO contract can be viewed through DISCO Participation Matrix (DPM) as given by

$$DPM = \begin{bmatrix} cpf_{11} & \dots & \dots & \dots & cpf_{1n} \\ cpf_{21} & \dots & \dots & \dots & \vdots \\ \vdots & \dots & cpf_{ij} & \dots & \vdots \\ \vdots & \dots & \dots & \dots & \vdots \\ cpf_{m1} & cpf_{m2} & \dots & \dots & cpf_{mn} \end{bmatrix}_{m \times n} \quad (5.1)$$

Number of rows and columns of DPM indicate the number of GENCOs (m) and number of DISCOs (n), respectively, participating in the energy market [132]. Each entry of DPM refers to the load contract made by the j^{th} DISCO to the i^{th} GENCO, which is termed as contract participation factor (cpf_{ij}). Sum of all elements in each column in the DPM is unity [130].

$$\sum_{i=1}^{i=n} cpf_{ij} = 1; \text{ for } j = 1, 2, \dots, n \quad (5.2)$$

The concept of DPM in deregulated power systems was introduced by [32]. The sum of the individual elements in each row of the DPM indicates the generation of individual GENCO.

$$\Delta P_{Gi} = \sum_{j=1}^n cpf_{ij} \Delta P_{Lj}; \text{ for } i = 1, 2, \dots, n, \quad (5.3)$$

where ΔP_{Gi} is the power generation from the i^{th} GENCO and ΔP_{Lj} is the load demand by j^{th} DISCO.

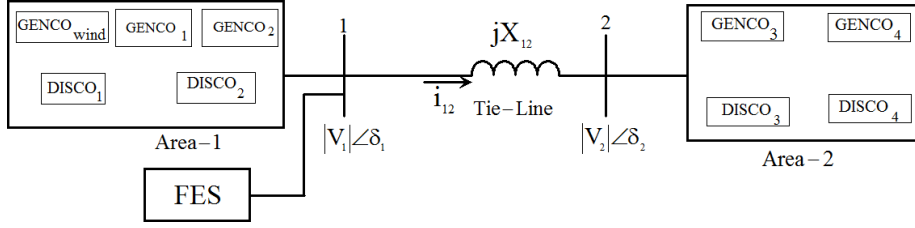


Fig. 5.2: Schematic model of a two area deregulated power system

Due to bilateral transactions, the tie-line power flow changes with load contract, when DISCOs have power contract with GENCOs in other areas. Traditionally, tie-line bias frequency control aims at bringing back the system frequency and tie-line power exchange to their respective scheduled value immediately after the loss of power balance [133]. Hence, in order to take account of bilateral transactions, in deregulated power systems, the area control error (ACE) is formulated in such a way to serve the objective of load following. For i^{th} area, the ACE is formulated as

$$ACE_i = B_i \Delta f_i + \Delta P_{tie\ ij\ error}, \quad (5.4)$$

where B_i is the biasing factor, Δf_i is the deviation in the area frequency of the i^{th} area and $\Delta P_{tie\ ij\ error}$ is the error in the tie-line power flow from i^{th} area to j^{th} area.

$$\Delta P_{tie\ ij\ error} = \Delta P_{tie\ ij\ actual} - \Delta P_{tie\ ij\ sched}, \quad (5.5)$$

where $\Delta P_{tie\ ij\ actual}$ is the actual tie-line power flow from i^{th} area to j^{th} area.

Scheduled tie-line power flow = \sum (load contract made by DISCOs in Area-2 from GENCOs in Area-1) – \sum (load contract made by DISCOs in Area-1 from GENCOs in Area-2)

A schematic diagram of the two area deregulated power system with Wind based GENCO and FES system used for the analysis is shown in Fig. 5.2.

5.3.1 Power Market with Wind Energy System

At each instant, total electricity produced must match with varying load. Thus, efficiently regulating or balancing the power imbalance seems interesting for market operators, as

they earn extra incentive for regulation [77]. Moreover, the system operator should identify the market reserve for unpredictable load variations other than the usual load swings. System load profile and wind power forecastings are normally done in a day-ahead basis in order to schedule the conventional generating units. Usually in a modern liberalized power market, supply-demand biddings are done in a cost effective way. However, forecasting errors typically in wind power output leads to departing from the energy bid, which reduces the net profit of the operator/utilities as they need to buy extra power at extra cost for balancing. Thus, efficient and effective forecasting method is one of the best way to avoid loss of profit. Another solution is the effective utilization of energy storage devices in conjunction with wind power plant as they provides a better regulation reserve immediately after the load swing.

When a wind based GENCO violates contract by supplying a lesser power than it has contracted early, for balancing, the other conventional generating units are called to fill in the deviation made by wind energy system. As wind penetration level increases, the unit commitment becomes complex due to the stochastic nature of wind, which becomes an interesting problem for researchers. Intermittent nature of power output from WECS hinders them in participation in ancillary service market [134]. Hence, deviations from forecasted production schedules needs immediate balancing with the help of conventional sources [77]. In this regard, the system operator must compensate for the power imbalance through proper regulation reserve. The penalty for compensation cost is imposed on participants who failed to fulfill their load contract, especially the wind based GENCOs [83].

Normally wind based power plants are designed and operated for *must run condition* so as to exploit maximum available energy from the wind. The inter-temporal variations in power market and intermittency in the power production results in the wind power curtailment without any storage devices [85].

5.4 Case Studies

The analysis of load following on a wind integrated power system is done in following cases.

1. Case 1: Thermal-Thermal Systems
2. Case 2: Hydro-Thermal Systems

5.4.1 Case-1: Thermal-Thermal Systems

5.4.1.1 System Investigated

A detailed transfer function block diagram model of the sample two area thermal-thermal wind integrated deregulated power system in which analysis has been carried out is shown in Fig. 5.3. The two area deregulated system consists of two conventional GENCOs ($GENCO_1$ and $GENCO_2$) and one wind power plant based GENCO ($GENCO_{wind}$) in Area-1, and two conventional GENCOs ($GENCO_3$ and $GENCO_4$) in Area-2. Each area comprises two DISCOs each. A Flywheel Energy Storage (FES) system is also kept near to Area-1. The DPM pertains to load contract made by DISCOs and GENCOs of the sample two area deregulated power system is given as,

$$DPM = \begin{matrix} & & \begin{matrix} DISCO_1 & DISCO_2 & DISCO_3 & DISCO_4 \end{matrix} \\ \begin{matrix} GENCO_{wind} \\ GENCO_1 \\ GENCO_2 \\ GENCO_3 \\ GENCO_4 \end{matrix} & \left[\begin{array}{cccc} cpf_{w1} & cpf_{w2} & cpf_{w3} & cpf_{w4} \\ cpf_{11} & cpf_{12} & cpf_{13} & cpf_{14} \\ cpf_{21} & cpf_{22} & cpf_{23} & cpf_{24} \\ \hline cpf_{31} & cpf_{32} & cpf_{33} & cpf_{34} \\ cpf_{41} & cpf_{42} & cpf_{43} & cpf_{44} \end{array} \right] \end{matrix}$$

First row in the above DPM represents the load contract made by various DISCOs to the wind power plant based GENCO ($GENCO_{wind}$), i.e., cpf_{wi} indicates the load share of i^{th} DISCO to the $GENCO_{wind}$. As explained in earlier sections, the supply-load bidding are done in a day-ahead market.

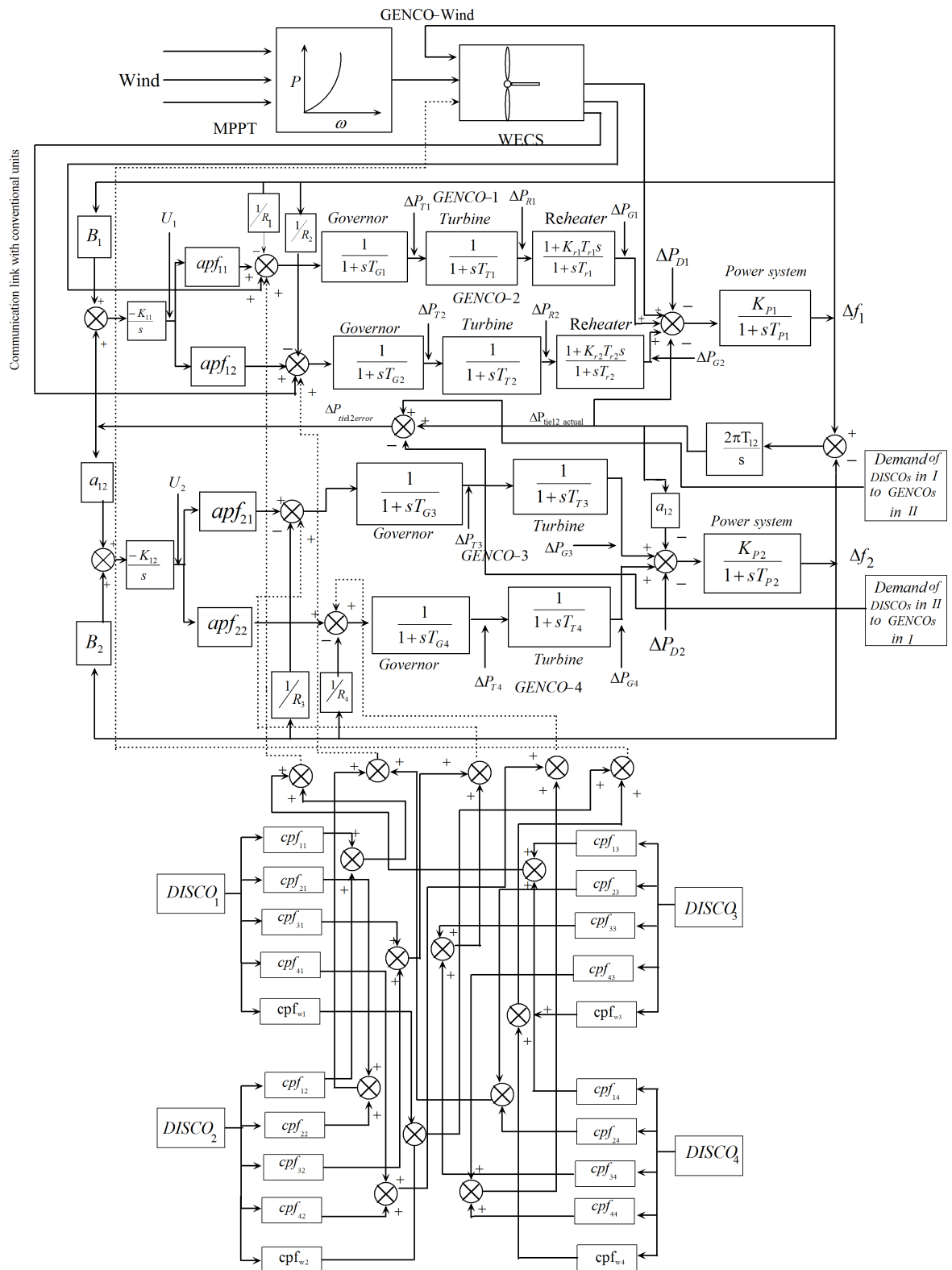


Fig. 5.3: Linearized model of an interconnected thermal-thermal system with high wind integration under deregulation

5.4.1.2 Optimizing the Controller Gains

In deregulated power systems, load following is considered as one of the ancillary services which tries to maintain area frequencies and tie-line power flows at their respective scheduled values and at the same time, keeping settling time and overshoot as low as possible. An objective function that takes into account of the changes in wind power generation (ΔP_{wind}) in addition to frequency perturbations ($\Delta f_1, \Delta f_2$) and error in tie-line power deviation ($\Delta P_{tie12error}$) is formulated to tune the controller gains as given below.

$$J = \int_0^t [\Delta f_1^2 + \Delta f_2^2 + \Delta P_{tie12error}^2 + \Delta P_{wind}^2] dt \quad (5.6)$$

J is minimized to obtain the optimum values of controller gains.

Teaching Learning based Optimization (TLBO), an algorithm inspired from nature, is used to find the optimal values of integral gains instead of the analytic calculus based methods due to their reliability, consistency and computational friendliness.

5.4.1.3 Teaching Learning Based Optimization (TLBO)

TLBO is an algorithm proposed by [3, 4] and is used for obtaining the global best solutions, with less computational effort and high consistency, for functions which are continuous and nonlinear. TLBO is based on the influence of the teacher on the performance of the students in the class. Each design variable is considered as a subject for which the performance is seen and each student tries to improve his performance based on his own capability [4]. The performance of the students improve either by interaction with teacher and also with other students. Therefore, the method is divided into teacher phase and student phase [3]. In teacher phase, the best student in the class is considered as teacher and the teacher's aim is to bring up knowledge of students to his level. The teacher brings up the class average near to his level based on the capability of class. In learner phase a student learns from another student who has more knowledge than him. A flowchart shown in Fig. 5.4 gives the schematic overview of TLBO algorithm.

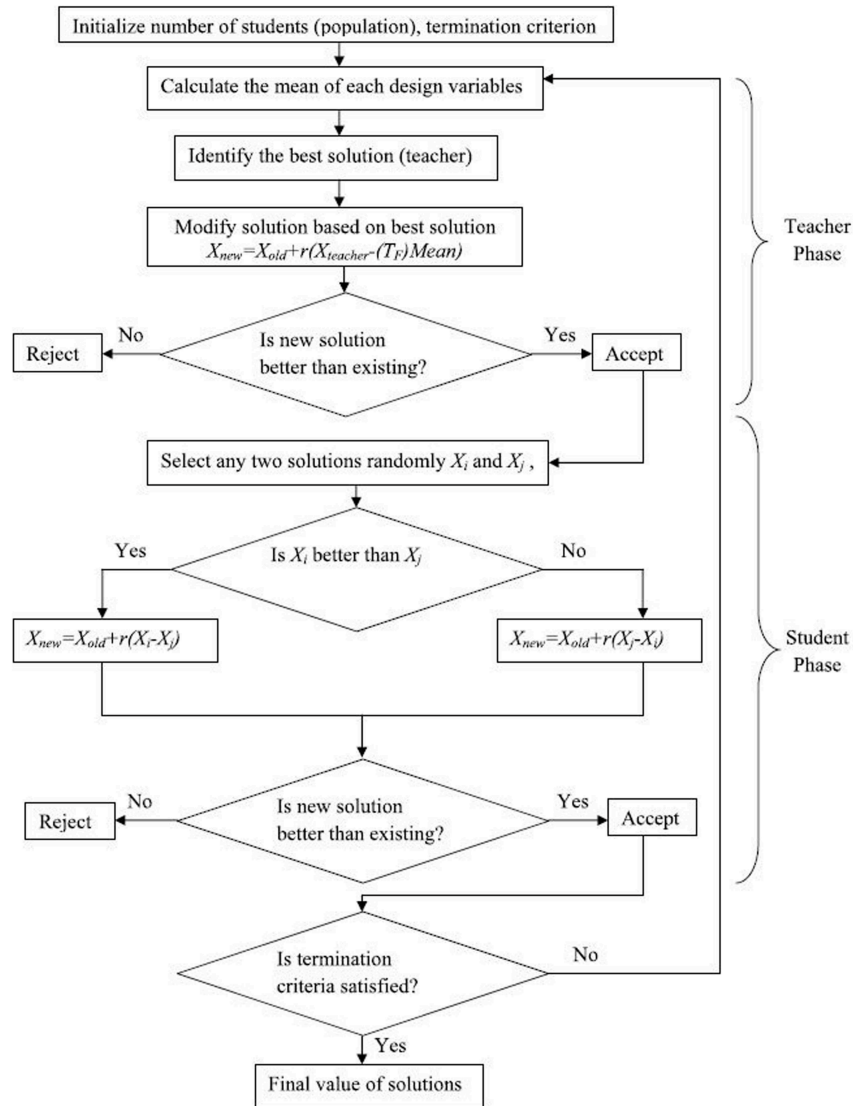


Fig. 5.4: Flow chart of TLBO algorithm [3, 4].

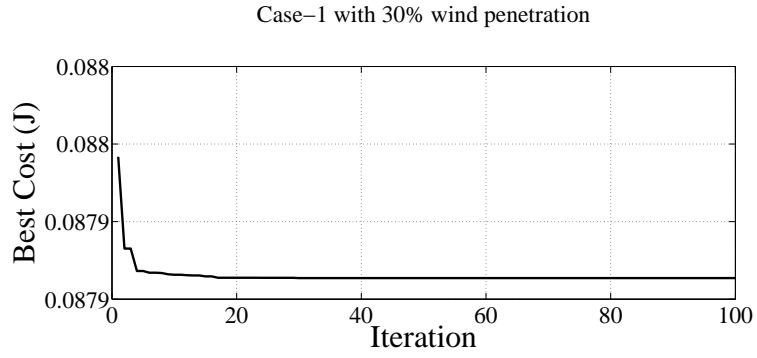
Table 5.1
Optimization parameters used for tuning

Population size	100
Number of generations	100
Number of design variables	4

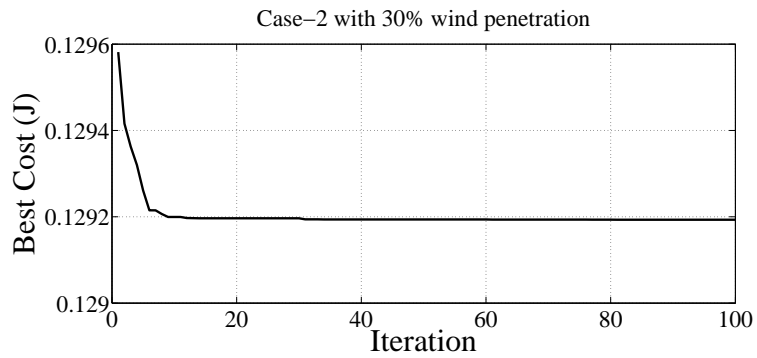
Optimum values of controller gains for various cases with 30% wind penetration level

Table 5.2

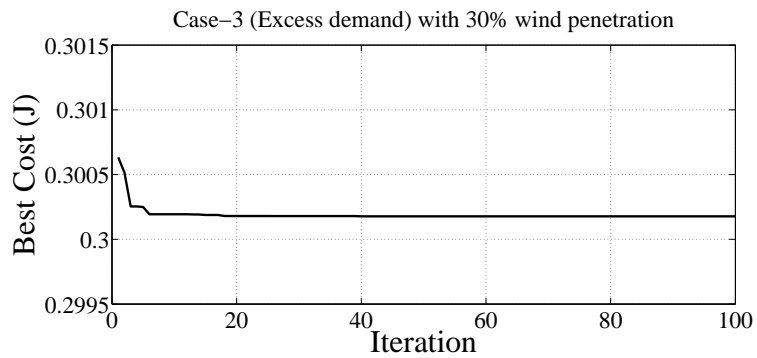
	Unilateral contract		Bilateral contract		Contract violation			
	Without FES	With FES	Without FES	With FES	Excess demand		Wind power deficit	
	Without FES	With FES	Without FES	With FES	Without FES	With FES	Without FES	With FES
K_{I1}	0.6305	0.3662	0.6700	0.4090	0.8317	0.4954	0.6589	0.3610
K_{I2}	0.00125	0.001357	0.0178	0.0019	0.0174	0.00261	0.00238	0.02930
K_P	9.5865	10.0840	9.5504	10.2978	8.2798	9.9048	8.2627	9.1758
K_I	1.243	8.4593	5.0286	10.004	1.0458	5.9132	1.0917	6.5740



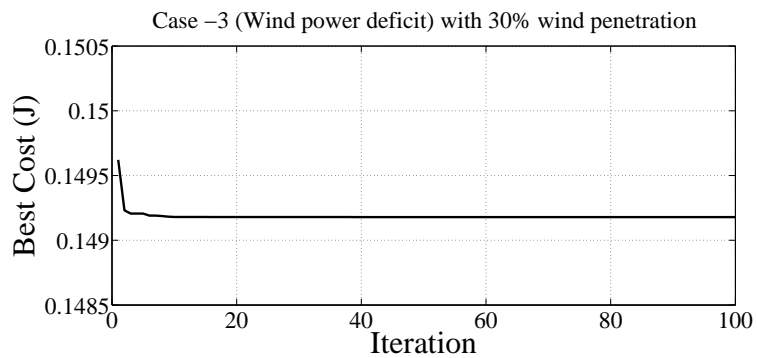
(a) Unilateral contact without FES



(b) Bilateral contact without FES



(c) Contact violation (excess demand) without FES



(d) Contact violation (deficit in wind power) without FES

Fig. 5.5: Iteration vs fitness values obtained from TLBO for 30% wind penetration

The optimization parameters used for tuning the controller values are shown in Table 5.1. The optimized gain settings for (1) unilateral, (2) bilateral contract and (3) contract violation cases for 30% wind penetration level with and without FES for Areas 1 and 2 are given in Table 5.2. Presented in Fig. 5.5 are plots showing the best function versus iteration no. for different cases.

5.4.1.4 Simulation Results and Discussion

Analysis has been carried on the given two area wind integrated deregulated power system shown in Fig. 5.3. It is assumed that each DISCO demands 10%, i.e., $\Delta P_{L1} = \Delta P_{L2} = \Delta P_{L3} = \Delta P_{L4} = 0.1$ pu MW. Fourth-order Runge-Kutta method with an integration step size of 0.01 s is used for simulations. Studies are carried out for three different possibilities as given below.

- Case 1: Unilateral contract
- Case 2: Bilateral contract
- Case 3: With contract violation

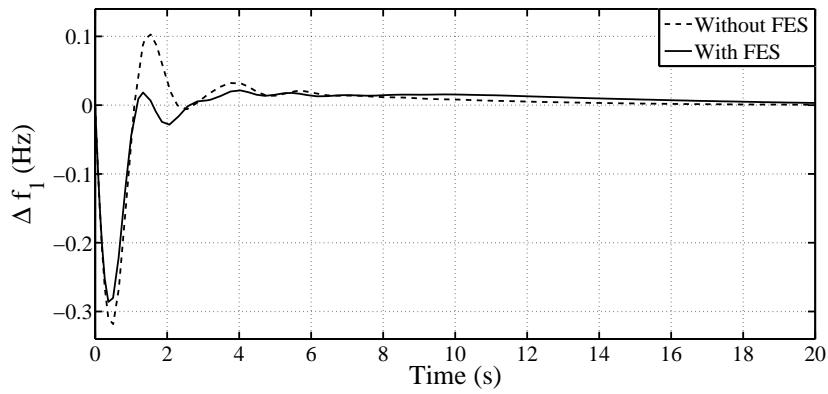
Case 1: Unilateral Contract

In this scenario, DISCOs in an area has the load contract with GENCOs in the same area [81], i.e., there is no inter area load contract by DISCOs, so that during load following $\Delta P_{tie\ 12\ sched}$ settles down to zero. For analysis, it is assumed that each DISCO demands 0.1 pu MW load. The DISCO-GENCO load contract during unilateral transaction can be visualized through the following DPM,

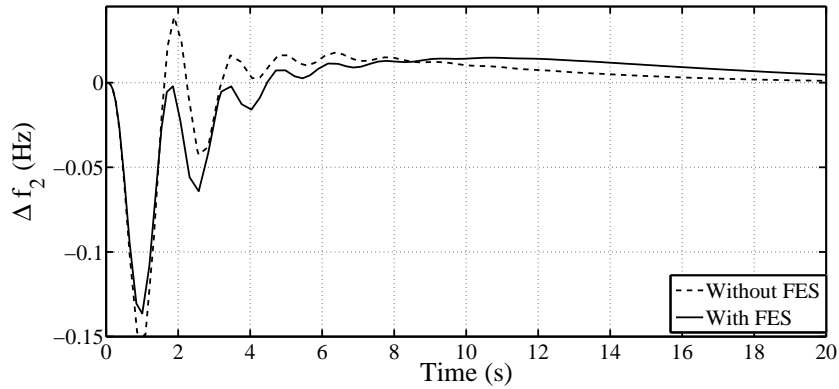
$$DPM = \begin{bmatrix} 0.1 & 0.05 & 0 & 0 \\ 0.7 & 0.3 & 0 & 0 \\ 0.2 & 0.65 & 0 & 0 \\ 0 & 0 & 0 & 0 \\ 0 & 0 & 0 & 0 \end{bmatrix} \quad (5.7)$$

First row in the above DPM shows the load contract made by various DISCOs to the GENCO-wind.

$$\begin{aligned}
 \Delta P_{wind} &= \sum_{j=1}^4 cp f_{wj} \times \Delta P_{Lj} \\
 &= (0.1 \times 0.1) + (0.05 \times 0.1) + (0 \times 0) + (0 \times 0) \\
 &= 0.01 + 0.005 \\
 &= 0.015 \text{ pu MW}
 \end{aligned}$$



(a) Deviation in frequency of Area-1

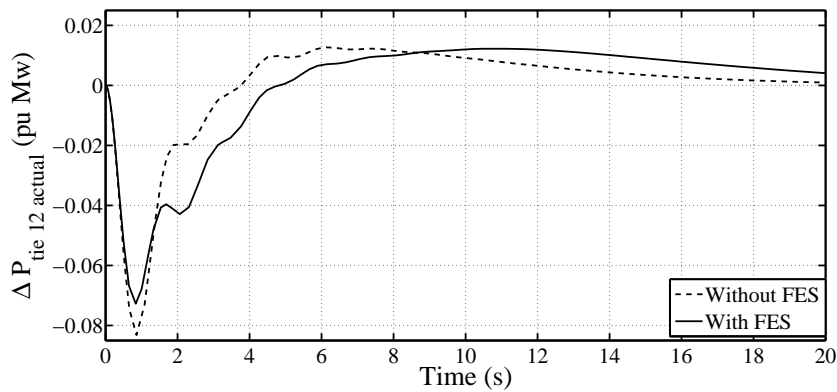


(b) Deviation in frequency of Area-2

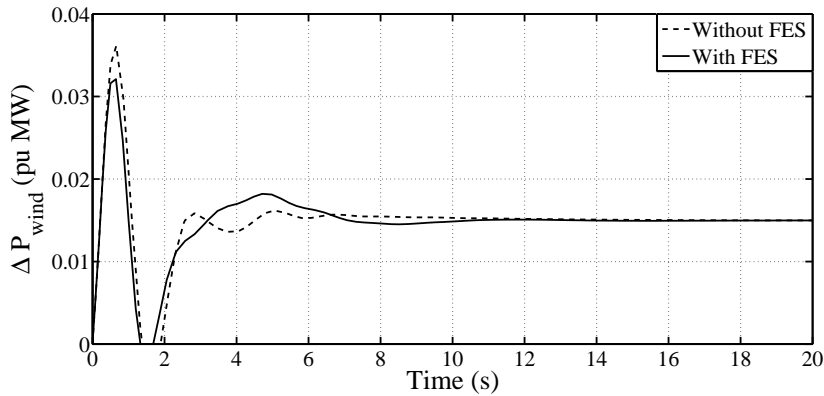
Fig. 5.6: Variations in area frequencies (Δf_1 and Δf_2) and tie-line power (ΔP_{tie12}) in unilateral contract case

Simulations are carried out for 30% wind penetration level. Figs. 5.6-5.9 show the dynamic responses with and without FES for 30% wind penetration level. It is seen that

with FES, transient responses have been improved in terms of peak overshoot and ripples. From the DPM shown above, it is evident that during unilateral contract, the load contracts of DISCOs in Area-1 are met by the GENCOs in Area-1 only. As expected, tie-line power flow settles to zero, which is seen in Fig. 5.7(a). Fig. 5.7(b) shows the power output from the wind based GENCO in Area-1. It is evident that load of DISCOs in Area-1 are also supplied by the wind power plants in Area-1. i.e., it is following the load contract made in the energy market.



(a) Deviation in tie-line power flow



(b) Deviation in power output of GENCO-wind

Fig. 5.7: Variations in tie-line power ($\Delta P_{tie\ 12\ actual}$) and power output of wind power plant (ΔP_{wind}) in unilateral contract case

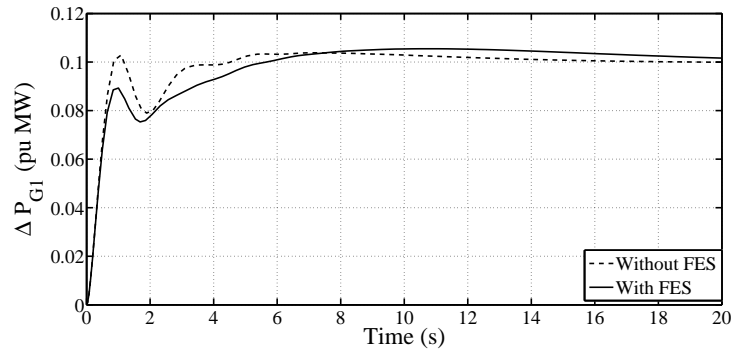
It is also observed that at steady state, power output of GENCO-1 settles to 0.1

pu MW, i.e.,

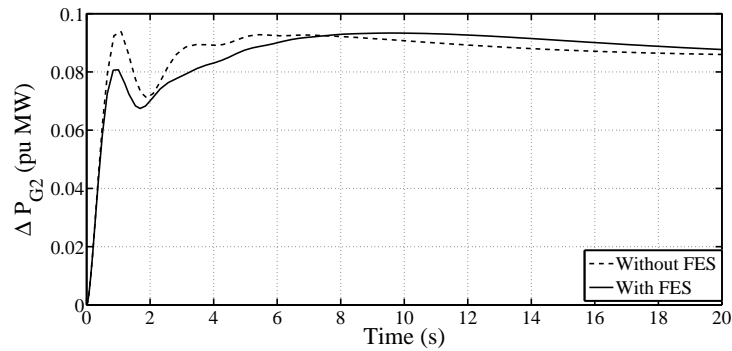
$$\begin{aligned}
 \Delta P_{G1} &= (cpf_{11} \times \Delta P_{L1}) + (cpf_{12} \times \Delta P_{L2}) + \\
 &\quad (cpf_{13} \times \Delta P_{L3}) + (cpf_{14} \times \Delta P_{L4}) \\
 &= (0.7 \times 0.1) + (0.3 \times 0.1) + (0 \times 0.1) + (0 \times 0.1) \\
 &= 0.10 \text{ pu MW}
 \end{aligned}$$

and power output of GENCO-2 becomes,

$$\begin{aligned}
 \Delta P_{G2} &= (cpf_{21} \times \Delta P_{L1}) + (cpf_{22} \times \Delta P_{L2}) + (cpf_{23} \times \Delta P_{L3}) + (cpf_{24} \times \Delta P_{L4}) \\
 &= (0.2 \times 0.1) + (0.65 \times 0.1) + (0 \times 0.1) + (0 \times 0.1) \\
 &= 0.085 \text{ pu MW.}
 \end{aligned}$$



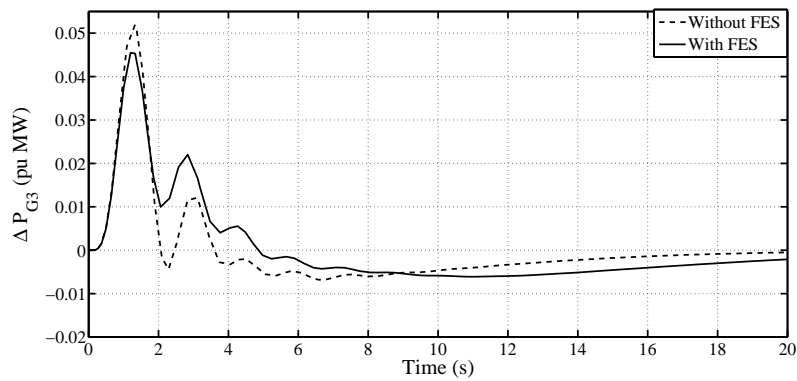
(a) Deviation in power output of GENCO-1



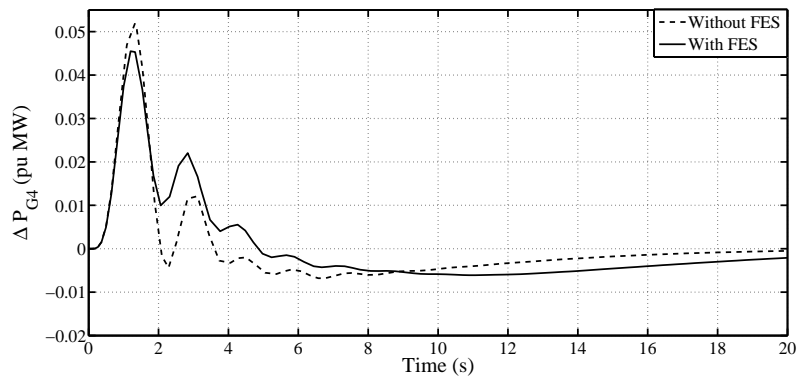
(b) Deviation in power output of GENCO-2

Fig. 5.8: Deviation in generation (ΔP_{G1} and ΔP_{G2}) of GENCOs in Area-1 for unilateral contract case

Similarly at steady state, as anticipated earlier, the power output of GENCOs in area-2 ($GENCO_3$ & $GENCO_4$) settles down to zero, which can be easily calculated as per the DPM. Figs. 5.7(b)-5.9 show the generation output of various GENCOs with and without FES for 30% wind penetration level.



(a) Deviation in power output of GENCO-3

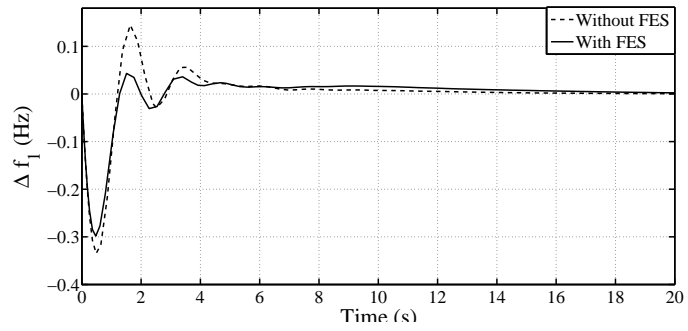


(b) Deviation in power output of GENCO-4

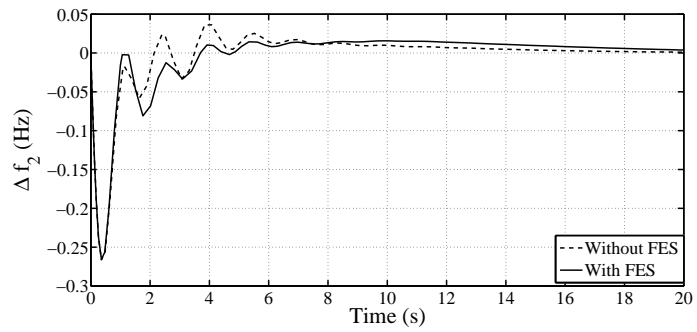
Fig. 5.9: Deviation in generation (ΔP_{G3} and ΔP_{G4}) of GENCOs in Area-2 for unilateral contract case

Case 2: Bilateral Transactions

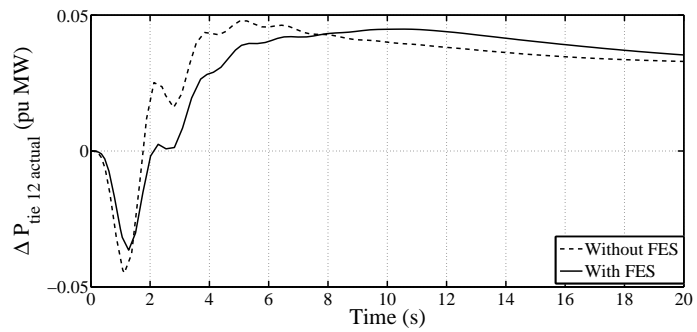
In bilateral contract, a DISCO in an area has the freedom to contract with any GENCOs from its own and other areas as well [79]. Due to bilateral transactions, during load demands the tie-line power flow settles down to new scheduled value as per the net contract made by various DISCOs and GENCOs through competitive bidding in the power market.



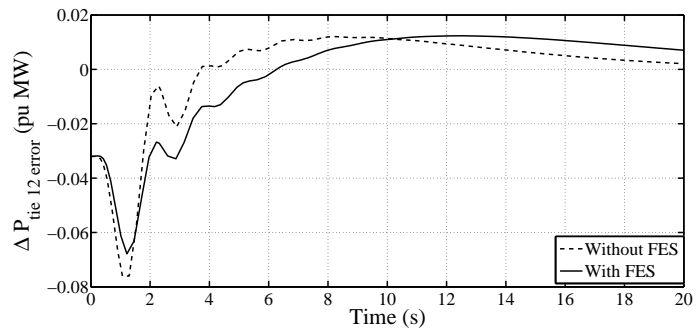
(a) Deviation in frequency of Area-1



(b) Deviation in frequency of Area-2



(c) Deviation in tie-line power flow



(d) Deviation in tie-line power flow error

Fig. 5.10: Variations in area frequencies (Δf_1 and Δf_2) actual tie-line power (ΔP_{tie12}) and tie-line power error ($\Delta P_{tie12error}$) in bilateral contract case

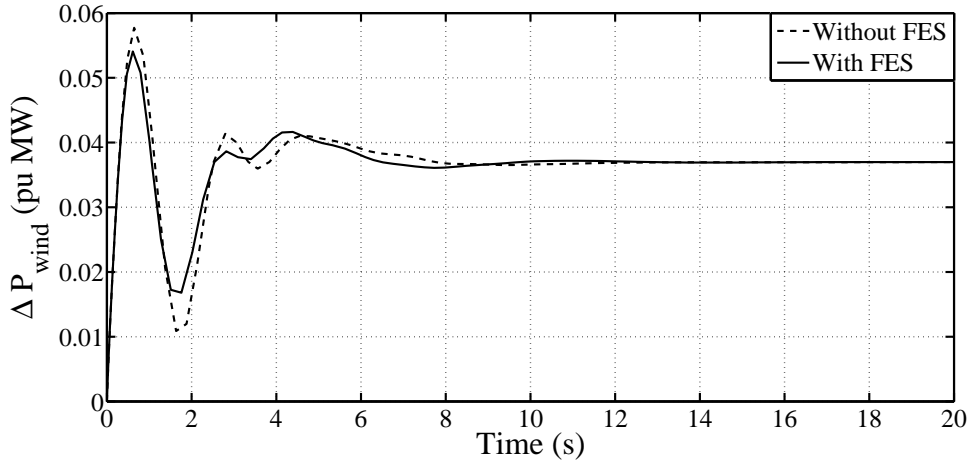


Fig. 5.11: Deviation in power output of GENCO-wind

The load contracts by GENCOs and DISCOs are given as,

$$DPM = \begin{bmatrix} 0.1 & 0.06 & 0.07 & 0.14 \\ 0.3 & 0.24 & 0.37 & 0.11 \\ 0.45 & 0.2 & 0.16 & 0.12 \\ 0.15 & 0.14 & 0.21 & 0.33 \\ 0 & 0.36 & 0.19 & 0.3 \end{bmatrix} \quad (5.8)$$

Figs. 5.10-5.13 depict the corresponding simulation results pertains to bilateral contract with and without FES for 30% wind penetration level. It can be seen that with FES, the peak overshoot and ripples settles down faster. Fig. 5.10(c) corresponds to the tie-line power flow during bilateral transactions. It is found that, the tie-line power flow settles down to its respective scheduled value (i.e., 0.032 pu MW) as calculated earlier,

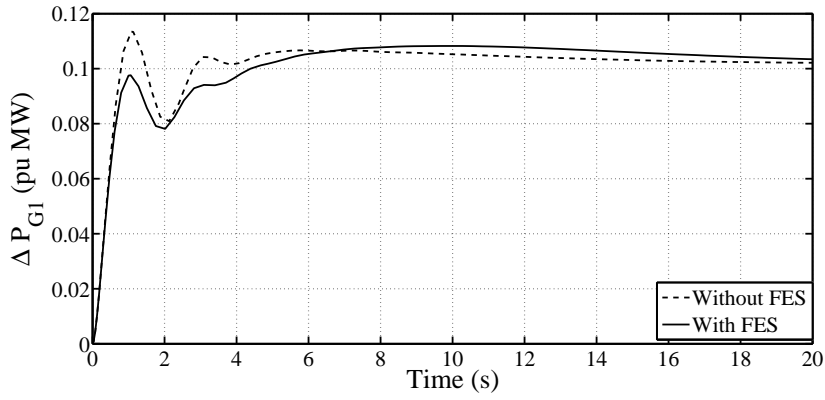
$$\Delta P_{tie\ 12\ sched} = \sum_{\substack{i=1 \\ j=3}}^{\substack{j=4 \\ i=2,w}} cpf_{ij} \times \Delta P_{Lj} - \sum_{\substack{i=3 \\ j=1}}^{\substack{j=2 \\ i=4}} cpf_{ij} \times \Delta P_{Lj} \quad (5.9)$$

At steady state, the power output of various GENCOs matches with values as calculated from the DPM given in Eqn. 5.8.

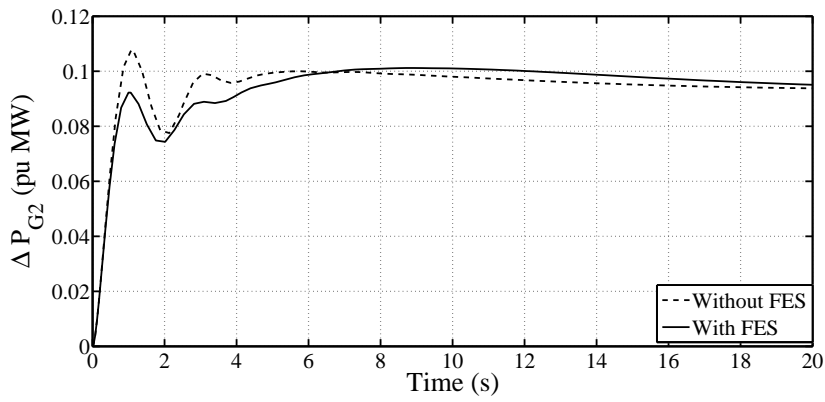
$$\begin{aligned}
\text{Power output of wind power plant, } \Delta P_{wind} &= \sum_{j=1}^{j=4} cpf_{wj} \times \Delta P_{Lj} \\
&= cpf_{w1} \times \Delta P_{L1} + cpf_{w2} \times \Delta P_{L2} + cpf_{w3} \times \Delta P_{L3} \\
&\quad + cpf_{w4} \times \Delta P_{L4} \\
&= (0.1 \times 0.1) + (0.06 \times 0.1) + (0.07 \times 0.1) \\
&\quad + (0.14 \times 0.1) \\
&= 0.037 \text{ pu MW}
\end{aligned}$$

$$\begin{aligned}
\text{Power output of GENCO-1, } \Delta P_{G1} &= \sum_{j=1}^{j=4} cpf_{1j} \times \Delta P_{Lj} \\
&= cpf_{11} \times \Delta P_{L1} + cpf_{12} \times \Delta P_{L2} + cpf_{13} \times \Delta P_{L3} \\
&\quad + cpf_{14} \times \Delta P_{L4} \\
&= (0.3 \times 0.1) + (0.24 \times 0.1) + (0.37 \times 0.1) \\
&\quad + (0.11 \times 0.1) \\
&= 0.103 \text{ pu MW}
\end{aligned}$$

$$\begin{aligned}
\text{Power output of GENCO-2, } \Delta P_{G2} &= \sum_{j=1}^{j=4} cpf_{2j} \times \Delta P_{Lj} \\
&= cpf_{21} \times \Delta P_{L1} + cpf_{22} \times \Delta P_{L2} + cpf_{23} \times \Delta P_{L3} \\
&\quad + cpf_{24} \times \Delta P_{L4} \\
&= (0.45 \times 0.1) + (0.2 \times 0.1) + (0.16 \times 0.1) \\
&\quad + (0.12 \times 0.1) \\
&= 0.093 \text{ pu MW}
\end{aligned}$$



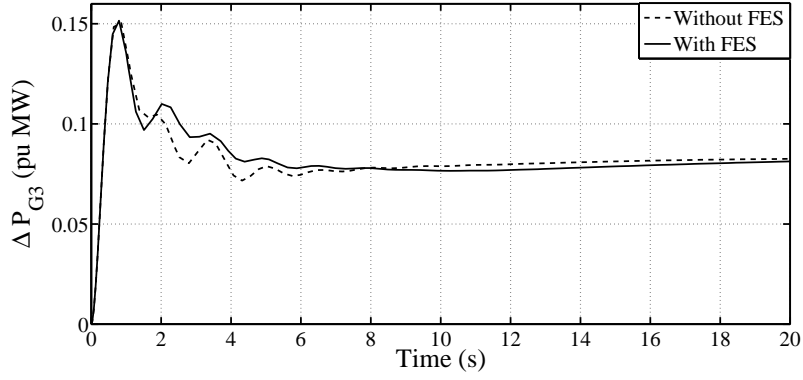
(a) Deviation in power output of GENCO-1



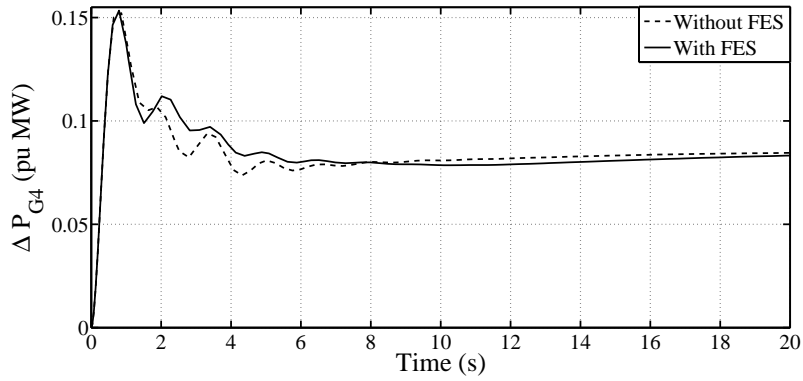
(b) Deviation in power output of GENCO-2

Fig. 5.12: Deviation in generation (ΔP_{G1} and ΔP_{G2}) of GENCOs in Area-1 for bilateral contract case

$$\begin{aligned}
 \text{Power output of GENCO-3, } \Delta P_{G3} &= \sum_{j=1}^{j=4} cpf_{3j} \times \Delta P_{Lj} \\
 &= cpf_{31} \times \Delta P_{L1} + cpf_{32} \times \Delta P_{L2} + cpf_{33} \times \Delta P_{L3} \\
 &\quad + cpf_{34} \times \Delta P_{L4} \\
 &= (0.15 \times 0.1) + (0.14 \times 0.1) + (0.21 \times 0.1) \\
 &\quad + (0.33 \times 0.1) \\
 &= 0.083 \text{ pu MW}
 \end{aligned}$$



(a) Deviation in power output of GENCO-3



(b) Deviation in power output of GENCO-4

Fig. 5.13: Deviation in generation (ΔP_{G3} and ΔP_{G4}) of GENCOs in Area-2 for bilateral contract case

$$\begin{aligned}
 \text{Power output of GENCO-4, } \Delta P_{G4} &= \sum_{j=1}^{j=4} cpf_{4j} \times \Delta P_{Lj} \\
 &= cpf_{41} \times \Delta P_{L1} + cpf_{42} \times \Delta P_{L2} + cpf_{43} \times \Delta P_{L3} \\
 &\quad + cpf_{44} \times \Delta P_{L4} \\
 &= (0 \times 0.1) + (0.36 \times 0.1) + (0.19 \times 0.1) \\
 &\quad + (0.3 \times 0.1) \\
 &= 0.085 \text{ pu MW}
 \end{aligned}$$

It is clear from Figs. 5.11-5.13 that at steady state, the generations at each GENCO settles

down to their respective calculated values as above. It is also evident that FES improves the transient performances of the system.

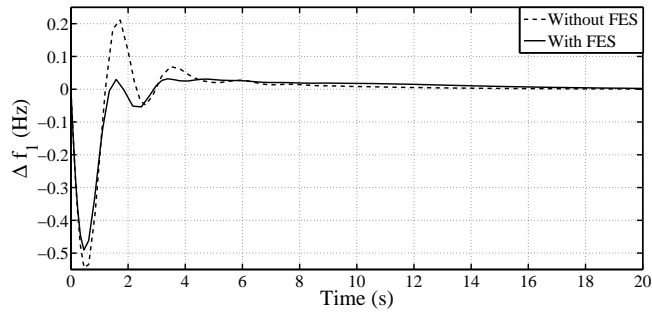
Case 3: Contract Violation

In a typical deregulated power system, during load following, any of the DISCOs may violate the contract by demanding more or less power as contracted early. In order to maintain the system power balance and frequency, the system operator has to intervene and restore the power balance. In classical tie-line bias control for bilateral transactions, the tie-line power flow must be maintained at its scheduled value at steady state. This scheme is normally employed to avoid unscheduled power exchanges, for which TRANSCOs charge more wheeling charges. In this work, the contract violation can be sub divided into

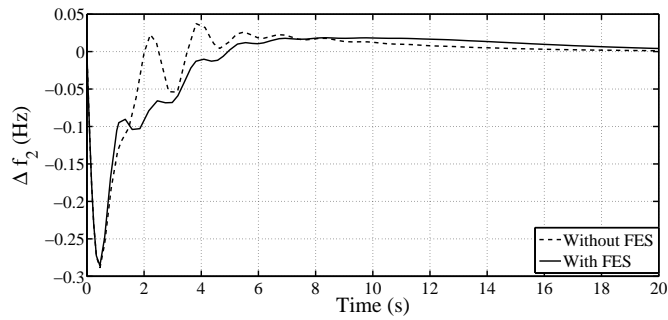
- Contract violation due to
 - Excess DISCO demand
 - Deficit in wind power generation

Excess Demand

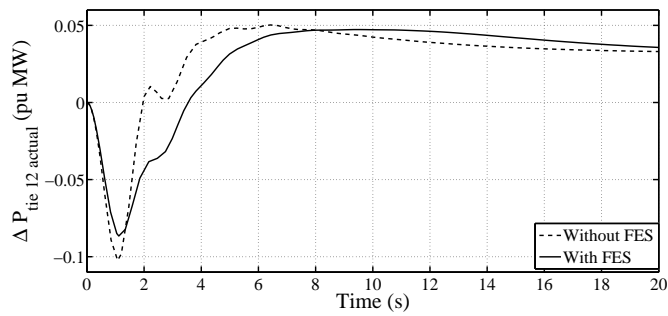
In this scenario, any of the DISCOs may violate the load contract by demanding excess power, which it is contracted early. As explained previously, in order to maintain the tie-line power flow at its scheduled value, this extra uncontracted load will be supplied from the GENCOs in the area in which DISCO locates. In this analysis, we have analyzed a case where DISCO-1 demands 0.1 pu MW extra load. As per the prevailing practices, this extra load must be met from the GENCOs in Area-1. However, the presence of GENCO-wind poses a new case as the GENCO-wind had already made load contract according to wind power forecast and it is expected to deliver its maximum available energy from the wind. Since, there is no control over input of GENCO-wind, in high wind integrated power systems, conventional units in Area-1 have to deliver this excess load as per the area participation factor. Normally, conventional generators are slow responding as they are unable to absorb the frequency fluctuations faster without any energy storage devices because of their heavy inertia.



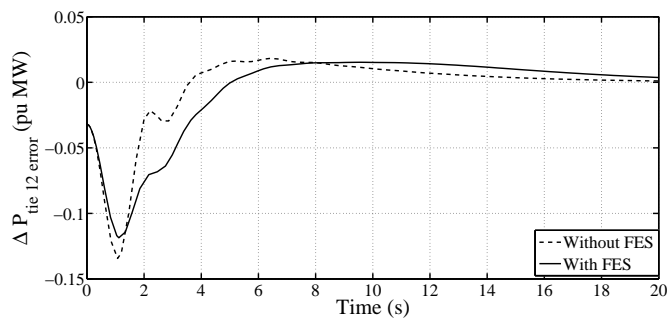
(a) Deviation in frequency of Area-1



(b) Deviation in frequency of Area-2



(c) Deviation in tie-line power flow



(d) Deviation in tie-line power flow error

Fig. 5.14: Variations in area frequencies (Δf_1 and Δf_2) and actual tie-line power (ΔP_{tie12}) and ($\Delta P_{tie12error}$) for contract violation (excess demand)

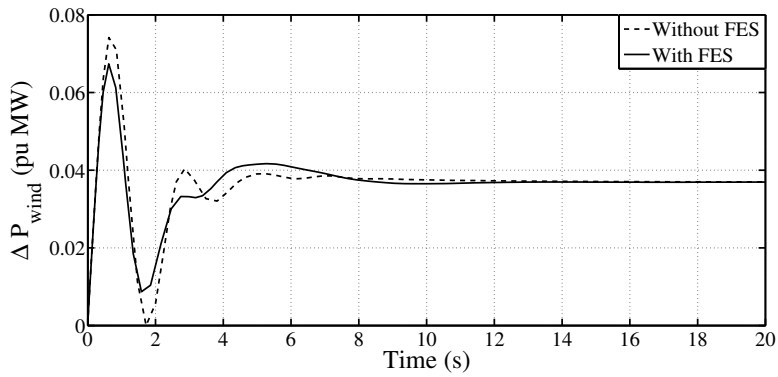
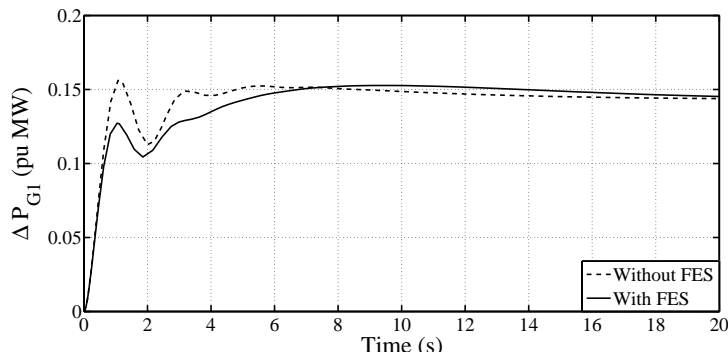
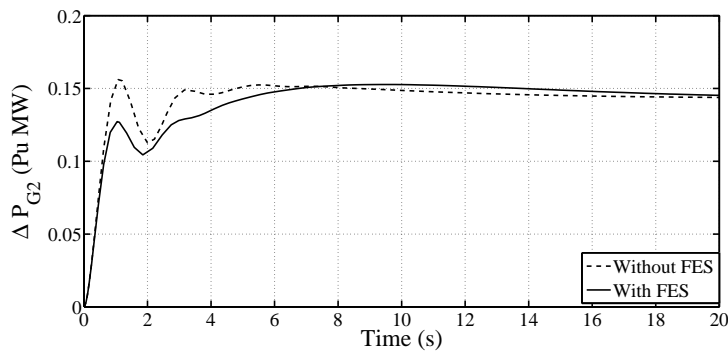


Fig. 5.15: Deviation in power output of GENCO-wind for contract violation (excess demand)



(a) Deviation in power output of GENCO-1



(b) Deviation in power output of GENCO-2

Fig. 5.16: Deviation in generation (ΔP_{G1} and ΔP_{G2}) of GENCOs in Area-1 for contract violation (excess demand)

With FES system, better system performances are observed during excess demand, as viewed in Figs. 5.14-5.17. Fig. 5.17 shows that the output of GENCOs in Area-2 re-

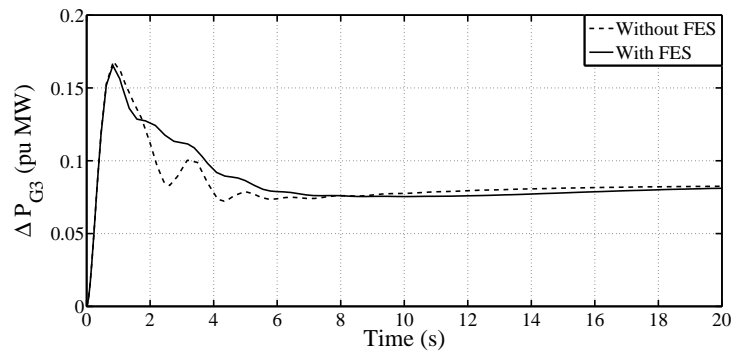
mains unchanged. It is clear that outputs of GENCO-1 and GENCO-2 are increased to accommodate this new load demand. At steady state, ΔP_{G1} becomes 0.0153 pu MW ,

$$\Delta P_{G1 \text{ old}} + apf_{11} \times 0.1 = 0.103 + 0.05 = 0.153 \text{ pu MW}$$

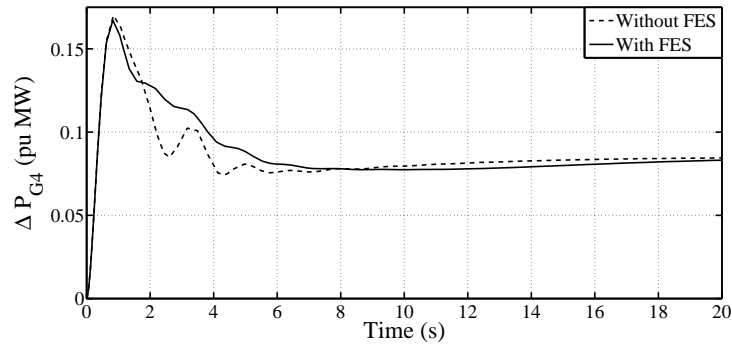
and ΔP_{G2} becomes 0.143 pu MW,

$$\Delta P_{G2 \text{ old}} + apf_{12} \times 0.1 = 0.093 + 0.05 = 0.143 \text{ pu MW}$$

Fig. 5.15 again validates the fact that extra load cannot be met from wind based GENCO.



(a) Deviation in power output of GENCO-3

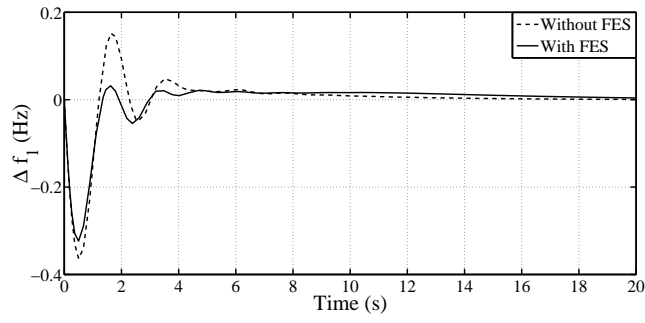


(b) Deviation in power output of GENCO-4

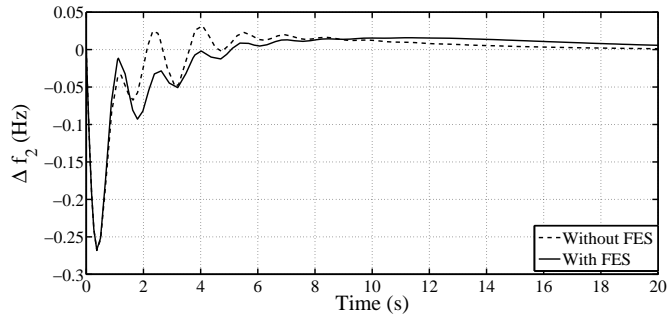
Fig. 5.17: Deviation in generation (ΔP_{G3} and ΔP_{G4}) of GENCOs in Area-2 for contract violation (excess demand)

Wind power deficit

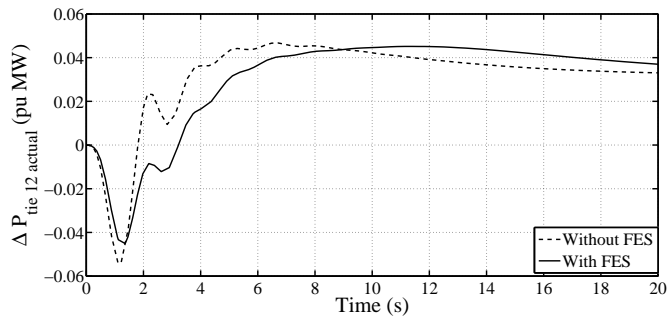
Even though wind energy is available ubiquitous, due to its stochastic nature hinders WECS from connecting it to grid [84].



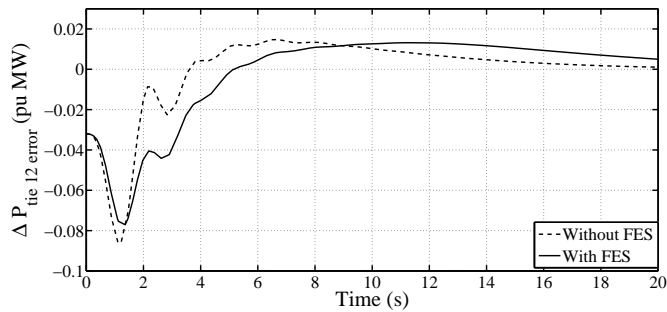
(a) Deviation in frequency of Area-1



(b) Deviation in frequency of Area-2



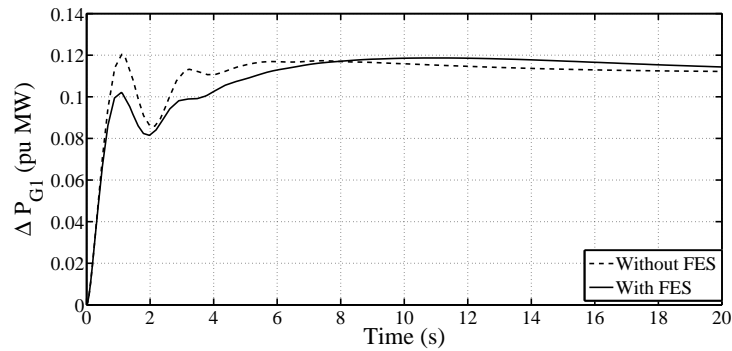
(c) Deviation in tie-line power flow



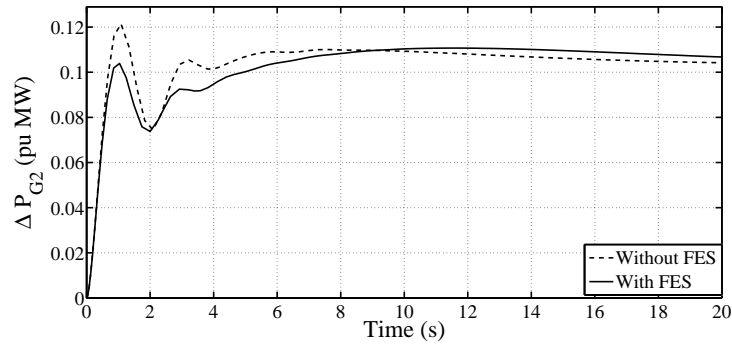
(d) Deviation in tie-line power flow error

Fig. 5.18: Variations in area frequencies (Δf_1 and Δf_2) and actual tie-line power (ΔP_{tie12}) and ($\Delta P_{tie12error}$) for contract violation (deficit in wind power)

Availability of various forecasting algorithms for predicting the wind power plant output enables WECS in participating in power market. Increase in wind penetration level compels wind power producers to behave like other conventional market participants. However, wind power producers have to pay penalty if they violate from the contract. In this scenario of contract violation, the wind power generation deviates from its scheduled value. i.e., it violates the contract by delivering less power than it contracted. Contract violation may be due to the error in forecasting or due to technical issues.



(a) Deviation in power output of GENCO-1

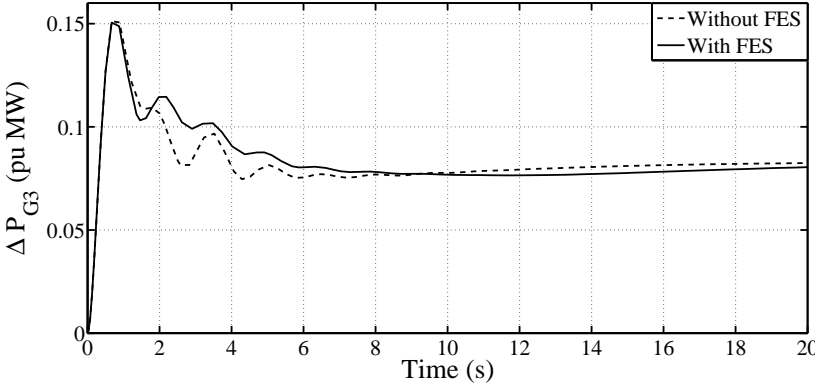


(b) Deviation in power output of GENCO-2

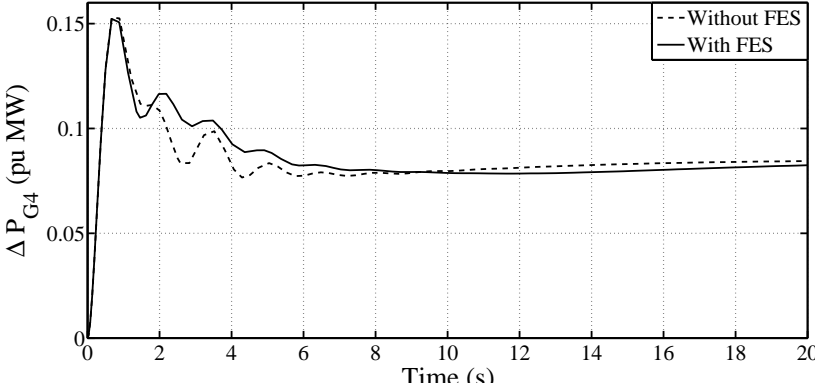
Fig. 5.19: Deviation in generation (ΔP_{G1} and ΔP_{G2}) of GENCOs in Area-1 for contract violation (deficit in wind power)

Figs. 5.18-5.20 correspond to various system variables with and without FES when there is a deficit in power generation from GENCO-wind. Fig. 5.21 depicts the power output of GENCO-wind, where it lacks 0.02 pu MW from the contracted value. It is also clear that this deficit should be met from the conventional GENCOs in the same area. The deficit in load demand may be shared themselves according to the area participation

factor. GENCO-1 and GENCO-2 increase their output by 0.01 pu MW ($\frac{0.02}{0.5}$ pu MW), which can be viewed in Fig. 5.19. On the other hand, power outputs of conventional GENCOs in Area-2 remain unaltered (see Fig. 5.20).



(a) Deviation in power output of GENCO-3



(b) Deviation in power output of GENCO-4

Fig. 5.20: Deviation in generation (ΔP_{G3} and ΔP_{G4}) of GENCOs in Area-2 for contract violation (deficit in wind power)

It is also evident from all the above scenarios that system performance is improved with FES. This establishes the fact that fast real power balancing can be achieved with FES, where it stores the excess energy and also releases it during power shortage. This also avoids the wind power curtailment during excess wind power generation.

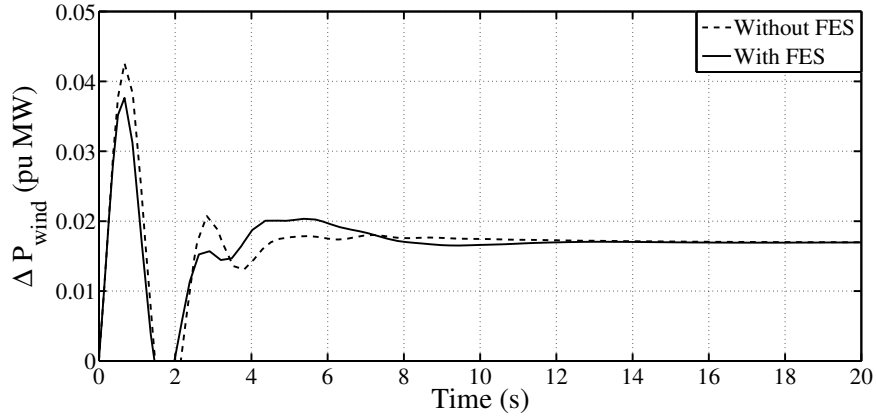


Fig. 5.21: Deviation in power output of GENCO-wind for contract violation (deficit in wind power)

5.4.2 Case-2: Hydro-Thermal System

5.4.2.1 System Investigated

Fig. 5.22 shows the two area hydro-thermal wind integrated power system in which investigations are carried out. For analysis, three GENCOs are considered in Area-1 of which two are conventional thermal generating units (GENCO-1 and GENCO-2) and a wind power plant based GENCO-wind whereas, Area-2 comprises two hydro generating units. An FES system is placed near Area-1. The power contracts made by various DISCOs to GENCOs are given in DPM.

$$DPM = \begin{bmatrix} cpf_{w1} & cpf_{w2} & cpf_{w3} & cpf_{w4} \\ cpf_{11} & cpf_{12} & cpf_{13} & cpf_{14} \\ cpf_{21} & cpf_{22} & cpf_{23} & cpf_{24} \\ cpf_{31} & cpf_{32} & cpf_{33} & cpf_{34} \\ cpf_{41} & cpf_{42} & cpf_{43} & cpf_{44} \end{bmatrix}_{5 \times 4} \quad (5.10)$$

Gains are optimized by TLBO for (1) unilateral, (2) bilateral contract and (3) contract violation cases for 30% wind penetration level with and without FES for Areas 1 and 2 are given in Table 5.3.

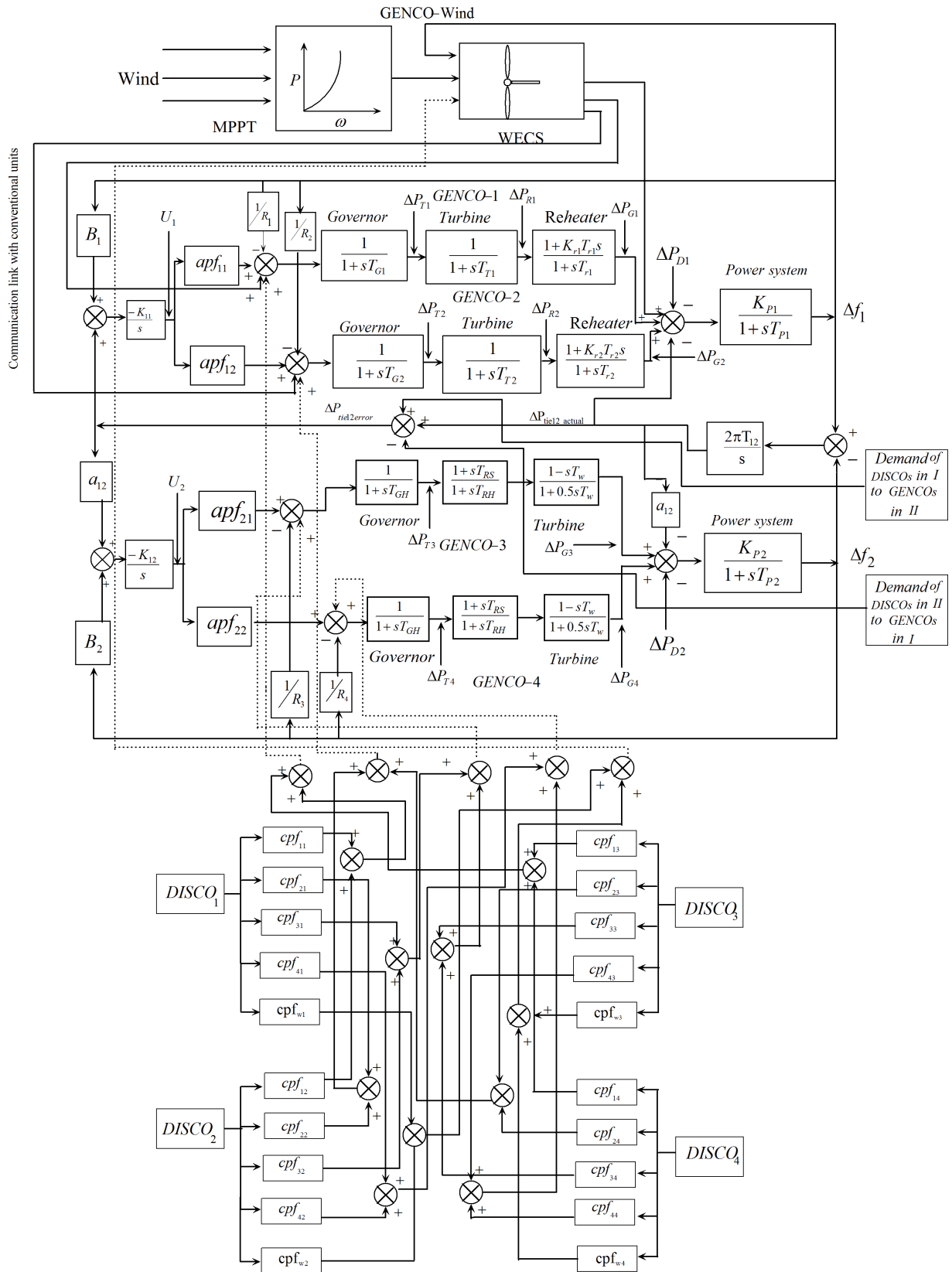


Fig. 5.22: Linearized model of an interconnected thermal-thermal system with high wind integration under deregulation

5.4.2.2 Simulation Results and Discussion

In order to analyze the effect of load following by wind power plants a hydro-thermal deregulated power system shown in Fig. 5.22 is considered. The entire analysis are carried out for 30% wind penetration levels with and without FES case. For analysis, it is assumed that each DISCO demands 0.1 pu MW load. As already done, simulations are carried out for three possible market conditions.

- Case 1: Unilateral contract
- Case 2: Bilateral contract
- Case 3: With contract violation

Case 1: Unilateral Contract

Simulations are carried out on a hydro-thermal deregulated power system to study the effect of wind power plants in competitive market environment. Unilateral case as considered, where DISCOs in area have the power contract with GENCOs in the same area. The corresponding power contract for unilateral transactions can be viewed in DPM.

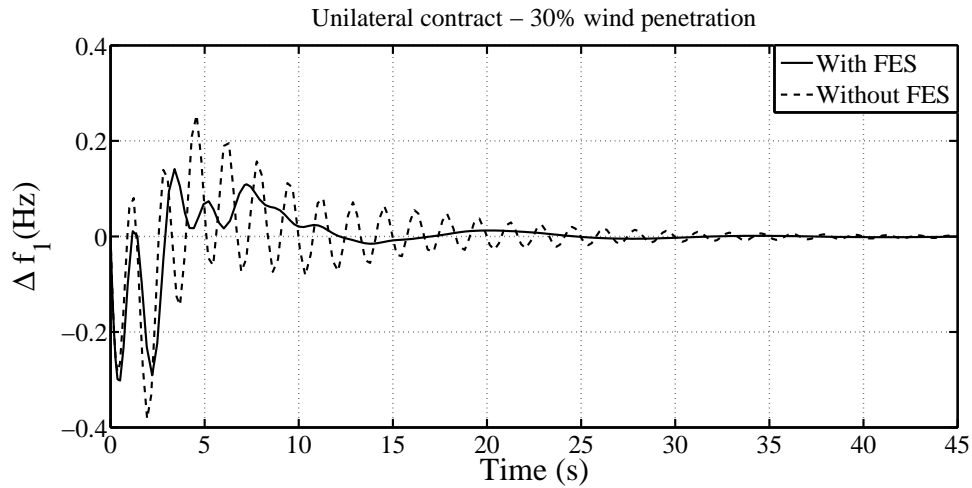
$$DPM = \begin{bmatrix} 0.15 & 0.16 & 0 & 0 \\ 0.6 & 0.24 & 0 & 0 \\ 0.25 & 0.6 & 0 & 0 \\ 0 & 0 & 0 & 0 \\ 0 & 0 & 0 & 0 \end{bmatrix} \quad (5.11)$$

The results also confirm conclusions drawn out from the thermal-thermal system. The net power contract made by various DISCOs to GENCO-wind is given as,

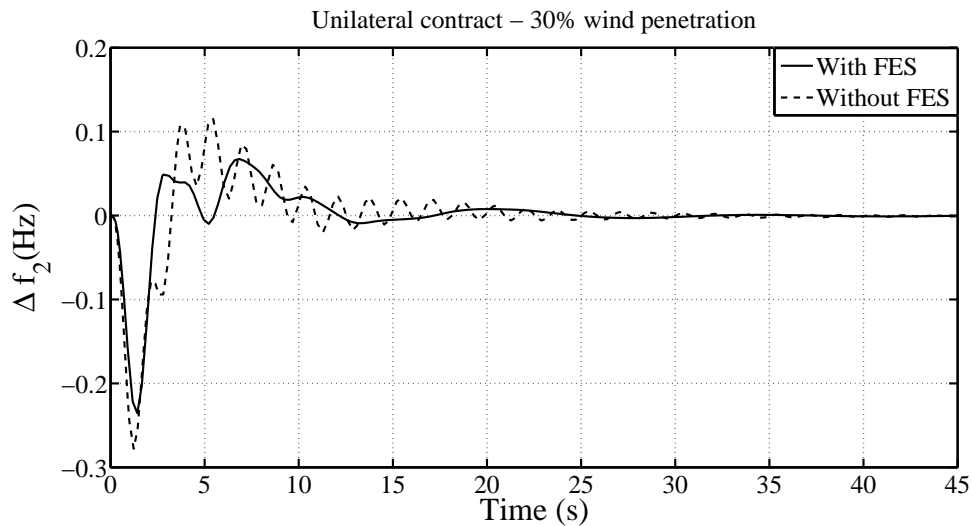
$$\begin{aligned} \Delta P_{wind} &= \sum_{j=1}^4 cpf_{wj} \times \Delta P_{Lj} \\ &= (0.15 \times 0.1) + (0.16 \times 0.1) + (0 \times 0) + (0 \times 0) \\ &= 0.015 + 0.016 \\ &= 0.031 \text{ pu MW} \end{aligned}$$

Table 5.3
Optimum values of controller gains for various cases

	Unilateral contract		Bilateral contract		Contract violation		
	Without FES	With FES	Without FES	With FES	Wind power deficit		
					Excess demand	Without FES	With FES
K_{T1}	0.4645	0.5025	0.5236	0.9474	0.5144	0.6123	0.7296
K_{T2}	0.00129	0.00166	0.0489	0.3427	0.2890	0.3125	0.3860
K_P	4.0384	6.936	5.0124	9.7844	2.7598	2.9635	6.0651
K_I	1.7351	2.0339	1.8926	2.4076	0.3649	0.4391	1.680



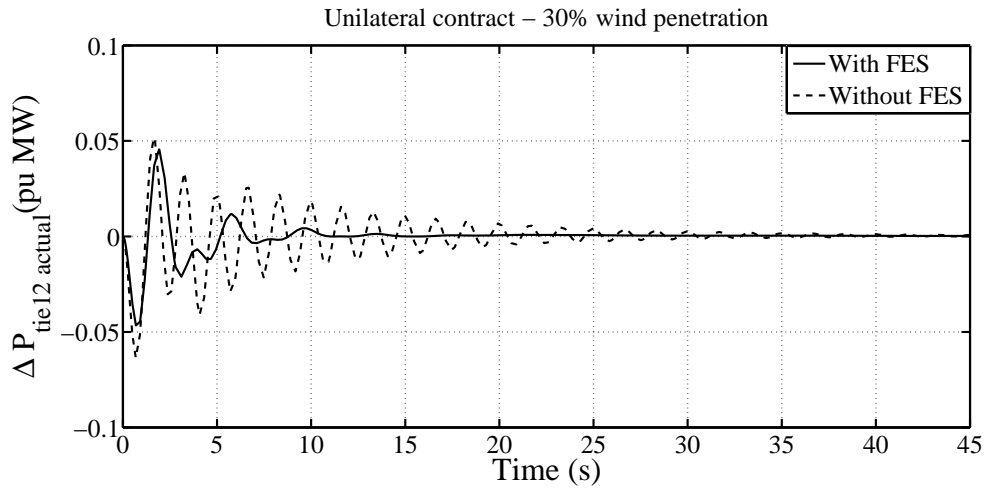
(a) Deviation in frequency of area-1



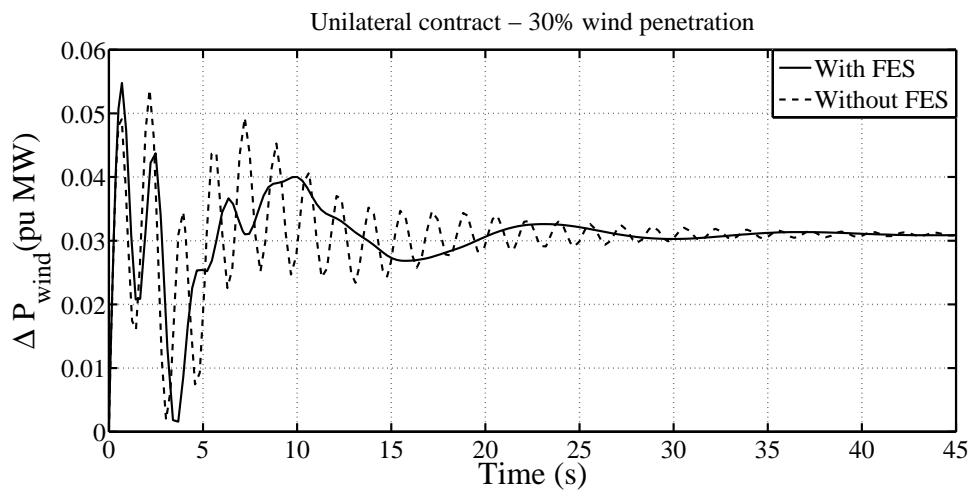
(b) Deviation in frequency of area-2

Fig. 5.23: Variations in area frequencies (Δf_1 and Δf_2) and tie-line power (ΔP_{tie12}) in case-1

Dynamic response of system parameters are shown in Figs. 5.23-5.26. It is found that with FES the system performance improved in terms of settling time, peak overshoot etc.. It is clear that at steady state, GENCOs generate power as per the available power contract, which is realized through the given DPM. The output of GENCOs are matching with the calculated values that can be Figs. 5.24-5.26.



(a) Deviation in tie-line power flow



(b) Deviation in power output of GENCO-wind

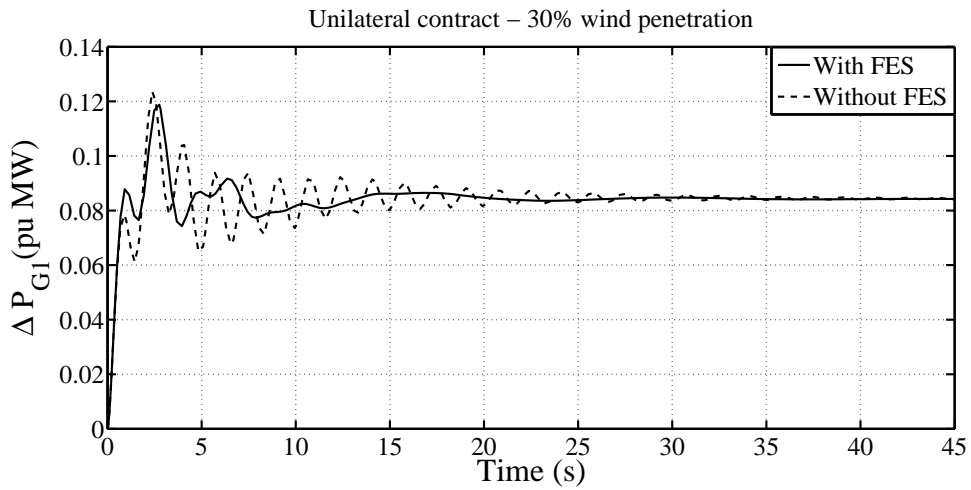
Fig. 5.24: Variations in tie-line power ($\Delta P_{tie\ 12\ actual}$) and power output of wind power plant (ΔP_{wind}) in Case-1

Case 2: Bilateral Transactions

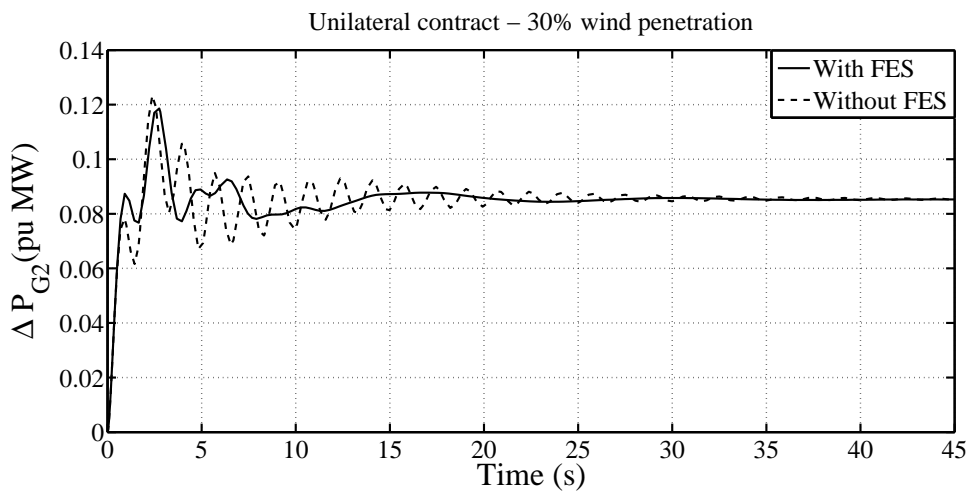
As explained in thermal-thermal system, DISCOs have freedom to make power contract with GENCOs in any areas. The bilateral contract by DISCOs-GENCOs can be viewed

in DPM shown below,

$$DPM = \begin{bmatrix} 0.07 & 0.08 & 0 & 0.16 \\ 0.1 & 0.22 & 0.52 & 0.11 \\ 0.07 & 0.58 & 0.08 & 0.2 \\ 0.5 & 0.12 & 0.05 & 0.23 \\ 0.26 & 0 & 0.35 & 0.3 \end{bmatrix} \quad (5.12)$$

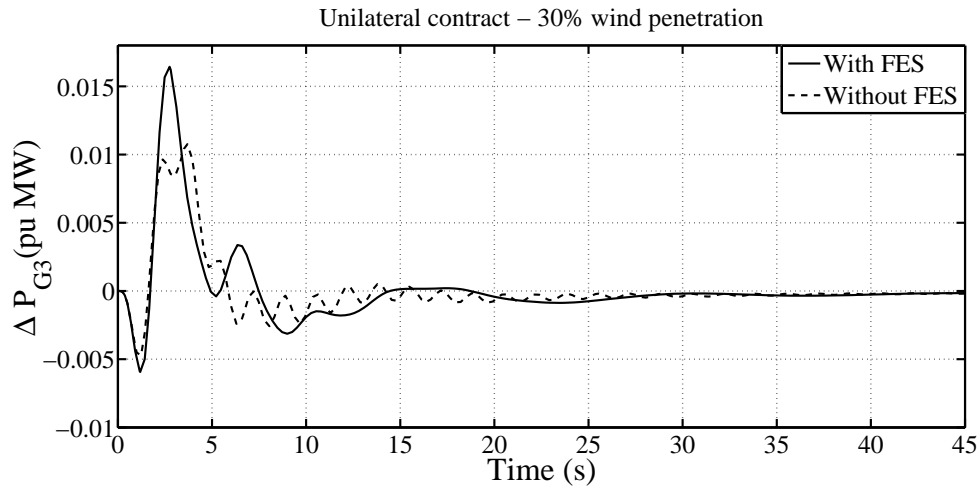


(a) Deviation in power output of GENCO-1

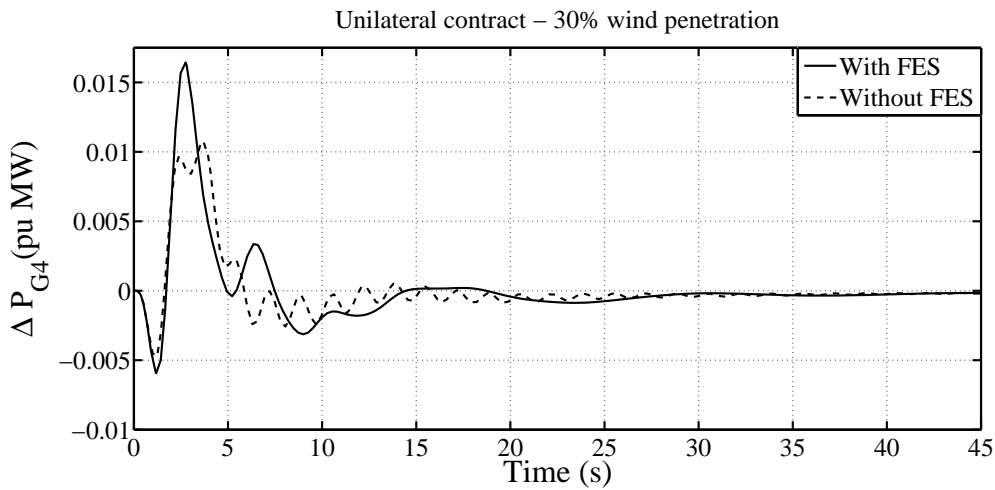


(b) Deviation in power output of GENCO-2

Fig. 5.25: Deviation in generation (ΔP_{G1} and ΔP_{G2}) of GENCOs in Area-1 for Case-1



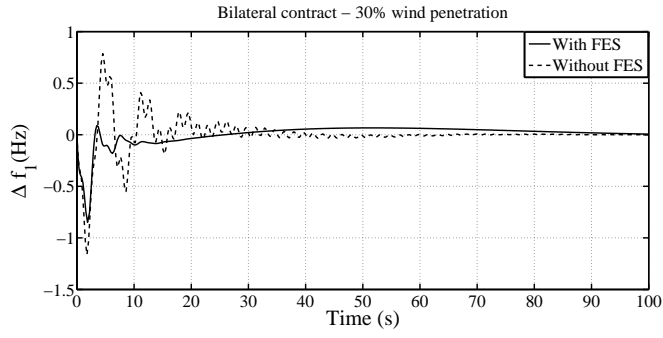
(a) Deviation in power output of GENCO-3



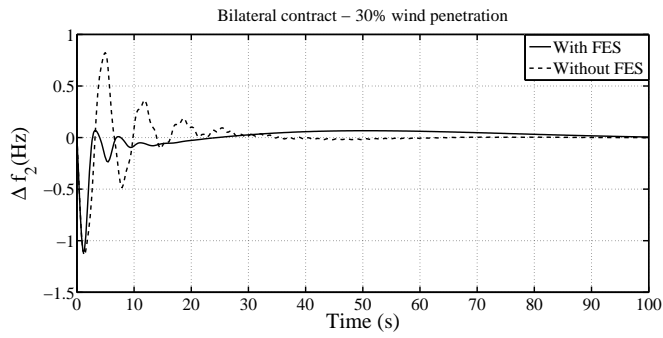
(b) Deviation in power output of GENCO-4

Fig. 5.26: Deviation in generation (ΔP_{G3} and ΔP_{G4}) of GENCOs in Area-2 for Case-1

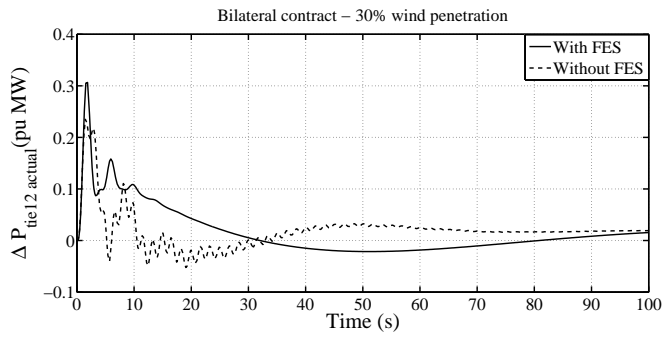
Figs. 5.27-5.30 depict the corresponding simulation results pertains to bilateral contract with and without FES for 30% wind penetration level on a hydro-thermal restructured power system. The immediate energy release from FES system during load demand helps in improving the system performance with fast settling and less overshoot. In order to have a better regulation, normally service providers incorporates energy storage devices to improve system regulation margin.



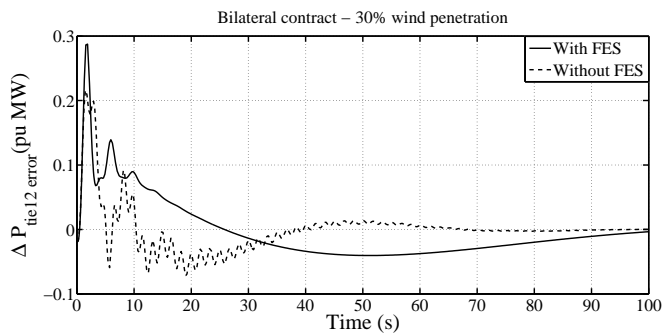
(a) Deviation in frequency of Area-1



(b) Deviation in frequency of Area-2



(c) Deviation in tie-line power flow



(d) Deviation in tie-line power flow error

Fig. 5.27: Variations in area frequencies (Δf_1 and Δf_2) actual tie-line power (ΔP_{tie12}) and tie-line power error ($\Delta P_{tie12 \text{ error}}$)

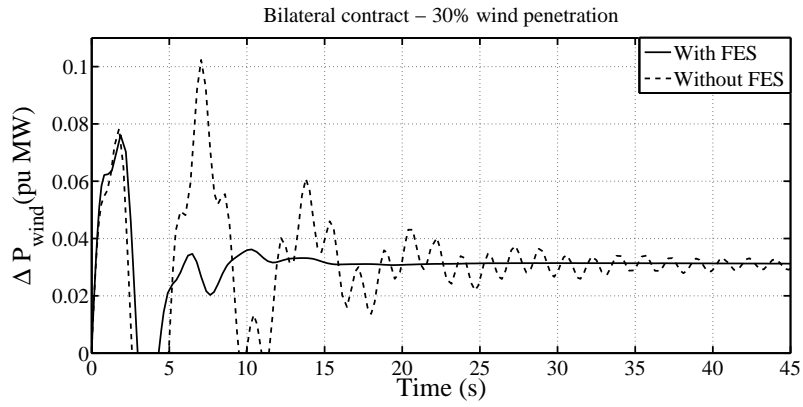
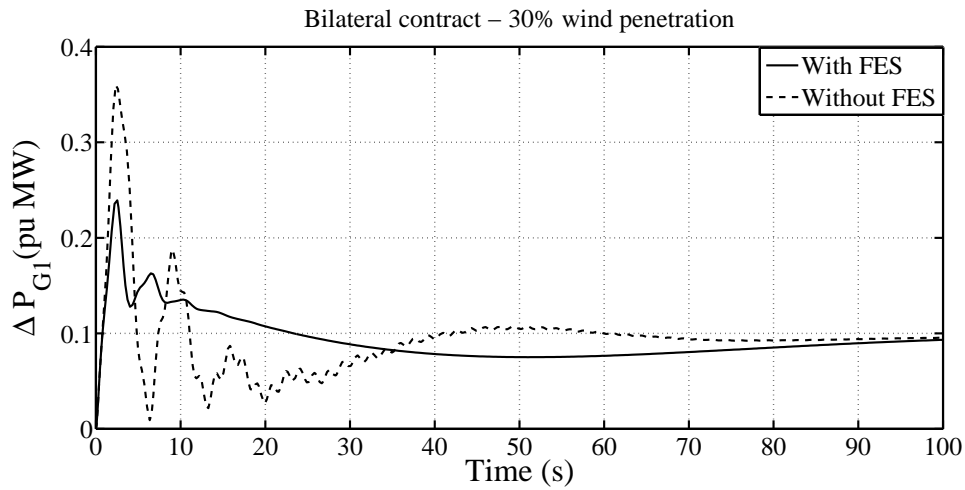
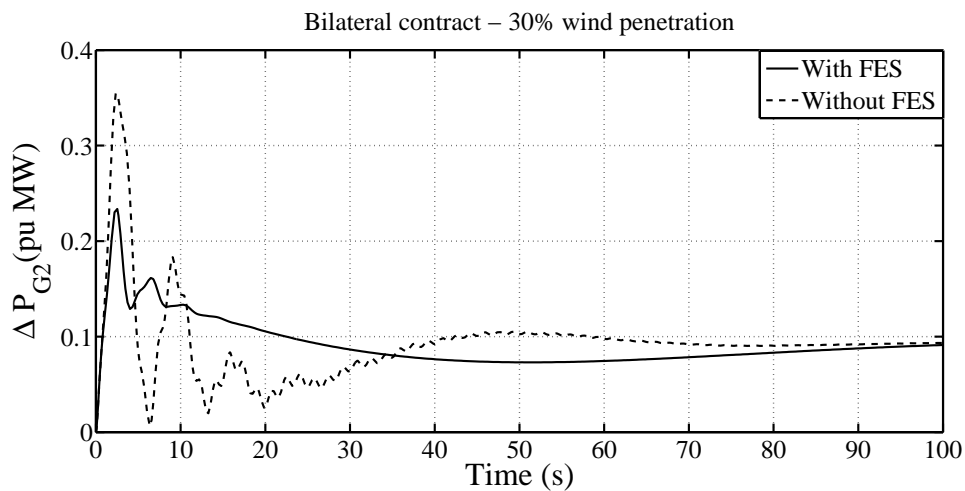


Fig. 5.28: Deviation in power output of GENCO-wind



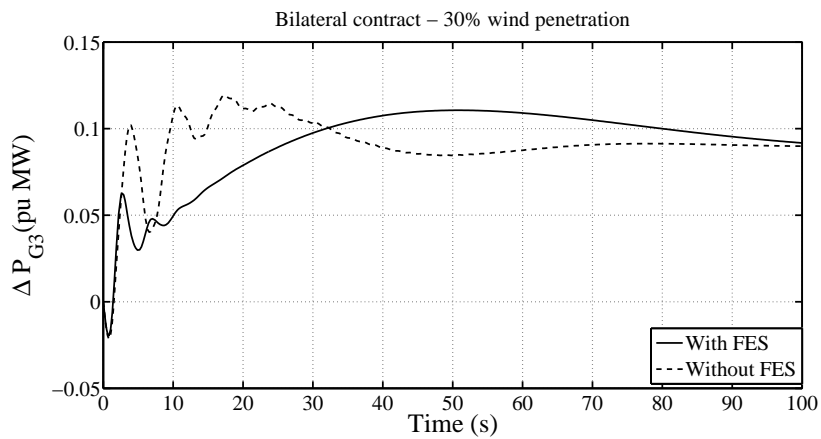
(a) Deviation in power output of GENCO-1



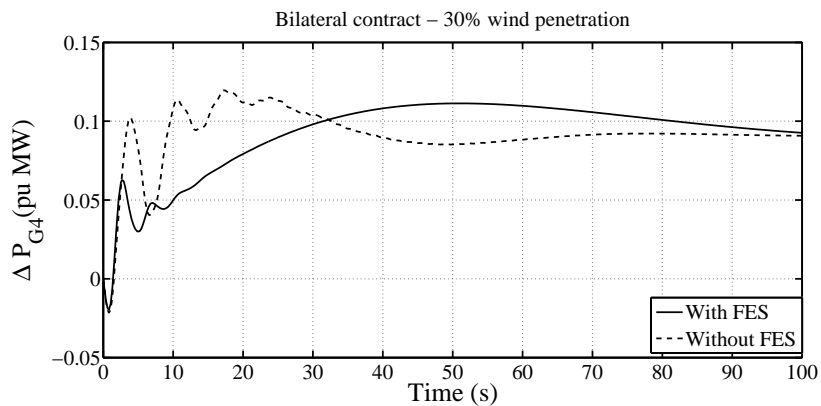
(b) Deviation in power output of GENCO-2

Fig. 5.29: Deviation in generation (ΔP_{G1} and ΔP_{G2}) of GENCOs in Area-1 for Case-2

Presence of FES system near to GENCO-wind in Area-1 avoids the chances of wind power curtailment during excess production during off peak hours. From the results, we can conclude that the similar response were obtained in hydro-thermal system during load following by wind power plants. Simulation results also confirms the need for energy storage devices along with wind power sources. The open market scenario during bilateral transactions urges the need of better system performance during load perturbations in deregulated power system where frequency control is considered as one of the ancillary services.



(a) Deviation in power output of GENCO-3



(b) Deviation in power output of GENCO-4

Fig. 5.30: Deviation in generation (ΔP_{G3} and ΔP_{G4}) of GENCOs in Area-2 for Case-2

Case 3: Contract Violation

Contract violation is an extension of bilateral transaction where any of DISCOs or GENCOs may violate the power contract, which is already made either in day ahead or hour ahead market. For analysis we have considered two cases of contract violation.

■ Contract violation due to

- Excess DISCO demand
- Deficit in wind power generation

Excess Demand

Here, DISCO-1 of Area-1 violates the power contract by demanding 0.1 pu MW extra power than it contracted earlier. This extra load act as a local load to Area-1. Normally this excess load will be met by the conventional GENCOs-1 and GENCO-2 of Area-1. The results pertain to contract violation due to excess is shown in Figs. 5.32-5.34.

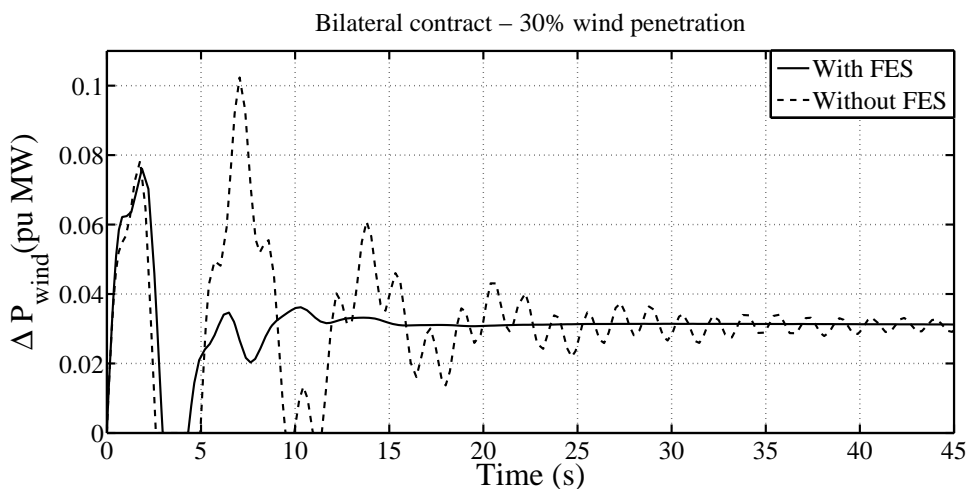
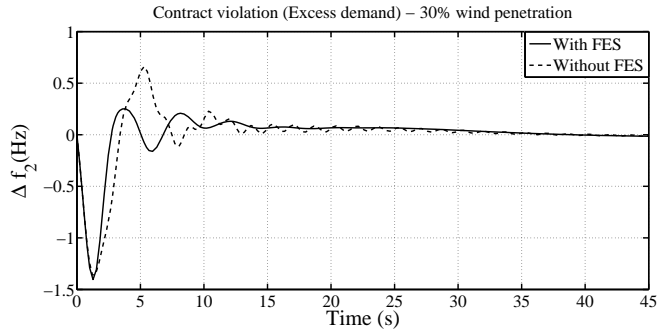
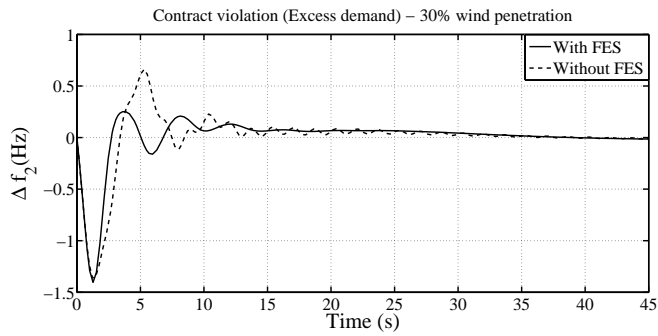


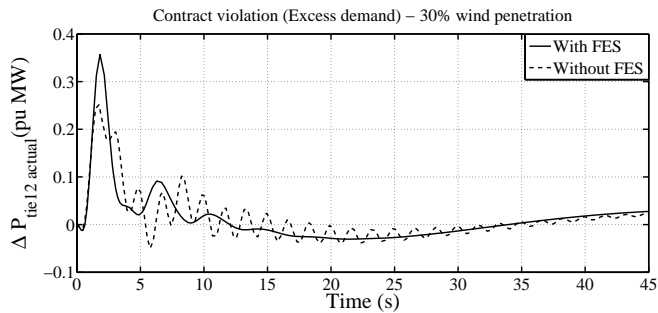
Fig. 5.31: Deviation in power output of GENCO-wind for Case-3 (excess demand)



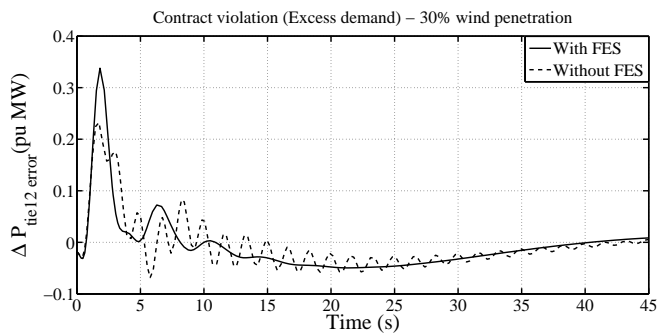
(a) Deviation in frequency of Area-1



(b) Deviation in frequency of Area-2



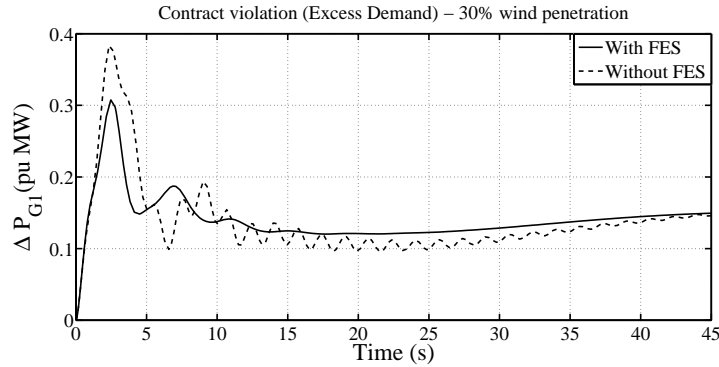
(c) Deviation in tie-line power flow



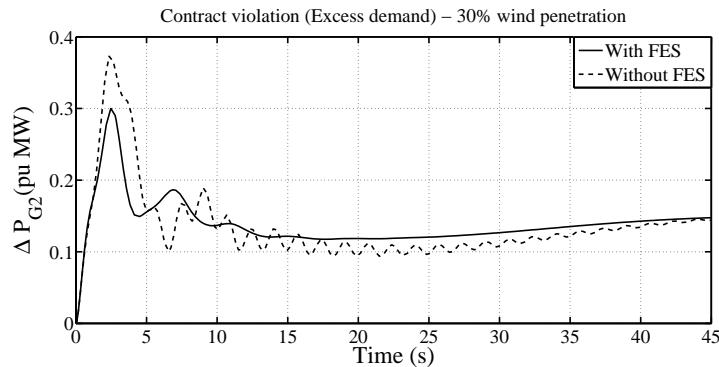
(d) Deviation in tie-line power flow error

Fig. 5.32: Variations in area frequencies (Δf_1 and Δf_2) and actual tie-line power (ΔP_{tie12}) and ($\Delta P_{tie12error}$) for Case-3 (excess demand)

In this scenario, presence of FES improves the dynamic frequency control during contract violation. This can be visualized through Fig. 5.32. As expected, at steady state, the output of various GENCOs in Area-2 settles down to their respective values (see Fig. 5.34). At the same time, it is also seen that at steady state, $\Delta P_{tie12sched}$ remains unaltered since extra load is met by the conventional GENCOs in Area-1. It is clear from Fig. 5.31 that the output of GENCO-wind remains unchanged since there is no control of input power.



(a) Deviation in power output of GENCO-1



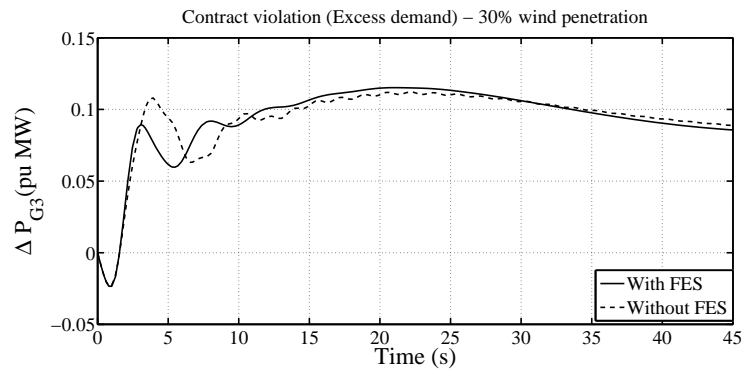
(b) Deviation in power output of GENCO-2

Fig. 5.33: Deviation in generation (ΔP_{G1} and ΔP_{G2}) of GENCOs in Area-1 for Case-3 (excess demand)

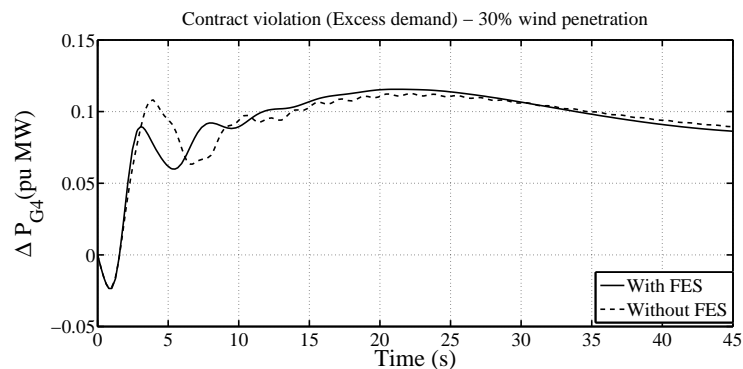
Wind Power Deficit

Stochastic nature of wind hinders wind power plants to participate in conventional power market. Due to the high integration of WECS and various incentives to operators forces wind power plant owners to actively involve in energy trade. This market operation is possible only with wind power forecasting. Among the available renewable sources wind

energy is least predictable due to the variability associated with wind. In this scenario of market operation, one has to taken care of the effect of this uncertainty associated with wind power forecasting.



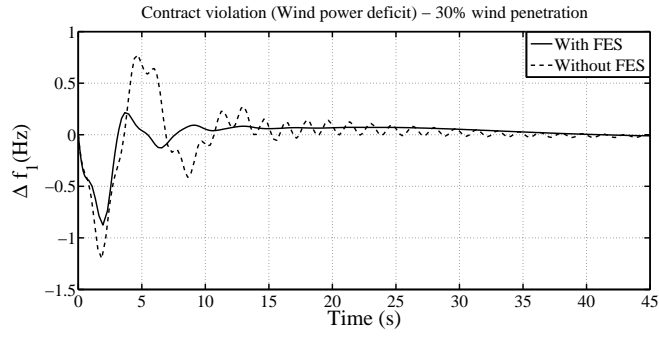
(a) Deviation in power output of GENCO-3



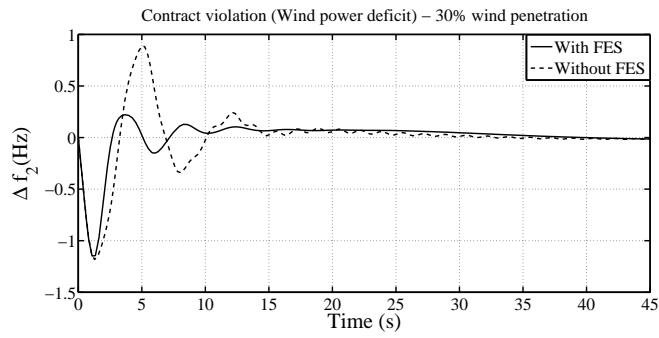
(b) Deviation in power output of GENCO-4

Fig. 5.34: Deviation in generation (ΔP_{G3} and ΔP_{G4}) of GENCOs in Area-2 for Case-3 (excess demand)

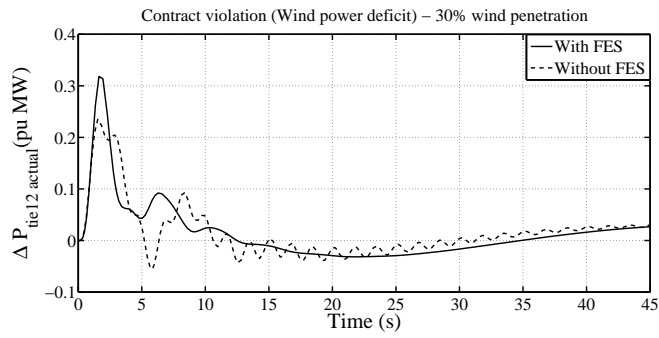
In our analysis, we have considered a case of contract violation where WECS generates less power than it contracted earlier. In order to maintain the power balance, this deficit in wind power should be met by the conventional generators in same area. Dynamic performances of system for are depicted in Fig. 5.35-5.38. The auxillary support from FES during load imbalance helps in maintaining frequency variation over a small range.



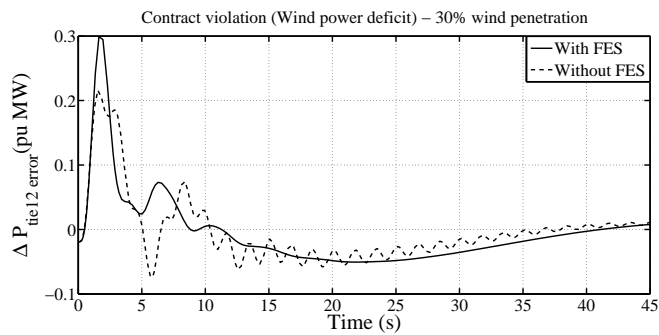
(a) Deviation in frequency of Area-1



(b) Deviation in frequency of Area-2



(c) Deviation in tie-line power flow



(d) Deviation in tie-line power flow error

Fig. 5.35: Variations in area frequencies (Δf_1 and Δf_2) and actual tie-line power (ΔP_{tie12}) and ($\Delta P_{tie12 error}$) for Case-3 (deficit in wind power)

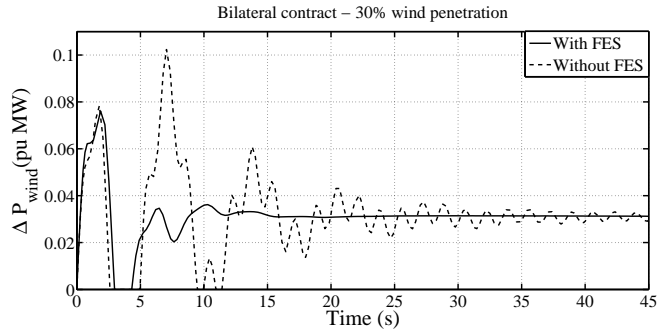
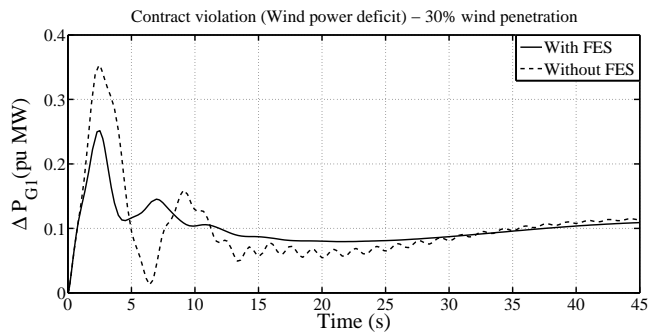
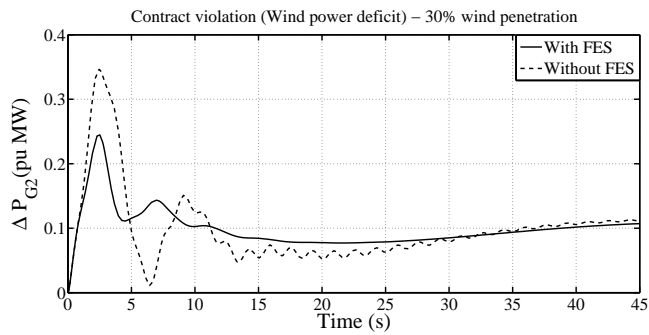


Fig. 5.36: Deviation in power output of GENCO-wind for Case-3 (deficit in wind power)



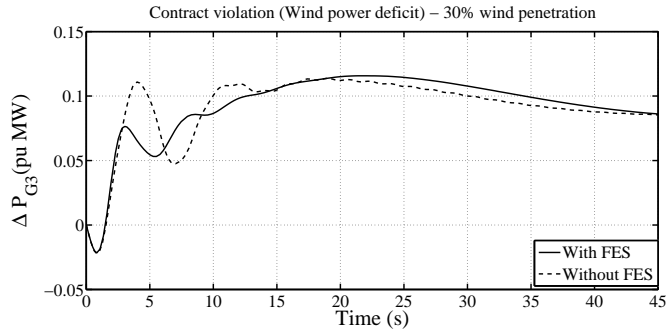
(a) Deviation in power output of GENCO-1



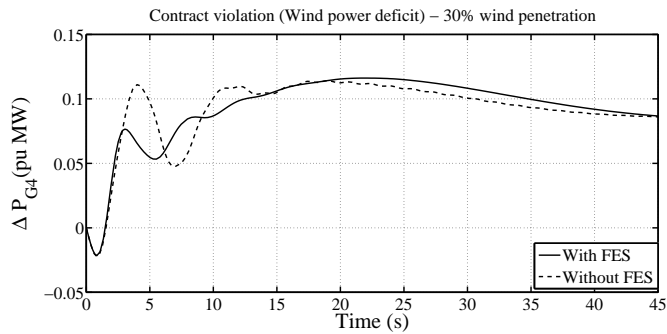
(b) Deviation in power output of GENCO-2

Fig. 5.37: Deviation in generation (ΔP_{G1} and ΔP_{G2}) of GENCOs in Area-1 for Case-3 (deficit in wind power)

The variation associated with frequency and tie-line power flow (see Fig. 5.35) in with and without FES cases validates the advantage of FES system in imperialistic market operation.



(a) Deviation in power output of GENCO-3



(b) Deviation in power output of GENCO-4

Fig. 5.38: Deviation in generation (ΔP_{G3} and ΔP_{G4}) of GENCOs in Area-2 for Case-3 (deficit in wind power)

5.5 Summary

Increase in wind penetration level has necessitated wind energy system to participate in open energy market. This introduced complexity in system balancing during load following as wind power is highly stochastic and also reduces the system reserve margin. In this work, we analyzed the effect of WECS in three market conditions, (i) Unilateral contract (ii) Bilateral contract and (iii) Contract violation with and without FES system. It is found that the use of FES system improves the system regulation margin during market operations. WECS based GENCO posed a problem to market operators by delivering power at a reduced level as contracted early resulted due to error in forecasting. Maintaining system balance, which is one of the ancillary services in deregulated system is done by sharing unsupplied load contract among the conventional GENCOs in the same area of GENCO-wind. It also establishes that operation of fast acting storage improves the load following in competitive power market with wind energy systems.

Chapter 6

Conclusions and Future Scope of Work

6.1 Conclusions

In this thesis, we have considered the effect of Thyristor Controlled Series Compensator (TCSC) on improving the frequency regulation of conventional, deregulated and wind integrated power system. It is found that TCSC improves the performance of the system following a small perturbation by damping the low frequency oscillations in the area frequencies and tie-line power flow. Hence, in this work we have explored inherent advantages of TCSC for improving the frequency regulation of the system. However, even now, frequency regulation is still challenging due to non-availability of energy immediately after the load demand. Most of the conventional energy sources are slow responding and need quite a long time to enhance the generation, which forces to use fast responding energy storage devices such as Flywheel, Superconducting Magnetic Energy Storage and Batteries. Through our analysis, we have found that use of energy storage devices like Flywheel Energy Storage System (FES) can improve the frequency regulation in wind integrated system.

Initial stage of our work is concerned with developing a linear incremental model for a TCSC and its application to improve the performance of Automatic Generation Control of two-area interconnected power system. The optimized integral gain values of AGC are obtained using Integral Squared Error (ISE) technique. A quadratic performance index considering a step load perturbation in either of the areas is considered for minimization. Simulation results suggest that, incorporating a TCSC is very effective in damping the low frequency oscillations in area frequencies as well as the tie-power after a sudden load perturbation in any of area compared to AGC without TCSC.

The effect of a TCSC for load following in a deregulated two area interconnected power system with two GENCOs and two DISCOs in either areas is also examined. Opti-

mal gain settings of the integral controllers in the control areas are obtained using Genetic Algorithm by minimizing a quadratic performance index. Simulation studies carried out in MATLAB validates that a Thyristor Controlled Series Compensator in series with tie-line can effectively improve the load following performance of the power system in a deregulated environment.

The impact of wind penetration levels on primary frequency control of a power system considering non-linearities are studied, where Flywheel Energy Storage (FES) is deployed in a wind integrated power system to overcome the intermittent nature of wind power generation. The effect of TCSC in damping out low frequency oscillations in area frequencies and tie-line power flow in a wind penetrated power system is also analyzed. A strategy comprising inertia control combined with coordinated operation of conventional generation units with wind energy and TCSC-FES has been proposed for frequency support in a wind penetrated power system. Simulation results establish the effectiveness of the TCSC-FES combination in enhancing the primary frequency control from wind integrated power system during frequency excursions.

At last, our work addresses issues pertaining to load following by wind power plants in a deregulated power system. At present, a significant share of the power generated in the electric grid is from wind power plants. Availability of various forecasting algorithms makes wind power plants a competitive candidate in the open power market. However, the stochastic nature of wind generating units primarily affects power balancing of the grid. This thesis aims at enhancing the system regulation reserve by combining wind energy source with energy storage such as FES system in a deregulated power system. For our analysis, we consider a wind energy system model capable of primary frequency control. Load following with wind energy system is studied in various market scenarios - unilateral contract, bilateral contract and contract violation cases. In addition, a new case of contract violation is considered, where wind energy system supplies power less than that contracted earlier. Teaching-Learning Based Optimization (TLBO), a nature inspired algorithm, is used to tune the controller parameters for various market conditions. Simulation results show the effectiveness of FES system in improving the frequency regulation and system regulation margin during load following in a deregulated power system.

6.2 Future Scope

Electric industry is growing with the aim to reduce fossil fuel consumption and carbon emission. This even affected the automobile industry with the emergence of electric vehicles. Now a days the advancements in technologies and reduction in capital expenditure have paved way for more customers to opt for Plug in Electric Vehicles (PEVs). To attract more customers, government and other power producers offer incentives to PEVs to participate effectively in load balancing. This becomes more attractive when we have sufficient renewable integration in the grid. Hence, there is still potential gap in utilizing effectiveness of PEVs in power balancing.

Meanwhile, in an era of deregulation, utilities are interested in maximizing their profit rather than bringing power balance. The use of frequency linked tariff may be an alternate option to make utilities to participate in load balance. This becomes more important with wind energy source where unscheduled interchange may be due to contract violation resulting from improper forecasting. Availability Based Tariff (ABT) based LFC may be a suitable candidate to bring back the frequency equilibrium in deregulated power system with significant renewable integration. Hence, there is a need to address the effect of ABT with wind power plants in open market operation.

Appendix

1. System Data [96,98,135]

$$K_{P1} = K_{P2} = 120 \text{ Hz/p.u MW}$$

$$T_{P1} = T_{P2} = 20 \text{ s}$$

$$R_1 = R_2 = R_3 = R_4 = 2.4 \text{ Hz/p.u.MW}$$

$$T_{G1} = T_{G2} = T_{G3} = T_{G4} = 0.08 \text{ s}$$

$$T_{T1} = T_{T2} = T_{T3} = T_{T4} = 0.3 \text{ s}$$

$$T_{R1} = T_{R2} = 10 \text{ s}$$

$$K_{R1} = K_{R2} = 0.5$$

$$P_{r1} = P_{r2} = 1200 \text{ MW}$$

$$T_{12} = 0.0866$$

$$T_{GH} = 48.7$$

$$T_{RH} = 0.513$$

$$T_{RS} = 5 \text{ s}$$

$$T_W = 1 \text{ s}$$

2. TCSC Data [90,136]

System voltage : 400 kV

Rated continuous current : 1500 A

Rated overall power : 493 MVAR

$$K_{TCSC} = 2$$

$$T_{TCSC} = 0.02 \text{ s}$$

3. Wind System [45]

$$T_w = 6.0 \text{ s}$$

$$T_R = 0.1 \text{ s}$$

$$T_A = 0.2 \text{ s}$$

$$T_c = 0.2 \text{ s}$$

$$\Delta P_{windMin}/\Delta P_{windMax} = 0.0/1.2 \text{ pu}$$

$$\omega_e^{min}/\omega_e^{max} = 0.8/1.2 \text{ pu}$$

4. FES data[137–139]

Nominal output rating : Up to 100 kW

Usable energy at full charge : 200 kWh

$$K_{FES} = 1$$

$$T_{FES} = 0.1 \text{ s}$$

Bibliography

- [1] E. Ela, V. Gevorgian, P. Fleming, Y. Zhang, M. Singh, E. Muljadi, A. Scholbrook, J. Aho, A. Buckspan, L. Pao *et al.*, “Active power controls from wind power: Bridging the gaps,” National Renewable Energy Laboratory (NREL), Golden, CO., Tech. Rep., 2014.
- [2] R. C. Eberhart and Y. Shi, “Comparing inertia weights and constriction factors in particle swarm optimization,” *Evolutionary Computation, Proceedings of the 2000 Congress on*, vol. 1, pp. 84–88, 2000.
- [3] R. V. Rao, V. J. Savsani, and D. Vakharia, “Teaching - learning - based optimization: a novel method for constrained mechanical design optimization problems,” *Computer-Aided Design*, vol. 43, no. 3, pp. 303–315, 2011.
- [4] R. Rao, V. Savsani, and D. Vakharia, “Teaching - learning - based optimization: An optimization method for continuous non-linear large scale problems,” *Information Sciences*, vol. 183, no. 1, pp. 1 – 15, 2012. [Online]. Available: <http://www.sciencedirect.com/science/article/pii/S0020025511004191>
- [5] O. I. Elgerd and C. E. Fosha, “Optimum megawatt-frequency control of multiarea electric energy systems,” *IEEE Transactions on Power Apparatus and Systems*, no. 4, pp. 556–563, 1970.
- [6] C. E. Fosha and O. I. Elgerd, “The megawatt-frequency control problem: A new approach via optimal control theory,” *IEEE Transactions on Power Apparatus and Systems*, no. 4, pp. 563–577, 1970.
- [7] A. J. Wood and B. F. Wollenberg, *Power generation, operation, and control*. John Wiley & Sons, 2012.

- [8] P. Kundur, N. J. Balu, and M. G. Lauby, *Power system stability and control*. McGraw-hill New York, 1994, vol. 7.
- [9] F. Daneshfar and H. Bevrani, "Load–frequency control: a GA-based multi-agent reinforcement learning," *IET generation, transmission & distribution*, vol. 4, no. 1, pp. 13–26, 2010.
- [10] R. de Almeida and J. Peas Lopes, "Participation of Doubly Fed Induction Wind Generators in System Frequency Regulation," *IEEE Transactions on Power Systems*, vol. 22, no. 3, pp. 944–950, August 2007.
- [11] P.-K. Keung, P. Li, H. Banakar, and B. Ooi, "Kinetic Energy of Wind-Turbine Generators for System Frequency Support," *IEEE Transactions on Power Systems*, vol. 24, no. 1, pp. 279–287, February 2009.
- [12] A. Tenenge, C. Jecu, D. Roye, S. Bacha, J. Duval, and R. Belhomme, "Contribution to frequency control through wind turbine inertial energy storage," *IET Renewable Power Generation*, vol. 3, no. 3, pp. 358–370, September 2009.
- [13] Z.-S. Zhang, Y.-Z. Sun, J. Lin, and G.-J. Li, "Coordinated frequency regulation by doubly fed induction generator-based wind power plants," *IET Renewable Power Generation*, vol. 6, no. 1, pp. 38–47, January 2012.
- [14] M. Kayikci and J. Milanovic, "Dynamic contribution of dfig-based wind plants to system frequency disturbances," *IEEE Transactions on Power Systems*, vol. 24, no. 2, pp. 859–867, May 2009.
- [15] Y. Wang, R. Zhou, and C. Wen, "New robust adaptive load-frequency control with system parametric uncertainties," *IEE Proceedings-Generation, Transmission and Distribution*, vol. 141, no. 3, pp. 184–190, 1994.
- [16] A. Stankovic, G. Tadmor, and T. A. Sakharuk, "On robust control analysis and design for load frequency regulation," *IEEE Transactions on Power Systems*, vol. 13, no. 2, pp. 449–455, 1998.

- [17] T. Sasaki, T. Kadoya, and K. Enomoto, "Study on load frequency control using redox flow batteries," *IEEE Transactions on Power Systems*, vol. 19, no. 1, pp. 660–667, 2004.
- [18] P. Subbaraj and K. Manickavasagam, "Generation control of interconnected power systems using computational intelligence techniques," *IET Generation, Transmission & Distribution*, vol. 1, no. 4, pp. 557–563, 2007.
- [19] M. Farahani, S. Ganjefar, and M. Alizadeh, "PID controller adjustment using chaotic optimisation algorithm for multi-area load frequency control," *IET Control Theory & Applications*, vol. 6, no. 13, pp. 1984–1992, 2012.
- [20] A. Keyhani and A. Chatterjee, "Automatic generation control structure for smart power grids," *IEEE Transactions on Smart Grid*, vol. 3, no. 3, pp. 1310–1316, 2012.
- [21] K. Yamashita and H. Miyagi, "Multivariable self-tuning regulator for load frequency control system with interaction of voltage on load demand," in *IEE Proceedings D-Control Theory and Applications*, vol. 138, no. 2. IET, 1991, pp. 177–183.
- [22] L. Chang-Chien, Y. Wu, and J. Cheng, "Online estimation of system parameters for artificial intelligence applications to load frequency control," *IET generation, transmission & distribution*, vol. 5, no. 8, pp. 895–902, 2011.
- [23] L. R. Chang-Chien, N.-B. Hoonchareon, C.-M. Ong, and R. A. Kramer, "Estimation of beta; for adaptive frequency bias setting in load frequency control," *IEEE Transactions on Power Systems*, vol. 18, no. 2, pp. 904–911, May 2003.
- [24] S. Doolla and T. S. Bhatti, "Load frequency control of an isolated small-hydro power plant with reduced dump load," *IEEE Transactions on Power Systems*, vol. 21, no. 4, pp. 1912–1919, November 2006.
- [25] K. Vrdoljak, N. Peric, and I. Petrovic, "Sliding mode based load-frequency control in power systems," *Electric Power Systems Research*, vol. 80, no. 5, pp. 514 –

527, 2010. [Online]. Available: <http://www.sciencedirect.com/science/article/pii/S0378779609002673>

- [26] N. Hasan, Ibraheem, P. Kumar, and Nizamuddin, "Sub-optimal automatic generation control of interconnected power system using constrained feedback control strategy," *International Journal of Electrical Power & Energy Systems*, vol. 43, no. 1, pp. 295 – 303, 2012. [Online]. Available: <http://www.sciencedirect.com/science/article/pii/S0142061512001664>
- [27] D. Zhu and G. Hug-Glanzmann, "Coordination of storage and generation in power system frequency control using an h_∞ approach," *IET Generation, Transmission Distribution*, vol. 7, no. 11, pp. 1263–1271, November 2013.
- [28] M. Shiroei, M. R. Toulabi, and A. M. Ranjbar, "Robust multivariable predictive based load frequency control considering generation rate constraint," *International Journal of Electrical Power & Energy Systems*, vol. 46, pp. 405 – 413, 2013. [Online]. Available: <http://www.sciencedirect.com/science/article/pii/S0142061512006023>
- [29] A. Khodabakhshian, "Enhancement of power system performance by lfc analysis of hydro power plants using QFT," *European Transactions on Electrical Power*, vol. 19, no. 2, pp. 323–338, 2009. [Online]. Available: <http://dx.doi.org/10.1002/etep.223>
- [30] M. Shiroei, A. M. Ranjbar, and T. Amraee, "A functional model predictive control approach for power system load frequency control considering generation rate constraint," *International Transactions on Electrical Energy Systems*, vol. 23, no. 2, pp. 214–229, 2013. [Online]. Available: <http://dx.doi.org/10.1002/etep.653>
- [31] R. Hooshmand, M. Ataei, and A. Zargari, "A new fuzzy sliding mode controller for load frequency control of large hydropower plant using particle swarm optimization algorithm and kalman estimator," *European Transactions on Electrical Power*, vol. 22, no. 6, pp. 812–830, 2012. [Online]. Available: <http://dx.doi.org/10.1002/etep.609>

- [32] V. Donde, M. A. Pai, and I. A. Hiskens, "Simulation and optimization in an AGC system after deregulation," *IEEE Transactions on Power Systems*, vol. 16, no. 3, pp. 481–489, August 2001.
- [33] W. Tan, H. Zhang, and M. Yu, "Decentralized load frequency control in deregulated environments," *International Journal of Electrical Power & Energy Systems*, vol. 41, no. 1, pp. 16 – 26, 2012. [Online]. Available: <http://www.sciencedirect.com/science/article/pii/S0142061512000403>
- [34] H. Bevrani, Y. Mitani, K. Tsuji, and H. Bevrani, "Bilateral based robust load frequency control," *Energy Conversion and Management*, vol. 46, no. 7-8, pp. 1129 – 1146, 2005. [Online]. Available: <http://www.sciencedirect.com/science/article/pii/S0196890404001633>
- [35] H. Shayeghi and H. A. Shayanfar, "Design of decentralized robust LFC in a competitive electricity environment," *Journal of Electrical Engineering*, vol. 56, no. 9-10, pp. 225–236, 2005.
- [36] E. Rakhshani and J. Sadeh, "Practical viewpoints on load frequency control problem in a deregulated power system," *Energy Conversion and Management*, vol. 51, no. 6, pp. 1148 – 1156, 2010. [Online]. Available: <http://www.sciencedirect.com/science/article/pii/S0196890409005305>
- [37] H. Shayeghi, H. Shayanfar, and O. Malik, "Robust decentralized neural networks based LFC in a deregulated power system," *Electric Power Systems Research*, vol. 77, no. 3–4, pp. 241 – 251, 2007. [Online]. Available: <http://www.sciencedirect.com/science/article/pii/S0378779606000587>
- [38] I. Chidambaram and B. Paramasivam, "Optimized load-frequency simulation in restructured power system with Redox Flow Batteries and Interline Power Flow Controller," *International Journal of Electrical Power & Energy Systems*, vol. 50, pp. 9 – 24, 2013. [Online]. Available: <http://www.sciencedirect.com/science/article/pii/S0142061513000641>

- [39] H. Shayeghi, A. Jalili, and H. Shayanfar, "A robust mixed h_2/h_∞ based LFC of a deregulated power system including SMES," *Energy Conversion and Management*, vol. 49, no. 10, pp. 2656 – 2668, 2008. [Online]. Available: <http://www.sciencedirect.com/science/article/pii/S0196890408001465>
- [40] K. S. Parmar, S. Majhi, and D. Kothari, "LFC of an interconnected power system with multi-source power generation in deregulated power environment," *International Journal of Electrical Power & Energy Systems*, vol. 57, pp. 277 – 286, 2014. [Online]. Available: <http://www.sciencedirect.com/science/article/pii/S0142061513005164>
- [41] H. Bevrani, Y. Mitani, and K. Tsuji, "Robust decentralized AGC in a restructured power system," *Energy Conversion and Management*, vol. 45, no. 15, pp. 2297 – 2312, 2004. [Online]. Available: <http://www.sciencedirect.com/science/article/pii/S0196890403003625>
- [42] H. S. Moghanlou and H. A. Shayanfar, "Robust decentralized LFC design in a restructured power system," *International Journal of Emerging Electric Power Systems*, vol. 6, no. 2, p. 4, 2006.
- [43] F. Daneshfar, "Intelligent load-frequency control in a deregulated environment: Continuous-valued input, extended classifier system approach," *IET Generation, Transmission Distribution*, vol. 7, no. 6, pp. 551–559, June 2013.
- [44] L.-R. Chang-Chien, C.-M. Hung, and Y.-C. Yin, "Dynamic reserve allocation for system contingency by DFIG wind farms," *IEEE Transactions on Power Systems*, vol. 23, no. 2, pp. 729–736, May 2008.
- [45] J. Mauricio, A. Marano, A. Gomez-Exposito, and J. Martinez Ramos, "Frequency regulation contribution through variable-speed wind energy conversion systems," *IEEE Transactions on Power Systems*, vol. 24, no. 1, pp. 173–180, February 2009.
- [46] N. Ullah, T. Thiringer, and D. Karlsson, "Temporary primary frequency control support by variable speed wind turbines - potential and applications," *IEEE Transactions on Power Systems*, vol. 23, no. 2, pp. 601–612, May 2008.

- [47] J. Morren, S. de Haan, W. Kling, and J. Ferreira, "Wind turbines emulating inertia and supporting primary frequency control," *IEEE Transactions on Power Systems*, vol. 21, no. 1, pp. 433–434, February 2006.
- [48] O. Anaya-Lara, F. Hughes, N. Jenkins, and G. Strbac, "Contribution of DFIG-based wind farms to power system short-term frequency regulation," *Generation, Transmission and Distribution, IEE Proceedings-*, vol. 153, no. 2, pp. 164–170, March 2006.
- [49] D. Gautam, L. Goel, R. Ayyanar, V. Vittal, and T. Harbour, "Control strategy to mitigate the impact of reduced inertia due to doubly fed induction generators on large power systems," *IEEE Transactions on Power Systems*, vol. 26, no. 1, pp. 214–224, February 2011.
- [50] L.-R. Chang-Chien, W.-T. Lin, and Y.-C. Yin, "Enhancing frequency response control by DFIGs in the high wind penetrated power systems," *IEEE Transactions on Power Systems*, vol. 26, no. 2, pp. 710–718, May 2011.
- [51] Z. Miao, L. Fan, D. Osborn, and S. Yuvarajan, "Wind farms with HVdc delivery in inertial response and primary frequency control," *Energy Conversion, IEEE Transactions on*, vol. 25, no. 4, pp. 1171–1178, December 2010.
- [52] Y. Fu, Y. Wang, and X. Zhang, "Integrated wind turbine controller with virtual inertia and primary frequency responses for grid dynamic frequency support," *IET Renewable Power Generation*, vol. 11, no. 8, pp. 1129–1137, 2017.
- [53] T. Taj, H. Hasanien, A. Alolah, and S. Muyeen, "Transient stability enhancement of a grid-connected wind farm using an adaptive neuro-fuzzy controlled-flywheel energy storage system," *IET Renewable Power Generation*, vol. 9, no. 7, pp. 792–800, 2015.
- [54] G. Ramtharan, J. Ekanayake, and N. Jenkins, "Frequency support from doubly fed induction generator wind turbines," *IET Renewable Power Generation*, vol. 1, no. 1, pp. 3–9, March 2007.

- [55] GE. (2009) GE Energy WindINERTIA control fact sheet. [Online]. Available: http://site.ge-energy.com/prod_serv/products/renewable_energy/en/downloads/GEA17210.pdf
- [56] N. Miller, K. Clark, M. E. Cardinal, R. W. Delmerico, and G. Energy, “GE wind plant dynamic performance for grid and wind events,” *AEE TECH WIND GRID*, 2009.
- [57] GE Energy. (2009) 1.5MW wind turbine. [Online]. Available: <http://geosci.uchicago.edu/~moyer/GEOS24705/Readings/GEA14954C15-MW-Broch.pdf>
- [58] A. Zertek, G. Verbic, and M. Pantos, “A novel strategy for variable-speed wind turbines’ participation in primary frequency control,” *Sustainable Energy, IEEE Transactions on*, vol. 3, no. 4, pp. 791–799, October 2012.
- [59] R. Doherty, A. Mullane, G. Nolan, D. Burke, A. Bryson, and M. O’Malley, “An assessment of the impact of wind generation on system frequency control,” *IEEE Transactions on Power Systems*, vol. 25, no. 1, pp. 452–460, February 2010.
- [60] I. Margaris, S. Papathanassiou, N. Hatziargyriou, A. Hansen, and P. Sorensen, “Frequency control in autonomous power systems with high wind power penetration,” *Sustainable Energy, IEEE Transactions on*, vol. 3, no. 2, pp. 189–199, April 2012.
- [61] T. H. Mohamed, J. Morel, H. Bevrani, and T. Hiyama, “Model predictive based load frequency control design concerning wind turbines,” *International Journal of Electrical Power & Energy Systems*, vol. 43, no. 1, pp. 859–867, 2012.
- [62] P. Moutis, S. A. Papathanassiou, and N. D. Hatziargyriou, “Improved load-frequency control contribution of variable speed variable pitch wind generators,” *Renewable Energy*, vol. 48, no. 0, pp. 514 – 523, 2012.
- [63] K. Vidyanandan and N. Senroy, “Primary frequency regulation by deloaded wind turbines using variable droop,” *IEEE Transactions on Power Systems*, vol. 28, no. 2, pp. 837–846, May 2013.

- [64] A. Pappachen and A. P. Fathima, "Load frequency control in deregulated power system integrated with SMES-TCPS combination using ANFIS controller," *International Journal of Electrical Power & Energy Systems*, vol. 82, pp. 519 – 534, 2016. [Online]. Available: <http://www.sciencedirect.com/science/article/pii/S0142061516307037>
- [65] R. J. Abraham, D. Das, and A. Patra, "Agc system after deregulation considering TCPS in series with the tie-line," *International Journal of Emerging Electric Power Systems*, vol. 16, no. 3, pp. 281–295, 2015.
- [66] P. Bhatt, S. Ghoshal, and R. Roy, "Coordinated control of TCPS and SMES for frequency regulation of interconnected restructured power systems with dynamic participation from DFIG based wind farm," *Renewable Energy*, vol. 40, no. 1, pp. 40 – 50, 2012.
- [67] P. Ribeiro, B. Johnson, M. Crow, A. Arsoy, and Y. Liu, "Energy storage systems for advanced power applications," *Proceedings of the IEEE*, vol. 89, no. 12, pp. 1744–1756, December 2001.
- [68] A. Thatte, F. Zhang, and L. Xie, "Coordination of wind farms and flywheels for energy balancing and frequency regulation," in *Power and Energy Society General Meeting, 2011 IEEE*, July 2011, pp. 1–7.
- [69] F. W. Capp, M. L. Lazarewicz, A. J. Arseneaux, P. Dresens, and H. A. Rojas, "Methods, systems and apparatus for regulating frequency of generated power using flywheel energy storage systems with varying load and/or power generation," Jun. 23 2015, US Patent 9,065,295.
- [70] H. Shayeghi, H. Shayanfar, and O. Malik, "Robust decentralized neural networks based LFC in a deregulated power system," *Electric Power Systems Research*, vol. 77, no. 3–4, pp. 241 – 251, 2007. [Online]. Available: <http://www.sciencedirect.com/science/article/pii/S0378779606000587>
- [71] H. Shayeghi, H. Shayanfar, and A. Jalili, "Multi-stage fuzzy PID power system automatic generation controller in deregulated environments," *Energy Conversion*

- and Management*, vol. 47, no. 18, pp. 2829 – 2845, 2006. [Online]. Available: <http://www.sciencedirect.com/science/article/pii/S0196890406001257>
- [72] S. Hosseini and A. Etemadi, “Adaptive neuro-fuzzy inference system based automatic generation control,” *Electric Power Systems Research*, vol. 78, no. 7, pp. 1230 – 1239, 2008. [Online]. Available: <http://www.sciencedirect.com/science/article/pii/S0378779607002180>
- [73] A. A. Hussein, N. Kutkut, Z. J. Shen, and I. Batarseh, “Distributed battery micro-storage systems design and operation in a deregulated electricity market,” *IEEE Transactions on Sustainable Energy*, vol. 3, no. 3, pp. 545–556, July 2012.
- [74] D. Menniti, A. Pinnarelli, N. Scordino, and N. Sorrentino, “Using a FACTS device controlled by a decentralised control law to damp the transient frequency deviation in a deregulated electric power system,” *Electric power systems research*, vol. 72, no. 3, pp. 289–298, 2004.
- [75] A. Demiroren and H. Zeynelgil, “GA application to optimization of AGC in three-area power system after deregulation,” *International Journal of Electrical Power & Energy Systems*, vol. 29, no. 3, pp. 230 – 240, 2007. [Online]. Available: <http://www.sciencedirect.com/science/article/pii/S0142061506001475>
- [76] Y. Arya, “AGC performance enrichment of multi-source hydrothermal gas power systems using new optimized FOPID controller and redox flow batteries,” *Energy*, vol. 127, pp. 704 – 715, 2017. [Online]. Available: <http://www.sciencedirect.com/science/article/pii/S0360544217305212>
- [77] I. Gonzalez-Aparicio and A. Zucker, “Impact of wind power uncertainty forecasting on the market integration of wind energy in Spain,” *Applied Energy*, vol. 159, pp. 334 – 349, 2015. [Online]. Available: <http://www.sciencedirect.com/science/article/pii/S0306261915010405>
- [78] C. Archer, H. Simao, W. Kempton, W. Powell, and M. Dvorak, “The challenge of integrating offshore wind power in the U.S. electric grid. part I: Wind forecast

- error,” *Renewable Energy*, vol. 103, pp. 346 – 360, 2017. [Online]. Available: <http://www.sciencedirect.com/science/article/pii/S096014811631031X>
- [79] B. Mohanty and P. K. Hota, “Comparative performance analysis of fruit fly optimisation algorithm for multi-area multi-source automatic generation control under deregulated environment,” *IET Generation, Transmission Distribution*, vol. 9, no. 14, pp. 1845–1855, 2015.
- [80] H. Simáč, W. Powell, C. Archer, and W. Kempton, “The challenge of integrating offshore wind power in the U.S. electric grid. part ii: Simulation of electricity market operations,” *Renewable Energy*, vol. 103, pp. 418 – 431, 2017. [Online]. Available: <http://www.sciencedirect.com/science/article/pii/S0960148116310333>
- [81] A. Banswar, N. K. Sharma, Y. R. Sood, and R. Shrivastava, “Market based procurement of energy and ancillary services from renewable energy sources in deregulated environment,” *Renewable Energy*, vol. 101, pp. 1390 – 1400, 2017. [Online]. Available: <http://www.sciencedirect.com/science/article/pii/S0960148116308825>
- [82] K. Valentine, W. Temple, R. J. Thomas, and K. M. Zhang, “Relationship between wind power, electric vehicles and charger infrastructure in a two-settlement energy market,” *International Journal of Electrical Power & Energy Systems*, vol. 82, pp. 225 – 232, 2016. [Online]. Available: <http://www.sciencedirect.com/science/article/pii/S0142061516303052>
- [83] H. H. Abdeltawab and Y. A. R. I. Mohamed, “Market-oriented energy management of a hybrid wind-battery energy storage system via model predictive control with constraint optimizer,” *IEEE Transactions on Industrial Electronics*, vol. 62, no. 11, pp. 6658–6670, November 2015.
- [84] A. P. Antony and D. T. Shaw, “Empowering the electric grid: Can SMES coupled to wind turbines improve grid stability?” *Renewable Energy*, vol. 89, pp. 224 – 230, 2016. [Online]. Available: <http://www.sciencedirect.com/science/article/pii/S0960148115305103>

- [85] H. Akhavan-Hejazi and H. Mohsenian-Rad, "Optimal operation of independent storage systems in energy and reserve markets with high wind penetration," *IEEE Transactions on Smart Grid*, vol. 5, no. 2, pp. 1088–1097, March 2014.
- [86] M. Klein, G. Rogers, and P. Kundur, "A fundamental study of inter-area oscillations in power systems," *IEEE Transactions on Power Systems*, vol. 6, no. 3, pp. 914–921, 1991.
- [87] E. V. Larsen, J. J. Sanchez-Gasca, and J. H. Chow, "Concepts for design of FACTS controllers to damp power swings," *IEEE Transactions on power systems*, vol. 10, no. 2, pp. 948–956, 1995.
- [88] B. Chaudhuri, B. C. Pal, A. C. Zolotas, I. M. Jaimoukha, and T. C. Green, "Mixed-sensitivity approach to H/sub/spl infin//control of power system oscillations employing multiple FACTS devices," *IEEE Transactions on Power Systems*, vol. 18, no. 3, pp. 1149–1156, 2003.
- [89] B. Chaudhuri and B. C. Pal, "Robust damping of multiple swing modes employing global stabilizing signals with a TCSC," *IEEE Transactions on Power Systems*, vol. 19, no. 1, pp. 499–506, 2004.
- [90] B. Pal and B. Chaudhuri, *Robust control in power systems*. Springer Science & Business Media, 2006.
- [91] L. Gyugyi, "Unified power-flow control concept for flexible AC transmission systems," in *IEE proceedings C (generation, transmission and distribution)*, vol. 139, no. 4. IET, 1992, pp. 323–331.
- [92] J. J. Paserba, N. W. Miller, E. V. Larsen, and R. J. Piwko, "A thyristor controlled series compensation model for power system stability analysis," *IEEE Transactions on Power Delivery*, vol. 10, no. 3, pp. 1471–1478, Jul 1995.
- [93] A. D. D. Rosso, C. A. Canizares, and V. M. Dona, "A study of TCSC controller design for power system stability improvement," *IEEE Transactions on Power Systems*, vol. 18, no. 4, pp. 1487–1496, November 2003.

- [94] N. G. Hingorani and L. Gyugyi, *Understanding FACTS*. IEEE press, 2000.
- [95] S. Tripathy, G. Hope, and O. Malik, "Optimisation of load-frequency control parameters for power systems with reheat steam turbines and governor deadband non-linearity," in *IEE Proceedings C (Generation, Transmission and Distribution)*, vol. 129, no. 1. IET, 1982, pp. 10–16.
- [96] R. Abraham, D. Das, and A. Patra, "Effect of TCPS on oscillations in tie-power and area frequencies in an interconnected hydrothermal power system," *IET Generation, Transmission & Distribution*, vol. 1, no. 4, pp. 632–639, 2007.
- [97] "IEEE recommended practice for functional and performance characteristics of control systems for steam turbine-generator units," *IEEE Std 122-1991*, pp. 1–, 1992.
- [98] D. Das, J. Nanda, M. Kothari, and D. Kothari, "Automatic generation control of a hydrothermal system with new area control error considering generation rate constraint," *Electric Machines & Power Systems*, vol. 18, no. 6, pp. 461–471, 1990.
- [99] J. Nanda, M. Kothari, and P. Satsang, "Automatic generation control of an interconnected hydrothermal system in continuous and discrete modes considering generation rate constraints," in *IEE Proceedings D-Control Theory and Applications*, vol. 130, no. 1. IET, 1983, pp. 17–27.
- [100] S. C. Tripathy, T. S. Bhatti, C. S. Jha, O. P. Malik, and G. S. Hope, "Sampled data automatic generation control analysis with reheat steam turbines and governor dead-band effects," *IEEE Transactions on Power Apparatus and Systems*, vol. PAS-103, no. 5, pp. 1045–1051, May 1984.
- [101] L.-R. Chang-Chien and I.-C. Chu, "Formulating customer's power deficiency for GENCOs to perform third-party supply," *Electric Power Systems Research*, vol. 78, no. 2, pp. 177 – 191, 2008. [Online]. Available: <http://www.sciencedirect.com/science/article/pii/S0378779607000211>

- [102] E. Nobile, A. Bose, and K. Tomsovic, “Feasibility of a bilateral market for load following,” *IEEE Transactions on Power Systems*, vol. 16, no. 4, pp. 782–787, November 2001.
- [103] H. Bevrani, *Robust power system frequency control*. Springer, 2009, vol. 85.
- [104] T. McGovern and C. Hicks, “Deregulation and restructuring of the global electricity supply industry and its impact upon power plant suppliers,” *International Journal of Production Economics*, vol. 89, no. 3, pp. 321 – 337, 2004, manufacturing Strategy. [Online]. Available: <http://www.sciencedirect.com/science/article/pii/S0925527304000660>
- [105] D. Menniti, A. Pinnarelli, N. Scordino, and N. Sorrentino, “Using a FACTS device controlled by a decentralised control law to damp the transient frequency deviation in a deregulated electric power system,” *Electric Power Systems Research*, vol. 72, no. 3, pp. 289 – 298, 2004. [Online]. Available: <http://www.sciencedirect.com/science/article/pii/S037877960400121X>
- [106] D. Lawrence *et al.*, “Handbook of genetic algorithms,” *Van No strand Reinhold, New York*, 1991.
- [107] Y. Abdel-Magid and M. Dawoud, “Optimal AGC tuning with genetic algorithms,” *Electric Power Systems Research*, vol. 38, no. 3, pp. 231 – 238, 1996. [Online]. Available: <http://www.sciencedirect.com/science/article/pii/S0378779696010917>
- [108] S. Ghosh, S. Kamalasan, N. Senroy, and J. Enslin, “Doubly fed induction generator (DFIG)-Based Wind Farm Control Framework for Primary Frequency and Inertial Response Application,” *IEEE Transactions on Power Systems*, vol. 31, no. 3, pp. 1861–1871, May 2016.
- [109] R. Yan and T. K. Saha, “Frequency response estimation method for high wind penetration considering wind turbine frequency support functions,” *IET Renewable Power Generation*, vol. 9, no. 7, pp. 775–782, 2015.
- [110] M. Dreidy, H. Mokhlis, and S. Mekhilef, “Inertia response and frequency control techniques for renewable energy sources: A review,” *Renewable and*

- Sustainable Energy Reviews*, vol. 69, pp. 144 – 155, 2017. [Online]. Available: <http://www.sciencedirect.com/science/article/pii/S1364032116309212>
- [111] S. Muller, M. Deicke, and R. W. D. Doncker, “Doubly fed induction generator systems for wind turbines,” *IEEE Industry Applications Magazine*, vol. 8, no. 3, pp. 26–33, May 2002.
- [112] Y. Lei, A. Mullane, G. Lightbody, and R. Yacamini, “Modeling of the wind turbine with a doubly fed induction generator for grid integration studies,” *IEEE Transactions on Energy Conversion*, vol. 21, no. 1, pp. 257–264, March 2006.
- [113] R. de Almeida, E. Castronuovo, and J. Peas Lopes, “Optimum generation control in wind parks when carrying out system operator requests,” *IEEE Transactions on Power Systems*, vol. 21, no. 2, pp. 718–725, May 2006.
- [114] C. Hearn, M. Lewis, S. Pratap, R. Hebner, F. Uriarte, D. Chen, and R. Longoria, “Utilization of optimal control law to size grid-level flywheel energy storage,” *Sustainable Energy, IEEE Transactions on*, vol. 4, no. 3, pp. 611–618, July 2013.
- [115] G. O. Cimuca, C. Saudemont, B. Robyns, and M. M. Radulescu, “Control and performance evaluation of a flywheel energy-storage system associated to a variable-speed wind generator,” *IEEE Transactions on Industrial Electronics*, vol. 53, no. 4, pp. 1074–1085, June 2006.
- [116] J. P. Barton and D. G. Infield, “Energy storage and its use with intermittent renewable energy,” *IEEE Transactions on Energy Conversion*, vol. 19, no. 2, pp. 441–448, June 2004.
- [117] M. Kothari, P. Satsangi, and J. Nanda, “Sampled-data automatic generation control of interconnected reheat thermal systems considering generation rate constraints,” *Power Apparatus and Systems, IEEE Transactions on*, vol. PAS-100, no. 5, pp. 2334–2342, May 1981.
- [118] Essential Reliability Services Task Force (ERSTF), “Measures framework report,” North American Electric Reliability Corporation (NERC), 3353 Peachtree Road NE, Suite 600, North Tower, Atlanta, GA 30326, Tech. Rep., December 2015.

- [119] S. Tripathy, R. Balasubramanian, and P. Nair, "Effect of superconducting magnetic energy storage on automatic generation control considering governor deadband and boiler dynamics," *IEEE Transactions on Power Systems*, vol. 7, no. 3, pp. 1266–1273, August 1992.
- [120] M. P. K. T. Chaturvedi and L. Srivastava, "Self-organizing hierarchical particle swarm optimization for nonconvex economic dispatch," *IEEE Transactions on Power Systems*, vol. 23, no. 3, pp. 1079–1087, 2008.
- [121] R. Poli, "Analysis of the publications on the applications of particle swarm optimization," *Journal of Artificial Evolution and Applications*, p. 10, 2008.
- [122] Y. Del Valle, G. K. Venayagamoorthy, S. Mohagheghi, J.-C. Hernandez, and R. G. Harley, "Particle swarm optimization: basic concepts, variants and applications in power systems," *IEEE Transactions on evolutionary computation*, vol. 12, no. 2, pp. 171–195, 2008.
- [123] WWEA Half-year report: World wind capacity reached 456 GW. <http://www.wwindea.org/wwea-half-year-report-worldwind-wind-capacity-reached-456-gw/>. Accessed: 2017-04-10.
- [124] M. Dreidy, H. Mokhlis, and S. Mekhilef, "Inertia response and frequency control techniques for renewable energy sources: A review," *Renewable and Sustainable Energy Reviews*, vol. 69, pp. 144 – 155, 2017. [Online]. Available: <http://www.sciencedirect.com/science/article/pii/S1364032116309212>
- [125] J. Serrano-Gonzalez and R. Lacal-Arantequi, "Technological evolution of onshore wind turbines – A market-based analysis," *Wind Energy*, vol. 19, no. 12, pp. 2171–2187, 2016, wE-15-0200.R2. [Online]. Available: <http://dx.doi.org/10.1002/we.1974>
- [126] J. Ekanayake and N. Jenkins, "Comparison of the response of doubly fed and fixed-speed induction generator wind turbines to changes in network frequency," *IEEE Transactions on Energy Conversion*, vol. 19, no. 4, pp. 800–802, December 2004.

- [127] L. Wu and D. G. Infield, "Towards an assessment of power system frequency support from wind plant - modeling aggregate inertial response," *IEEE Transactions on Power Systems*, vol. 28, no. 3, pp. 2283–2291, August 2013.
- [128] Z. S. Zhang, Y. Z. Sun, J. Lin, and G. J. Li, "Coordinated frequency regulation by doubly fed induction generator-based wind power plants," *IET Renewable Power Generation*, vol. 6, no. 1, pp. 38–47, January 2012.
- [129] A. Rahman, L. C. Saikia, and N. Sinha, "Load frequency control of a hydro-thermal system under deregulated environment using biogeography-based optimised three-degree-of-freedom integral-derivative controller," *IET Generation, Transmission & Distribution*, vol. 9, no. 15, pp. 2284–2293, 2015.
- [130] W. Tan, Y. Hao, and D. Li, "Load frequency control in deregulated environments via active disturbance rejection," *International Journal of Electrical Power & Energy Systems*, vol. 66, pp. 166 – 177, 2015. [Online]. Available: <http://www.sciencedirect.com/science/article/pii/S0142061514006395>
- [131] C. K. Shiva and V. Mukherjee, "Automatic generation control of multi-unit multi-area deregulated power system using a novel quasi-oppositional harmony search algorithm," *IET Generation, Transmission Distribution*, vol. 9, no. 15, pp. 2398–2408, 2015.
- [132] S. B. Shree and N. Kamaraj, "Hybrid neuro fuzzy approach for automatic generation control in restructured power system," *International Journal of Electrical Power & Energy Systems*, vol. 74, pp. 274 – 285, 2016. [Online]. Available: <http://www.sciencedirect.com/science/article/pii/S0142061515002343>
- [133] R. K. Selvaraju and G. Somaskandan, "Impact of energy storage units on load frequency control of deregulated power systems," *Energy*, vol. 97, pp. 214 – 228, 2016. [Online]. Available: <http://www.sciencedirect.com/science/article/pii/S0360544215017661>
- [134] A. Shayegan-Rad, A. Badri, and A. Zangeneh, "Day-ahead scheduling of virtual power plant in joint energy and regulation reserve markets under

- uncertainties,” *Energy*, vol. 121, pp. 114 – 125, 2017. [Online]. Available: <http://www.sciencedirect.com/science/article/pii/S0360544217300063>
- [135] R. J. Abraham, D. Das, and A. Patra, “Load following in a bilateral market with local controllers,” *International Journal of Electrical Power & Energy Systems*, vol. 33, no. 10, pp. 1648 – 1657, 2011. [Online]. Available: <http://www.sciencedirect.com/science/article/pii/S0142061511001426>
- [136] ABB. (2016) TCSCthyristor controlled series compensation keeping grids together. [Online]. Available: <https://library.e.abb.com/public/dfd0b019e1fe08a48325771f002dbfc5/A02-0158.pdf>
- [137] G. Thijssen and J. Enslin, “Cost comparison for a 20 MW flywheel-based frequency regulation power plant,” *KEMA-Inc. Project: BPCC*, vol. 3, 2007. [Online]. Available: http://library.corporate-ir.net/library/12/123/123367/items/278586/KEMA_CostComparisonReport.pdf
- [138] I. Pan and S. Das, “Fractional order AGC for distributed energy resources using robust optimization,” *Smart Grid, IEEE Transactions on*, vol. PP, no. 99, pp. 1–1, 2015.
- [139] R. Rounds and G. Peek, “Design & development of a 20-MW flywheel-based frequency regulation power plant,” 2008. [Online]. Available: <http://prod.sandia.gov/techlib/access-control.cgi/2008/088229.pdf>

Publications Based on Thesis

Papers in Refereed Journals

1. **M. Deepak**, Rajesh Joseph Abraham (2015). Load following in a deregulated power system with Thyristor Controlled Series Compensator. *International Journal of Electrical Power & Energy Systems*, 65, 136-145.
2. **M. Deepak**, Dibyaranjan Senapati, Rajesh Joseph Abraham (2017). Damping of Low Frequency Oscillations in a Hydro-Thermal Power System Using Thyristor Controlled Series Compensator. *International Journal of Power and Energy Conversion*, 8(1),1-19.
3. **M. Deepak**, Rajesh Joseph Abraham (2017). Improving the dynamic frequency regulation of a Multisource Power System considering GRC and Deadband with TCSC and SMES. *International Journal of Power and Energy Conversion*, (in press)
4. **M. Deepak**, Rajesh Joseph Abraham, Francisco M Gonzalez-Longatt, David M Greenwood, Haile-Selassie Rajamani (2017). A novel approach to Frequency Support in a Wind Integrated Power System. *Renewable Energy*, 108, 194-206.
5. **M. Deepak**, Rajesh Joseph Abraham. Bilateral Load Following in a Competitive Power Market with Wind Power Plants. Submitted to *IET Smart Grid* (Revision submitted)

Presentations in Conferences

1. **M. Deepak**. *Analysis of TCPS-SMES coordination in a multi area thermal system with Automatic Generation Control*, 2014 **International Conference on Circuit**,

Power and Computing Technologies (ICCPCT), Nagarcoil, 20-21 March 2014.

2. **M. Deepak**. *Improving the dynamic performance in load frequency control of an interconnected power system with multi source power generation using superconducting magnetic energy storage (SMES)* at the **2014 International Conference on Advances in Green Energy (ICAGE)**, Thiruvananthapuram, 17-18 Dec. 2014.
3. **M. Deepak**, Rajesh Joseph Abraham. *Improving the AGC performance in a power system with Thyristor Controlled Series Compensator*, **2016 10th International Conference on Intelligent Systems and Control (ISCO)**, Coimbatore, 7-8 Jan. 2016
4. **M. Deepak**, Rajesh Joseph Abraham. *Comparative analysis of AGC performance in an interconnected power system with HVDC and TCSC considering GRC and deadband non-linearities*, **2016 IEEE 6th International Conference on Power Systems (ICPS)**, Delhi, 4-6 March 2016.